



I.R.Iran

ISSN:2423-5547
e-ISSN:2423-7469



Journal of Renewable Energy and Environment

Volume 10, Number 2, Spring 2023



Materials and Energy
Research Center



Iranian Association of
Chemical Engineers

In the Name of God

Journal of Renewable Energy and Environment

DIRECTOR-IN-CHARGE

H. Omidvar

Amirkabir University of Technology Tehran Polytechnic), Tehran, Iran

EDITOR-IN-CHIEF

M. Pazouki

Materials and Energy Research Center, Karaj, Iran

EDITORIAL BOARD

M. Ameri, Shahid Beheshti University, Tehran, Iran

S.S. Chandel, Shoolini University, Solan, Himachal Pradesh, India

J. Chaouki, Polytechnique Montréal, Montreal, Canada

H. Ghadamian, Materials and Energy Research Center, Karaj, Iran

B. Ghobadian, Tarbiat Modares University, Tehran, Iran

W.K.H. Hogland, Linnaeus University, Kalmar, Sweden

S.M. Hosseinalipoor, Iran University of Science & Technology, Tehran, Iran

H.A. Kazem, Sohar University, Sohar, Sultanate of Oman

K. Kaygusuz, Karadeniz Technical University, Trabzon, Turkey

A. Mostafaipoor, Yazd University, Yazd, Iran

G.H. Najafi, Tarbiat Modares University, Tehran, Iran

M.R. Omidkhah, Tarbiat Modares University, Tehran, Iran

M.H. Panjeshahi, Tehran University, Tehran, Iran

M. Pazouki, Materials and Energy Research Center, Karaj, Iran

R. Roshandel, Sharif University of Technology, Tehran, Iran

M.B. Shafii, Sharif University of Technology, Tehran, Iran

J. Shayegan, Sharif University of Technology, Tehran, Iran

T. Yusaf, Federation University Australia, Ballarat, Australia

S.A.H. Zamzamin, Materials and Energy Research Center, Karaj, Iran

EDITORIAL ADVISORY BOARD

N. Azbar, Ege University, Izmir, Turkey

M. El Haj Assad, University of Sharjah, Sharjah, United Arab Emirates

A.R. Maheri, University of Aberdeen, Aberdeen, United Kingdom

M. Mohanraj, Hindusthan College of Engineering and Technology, Coimbatore, Tamil Nadu, India

A. Sedaghat, Australian College of Kuwait, Kuwait

MANAGING EDITOR: M. Fouladian

COPY EDITOR: S. Saberi

PAGE DESIGNER: F. Hajizadeh

JOURNAL STAFF: M. Fouladian, V. Hajabdolali Bazzaz, E. Pouladi, R. Chaluei

DISCLAIMER

The publication of papers in *Journal of Renewable Energy and Environment* does not imply that the editorial board, reviewers, or the publisher accept, approve, or endorse the data and conclusions of authors.

Journal of Renewable Energy and Environment: (ISSN: 2423-5547) (e-ISSN: 2423-7469)

Website: www.jree.ir, E-mail: jree@merc.ac.ir

Tel: (+9826)36280040-49 (Ext 381), Fax: (+9826)36201888

Materials and Energy Research Center (MERC); Iranian Association of Chemical Engineers (IACChE)

AIMS AND SCOPE

Journal of Renewable Energy and Environment (JREE) publishes original papers, review articles, short communications and technical notes in the field of science and technology of renewable energies and environmental-related issues including:

- Generation
- Storage
- Conversion
- Distribution
- Management (economics, policies and planning)
- Environmental Sustainability

INSTRUCTIONS FOR AUTHORS

Submission of manuscript represents that it had neither been published nor submitted for publication elsewhere and is result of research carried out by author(s). Only the extended and upgraded articles presented in a conference and/or appeared in a symposium proceedings could be evaluated for publication.

Authors are required to include a list describing all the symbols and abbreviations in the paper. Use of the international system of measurement units is mandatory.

- On-line submission of manuscripts results in faster publication process and is recommended. Instructions are given in the JREE web sites: www.jree.ir
- References should be numbered in brackets and appear in sequence through the text. List of references should be given at the end of the paper. All journal articles listed in the References section must follow with article doi.
- Figure captions are to be indicated under the illustrations. They should sufficiently explain the figures.
- Illustrations should appear in their appropriate places in the text.
- Tables and diagrams should be submitted in a form suitable for reproduction.
- Photographs should be of high quality saved as jpg files.
- Tables' illustrations, figures and diagrams will be normally printed in single column width (8 cm). Exceptionally large ones may be printed across two columns (17 cm).

CONTENTS

Krishnarao Rajaram Patil	Experimental Investigation into the Combustion, Performance, and Emission Characteristics of Oxygenated DEE and Ethanol Blending with KOMÉ Biodiesel Fuelled CI Engine	1-8
Ming Hung Lin Jiun Hung Lin Mamdouh El Haj Assad Reza Alayi Seyed Reza Seyednouri	Optimal Location and Sizing of Wind Turbines and Photovoltaic Cells in the Grid for Load Supply Using Improved Genetic Algorithm	9-18
Armin Motamed Sadr Mehran Ameri Ebrahim Jahanshahi Javaran	Evaluation of the Experimental Performance of an Asphalt Solar Air Collector	19-26
Zeinab Sabzian-Molaei Esmaeel Rokrok Meysam Doostizadeh	An Optimal Master-Slave Model for Stochastic Planning of AC-DC Hybrid Distribution Systems	27-38
Uttam Bista Bhawana Rayamajhi Bipasyana Dhungana Sunil Prasad Lohani	Biogas Production by Co-Digestion of Food Waste with Sewage Sludge and Poultry Litter: A Way Towards Sustainable Waste-to-Energy Conversion	39-44
Seyed Amir Hassan Bathaei Masoud Iranmanesh Hossein Amiri Hajir Kourki	Investigation of the Enhancement of Thermophysical Properties of New Combinations of MWCNTs with Several PCMs Consisting of a Type of Paraffin in Comparison with Some Mineral Compounds (AN-MN-6H ₂ O)	45-55
Vasundhara Sen	Residential Consumer's Willingness to Pay for Renewable Energy: Evidence from a Double-Bounded Dichotomous Choice Survey from India	56-69
Ararsa Derese Seboka Fiseha Bekele Teshome Motuma Tolera Feyissa	Assessing the Environmental Impacts of Biomass Energy Production in Loka Abaya District, Sidama Region, Southern Ethiopia	70-80
Gokul Raghavendra Srinivasan Aditya Mahajan Rajiv Seth Rakesh Mahajan	Impact of Organic Hydrocarbons on Fuel Properties and Engine Characteristics of Thermally Cracked Cashew Nut Shell Liquid	81-94
Ritu Jain Vasundhara Mahajan	Energy Management of Multi-Microgrids in Joint Energy and Ancillary Service Market Considering Uncertainties of Renewables	95-107
Mohammad Hossein Jahangir Arash Kargarzadeh Mohammad Montazeri	Development of the Low-Economic-Risk Microgrids to Establish Environmental-Friendly Industries	108-124
Fatemeh Norouzi Morteza Hosseinpour Saeed Talebi	Analysis of Biogas Recovery from Liquid Dairy Manure Waste by Anaerobic Digestion	125-132



Research Article

Experimental Investigation into the Combustion, Performance, and Emission Characteristics of Oxygenated DEE and Ethanol Blending with KOME Biodiesel Fuelled CI Engine

Krishnarao Rajaram Patil*

Department of Mechanical Engineering, Marathwada Mitramandal's College of Engineering, Pune Affiliated to Savitribai Phule Pune University, P. O. Box: 411052, Pune, Maharashtra, India.

PAPER INFO

Paper History:

Received: 15 February 2022

Revised: 19 April 2022

Accepted: 26 April 2022

Keywords:

DEE-Ethanol-KOME Biodiesel Blend,
CI Engine,
Combustion Behaviour,
Engine Performance,
Emission Characteristics

ABSTRACT

The present study aims to develop different strategies for better utilization of oxygenated Diethyl ether and ethanol as supplementary fuels by blending them with biodiesel as the base fuel in CI engines. The used biodiesel used was readily available Karanja Oil Methyl Ester (KOME), its scientific name being *Pongamia Pinnata*. Initially, 5 %, 10 %, 15 %, and 20 % amounts of ethanol (volume) were mixed with biodiesel. Further, the optimum selected blend BE15 was mixed with 5 %, 10 %, 15 %, and 20 % DEE by volume to make the ternary blend. This DEE-ethanol-biodiesel blend was tested on the same engine under the same conditions. The experimental results exhibited that the DEE-ethanol-biodiesel ternary blend, BE15DE10, mitigated BTE by 8.89 % and the smoke, NO_x, and CO emissions by 15.66 %, 50.7 %, and 18.5 %, respectively, compared with neat biodiesel. The HC emission exhibited a slightly increasing trend. The results summarize the trade-off between smoke and NO_x reduction using DEE and ethanol oxygenated fuels. The addition of ethanol by 15 % and DEE up to 10 % by volume to biodiesel could be considered the most favorable blend without any significant modifications in the CI engine.

<https://doi.org/10.30501/jree.2022.328607.1330>

1. INTRODUCTION

A 'green' move to adopt alternative fuels over conventional petroleum-based fuels such as biodiesel, biogas, ethanol, methanol, DEE, DME, CNG, HCNG, LPG, LNG, hydrogen, propane, and P-series fuels are primarily preferred as an energy source for the transportation sector. Biofuels offer much potential on these frontiers as alternative energy [1, 2]. Vegetable oils fulfill the requirements of an alternative source of energy [3, 4]. Edible oils like Coconut oil, Rapeseed oil, Palm oil, Soyabean oil, Mustard oil, Sunflower oil, Waste cooking oil, and Rice bran oil can be used as biofuels. Also, non-edible oils like *Jatropha Curcas* oil, Castor oil, Karanja (*Pongamia Pinnata*) oil, Mahua oil, Canola oil, and Neem oil can be used as biofuels with minor modifications to automotive engines [5, 6].

Biodiesel is a clean alternative fuel produced from vegetable oils and animal fats considered safe and biodegradable [7, 8]. Biodiesel production from edible oil is not economical and non-edible seed like Karanja is less costly and widely available in India. Karanja trees can grow on non-agricultural lands with minimum care [9]. The seeds of Karanja contain

27-39 % of the oil and have the potential to be used as basic feedstock for biodiesel production [10, 11]. Hence, the oil can be easily converted into KOME biodiesel through transesterification or pyrolysis [12]. It can be used as a neat fuel in the CI engines or by blending with diesel fuel. Its reasonable cetane number, almost no sulfur, no aromatics, and about 10 % inherent oxygen reduce harmful emissions [13]. Compared to petroleum diesel, biodiesel suffers from higher viscosity, increased NO_x emission, and cold starting problems [14].

Ethanol (CH₃-CH₂-OH) is another promising renewable bio-based and highly oxygenated alternative fuel. Ethanol is derived from biomass by fermenting and distilling the crops. It is a clear, volatile, flammable, and colorless liquid. Its high oxygen content improves emission quality in CI engines and its high-octane level makes it suitable for SI engines. However, CI engine fuel suffers from low cetane value, no ignition features, and inadequate solubility in diesel fuel. In ambient conditions, ethanol blends readily with diesel fuel. At a temperature below 10 °C, ethanol separates from diesel fuel. On the other hand, ethanol and biodiesel can be easily mixed at any ratio and it forms a true solution [15]. The lower viscosity of ethanol than diesel is a concern for lubricity [16].

Diethyl ether (DEE) consists of two ethyl groups that are bonded to central oxygen specified by the chemical formula

*Corresponding Author's Email: krpatil@mmcoe.edu.in (K.R. Patil)
URL: https://www.jree.ir/article_154882.html



$\text{CH}_3\text{CH}_2\text{-O-CH}_2\text{CH}_3$. DEE has a low autoignition temperature, high cetane number, and high oxygen content. Its energy density, solubility with diesel, and broad flammability limits make it suitable for the CI engine [17, 18]. It appears as a clear colorless, volatile, highly inflammable liquid with an anesthetic odor [19]. DEE is safe because of its broad flammability and ease of handling as it remains liquid under ambient conditions [20, 21]. The acid ether synthesis process

is used to produce DEE on a large scale. The properties of test fuels are shown in Table 1.

The blending of oxygenated additives like ethanol or DEE with biodiesel enhances the oxygen percentage of the fuel-air mixture. Ethanol has the potential to reduce soot. While high ignition quality of DEE works as a co-solver and boosts the emission performance when blended with ethanol and KOME biodiesel.

Table 1. Properties of test fuels [22, 23]

Properties	Unit	DEE	Ethanol	KOME Biodiesel	Diesel
Chemical structure	-	$\text{CH}_3\text{CH}_2\text{-O-CH}_2\text{CH}_3$	$\text{CH}_3\text{-CH}_2\text{-OH}$	C_{12} to C_{22}	C_{10} to C_{25}
Oxygen content	mass %	21.6	34.7	10-12	0
Cetane number	-	>125	8	48-60	40-55
LCV	MJ/kg	33.8	26	38.3	34.9
Density at NTP	kg/m ³	713	785-789	875-885	815-860
Viscosity at NTP	cSt	0.23	1.2	1.9-6	2.4-4.1
Autoignition temp.	°C	160	420	-	316
Boiling point at 1 atm	°C	34.6	78	182-337	180-360
Stoichiometric A/F ratio	mass	11.1	9.06	13.8	14-14.7
Molecular weight	g/mol	74	46	-	-
Flammability limit in the air	vol %	3.4-18.6	4.3-19	-	7.6-1.4

2. EVALUATION OF BLENDED FUEL PROPERTIES

In this work, the used biodiesel was readily available Karanja Oil Methyl Ester (KOME) known by its local Indian name and its scientific name is *Pongamia Pinnata*. The commercial ethanol of analysis grade has 99.5 % purity and the analytical grade DEE has purity ≥ 99.5 % used in this research work. Different ratios of DEE and ethanol were added as supplementary oxygenated fuels to the base biodiesel fuel. Initially, 5 %, 10 %, 15 %, and 20 % volumes of ethanol were mixed with biodiesel and denoted by BE5, BE10, BE15, and BE20, respectively. The optimum blending ratio of the ethanol-biodiesel blend was found as BE15 considering various performance parameters of combustion and emissions of the test fuels. Then, for further investigation, the optimized

blend BE15 was mixed with 5 %, 10 %, 15 %, and 20 % DEE by volume to prepare the ternary blend and they are denoted by BE15DE5, BE15DE10, BE15DE15, and BE15DE20, respectively.

Initially, the solubility of both oxygenated fuels, DEE, and ethanol in the biodiesel was checked, which is the requirement for the stable working of the engine. It was observed that there was no phase separation for many days. This reveals that DEE and ethanol are completely miscible with biodiesel. Various instruments and standard methods used to measure fuel properties are shown in Table 2. As per the standard test method (IS 1448), the properties of test fuels were measured. The properties of test fuels are summarized in Table 3.

Table 2. Standard methods and instruments used to measure properties of blended fuels

Properties	ASTM method	Instrument used
Distillation profile	D86	Distillation apparatus
Higher calorific value	D240	Rajdhani make isothermal bomb calorimeter
Density	D941	Pyknometer, elect balance
Kinematic viscosity	D445	Stevis viscometer

Table 3. Properties of DEE-ethanol-KOME biodiesel blends

Properties/Abbreviations	Unit	Blend fuels							
		BE5	BE10	BE15	BE20	BE15DE5	BE15DE10	BE15DE15	BE15DE20
Oxygen content	mass %	12.07	13.26	14.36	15.64	14.49	15.52	16.02	17.68
HCV	MJ/kg	39.71	39.39	38.37	37.88	38.01	37.86	37.73	37.08
Density at NTP	kg/m ³	878	871.4	865	858.5	860.9	858.7	850.1	841.4
Viscosity at 40 °C	cSt	3.92	3.43	3.14	3.00	2.94	2.36	2.03	1.82

The boiling range characteristics of hydrocarbon fuels are studied by using distillation tests [24]. This study uses the ASTM D86 distillation test method for various ethanol-biodiesel blends. The distillation test results are shown in Figure 1. It is shown that the front-end volatility increases upon the addition of ethanol with biodiesel. The initial boiling point of biodiesel observed is 175 °C. The BE20 blend shows an IBP of 38 °C only. Although it reveals that increase in the ethanol concentration in biodiesel rises the front-end volatility. This effect improves the cold start condition. Consequently, it reduces exhaust emissions at a low load. A considerable change in the tail-end volatility of the ethanol-biodiesel blends was not observed. The studies carried out by Menezes et al. [20] reported similar results.

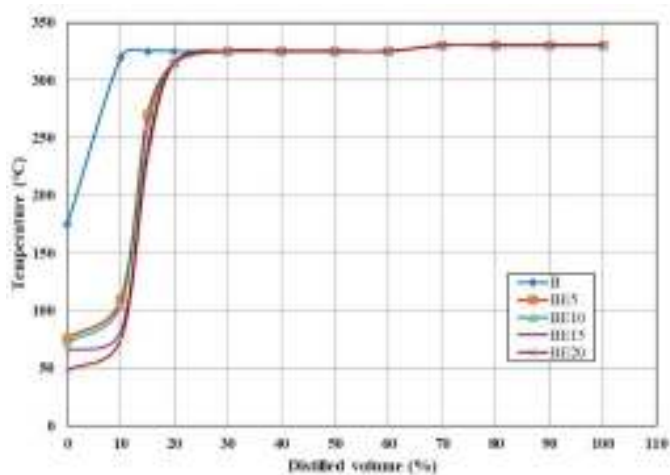


Figure 1. Distillation profile for ethanol-biodiesel blend

The laboratory tests show that the viscosity of the DEE-ethanol-biodiesel blends reduces upon increase in the concentration of ethanol and DEE in it. However, this decreased viscosity is greater than required for CI engines. It reveals that modifications of the fuel injection system are not required. The calorific value and density of DEE-ethanol-biodiesel blends are reduced because of the lower calorific value of ethanol and DEE than biodiesel. The inbound oxygen percentage of the fuel or various blends is an important factor in evaluating the properties of the fuel. It is observed that

adding ethanol and DEE increases the oxygen content of blends.

3. EXPERIMENTAL SETUP AND PROCEDURE

In this experimental investigation, the engine test rig was developed with necessary instruments for conducting the experimental tests at a constant speed of 1300 rpm in different brake load conditions. A single-cylinder, four-stroke cycle CI, direct injection, 3.5 kW, 17.5:1 CR, 661 CC engine was used. The engine specifications are tabulated in Table 4. This naturally aspirated, water-cooled, stationary engine is typically used for pump sets in agricultural applications. The injection timing was set to 29° BTDC. The eddy current dynamometer (400 kW) was used for loading the engine. The pressure inside the cylinder was monitored by a piezo sensor. The cooling water was measured using Rota-meter. The TDC and crank angle positions were observed by a Kuebler make crank angle encoder. The data acquisition system was used for collecting various inputs. The multi-gas analyzer, AVL Digas 444, was employed to measure CO, HC, and NO emissions. While the AVL 437 smoke meter was applied to measuring smoke opacity. The RTD and 'K' type thermocouples were used for various temperature measurements. The schematic diagram of the test engine is shown in Figure 2. The accuracies checked of measurement instruments are presented in Table 5.

Table 4. Test engine characteristics

Model	Kirloskar, TV1 Model
Brake power	3.7 kW @ 1300 rpm
Displacement	661 cm ³
Injection timing	29° BTDC
Intake air system	Naturally aspirated
Cylinders	Single cylinder
Comp. ratio	17.5:1
Inj. opening pressure	19.6 MPa
Type	Four-stroke cycle
Combustion System	Diesel direct injection

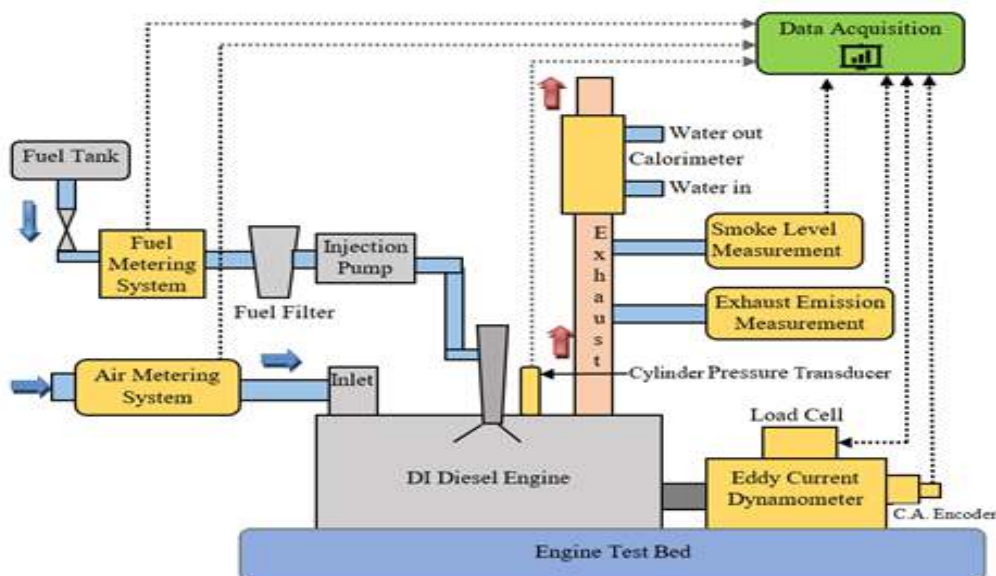


Figure 2. Schematic view of the test engine

Table 5. Accuracies of measurement parameters

Parameters	Measurement unit	Accuracy
Smoke opacity	%	± 1 % FSR
NO _x	ppm	± 1
CO	% vol	± 0.01 %
HC	ppm	± 1
CO ₂	% vol	± 0.1 %
Speed	rpm	± 0.5 % FSR
Temperature	°C	± 0.1 %
Mass fuel consumption	gm	± 0.01 %
Volumetric fuel consumption	ml	± 1 % FSR
Time	Sec	± 0.01 %
Density	kg/m ³	± 0.2
Calorific value	kJ/kg	± 0.15

The fuel samples were tested in various load conditions: no-load, 25 %, 50 %, 75 % of full load, and full load. These tests were carried out at a rated speed of 1300 rpm. Initially, the engine was run at no load for 30 mins to set in normal conditions. Every test was repeated at least three times for the accuracy of the results. The average values of combustion, performance, and emissions parameters were noted and analyzed.

4. RESULTS AND DISCUSSION

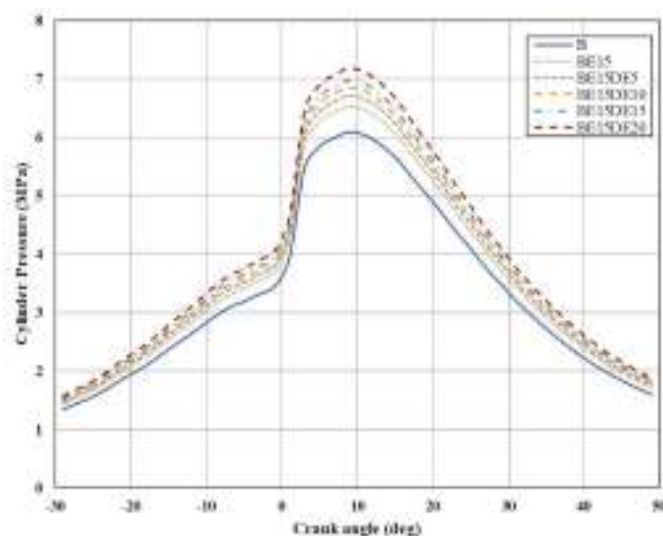
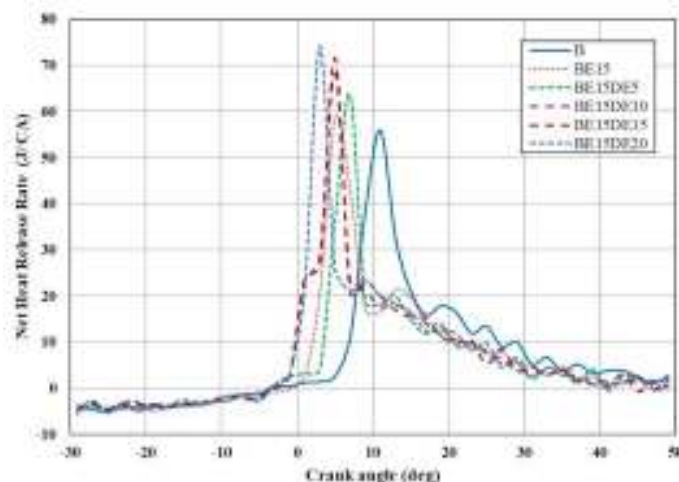
4.1. Combustion characteristics

The combustion in CI engine has two distinct phases of combustion viz. premixed and diffusion phase (mixing controlled) combustion. Once combustion starts, the fuel ignites immediately after injecting it into the cylinder and burns it at the diffusion combustion phase. It leads to a high heat release rate during premixed combustion than diffusion combustion [25]. The combustion characteristics of various DEE and ethanol blends with KOMBE biodiesel were monitored using in-cylinder pressure trace analysis under steady-state engine conditions. The prominent combustion behaviors such as cylinder pressure and heat release rate were observed at full load; hence, in this condition, the combustion characteristics have been analyzed.

The cylinder pressure for different DEE-ethanol-biodiesel blends is given in Figure 3. The results show that the ignition delay is extended with ethanol-biodiesel blends. This may be because of a reduction in cetane value, increased heat of evaporation, and a high level of auto-ignition temperature. Xin-Cai et al. [26] argued that in the ethanol-biodiesel blend, the biodiesel fuel burns first and then, it ignites the surrounding ethanol. The rise in peak pressure is observed because of an increase in fuel combustion at the premixed combustion phase. One can observe that the peak pressure attained for all the DEE-ethanol-biodiesel blends is moving away from TDC. It can be because of the effect of elongation in ignition delay and retardation of the start of combustion.

The net heat release rate for DEE-ethanol-biodiesel blends is shown in Figure 4. It shows that high HRR at the end of combustion leads to a longer duration of HRR. This is because of the elongated ignition delay of ethanol-biodiesel blends. The combustion start was observed with delay for all DEE blends and with an increase in DEE percentage, it turned into a prominent one. The increase in HRR for the diffusion

combustion phase is observed because of oxidation resulting from oxygen concentration in the blends [27].

**Figure 3.** Cylinder pressure variations for DEE-ethanol-biodiesel blends**Figure 4.** Net HRR variations for DEE-ethanol-biodiesel blends

4.2. Performance characteristics

The brake thermal efficiency assesses the fuel energy conversion efficiency into brake power. The other parameters like BSFC and BSEC have not been discussed in this work because they do not show different results from BTE.

The results of the BTE of ethanol-biodiesel are shown in Figure 5. The BTE increases with the addition of ethanol to biodiesel. The maximum BTE is observed for 15 % ethanol blending with biodiesel (BE15), especially in full-load conditions. This BE15 optimum blend is selected as a base fuel for the second step of the tests. Then, DEE is added to the BE15 blend in different proportions. The BTE for the DEE-ethanol-biodiesel blend is presented in Figure 6. The blending of DEE percentage of more than 15 % in BE15 blends shows the reduction in BTE near full load. The BE15DE10 blend shows maximum BTE than other blends at full load. This improvement in BTE results from fuel-bound oxygen concentration, particularly in the fuel-rich zone [28]. The erratic operation was observed in engine operation when more than 15 % DEE was added to the BE15 blend, thereby affecting the engine performance. It is observed that the BTE

of BE15DE10 blend has increased by 8.9 % more than the neat biodiesel fuel.

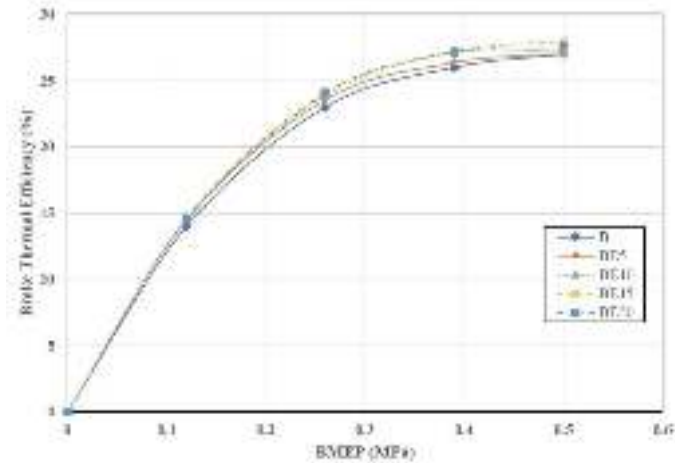


Figure 5. BTE for ethanol-biodiesel blends

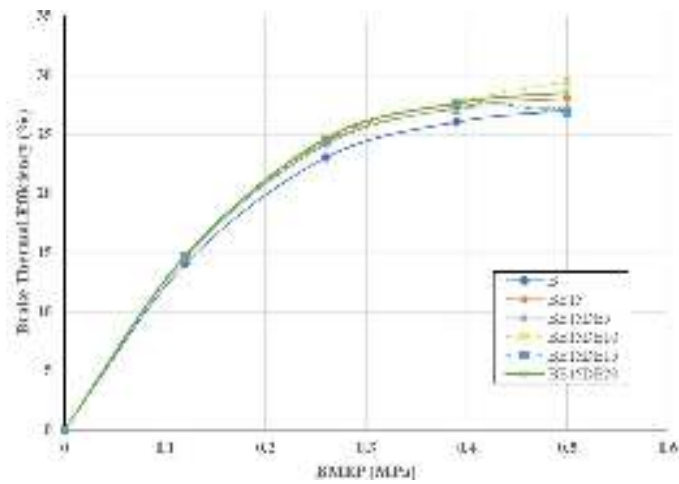


Figure 6. BTE for DEE-ethanol-biodiesel blends

4.3. Emission characteristics

The fuel ignition quality, proper mixing of air and fuel during ignition delay, and residence time lead to the burning of uneven air/fuel mixtures during combustion, and expansion processes have a significant impact on emission formation in diesel or biodiesel engines [25].

4.3.1. Smoke emission

The results of smoke for ethanol-biodiesel blends are given in Figure 7. It exhibits the trend of reduction in smoke by blending ethanol with biodiesel. The fuel-bound oxygen content in ethanol improves combustion quality, especially in diffusion combustion, which improves smoke emission [29]. At low load, the ethanol blends exhibit minor effect on smoke emission. It is because of the engine running at the overall lean mixture and the low flame temperature of the ethanol-biodiesel blends. Overall, the BE15 blend is the optimum blend and shows a smoke reduction of 13.8 % relative to biodiesel fuel.

The effect of DEE blending with BE15 on smoke is shown in Figure 8. The smoke emission reduction with DEE-ethanol-biodiesel blends is not as much as expected. On the other hand, when more than 15 % DEE is added to the BE15 base fuel, a minor increase in smoke emission is observed which

may result from erratic combustion, as discussed before. The findings reported by Anand et al. [30] are in line with these results. The DEE-ethanol-biodiesel ternary blends reduced 15.66 % smoke emissions on average, compared to neat biodiesel. The reduction in smoke may be because of the presence of inherent oxygen of DEE and ethanol in the fuel reach zone, which assists the engine to run leaner. The BE15DE15 blend exhibits the lowest smoke emissions overall and at full load condition as compared to other blends.

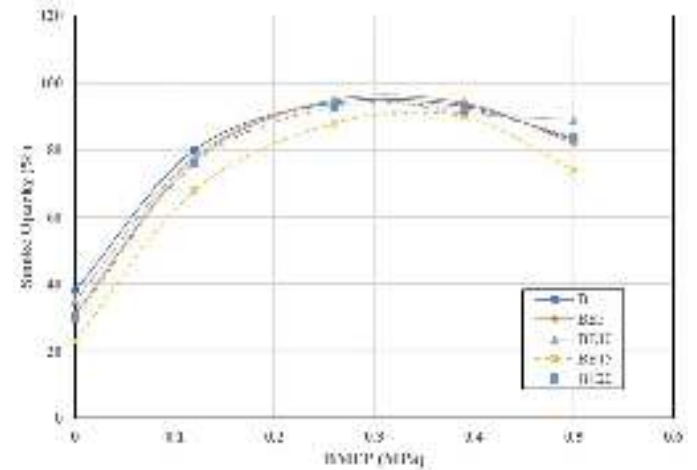


Figure 7. Smoke emission for ethanol-biodiesel blends

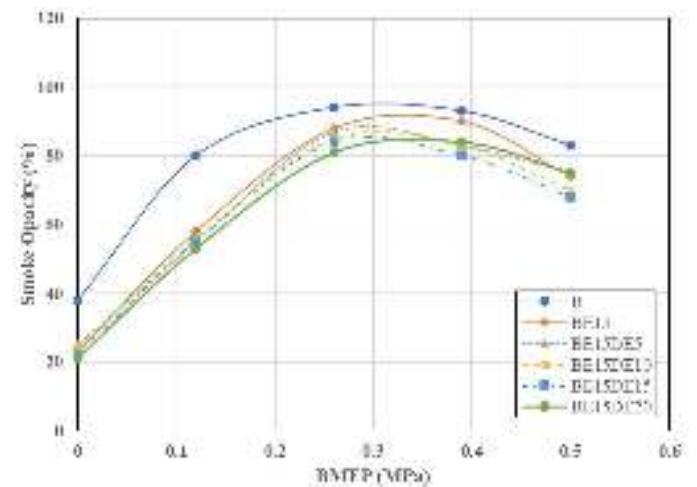


Figure 8. Smoke emission for DEE-ethanol-biodiesel blends

4.3.2. NOx emissions

The NOx produced in diesel or biodiesel engines is proportional to combustion efficiency. The results of NOx emissions of ethanol-biodiesel blends are presented in Figure 9. At high loads, when compared with biodiesel, the NOx emissions exhibit a prominent reduction. The ethanol addition to biodiesel reduces the viscosity and density of blends. Consequently, it retards the dynamic injection timing of the blends. Moreover, as discussed before, it leads to low combustion temperature because of the high evaporation rate of ethanol. These two factors cause a reduction in NOx emissions. It is seen that the NOx emission at lower ethanol ratios is not significant due to the poor ignition quality of ethanol. Overall, the studies reveal that the BE15 blend has the lowest NOx emission at high load.

Further, the DEE blended with the optimum selected blend BE15 and findings are presented in Figure 10. It can be said that there are further reductions in NOx emissions due to

blending in the presence of DEE in the blends. The experimental results exhibit that DEE-ethanol-biodiesel ternary blends reduce 50.7 % NO_x emissions on average as compared to neat biodiesel. As it is evident, the inherent oxygen of the fuels plays a more active role in the reduction of NO_x emission than the oxygen provided by air [31]. The BE15DE20 blend exhibits the lowest NO_x emissions and in full-load conditions. A reduction in NO_x emission level results from the joint effect of the engine running leaner as well as the lower combustion temperature and reaction time. It is to be noted that the mixture of DEE-diesel blends is effectively leaner with respect to the corresponding neat diesel fuel.

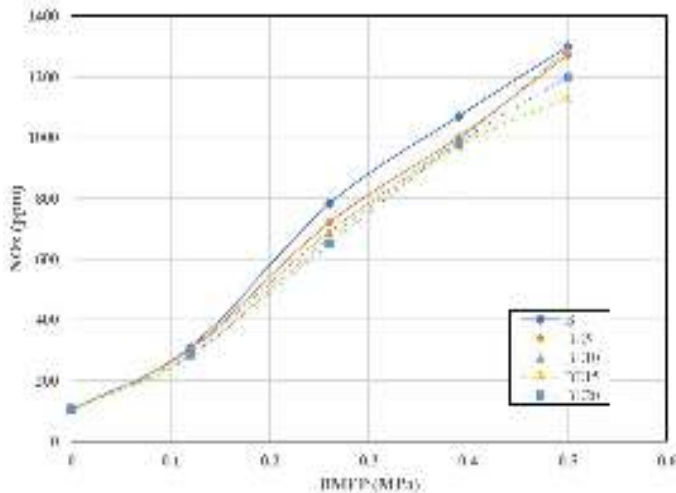


Figure 9. NO_x emissions for ethanol-biodiesel blends

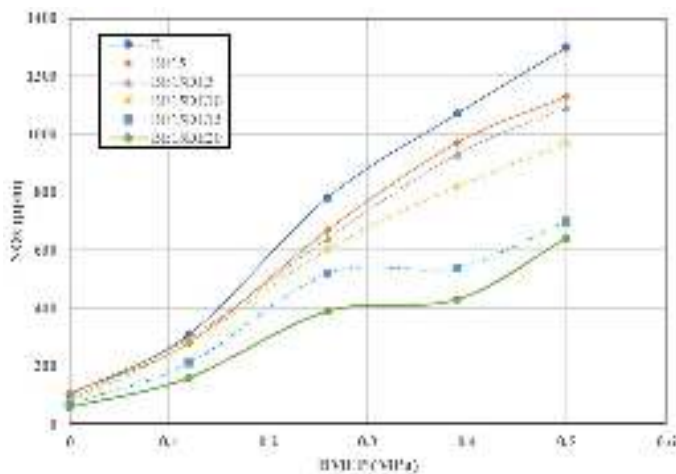


Figure 10. NO_x emissions for DEE-ethanol-biodiesel blends

4.3.3. CO emission

The effect of ethanol-biodiesel blends on CO emission is given in Figure 11. The results reveal that the CO emitted by all ethanol-biodiesel blends increased at low loads except for the BE20 blend. At lower loads, the incomplete combustion of the blended fuels increases the CO emission. However, a substantial reduction in the CO emission is observed at full load for all the blends. This effect results from the increase in oxygen concentration of the blends that encourages the additional oxidation of the CO emission during the engine expansion process [32, 33].

The CO emission for the DEE-ethanol-biodiesel blend is presented in Figure 12. Overall, the blend BE15DE10 exhibits

further reductions in the CO emission at high load. The experimental investigation exhibits that the CO emission of DEE-ethanol-biodiesel ternary blends is reduced by 18.5 %, compared to neat biodiesel. This effect is attributed to the reduction in density and viscosity of the DEE-ethanol-biodiesel blends and improvement in the start of injection and ignition timing because of the presence of DEE in the blends.

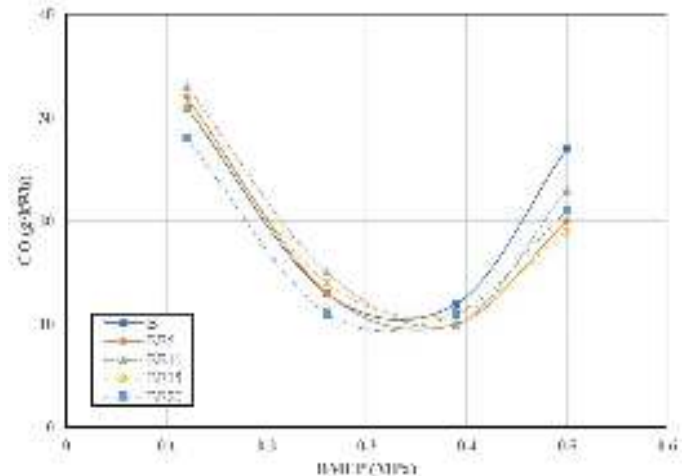


Figure 11. CO emission for ethanol-biodiesel blends

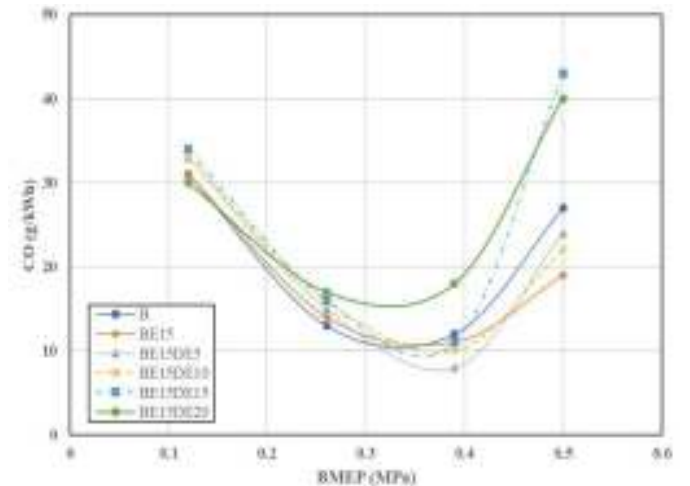


Figure 12. CO emission for DEE-ethanol-biodiesel blends

4.3.4. HC emission

The HC emission for ethanol-biodiesel blends is given in Figure 13. The studies reveal that the HC emission of ethanol-biodiesel blends is increased compared to the biodiesel fuel. Also, the rise in HC emission is observed as the concentration of ethanol in the blend increases. The considerable rise is displayed by HC emission at low loads and it increases moderately at high loads.

The HC emission for DEE-ethanol-biodiesel blends is shown in Figure 14. The outcomes of DEE-ethanol-biodiesel blends reveal that there is a rise in the HC emission for all blends, compared to the BE15 base fuel. At full load, the blend BE15DE10 exhibits the lowest level of HC emission among other DEE-ethanol-biodiesel blends. The HC emission is increased mainly because of higher heat of evaporation of the DEE-ethanol-biodiesel blends causing slower evaporation, which causes poor fuel-air mixing, flame quenching, and the increase of 'lean outer flame zone' where the flame is unable to exist [2].

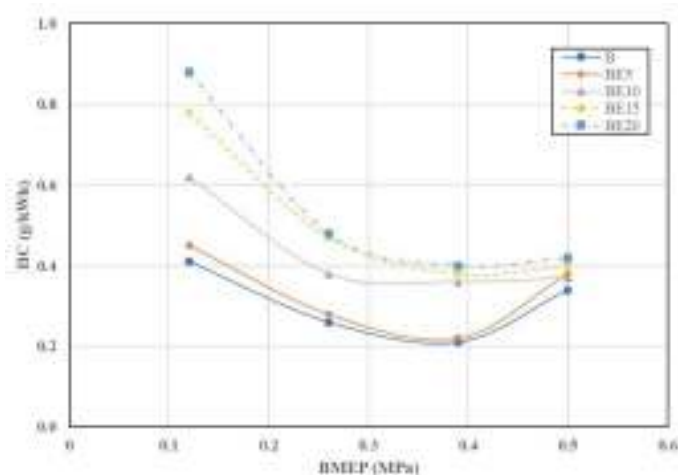


Figure 13. HC emission for Ethanol-Biodiesel blends

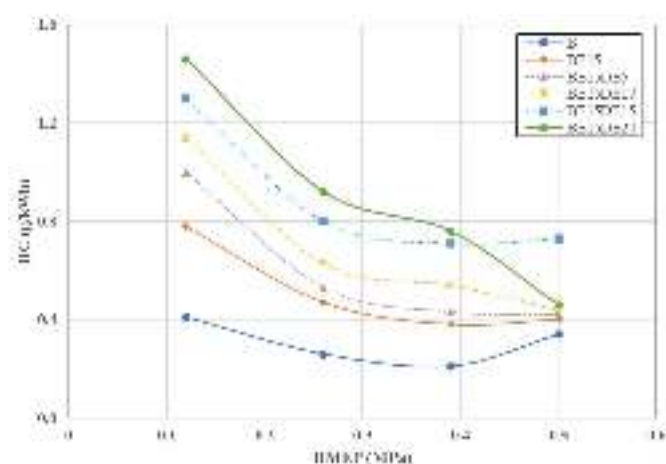


Figure 14. HC emission for DEE blends with BE15

5. CONCLUSIONS

The blending of oxygenated DEE and ethanol into biodiesel changes the physicochemical properties of the blends. The laboratory tests showed that DEE and ethanol remained completely soluble in biodiesel at any ratio. The experimental investigation revealed that the blending of DEE and ethanol with biodiesel up to 20 % by volume was possible. The DEE-ethanol-biodiesel blends resulted in a decrease in density, kinematic viscosity, and higher heating value, whereas the cetane value and oxygen concentration increased. The front-end volatility increased, while the boiling point of ternary blends was reduced compared to neat biodiesel because of the presence of DEE and ethanol. The combustion studies pointed to the increase in ignition delay, peak pressure, and peak HRR of the DEE-ethanol-biodiesel blends. The BE15DE10 ternary blend exhibited an increase in Brake Thermal Efficiency by 8.89 %, reduction in smoke by 15.66 %, drop in NO_x by 50.7 %, and decrease in CO emission by 18.5 %, as compared with neat KOME biodiesel. At full load, it exhibited the lowest level of HC emission compared to other DEE-ethanol-biodiesel blends. These results of BE15DE10 are optimum as compared to other blends. Overall, the trade-off between smoke and NO_x of biodiesel engines shows a reduction by blending DEE and ethanol with KOME biodiesel fuel. Thus, the BE15DE10 blend is recommended as the optimum blend without significant engine alterations.

6. ACKNOWLEDGEMENT

The author is grateful to Marathwada Mitramandal's College of Engineering Pune for providing the engine test facility; VIT, Pune for extending the equipment support; ARAI and Chem-Tech Labs for providing the fuel test facility.

NOMENCLATURE

ASTM	American Society for Testing and Materials
BMEP	Brake Mean Effective Pressure
BTDC	Before Top Dead Centre
BTE	Brake Thermal Efficiency
CA	Crank Angle
CI	Compression-Ignition
CNG	Compressed Natural Gas
CO	Carbon Monoxide
DI	Direct Injection
DEE	Diethyl Ether
DME	Dimethyl Ether
HC	Hydrocarbon
HCNG	Hydrogen CNG
HCV	Higher Calorific Value
HRR	Heat Release Rate
IS	Indian Standards
KOME	Karanja Oil Methyl Ester
LNG	Liquified Natural Gas
LPG	Liquified Petroleum Gas
NO	Nitric Oxide
NO _x	Oxides of Nitrogen
NTP	Normal Temp. and Pressure
PM	Particulate Matter
RTD	Resistance Temp. Detector
SI	Spark Ignition

REFERENCES

- Ibrahim, A., "Investigating the effect of using diethyl ether as a fuel additive on diesel engine performance and combustion", *Applied Thermal Engineering*, Vol. 107, (2016), 853-862. (<http://doi.org/10.1016/j.applthermaleng.2016.07.061>).
- Patil, K.R. and Thipse, S.S., "Experimental investigation of CI engine combustion, performance and emissions in DEE-kerosene-diesel blends of high DEE concentration", *Energy Conversion and Management*, Vol. 89, (2015), 396-408. (<http://doi.org/10.1016/j.enconman.2014.10.022>).
- Hariram, V., Seralathan, S., Paulson, V., Prakash, R. and Premkumar, T.M., "Production of biodiesel from eucalyptus tereticornis and its effect on combustion, performance and emission characteristics of a CI engine", *International Journal of Vehicle Structures and Systems*, Vol. 10, No. 6, (2018), 443-452. (<https://doi.org/10.4273/ijvss.10.6.13>).
- Kaimal, V.K. and Vijayabalan, P., "An investigation on the effects of using DEE additive in a DI diesel engine fuelled with waste plastic oil", *Fuel*, Vol. 180, (2016), 90-96. (<http://doi.org/10.1016/j.fuel.2016.04.030>).
- Patil, K.R. and Thipse, S.S., "Characteristics of performance and emissions in direct injection diesel engine fuelled with kerosene/diesel blends", *International Journal of Automotive & Mechanical Engineering*, Vol. 10, (2014), 2102-2111. (<http://doi.org/10.15282/ijame.10.2014.26.0177>).
- Oyegoke, T., Obadiah, E., Adah, F., Oguche, J.E., Timothy, G.T., Mantu, I.A. and Ado, A.D., "Trends of progress in setting up biorefineries in developing countries: A review of bioethanol exploration in Nigeria", *Journal of Renewable Energy and Environment (JREE)*, Vol. 9, No. 1, (2022), 37-52. (<https://doi.org/10.30501/jree.2021.278037.1197>).
- Rakopoulos, D.C., Rakopoulos, C.D., Giakoumis, E.G., Papagiannakis, R.G. and Kyritsis, D.C., "Influence of properties of various common bio-fuels on the combustion and emission characteristics of high-speed DI (direct injection) diesel engine: Vegetable oil, bio-diesel, ethanol, n-butanol, diethyl ether", *Energy*, Vol. 73, (2014), 354-366. (<https://doi.org/10.1016/j.ENERGY.2014.06.032>).
- Gharibian, M., Hosseinzadeh, S.B., Shimeshan, A.R. and Rostami, S., "Investigation and ranking of the effect of biodiesel produced from

- safflower oil by the hydrodynamic method in diesel generator engine using TOPSIS method", *Journal of Renewable Energy and Environment (JREE)*, Vol. 9, No. 1, (2022), 13-22. (<https://doi.org/10.30501/jree.2021.272074.1186>).
9. Patel, R.L. and Sankhavara, C.D., "Biodiesel production from karanja oil and its use in diesel engine: A review", *Renewable and Sustainable Energy Reviews*, Vol. 71, (2017), 464-474. (<https://doi.org/10.1016/j.rser.2016.12.075>).
 10. Naveen, S., Kannappan, P.G., Rajagopal, M., Jayaraman, R.S., Krishnan, A. and Jayaseelan, A., "A solar reactor for bio-diesel production from Pongamia oil: Studies on transesterification process parameters and energy efficiency", *Chinese Journal of Chemical Engineering*, Vol. 40, (2021), 218-224. (<https://doi.org/10.1016/j.cjche.2020.10.010>).
 11. Dhar, A. and Agarwal, A.K., "Performance, emissions and combustion characteristics of karanja biodiesel in a transportation engine", *Fuel*, Vol. 119, (2014), 70-80. (<https://doi.org/10.1016/j.fuel.2013.11.002>).
 12. Thangaraj, S. and Govindan, N., "Evaluating combustion, performance and emission characteristics of diesel engine using karanja oil methyl ester biodiesel blends enriched with HHO gas", *International Journal of Hydrogen Energy*, Vol. 43, No. 12, (2018) 6443-6455. (<https://doi.org/10.1016/j.ijhydene.2018.02.036>).
 13. Liaquata, A.M., "Application of blend fuels in a diesel engine", *Energy Procedia*, Vol. 14, (2012), 1124-1133. (<https://doi.org/10.1016/j.egypro.2011.12.1065>).
 14. Chang, Y., Lee, W., Wu, T., Wu, C. and Chen S., "Use of water containing acetone-butanol-ethanol for NOx-PM (nitrogen oxide-particulate matter) trade-off in the diesel engine fueled with biodiesel", *Energy*, Vol. 64, (2014), 678-687. (<https://doi.org/10.1016/j.energy.2013.10.077>).
 15. Agarwal, A.K., "Biofuels (alcohols and biodiesel) applications as fuels for internal combustion engines", *Progress in Energy and Combustion Science*, Vol. 33, (2007), 233-271. (<https://doi.org/10.1016/j.peccs.2006.08.003>).
 16. Nigam, P.S. and Singh, A., "Production of liquid biofuels from renewable resources", *Progress in Energy and Combustion Science*, Vol. 37, (2011), 52-68. (<https://doi.org/10.1016/j.peccs.2010.01.003>).
 17. Patil, K.R. and Thipse, S.S., "Characterisation of the key fuel properties of oxygenated diethyl ether-diesel blends", *Applied Mechanics and Materials*, Vol. 612, (2014), 175-180. (<http://doi.org.10.4028/www.scientific.net/AMM.612.175>).
 18. Bailey, B., Guguen, S. and Erwin J., "Diethyl ether (DEE) as a renewable fuel", *SAE Paper*, (1997), 972978. (<https://doi.org/10.4271/972978>).
 19. Patil, K.R. and Thipse, S.S., "Effect of injection timing on performance and emissions of direct injection CI engine running on diethyl ether-diesel blends", *International Journal of Automotive & Mechanical Engineering*, Vol. 13, No. 3, (2016), 3773-3787. (<https://doi.org/10.15282/ijame.13.3.2016.19.0309>).
 20. Menezes, E.W.D., Silva, R.D., Cataluna, R. and Ortega, R.J.C., "Effect of ethers and ether/ethanol additives on the physicochemical properties of diesel fuel and on engine tests", *Fuel*, Vol. 85, (2006), 815-822. (<https://doi.org/10.1016/j.fuel.2005.08.027>).
 21. Ortiz, Y., Sanchez, Florez E.G. and Mesa, D.H., "Analysis of the influence of droplet breakup time using kelvin-helmholtz model, on the diesel spray formation, evaporation and combustion", *International Journal of Automotive & Mechanical Engineering*, Vol. 18, No. 4, (2021), 9271-9283. (<https://doi.org/10.15282/ijame.18.4.2021.10.0713>).
 22. Patil, K.R., Thipse, S.S. and Warke, A., "Effect of oxygenate and cetane improver on performance and emissions of diesel engine fuelled with diethyl ether-diesel blends", *SAE Technical Papers*, Vol. 26, (2015), 0057. (<http://doi.org.10.4271/2015-26-0057>).
 23. Masoud, I., Subrahmanyam, J.P. and Babu M.K.G., "Potential of diethyl ether as supplementary fuel to improve combustion and emission characteristics of diesel engines", *SAE Technical Papers*, Vol. 28, (2008), 0044. (<https://doi.org/10.4271/2008-01-1805>).
 24. Gonca, G., "Investigation of the effects of steam injection on performance and NO emissions of a diesel engine running with ethanol-diesel blend", *Energy Conversion and Management*, Vol. 77, (2014), 450-457. (<http://doi.org.10.1016/j.enconman.2013.09.031>).
 25. Heywood, J.B., *Internal combustion engine fundamentals*, McGraw-Hill, New York, N.Y., (1988).
 26. Xing-cai, L., Jian-guang, Y., Wu-gao, Z. and Zhen, H., "Effect of cetane number improver on heat release rate and emissions of high-speed diesel engine fueled with ethanol-diesel blend fuel", *Fuel*, Vol. 83, (2004), 2013-2020. (<http://doi.org.10.1016/j.fuel.2004.05.003>).
 27. Rakopoulos, D.C., Rakopoulos, C.D., Giakoumis, E.G. and Dimaratos, A.M., "Characteristics of performance and emissions in high-speed direct injection diesel engine fueled with diethyl ether/diesel fuel blends", *Energy*, Vol. 43, No. 1, (2012), 214-224. (<http://doi.org.10.1016/j.energy.2012.04.039>).
 28. Rakopoulos, D.C., Rakopoulos, C.D., Giakoumis, E.G. and Dimaratos, A.M., "Studying combustion and cyclic irregularity of diethyl ether as supplement fuel in diesel engine", *Fuel*, Vol. 109, (2013), 325-335. (<http://doi.org.10.1016/j.fuel.2013.01.012>).
 29. Ali, O.M., Mamat, R., Masjuki, H.H. and Abdullah, A.A., "Analysis of blended fuel properties and cycle-to-cycle variation in a diesel engine with a diethyl ether additive", *Energy Conversion and Management*, Vol. 108, (2016), 511-519. (<http://doi.org.10.1016/j.enconman.2015.11.035>).
 30. Anand, R. and Mahalakshmi, N.V., "Simultaneous reduction of NOx and smoke from a direct-injection diesel engine with exhaust gas recirculation and diethyl ether", *Proceedings of Institution of Mechanical Engineers, Part D: Journal of Automobile Engineering*, (2007), 221. (<https://doi.org/10.1243%2F09544070JAUTO258>).
 31. Gorski, K. and Przedlacki, M., "Evaluation of the influence of diethyl ether (DEE) addition on selected physicochemical properties of diesel oil and ignition delay period", *Energy & Fuels*, Vol. 28, No. 4, (2014), 2608-2616. (<http://doi.org.10.1021/ef4025036>).
 32. Kowalewicz, A., "Eco-diesel engine fuelled with rapeseed oil methyl ester and ethanol, Part 1: Efficiency and emission", *Proceedings of Institution of Mechanical Engineers, Part D: Journal of Automobile Engineering*, Vol. 219, (2005). (<https://doi.org/10.1243%2F09544070JAUTO218>).
 33. Rakopoulos, C.D., Antonopoulos, K.A. and Rakopoulos, D.C., "Multi-zone modeling of diesel engine fuel spray development with vegetable oil, bio-diesel or diesel fuels", *Energy Conversion Management*, Vol. 47, (2006), 1550-1573. (<https://doi.org/10.1016/j.enconman.2005.08.005>).



Research Article

Optimal Location and Sizing of Wind Turbines and Photovoltaic Cells in the Grid for Load Supply Using Improved Genetic Algorithm

Ming Hung Lin^a, Jiun Hung Lin^b, Mamdouh El Haj Assad^{c*}, Reza Alayi^{d,e*}, Seyed Reza Seyednouri^f

^a Department of Electrical Engineering, Cheng Shiu University, 83347, Kaohsiung City, Taiwan, China.

^b College of Electrical Engineering and Computer Science, National Kaohsiung University of Science and Technology, 811, Kaohsiung City, Taiwan, China.

^c Department of Sustainable and Renewable Energy Engineering, University of Sharjah, P. O. Box: 27272, Sharjah, United Arab Emirates.

^d Department of Mechanics, Germe Branch, Islamic Azad University, P. O. Box: 5651763764, Germe, Ardabil, Iran.

^e Energy Research Center, Shahrekord Branch, Islamic Azad University, Shahrekord, Chaharmahal and Bakhtiari, Iran.

^f Young Researchers and Elite Club, Germe Branch, Islamic Azad University, P. O. Box: 5651763764, Germe, Ardabil, Iran.

PAPER INFO

Paper History:

Received: 30 January 2022

Revised: 19 June 2022

Accepted: 23 June 2022

Keywords:

Optimal Placement,
Improved Genetic Algorithm,
Distributed Production,
Loss Reduction,
Combined System

ABSTRACT

The optimal combination of distributed generation units in recent years has been designed to improve the reliability of distributed generation systems as well as to reduce losses in electrical distribution systems. In this research, the improved Genetic Algorithm has been proposed as a powerful optimization algorithm for optimizing problem variables. The objective function of this paper includes power loss reduction, hybrid system reliability, voltage profile, optimal size of distributed generation unit, and finally improvement of the construction cost of combined wind and solar power plants. Therefore, the problem variables are subject to reliable load supply and the lowest possible cost during the optimization process. In order to achieve this goal in this study, the IEEE standard 30-bus network is examined. The results of the system simulation show the reduction of total system losses after DG installation compared to the state without DG and the improvement of other variable values in this network. This loss index after installing DG in the desired bus has a reduction of about 200 kWh during the year and has a value equal to 126.42 kWh per year.

<https://doi.org/10.30501/jree.2022.327250.1321>

1. INTRODUCTION

Studies have shown that more than 70 % of the total power system losses are related to distribution networks, being more than 13 % of the total production capacity [1-3]. These electrical losses can be reduced by installing and controlling dispersed production devices. The use of distributed generation is widely used in distribution networks, the advantages of which include voltage regulation, loss reduction, power factor correction, and system capacity liberalization [4-6]. In order to determine the location, number, size, type, and control plan of distributed generation over a period of one to ten years, a complex optimization problem with conflicting objectives such as minimizing the cost of purchasing and installing distributed generation and reducing electrical losses can be addressed [7-9]. Since the 1960s, several methods have been proposed in this field. These methods can be divided into four groups: analytical, numerical programming, innovative methods, and artificial intelligence methods. Most of the research studies presented

in this field have not considered a number of important aspects such as considering distributed generation in a discrete way with real prices and quantities available in the market [10-12], considering unbalanced load and network [13-15], presence of harmonic currents and voltages due to extensive use of harmonic generating loads and electronic power devices [16-18], reaction and coupling between harmonic voltages and currents created by nonlinear loads [19-21], increase of harmonic currents due to intensification [22-24], and IEEE power quality constraints [25, 26]. Power plants are used as distributed generation in distribution networks.

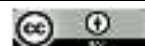
The main purpose of this research is to determine the location and optimal capacity of distributed generation units by considering these five objectives: reducing losses, improving voltage profile, improving system reliability, the optimal size of DG unit, and reducing the construction cost of combined wind and solar power plants. Each of these individual goals has been transformed into a single-objective function using weighting coefficients. These coefficients are determined using the AHP method and applied to the objective function of the problem.

2. MATERIAL AND METHOD

*Corresponding Authors' Email: massad@sharjah.ac.ae (M. El Haj Assad)

and reza_alayi@iaugermi.ac.ir (R. Alayi)

URL: https://www.jree.ir/article_155023.html



2.1. Case study

The intermittent behavior of the intensity of solar radiation has caused solar power plants to not have continuous and controllable characteristics. Wind power plants also do not have a uniform characteristic due to intermittent wind intensity. In this paper, in order to achieve uniform energy from renewable sources, a combination of wind and solar units is used. From the point of view of the power system, a solar power plant, which can include several photovoltaic panels with different capacities, is one of the sources of uncertainty in the system. In system studies in the presence of wind and solar power plants, their output power must first be determined. The output power of the combined wind and solar power plant depends on the intensity of the sun radiation and the intensity of the wind in the installation area. Therefore, the intensity of sunlight and wind in the study area must be

calculated and then, the solar and wind panel model must be determined. The studies of this paper are based on the data of solar radiation intensity and wind, which are the daily average of the New Energy Organization of Iran (SANA) for the Meshkinshahr region located in northwestern Iran, and the data has been applied in system simulation. Graphs related to the intensity of solar radiation and wind intensity in the study area can be seen in Figures 1 and 2, respectively.

Among the important issues that should be considered in the optimal placement of distributed generation sources in the distribution network is the existence of an unbalanced network and load and the effect of nonlinear and harmonic loads. Such network load is unbalanced. Therefore, it is necessary to optimize the house by considering the unbalanced load condition. This issue has not been considered in most of the research methods.

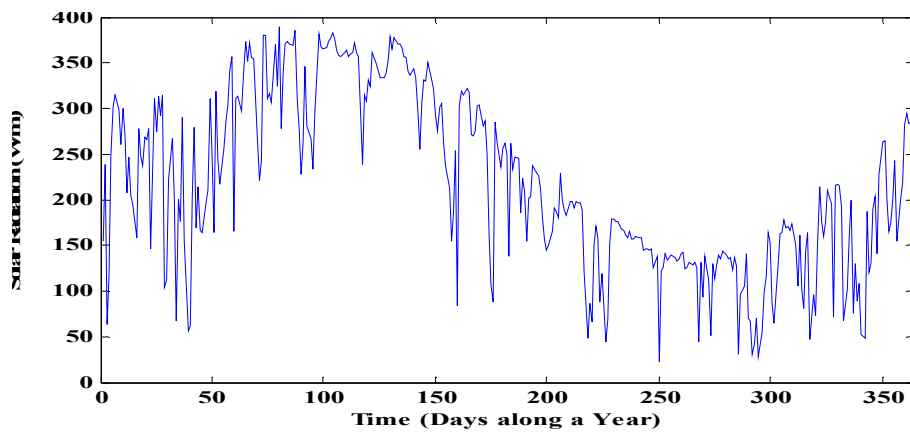


Figure 1. Intensity of solar radiation throughout the year for Meshginshahr

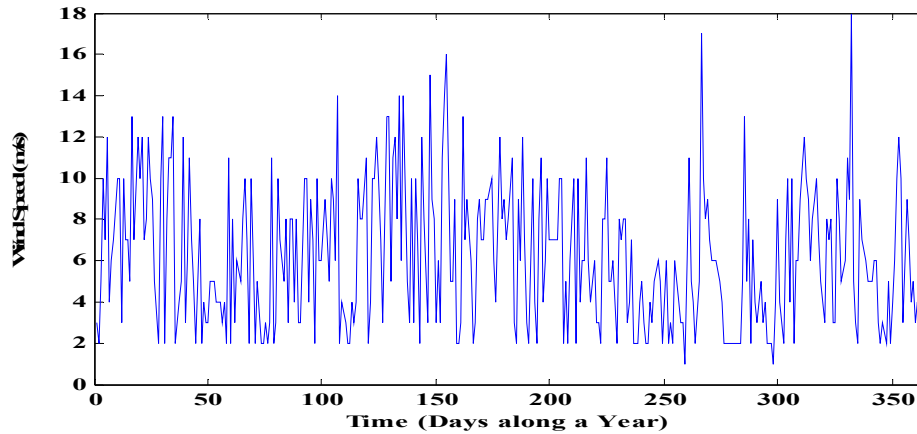


Figure 2. Intensity of wind speed throughout the year for Meshginshahr

2.2. System model in harmonic frequencies

At harmonic frequencies, accurate models are available for distribution lines and parallel capacitors. However, the exact harmonic model of the power supply system, distribution lines, transformer stations, and linearity and non-linearity is not available. If the skin effect is ignored, the capacitor and the lines can be shown as follows in the n^{th} harmonic [27, 28].

$$y_c^n = ny_c^1 \quad (1)$$

$$y_{i,i+1}^n = (R_{i,i+1} + jnX_{i,i+1}) \quad (2)$$

where $R_{i,i+1}$ and $X_{i,i+1}$ show the values of the position and reactance of the line between the i and $i + 1$ buses, respectively. Power sources and transformers are usually denoted by short-circuit admittances, y_c^n and y_c^1 , and entering the scale of harmonics. With respect to linear loads, a general resistance model parallel to the inductor is used to show the active and reactive powers at the main frequency. If only (w_i-1) which is the share of linear loads in the i th bus is assumed, the load admittance at the k th level is expressed as follows:

$$y_a^n = \frac{1 - w_i}{|V_a^2|} (P_a - j\frac{Q_a}{n}) \quad (3)$$

Nonlinear loads are also usually considered as ideal current sources. Composite loads are modeled as an impedance (linear load share) parallel to a current source (nonlinear load share). It should be noted that under harmonic conditions, there are negative and zero sequence components of the current even in the balanced networks. In addition, the multiples of three all appear in zero sequences; thus, a fundamental factor in voltages and multiples includes a three-fold approach connecting capacitive banks, transformers, and loads.

2.3. Network modeling in the presence of harmonics

The distribution network is modeled by considering the harmonic in the form of a single-line diagram shown in Figure 3. The distribution of the harmonic load after modeling the system is described below.

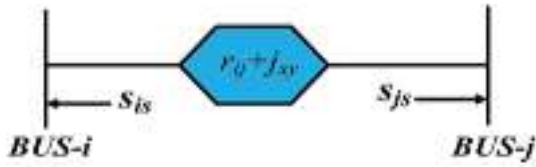


Figure 3. Single-line diagram of a feeder in a distribution network

Modeling a feeder is done according to the following steps:

- 1) The amplitude and angle of the voltage phase of each bus are obtained using the Backward/Forward Sweep Power Flow Method and based on the results, the resulting network losses are calculated.
- 2) At high frequencies, the power system is modeled as a combination of current sources and passive elements, because the admittance of system components changes with a harmonic order change. The admittance matrix must be modified in each harmonic order.
- 3) Linear loads are modeled as resistance and parallel reactance. Nonlinear loads are considered as current sources; thus, the harmonic current injected by the nonlinear loads in the i th bus is calculated according to Equation (4), and the index $C(h)$ in each harmonic order is based on Fourier analysis.

$$\begin{bmatrix} V_1^k \\ V_2^k \\ \vdots \\ V_{n-1}^k \\ V_n^k \end{bmatrix} = \begin{bmatrix} Y_{11}^k & Y_{12}^k & 0 \\ Y_{21}^k & Y_{22}^k & \vdots \\ \vdots & \vdots & \vdots \\ 0 & 0 & Y_{m-1,m-1}^k & Y_{m-1,m}^k \\ 0 & 0 & Y_{m,m-1}^k & Y_{m,m}^k \end{bmatrix}^{-1} \begin{bmatrix} I_1^k \\ I_2^k \\ \vdots \\ I_{n-1}^k \\ I_n^k \end{bmatrix} \quad (4)$$

$$I_i^k = \left[\frac{P_{hi} + jQ_{hi}}{V_{i1}} \right]^n \quad (5)$$

$$I_i^h = C(h)I_i^k \quad (6)$$

- 4) The effective value of voltage at bus i is calculated by Equation 7 as follows:

$$|V_i| = \sqrt{\sum_{h=1}^H |V_i^h|^2} \quad (7)$$

where P_i and Q_i are the active and reactive power of the 1st load in the 1st bus, respectively. R and X are the resistance and reactance between successive buses i and $i + 1$, respectively, and H is the highest harmonic order.

2.4. Power losses

Power loss is considered as one of the important goals in studies related to distributed generation. It is considered as the most important single goal and is stated as follows:

$$P_{L_{total}} = \sum_{i=1}^n R_i I_i^2 \quad (8)$$

$$F_1 = \frac{P_{loss,i}}{P_{loss,base}} \quad (9)$$

where I_i is the current passing through line i , n is the total number of lines, and R is the resistance of line i . $P_{loss,i}$ is the P_{loss} value for the i th branch after DG installation and $P_{loss,base}$ is the initial value of P_{loss} .

2.5. System reliability

To show a more tangible view of the overall network status, system-related reliability indicators are used to show the behavior of the entire feeder. Some of these indicators that are used in this work are:

- The system average interruption frequency index (SAIFI):

$$SAIFI = \frac{\sum \lambda_i \cdot N_i}{\sum N_i} \quad (10)$$

where λ_i is the failure rate and N_i is the number of customers for location i .

- The System Average Interruption Duration Index (SAIDI):

$$SAIDI = \frac{\sum_{i=1}^n U_i \cdot N_i}{\sum_{i=1}^n N_i} \quad (11)$$

In the above relation, U_i is the annual outage time for location i (h/year).

- The Average Energy Not Supplied (AENS):

$$AENS = \frac{ENS}{\sum N_i} \quad (12)$$

In the above relation, ENS is the Energy Not Supplied in terms of (kWh/year). The general system reliability index is examined through the following equation:

$$F_2 = \left[\left(\frac{SAIFI_i}{SAIFI_{base}} \right) + \left(\frac{SAIDI_i}{SAIDI_{base}} \right) + \left(\frac{AENS_i}{AENS_{base}} \right) \right] \quad (13)$$

where $SAIFI_i$ is the system average interruption frequency index after DG installation and $SAIFI_{base}$ is the system average interruption frequency index for the primary network without DG installation. The other indicators of the above relationship are the same.

2.6. The optimal size of DG

The optimal size of the DG can be calculated by the following index:

$$F_3 = \frac{P_{DG_{i,j}}}{\sum_{j=1}^{N_p} P_{load,j}} \quad (14)$$

where $P_{DG_{i,j}}$ is the power on the bus j for the i th branch, $P_{load,j}$ is the active power of the load point j , and N_p is the total number of load points.

2.7. Network voltage profile

The function F_4 is the voltage profile index and is calculated as follows:

$$F_4 = \sum_{i=1}^n (1 - |V_i|)^2 \quad (15)$$

In the above relation, V_i is the bus voltage at point j .

2.8. Cost of operating the hybrid system

The function F_5 is the index for the total cost of the wind and solar hybrid system, which is calculated by the following equation [29, 30]:

$$F_5 = \left(\frac{C_{DG}}{C_{DGT}} \right) \quad (16)$$

$$C_{DG} = \sum_S NPC(S) = N \times (\text{CapitalCost} + (\text{ReplacementCost} \times k)) + (\text{O\&MCost} \times \frac{1}{\text{CRF}(ir, R)}) \quad (17)$$

where the vector S is equal to $C_{DG, s} = (PV + WT)$ which is the base cost. In this case, it is equal to $C_{DGT} = 1000000$. CRF is the capital recovery factor that is calculated by the following equation [29, 30]:

$$\text{CRF}(ir, R) = \frac{ir(1 + ir)^R}{(1 + ir)^R - 1} \quad (18)$$

where ir is the discount rate and R is the project lifetime.

2.9. Modeling of the studied equipment

2.9.1. Photovoltaic system

The output power of photovoltaic panels can be calculated using Equations (19) to (21). This model includes the effects of solar radiation and panel temperature on its output power. These relationships at the maximum output power point are as follows [4, 9]:

$$P_{PV} = V_{MPP} \cdot I_{MPP} \quad (19)$$

$$V_{MPP} = V_{MPP,ref} + P_{v,oc}(T_C - T_{C,ref}) \quad (20)$$

$$I_{MPP} = I_{MPP,ref} + I_{SC,ref} \left(\frac{G_T}{G_{ref}} \right) + P_{I,SC}(T_C - T_{C,ref}) \quad (21)$$

where P_{PV} is the panel power, V_{mpp} is the potential voltage, $V_{mpp, ref}$ is the same as V_{mpp} in standard operating conditions (V), I_{mpp} is the panel current, $I_{SC, ref}$ is the short circuit current in standard operating conditions, G_T is the average daily radiation (W/m^2), and G_{ref} is equivalent to $1000 W/m^2$ for operation under standard conditions. $P_{v, oc}$, and $P_{I, SC}$ are the temperature coefficients for open-circuit voltage ($V/^\circ C$) and short circuit current ($A/^\circ C$), respectively. $T_{C,ref}$ is the

temperature of the photovoltaic panel under standard operating conditions, which is considered to be $25^\circ C$, and $T_C(t)$ is the operating temperature of the photovoltaic panel, which is calculated as follows:

$$T_C(t) = T_a(t) + \frac{\text{NOCT} - 20}{800} \cdot G_T \quad (22)$$

where $T_a(t)$ is the ambient temperature ($^\circ C$), NOCT (Nominal Operating Cell Temperature) is defined for the operation of the irradiated panel at $800 W/m^2$ and a temperature of $20^\circ C$ and is usually considered between $40^\circ C$ and $46^\circ C$.

Photovoltaic panels in series are defined using DC bus voltage and the nominal voltage of the panel as:

$$N_{PN,S} = \frac{V_{Bus}}{N_{pv,nom}} \quad (23)$$

where $N_{pv,nom}$ is the nominal voltage of the photovoltaic panel. It should be noted that $N_{PN,S}$ is not an optimized target and the number of connected panels in parallel is the optimized targets.

2.9.2. Wind turbine

The wind speed at the reference height h_r is used as the daily average to determine the wind speed colliding with the wind turbine in the model below. The wind turbine model is described as follows:

$$V(t) = V_r(t) \cdot \left(\frac{h}{h_r} \right)^\gamma \quad (24)$$

where $V(t)$ is the wind speed at height h , V_r is the wind speed recorded at height h , and γ is called the legal power view, which is between 0.14 and 0.25. This formula of wind speed calculation is used to calculate the turbine output power $P_{WT}(t)$ as follows [4, 9]:

$$P_{WT}(t) = \begin{cases} av^3(t) - bP_R & V_{Ci} < V < V_r \\ P_R & V_r < V < V_{Co} \\ 0 & \text{otherwise} \end{cases} \quad (25)$$

$$b = \frac{V_{Ci}^3}{(V_r^3 - V_{Ci}^3)}, a = \frac{P_r}{(V_r^3 - V_{Ci}^3)}$$

where P_r is the allowable power. V_{co} , V_r , and V_{Ci} are the low cut-off speed, nominal speed, and high cut-off speed of the turbine, respectively.

2.9.3. DC/AC converter

The DC/AC converter is used to convert the total DC power from the hybrid power plant into AC power at the desired frequency. In order to investigate the converter losses on the output power of the hybrid power plant, the following equation is used:

$$P_{inv-load} = (P_{Ren-inv}) \times \eta_{inv} \quad (26)$$

where η_{inv} is the converter efficiency. Costs related to investment, maintenance, replacement of parts, and operating costs of the system are shown in actual values in Table 1.

Table 1. Technical specifications of the used equipment

Equipment	Investment cost (\$/unit)	Replacement cost (\$/unit)	Annual fee (Repair and maintenance) (\$/unit-yr)	Life-time (yr)	Accessibility (%)	Efficiency (%)
PV	7000	6000	20	20	96	--
WG	19400	15000	75	20	96	--
DC/AC	800	750	8	15	99/89	90

2.10. Optimization

2.10.1. Improved GA algorithm

Considering the advantages and disadvantages of each of the real and binary coding methods and considering that there are both continuous and discrete variables in the problem of optimal placement of scattered products, the proposed genetic algorithm uses the combined coding method. In this coding method, each chromosome is divided into two parts: continuous variables and discrete variables. This coding method significantly reduces the length of the string and reduces the computational volume. Moreover, in this method, it is possible to use the advantages of both real and binary coding methods and no approximation is required to execute the obtained answer.

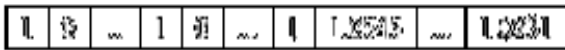


Figure 4. String structure

2.10.2. Genetic operators

Since in the proposed genetic algorithm, each chromosome is divided into two parts, continuous and discrete, it is necessary to define the genetic operators of mating and mutation in accordance with this coding.

2.10.3. Coupling

The genetic operator function selects the length of the binary and real parts of the operators proportional to the selected strings as the parent. The advantage of this method is that operators that respond better to continuous variables can be used for the real part while operators that work better for discrete variables can be used for the binary part. The mating operator presented in this dissertation is a scattered-exploration operator. This operator uses the scattered operator for the binary part and the more efficient exploration operator for the real part. The sparse operator first generates a random string of zeros and ones along the binary portion of the chromosome and then, replaces one of the corresponding genes of the first parent and zero of the corresponding genes of the second parent. The exploration operator generates a point from the pairing of the parent points that is on the line connecting these two points and closer to the better parent. If we assume that parent one is better than parent two, the resulting child will be as follows:

$$\text{Child} = R \times (\text{Parent 2} - \text{Parent 1})$$

where R is the ratio of the child to the better parent. The following figure shows how the sporadic genetic operator works and generates a new string of selected parents.

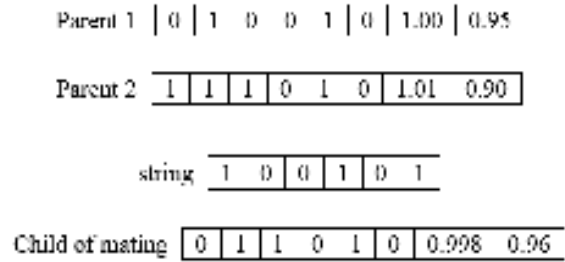


Figure 5. Scattered-exploration operator mutation

The mutation operator for the proposed method first generates a random string of zeros and ones in which the probability of one is equal to the probability defined for the mutation operator. Then in genes corresponding to one, if they are in the binary part, it converts zero to one and one to zero, and if it is in the real part, it puts a random number in the allowable range for that variable instead of the corresponding number. The function of the mutation operator can be seen in the figure below.

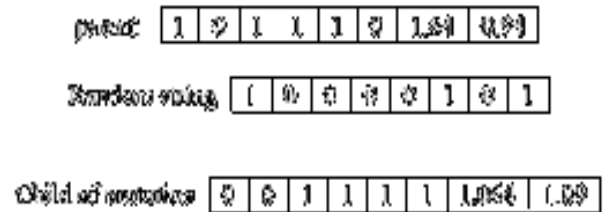


Figure 6. Mutation operator

Execution steps of GA-improved algorithm:

- 1) Obtain the value of t = 1
- 2) Produce x chromosome randomly in the desired range
- 3) Determine the fitness value of the function f(x) and assign this variable value as the best child (x_{best})
- 4) Calculate the child of the new generation using Equation (1)
- 5) Take the value t = t_{max}
- 6) Check the condition of completion of steps and determine x_{optimal} based on the following command:

$$\text{If } t=t_{\text{max}} \text{ go to step(2) else } x_{\text{optimal}}=x_{\text{best}}$$

- 7) The end

Figure 7 shows the GA-improved algorithm process.

2.10.4. Optimal placement of distributed generation

In this section, the objective function of the problem of optimal placement of distributed generation with equal and

unequal constraints is expressed. In this formulation, the effect of harmonic distortion of voltage sources on the network is considered.

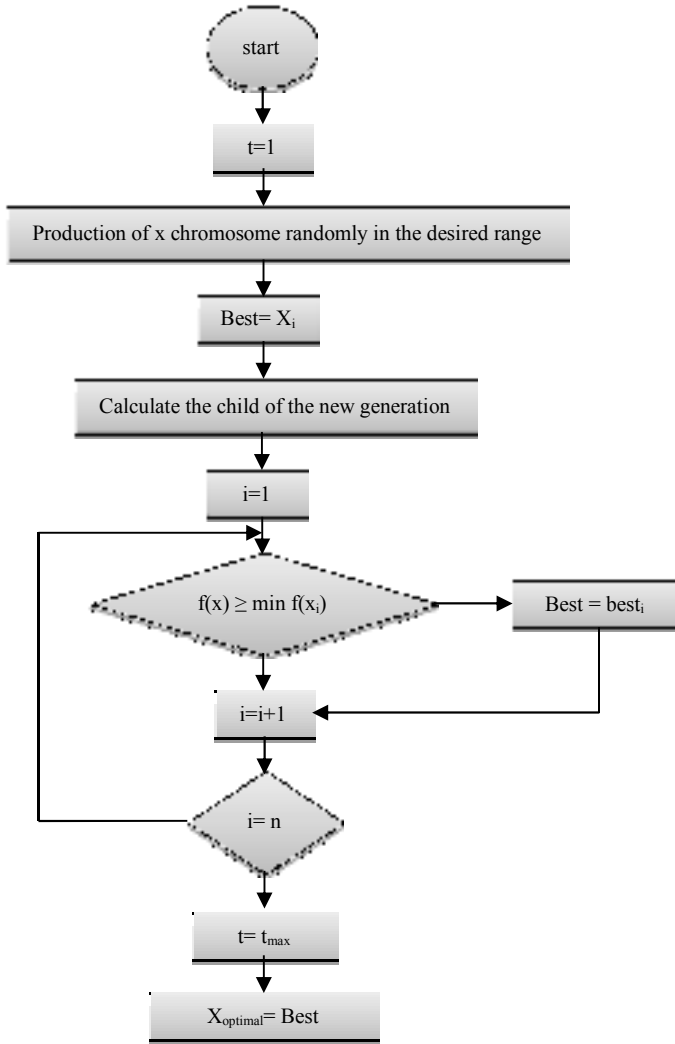


Figure 7. GA-Improved algorithm flowchart

The main purpose of this research is to determine the optimal location and capacity of distributed generation units by considering the five objectives of reducing losses, improving voltage profile, improving system reliability, the optimal size of DG unit, and construction cost of combined

wind and solar power plant. Each of these individual goals has been transformed into a single-objective function using weighting coefficients. These coefficients are determined using the AHP method and applied to the objective function of the problem. The AHP model was first used by Thomas L. Saaty in the 1970s. AHP is a simple computational method based on the main operation on the matrix, which calculates its specific values by creating a suitable hierarchy and processing step by step and constructing adaptive matrices at different levels, and in the vector of final weight coefficients, the relative importance of each option is determined according to the purpose of the hierarchy. The first step in calculating weighting coefficients is to prioritize the problem criteria. These values are applied as five priorities in this research in the following relation.

The criteria and sub-criteria used to evaluate sustainable energy options are summarized in the conceptual model shown in Figure 8.

The statistical population of this research dwell in Meshkinshahr. After determination of the potential of renewable energy and economic analysis, the level of prevention of environmental pollutants in comparison is determined with fossil resources. Then, using the analytical network process (ANP) for each of the sub-indicators of the economic dimension, the environmental dimension is assigned to each of the weighted renewable energies. Using the multi-criteria decision method of PROMETHEE, renewable energy (solar, wind) is used from the economic viewpoint and the environmental dimension is scored. Also, free R programming software is used for data analysis, which is an implementation of the ANP weighting method. The ANP method, which is a generalization of the Analytic Hierarchy Process (AHP) method, does not require a hierarchical structure and, therefore, shows the relationship between different levels of a decision in a network.

The preference linear function $p(d)$ is considered and a net superiority value $\Phi(\cdot)$ is obtained. The linear function $p(d)$ is obtained as follows:

$$p(d) = \begin{cases} 0 & d \leq 0 \\ d/p & 0 \leq d \leq p \\ 1 & d > p \end{cases} \quad (27)$$

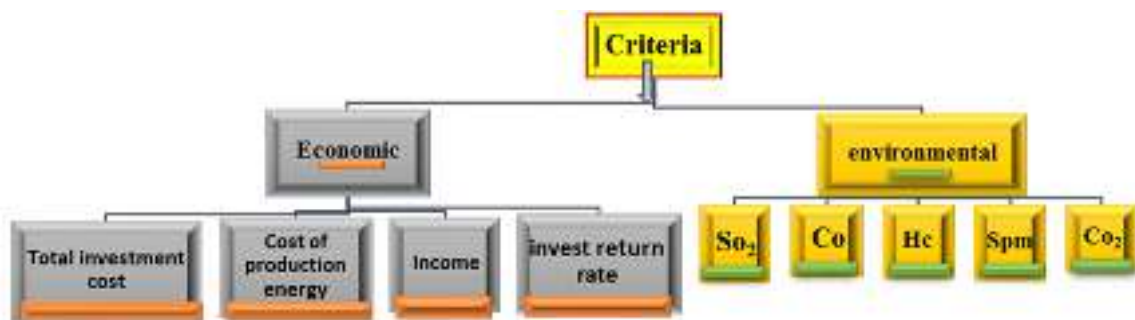


Figure 8. Conceptual model of influential factors of renewable energy

The net superiority value for region a , $\Phi(a)$ is calculated as follows:

$$\Phi(a) = \Phi^+(a) - \Phi^-(a) \quad (28)$$

$$\Phi^+(a) = \frac{1}{n-1} \sum_{x \in A} \pi(a, x), \quad (29)$$

$$\Phi^-(a) = \frac{1}{n-1} \sum_{x \in A} \pi(x, a), \quad (30)$$

And

$$\pi(a, x) = \sum_{j=1}^6 p_j(a, x) w_j, \quad (31)$$

$$\pi(x, a) = \sum_{j=1}^6 p_j(x, a) w_j, \quad (32)$$

and w_j 's are the weights assigned by the AHP method to each of the indicators of urban prosperity in terms of infrastructure. Now, if $\Phi(b) < \Phi(a)$, region a has less urban flourishing than region b, and vice versa.

Also, to make it easier to interpret the values of superiority between -1 and 1, it can be converted into a score between 0 and 100 using the following conversion:

$$\Phi'(a) = \frac{\Phi^+(a) + (1 - \Phi^-(a))}{2} \times 100 \quad (33)$$

According to the score presented by Equation (30), the status of operation of five types of renewable energy in Meshkinshahar studied is classified into (0-1) as:

$$A = \begin{bmatrix} W_1/W_1 \dots W_1/W_5 \\ \dots \dots \dots \\ W_5/W_1 \dots W_n/W_5 \end{bmatrix} \begin{bmatrix} W_1 \\ \dots \\ W_5 \end{bmatrix} \quad (34)$$

In the second step, the compatibility coefficient is calculated by the following equation:

$$CR = \frac{CI}{RI} \quad (35)$$

In the above equation, RI is random index and CI is obtained using the following relation:

$$CI = \frac{L - N}{N - 1} \quad (36)$$

$$L = \frac{1}{N} \left(\sum_i^N = \left(\frac{WA_i}{W_i} \right) \right) \quad (37)$$

According to the above relations, the value of weighting coefficients in this problem is calculated according to the preference and the order of importance is equal to $W_1=0.388$, $W_2=0.2186$, $W_3=0.1943$, $W_4=0.1564$, and $W_5=0.043$. In general, the objective function of the problem is to minimize the following equation:

$$\begin{aligned} \min \quad F = F = \sum_{m=1}^5 w_m \cdot F_m \\ w_m \in [0,1] \quad \sum_{m=1}^5 w_m = 1 \end{aligned} \quad (38)$$

2.10.5. Constraints

Problem constraints are applied in system simulation as follows:

- Power balance constraint:

$$P_{\text{Slack}} + \sum_{i=1}^N P_{DG_i} = \sum P_{D_i} + P_L \quad (39)$$

- Restrictions on active and reactive power:

$$\begin{aligned} Q_{DG_i}^{\min} \leq Q_{DG_i} \leq Q_{DG_i}^{\max} \\ P_{DG_i}^{\min} \leq P_{DG_i} \leq P_{DG_i}^{\max} \end{aligned} \quad (40)$$

- Losses:

$$\sum \text{Loss}_k(\text{withDG}) \leq \sum \text{Loss}_k(\text{withoutDG}) \quad (41)$$

- System reliability constraints:

$$\begin{aligned} \sum \text{SAIDI}_k(\text{withDG}) \leq \sum \text{SAIDI}_k(\text{withoutDG}) \\ \sum \text{SAIFI}_k(\text{withDG}) \leq \sum \text{SAIFI}_k(\text{withoutDG}) \\ \sum \text{AENS}_k(\text{withDG}) \leq \sum \text{AENS}_k(\text{withoutDG}) \end{aligned} \quad (42)$$

- The number of photovoltaic (PV) panels and wind turbines (WT):

$$\begin{aligned} N_{PV_{\min}} \leq N_{PV} \leq N_{PV_{\max}} \\ N_{WT_{\min}} \leq N_{WT} \leq N_{WT_{\max}} \end{aligned} \quad (43)$$

- Voltage and bus current:

$$\begin{aligned} |V_i|^{\min} \leq |V_i| \leq |V_i|^{\max} \\ |I_i| \leq |I_i|^{\max} \end{aligned} \quad (44)$$

3. RESULTS AND DISCUSSION

In order to demonstrate the accuracy and precision of the GA-Improved algorithm, the IEEE standard 30-bus network, which is shown in Figure 9, has been studied and evaluated. Taking into account the network losses before installing DG and the resulting voltage drop in the power system, the selected DG capacity for the network is equal to 3.43 MW. Considering that the purchase price of electricity by renewable units to the network in Iran is equal to 0.045 \$/kW, the rate of return on equity is equal to 7.6 years during the operation period of the system.



Figure 9. Single-line diagram of the studied network

The convergence process of the proposed algorithm is intended to solve the problem with the objectives and is shown in the form of a single-objective problem in Figure 10.

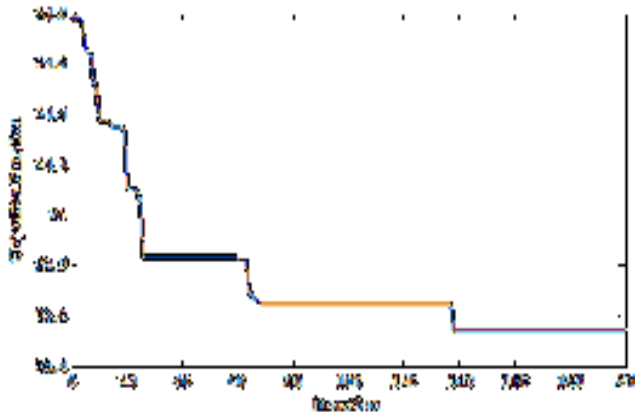


Figure 10. Convergence process of the GA-improved algorithm

The values obtained for system losses before and after DG installation and the rate of improvement of the network

voltage profile after DG installation are seen in Figures 11, 12, and 13, respectively.

According to Figure 11, with the placement of DG in bus 8 of the study network, system losses have been significantly reduced compared to the case of no DG installation and have a value equal to 72.48 kW. However, this amount of losses before installing DG had a value of 172.64 kW. The rate of reactive system losses in the two cases before and after the installation of DG is also seen in Figure 12.

According to Figure 12, the reactive loss rate after DG installation has a lower value than the case of no DG installation. According to the results of optimal placement of DG in the desired bus, the system reactive losses from the amount of 126.17 MVAR before installing DG have reached 37.46 MVAR after installing DG in the desired bus. Significant reduction of these losses for the installation of one DG unit with the aim of achieving the least losses is one of the important achievements of this study. Figure 13, which is related to the voltage profile of the studied network, shows the acceptable improvement of the system voltage profile after DG installation.

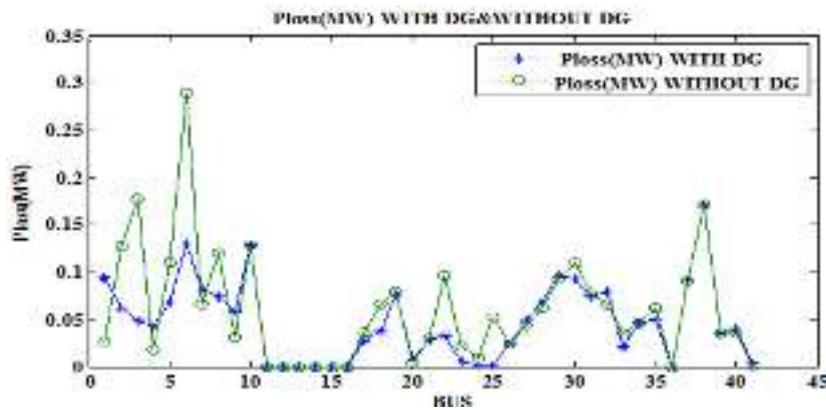


Figure 11. Active network losses before and after DG installation

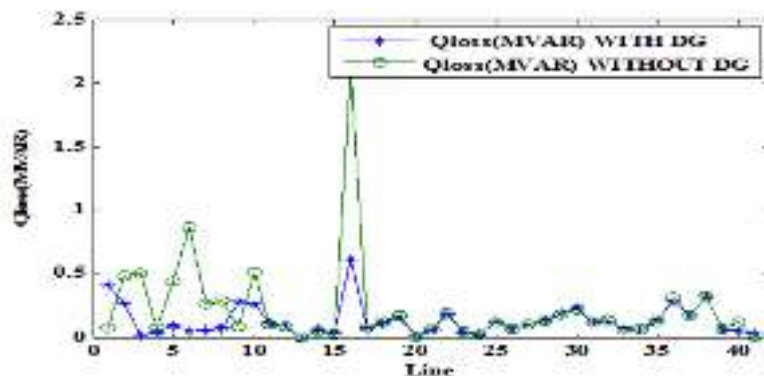


Figure 12. Reactive network losses before and after DG installation

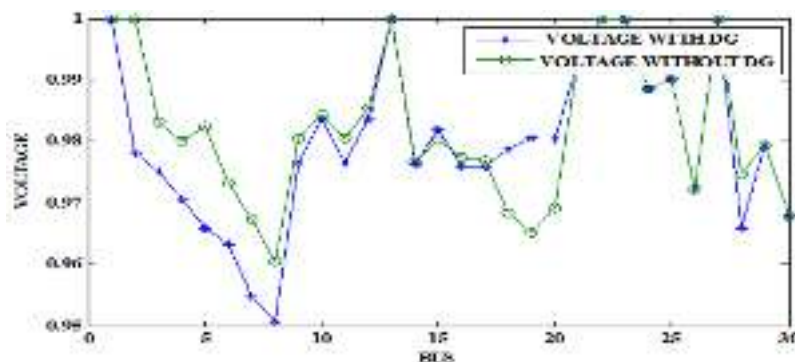


Figure 13. Network voltage profile before and after DG installation

According to Figure 13, the rate of the reduction of voltage profile in the case without using DG has a value equal to 0.7346 P.u, while after installing DG with a capacity of 3.43 MW in the bus 8 of the above network, this index reached 0.9424 P.u.

The results of the system simulation are also presented numerically in Table 2. According to Table 2, the total grid

voltage profile improved by 0.2078 (P.u) after DG installation. The optimal reduction of system reliability values according to the values obtained for SAIDI, SAIFI, and AENS indices can be seen in the table. The required capacity of the network for the design and installation of DG is equal to the amount of 3.43 MW, which includes 24 photovoltaic panels, 5 wind turbines, and 11 inverters at a cost of 1.552 M\$/MW.

Table 2. Results of the GA-improved algorithm

Parameter	Population size	Bus bar	Total capacity DG	Power losses (kW)	lowest voltage (P.u.)	SAIDI (h/yr.cent)	SAIFI (h/yr.cent)	AENS (kWh/yr)	PV (kW)	WT	Conv. (kW)	NPC (M\$/MW)
Without DG	50	-	-	172/64	0.7346	19/8	6/45	328/79	-	-	-	-
With DG	50	8	3/43	72/48	0.9424	4/36	1/04	126/42	24	5	11	1/552

According to the results related to system reliability, the index SAIFI has a value equal to 1.04 times of shutdown during the year and this means that this index, which indicates the average shutdown frequency of the entire network, has a value of 1.04 during the year, which is a very desirable amount in the design of distributed generation systems. It should be noted that the value of this index, as seen in Table 2, had a value of 6.45 times a year without the use of DG. By improving the reliability index of the second system, the SAIDI index was formed and calculated in this research and had an average value of 4.36 hours per year, while this index for the system without the use of DG was calculated and it accounted for 19.8 hours per year, which was a decrease in the indicator of the usefulness and obligation to install DG in the network during the operation period. Then, the third index of the system reliability, AENS is calculated for both cases before and after DG installation and is applied in the table resulting from the system simulation. This loss index after installing DG in the desired bus has a reduction of about 200 kWh during the year and has a value equal to 126.42 kWh per year.

According to the results, the total amount of losses after installing DG was reduced to 72.48 KW. The construction cost of the DG power plant, in this case, was quite smaller than that in previous studies, which was due to the selection of the optimal combination of wind and solar units to ensure the desired load in the study network.

4. CONCLUSIONS

In this research, the location and determination of the optimal capacity of distributed generation units for the IEEE standard network were done by the GA improved algorithm. The high accuracy and precision of the proposed algorithm was one of the main reasons for choosing this algorithm due to the lack of need for many control parameters. The objective function modeling of the problem included power losses, voltage profiles, reliability, DG size, and construction cost of the combined wind and solar combined generation unit in this study. The results of optimization show a 61.23 % reduction of total system losses after DG installation and improvement of system reliability indices, especially the SAIFI, from 6.45 (h/year) to 1.04 (h/year) after installing DG. Reducing the construction cost of DG unit, an optimal increase of network reliability, and significant reduction of power losses were the advantages of choosing the combined wind and solar mode in the studied network. The rate of return on capital was also calculated for the proposed hybrid system in this paper and

had a rate of 7.6 years during the operation period of the system. According to the results, the total amount of losses after installing DG was reduced to 72.48 kW. The construction cost of DG power plant, in this case, was quite smaller than that in previous studies due to the selection of the optimal combination of wind and solar units, thus ensuring the desired load in the study network.

5. ACKNOWLEDGEMENT

The authors appreciatively acknowledge the Islamic Azad University of Germe Branch.

NOMENCLATURE

R	Resistance (Ω)
X	Reactance (Ω)
Y	Harmonic
V	Voltage (V)
Q	Reactive power (VA)
P	Active power (kW)
I	Current (A)
λ	Failure rate
N	Number of customers
U	Annual outage time
Ir	Discount rate
T	Temperature (k)
GT	Average daily radiation (W/m^2)
h	Hour

REFERENCES

- Adebayo, T.S., Coelho, M.F., Onbaşıoğlu, D.Ç., Rjoub, H., Mata, M.N., Carvalho, P.V., Rita, J.X. and Adeshola, I., "Modeling the dynamic linkage between renewable energy consumption, globalization, and environmental degradation in South Korea: Does technological innovation matter?", *Energies*, Vol. 14, No. 14, (2021), 4265. (<https://doi.org/10.3390/en14144265>).
- Khosravi, A., Malekan, M., Pabon, J.J.G., Zhao, X. and Assad, M.E.H., "Design parameter modelling of solar power tower system using adaptive neuro-fuzzy inference system optimized with a combination of genetic algorithm and teaching learning-based optimization algorithm", *Journal of Cleaner Production*, Vol. 244, (2020), 118904. (<https://doi.org/10.1016/j.jclepro.2019.1189>).
- Alayi, R., Zishan, F., Mohkam, M., Hoseinzadeh, S., Memon, S. and Garcia, D.A., "A sustainable energy distribution configuration for microgrids integrated to the national grid using back-to-back converters in a renewable power system", *Electronics*, Vol. 10, No. 15, (2021), 1826. (<https://doi.org/10.3390/electronics10151826>).
- El Haj Assad, M., Ahmadi, M.H., Sadeghzadeh, M., Yassin, A. and Issakhov, A., "Renewable hybrid energy systems using geothermal energy: Hybrid solar thermal-geothermal power plant", *International*

- Journal of Low-Carbon Technologies*, Vol. 16, No. 2, (2021), 518-530. (<https://doi.org/10.1093/ijlct/ctaa084>).
5. Sina, M.A. and Adeel, M.A., "Assessment of stand-alone photovoltaic system and mini-grid solar system as solutions to electrification of remote villages in Afghanistan", *International Journal of Innovative Research and Scientific Studies*, Vol. 4, No. 2, (2021), 92-99. (<https://doi.org/10.53894/ijriss.v4i2.62>).
 6. Adewole, B.Z., Malomo, B.O., Olatunji, O.P. and Ikobayo, A.O., "Simulation and experimental verification of electrical power output of a microcontroller based solar tracking photovoltaic module", *International Journal of Sustainable Energy and Environmental Research*, Vol. 9, No. 1, (2020), 34-45. (<https://doi.org/10.18488/journal.13.2020.91.34.45>).
 7. Adebayo, T.S., Rjoub, H., Akinsola, G.D. and Oladipupo, S.D., "The asymmetric effects of renewable energy consumption and trade openness on carbon emissions in Sweden: New evidence from quantile-on-quantile regression approach", *Environmental Science and Pollution Research*, (2021), 1-12. (<https://doi.org/10.1007/s11356-021-15706-4>).
 8. Ghalandari, M., Ziamolki, A., Mosavi, A., Shamshirband, S., Chau, K.W. and Bornassi, S., "Aeromechanical optimization of first row compressor test stand blades using a hybrid machine learning model of genetic algorithm, artificial neural networks and design of experiments", *Engineering Applications of Computational Fluid Mechanics*, Vol. 13, No. 1, (2019), 892-904. (<https://doi.org/10.1080/19942060.2019.1649196>).
 9. Alayi, R., Zishan, F., Seyednouri, S.R., Kumar, R., Ahmadi, M.H. and Sharifpur, M., "Optimal load frequency control of island microgrids via a PID controller in the presence of wind turbine and PV", *Sustainability*, Vol. 13, No. 19, (2021), 10728. (<https://doi.org/10.3390/su131910728>).
 10. Kefif, N., Melzi, B., Hashemian, M., El Haj Assad, M. and Hoseinzadeh, S., "Feasibility and optimal operation of micro energy hybrid system (hydro/wind) in the rural valley region", *International Journal of Low-Carbon Technologies*, Vol. 17, (2022), 58-68. (<https://doi.org/10.1093/ijlct/ctab081>).
 11. Mostafaipoor, A., Saidi Mehrabad, M., Qolipour, M., Basirati, M., Rezaei, M. and Golmohammadi, A.M., "Ranking locations based on hydrogen production from geothermal in Iran using the Fuzzy Moora hybrid approach and expanded entropy weighting method", *Journal of Renewable Energy and Environment (JREE)*, Vol. 4, No. 4, (2017), 9-21. (<https://dx.doi.org/10.30501/jree.2017.88328>).
 12. Hsu, C.C., Zhang, Y., Ch, P., Aqdas, R., Chupradit, S. and Nawaz, A., "A step towards sustainable environment in China: The role of eco-innovation renewable energy and environmental taxes", *Journal of Environmental Management*, Vol. 299, (2021), 113609. (<https://doi.org/10.1016/j.jenvman.2021.113609>).
 13. AlShabi, M., Ghenai, C., Bettayeb, M., Ahmad, F.F. and El Haj Assad, M., "Multi-group grey wolf optimizer (MG-GWO) for estimating photovoltaic solar cell model", *Journal of Thermal Analysis and Calorimetry*, Vol. 144, No. 5, (2021), 1655-1670. (<https://doi.org/10.1007/s10973-020-09895-2>).
 14. Mughal, N., Arif, A., Jain, V., Chupradit, S., Shabbir, M.S., Ramos-Meza, C.S. and Zhanbayev, R., "The role of technological innovation in environmental pollution, energy consumption and sustainable economic growth: Evidence from South Asian economies", *Energy Strategy Reviews*, Vol. 39, (2022), 100745. (<https://doi.org/10.1016/j.esr.2021.100745>).
 15. Fu, L., Liu, B., Meng, K. and Dong, Z.Y., "Optimal restoration of an unbalanced distribution system into multiple microgrids considering three-phase demand-side management", *IEEE Transactions on Power Systems*, Vol. 36, No. 2, (2020), 1350-1361. (<https://doi.org/10.1109/TPWRS.2020.3015384>).
 16. Makkiabadi, M., Hoseinzadeh, S., Mohammadi, M., Nowdeh, S.A., Bayati, S., Jafaraghaei, U., Mirkiaei, S.M. and El Haj Assad, M., "Energy feasibility of hybrid PV/wind systems with electricity generation assessment under Iran environment", *Applied Solar Energy*, Vol. 56, No. 6, (2020), 517-525. (<https://doi.org/10.3103/S0003701X20060079>).
 17. Abbas, A.S., El-Sehiemy, R.A., El-Ela, A., Ali, E.S., Mahmoud, K., Lehtonen, M. and Darwish, M.M., "Optimal harmonic mitigation in distribution systems with inverter based distributed generation", *Applied Sciences*, Vol. 11, No. 2, (2021), 774. (<https://doi.org/10.3390/app11020774>).
 18. Marquez Alcaide, A., Monopoli, V.G., Wang, X., Leon, J.I., Buticchi, G., Vazquez, S., Liserre, M. and Franquelo, L.G., "Common-mode voltage harmonic reduction in variable speed drives applying a variable-angle carrier phase-displacement PWM method", *Energies*, Vol. 14, No. 10, (2021), 2929. (<https://doi.org/10.3390/en14102929>).
 19. Liu, Y., Xu, W., Long, T. and Blaabjerg, F., "An improved rotor speed observer for standalone brushless doubly-fed induction generator under unbalanced and nonlinear loads", *IEEE Transactions on Power Electronics*, Vol. 35, No. 1, (2019), 775-788. (<https://doi.org/10.1109/TPEL.2019.2915360>).
 20. Manito, A., Bezerra, U., Tostes, M., Matos, E., Carvalho, C. and Soares, T., "Evaluating harmonic distortions on grid voltages due to multiple nonlinear loads using artificial neural networks", *Energies*, Vol. 11, No. 12, (2018), 3303. (<https://doi.org/10.3390/en11123303>).
 21. Norozpour Niazi, A., Vasegh, N. and Motie Birjandi, A.A., "To study unplanned islanding transient response of microgrid by implementing MSOG and SRF-PLL based hierarchical control in the presence of non-linear loads", *IET Renewable Power Generation*, Vol. 14, No. 5, (2020), 881-890. (<https://doi.org/10.1049/iet-rpg.2019.0506>).
 22. Laffont, A., Pascaud, R., Callegari, T., Liard, L., Pascal, O. and Adam, J.P., "A harmonic oscillator model to study the intensification of microwave radiation by a subwavelength uniform plasma discharge", *Physics of Plasmas*, Vol. 28, No. 3, (2021), 033503. (<https://doi.org/10.1063/5.0038640>).
 23. Pan, C. and Su, H., "Research on excitation current and vibration characteristics of DC biased transformer", *CSEE Journal of Power and Energy Systems*, (2019). (<https://doi.org/10.17775/CSEEJPES.2019.00410>).
 24. Jamali-Abnavi, A., Hashemi-Dezaki, H., Ahmadi, A., Mahdavianesh, E. and Tavakoli, M.J., "Harmonic-based thermal analysis of electric arc furnace's power cables considering even current harmonics, forced convection, operational scheduling, and environmental conditions", *International Journal of Thermal Sciences*, Vol. 170, (2021), 107135. (<https://doi.org/10.1016/j.ijthermalsci.2021.107135>).
 25. Hemmati, M., Mohammadi-Ivatloo, B., Abapour, M. and Anvari-Moghaddam, A., "Optimal chance-constrained scheduling of reconfigurable microgrids considering islanding operation constraints", *IEEE Systems Journal*, Vol. 14, No. 4, (2020), 5340-5349. (<https://doi.org/10.1109/JSYST.2020.2964637>).
 26. Das, C.K., Bass, O., Kothapalli, G., Mahmoud, T.S. and Habibi, D., "Overview of energy storage systems in distribution networks: Placement, sizing, operation, and power quality", *Renewable and Sustainable Energy Reviews*, Vol. 91, (2018), 1205-1230. (<https://doi.org/10.1016/j.rser.2018.03.068>).
 27. Narimani, M. and Hosseinian, H., "Investigation of harmonic effects in locational marginal pricing and developing a framework for LMP calculation", *Scientia Iranica*, (2020). (<https://dx.doi.org/10.24200/sci.2020.54477.3776>).
 28. Das, T.K. and Chatterjee, S., "Multi-spurious harmonics suppression in folded hairpin line bandpass filter by meander spur-line", *International Journal of RF and Microwave Computer Aided Engineering*, Vol. 31, No. 11, (2021), e22858. (<https://doi.org/10.1002/mmce.22858>).
 29. Gu, Z., Malik, H.A., Chupradit, S., Albasher, G., Borisov, V. and Murtaza, N., "Green supply chain management with sustainable economic growth by CS-ARDL technique: Perspective to blockchain technology", *Frontiers in Public Health*, 2391. (<https://doi.org/10.3389%2Ffpubh.2021.818614>).
 30. Alayi, R., Jahangiri, M., Guerrero, J.W.G., Akhmadeev, R., Shichiyakh, R.A. and Zanghaneh, S.A., "Modelling and reviewing the reliability and multi-objective optimization of wind-turbine system and photovoltaic panel with intelligent algorithms", *Clean Energy*, Vol. 5, No. 4, (2021), 713-730. (<https://doi.org/10.1093/ce/zkab041>).



Research Article

Evaluation of the Experimental Performance of an Asphalt Solar Air Collector

Armin Motamed Sadr, Mehran Ameri*, Ebrahim Jahanshahi Javaran

Department of Mechanical Engineering, School of Engineering, Shahid Bahonar University of Kerman, P. O. Box: 76169-14111, Kerman, Iran.

PAPER INFO

Paper History:

Received: 17 March 2022

Revised: 26 June 2022

Accepted: 06 July 2022

Keywords:

Asphalt Collector,
Air,
Solar Energy,
Efficiency

ABSTRACT

In this research, the performance of an asphalt solar air collector was experimentally tested and the daily thermal and exergy efficiencies of the collector were analyzed. The sun's radiant energy is absorbed by asphalt and converted into thermal energy. Then, it is transmitted to aluminum pipes buried under the asphalt and, finally, to the air passing through the pipes. A suction fan induces the ambient air to the collector. The experimental results show that the daily thermal efficiencies at mass flow rates of 0.007 (kg/s) and 0.014 (kg/s) are 11.98 % and 24.10 % and daily exergy efficiencies are 0.34 % and 0.66 %, respectively, showing the increase in daily energy and exergy efficiencies with increasing the air mass flow rate. In addition, results show that as the flow rate increases, the outlet air temperature decreases. The presence of temperature difference between the inlet and outlet of the collector in the last hours of the day, when the sun's radiation is low, indicates that asphalt acts as a thermal energy storage medium.

<https://doi.org/10.30501/jree.2022.334587.1347>

1. INTRODUCTION

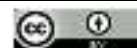
Nowadays, due to the growth of energy demands in communities and the reduction of fossil fuel sources in the world, there is a tendency to use renewable energies. Among the various types of renewable energies, solar energy has received more attention in recent decades. One of the most important applications of solar energy is the production of electricity using solar panels and also the heating of various fluids such as air and water by solar thermal collectors. Solar thermal collectors are responsible for converting the radiant energy received from the sun into the thermal energy required to heat the fluid. Solar air collectors are used in many applications such as dryers, indoor heating, cooking, etc. [1]. Researchers are interested in solar air heaters because of their affordable cost, simple structure, and ease of construction [2, 3].

Asphalt and concrete solar collectors are very popular due to their ease of construction and good efficiency. The asphalt and concrete solar collectors are commonly used for water or air heating; so far, researchers have pursued different goals for the study of these types of collectors. Concrete Solar Collectors (CSCs) are a solar thermal technology for low-temperature applications. They are particularly suitable for integration on precast concrete clad buildings [4]. Asphalt solar collectors have better performance in energy storage and efficiency due to higher absorption coefficient and lower thermal conductivity than concrete collectors [5, 6]. A group

of researchers by examining different types of pipe arrangements in asphalt collectors have tried to provide the best model of pipe placement to achieve the maximum performance of these types of collectors. In a laboratory study and numerical solution, Chiarelli et al. [7] discussed the arrangement, cross-sectional shape, and air volume of pipes in an asphalt air collector. In another study, Ehsan Hassan Zaim et al. [8] employed laboratory analysis and simulation of different models to investigate different arrangements of pipes in the thermal dynamics of an asphalt collector with water-working fluid. Then, they presented the best model for maximizing energy efficiency. Other studies have tried to investigate the effect of various factors on the efficiency of an asphalt solar collector such as the effect of using glass on the collector, the effect of solar radiation intensity in hot and cold seasons, and also the performance of the collector at different flow rates. In a study, Amirpooya Masoumi et al. [9] investigated the role of various factors in increasing the efficiency of an asphalt solar water collector in laboratory conditions. The results of this study in two cold and hot months of the year show that in general, the inlet temperature of the collector has a greater effect on increasing its performance than the surface temperature and conductivity of asphalt. Farzan et al. [10] experimentally investigated the effect of flow rate on the efficiency and dynamic behavior of an asphalt collector with water as working fluid. Results show that by increasing the flow rate, the thermal efficiency of the collector increases. In another experimental study by Farzan et al. [11], the effect of glass on the performance of an asphalt solar water collector was investigated, which showed the beneficial effect of using a glass shield on the collector

*Corresponding Author's Email: ameri_mm@mail.uk.ac.ir (M. Ameri)

URL: https://www.jree.ir/article_155030.html



surface. Studies on the pipes material in asphalt collectors show that metal pipes, which are often copper pipes, have a greater effect on increasing the performance of the collector than other materials [6]. In previous studies, the performance of asphalt collectors, which were often responsible for water heating, has been numerically and experimentally investigated, and few studies have only touched the issue of the operation and daily energy and exergy efficiency of an asphalt solar air heater in real conditions. Saad et al. [12] built a solar air heater with a free convection flow to investigate the effect of environmental parameters, such as ambient temperature and wind speed, on asphalt and outlet air temperature. In free convection flow, due to the low amount of flow rate, thermal efficiency is negligible.

To the best of authors' knowledge, experimental investigation of an asphalt air solar collector and evaluation of energy and exergy efficiency considering forced convection heat transfer have not been studied yet. In this research, an asphalt collector with 15 pipes and area of 1.4 m² has been tested for 8 hours during a day for two mass flow rates. The main objective of this study is to compare the thermal and exergy efficiencies of the asphalt solar air collector in a forced convection heat transfer regime. Based on the results for thermal and exergy daily efficiency as well as the output temperature of the collector at different hours of the day, the advantages of using asphalt solar air collectors can be realized further.

2. EXPERIMENTAL

In this experimental study, a wooden mold made of thick Russian wood was used. Russian wood is very suitable for outdoor use due to its high resistance to environmental conditions. On the other hand, due to its very low heat transfer

coefficient, it does not easily transfer the heat stored in the asphalt layers to the environment and reduces the heat losses as much as possible. The asphalt used in this experiment is the commonly used asphalt in Iran. Thermophysical properties of asphalt are seen in Table 1 [8]. The substrate of this test is divided into two parts that are separated to be examined simultaneously for two flow rates. The area of each collector is 1.4 (m²) and 15 aluminum pipes are buried at the asphalt depth of 3 (cm) in each collector. The inside and outside diameters of each pipe are 19 and 20 (mm), respectively. The pipes are installed at a distance of 2 (cm) from each other. Two sticks are placed between the two collectors so that the collectors are not connected. The complete geometric characteristics of the collector are given in Table 2. Schematic of the asphalt solar air collector is shown in Figure 1.

Table 1. Thermal properties of asphalt

k (W/m ² .K)	C_p (J/kg.K)	ρ (kg/m ³)	ϵ
1	1485	2450	0.95

Table 2. Asphalt solar collector specifications under investigation

Length of the collector (cm)	200
Width of the collector (cm)	70
Height of collector (cm)	20
Asphalt depth (cm)	8
Thickness of sand layer under asphalt (cm)	11
Buried depth of pipes from the asphalt surface (cm)	3
Distance between pipes (cm)	2
The inner diameter of pipes (cm)	1.9
The outer diameter of pipes (cm)	2
Number of pipes per collector	15

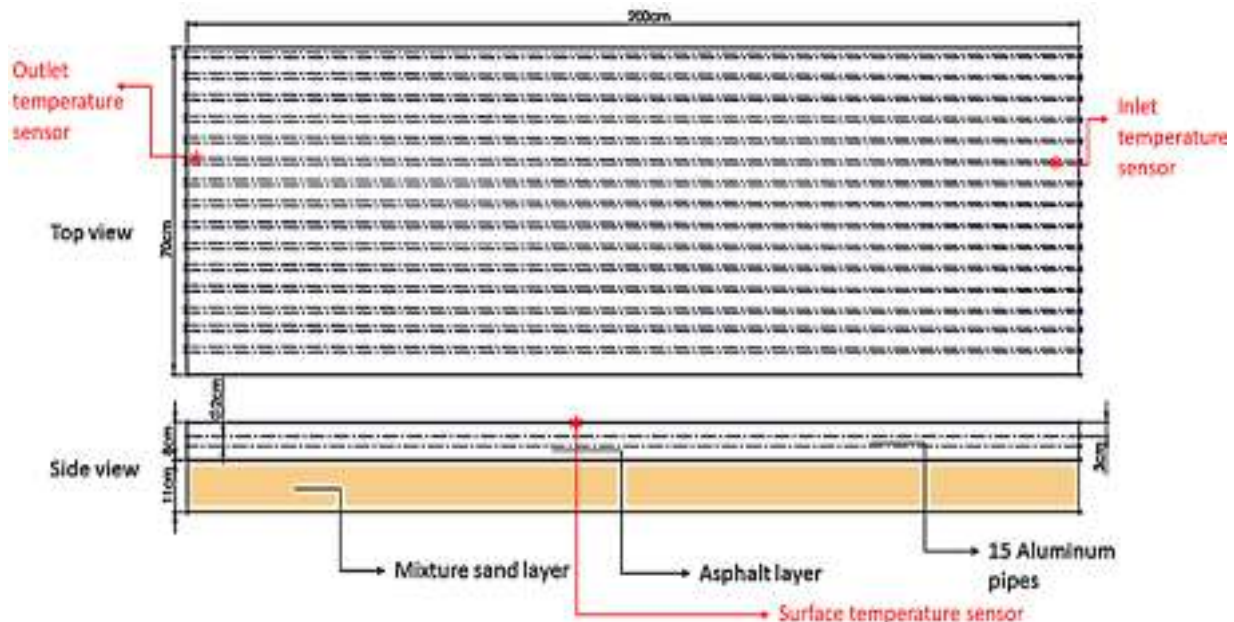


Figure 1. Schematic of the asphalt solar air collector

2.1. Test conditions

The test site was located in Kerman where the external factors such as trees and surrounding buildings do not affect the performance of the collector. Latitude and longitude in this place are 57.08 E and 30.28 N. The experiments were performed from 9 AM to 5 PM on November 3, when the

ambient temperature is relatively low. The Kipp & Zonen pyranometer model CMP 6B was used to measure the amount of total solar radiation. The intensity of the sun's rays is recorded every 15 minutes. Measurements at short intervals give a better comparison between the energy entering the collector by the sun and the energy leaving it by the air. An exhausted fan induces the ambient air into the collector.

Velocity measurement was done by an anemometer-type BENTECH GM816A and two desired flow rates were achieved by the changing outlet area. The flow rates considered in this experiment are 0.014 (kg/s) and 0.007 (kg/s), which change slightly due to a small change in the output density with time during the day and can be considered constant. For temperature measurements, temperature sensors TM1321 are used. The measurement accuracy for this sensor is up to three decimal places. Temperature sensors are used to measure the temperature of the surface of the asphalt as well as inlet and outlet air temperatures of the collector at any time, and they are recorded by connecting sensors to a computer. There is a temperature distribution on the collector surface; thus, the sensor at the surface temperature was placed at the center of the collector. The asphalt solar collector under consideration is shown in Figure 2. Pyranometer and temperature sensors are seen in Figures 3 and 4, respectively.



Figure 2. The asphalt solar collector under consideration



Figure 3. Pyranometer for measuring the intensity of solar radiation



Figure 4. Temperature sensor and transmitter type TM-1321

2.2. Uncertainty

Examining uncertainty in empirically conducted research is a very efficient and useful tool for calculating the number of errors in the results. The results extracted by the experiment may be subject to some errors, the main factor of which can be considered the accuracy of the measuring instrument. To obtain the amount of uncertainty during the experiment, Equation (1) is used [13].

$$w_R = \left[\sum_{i=1}^n \left(\frac{\partial R}{\partial x_i} w_{x_i} \right)^2 \right]^{1/2} \quad (1)$$

In this equation, R is a non-independent quantity and x is an independent quantity. w_R and w_{x_i} are the uncertainties for the quantities R and x, respectively.

The results of uncertainty along with the relative error based on the mean values defined by Equation (2) are seen in Table 3 [14].

$$E_R \% = \frac{w_R}{R} * 100 \quad (2)$$

Table 3. Relative errors and uncertainty of experimental data

Quantity	Uncertainty	E_R (%)
Temperature difference (°C)	± 0.1414	0.8
Mass flow rate (kg/s)	± 0.0009	6.3
Intensity of solar radiation (W/m ²)	± 5	0.6
Thermal efficiency (%)	± 0.010	5
Exergy efficiency (%)	± 0.012	0.2
Fan power consumption	± 0.04	3.8

Also, a graphical illustration of error bars is presented in Figure 5.

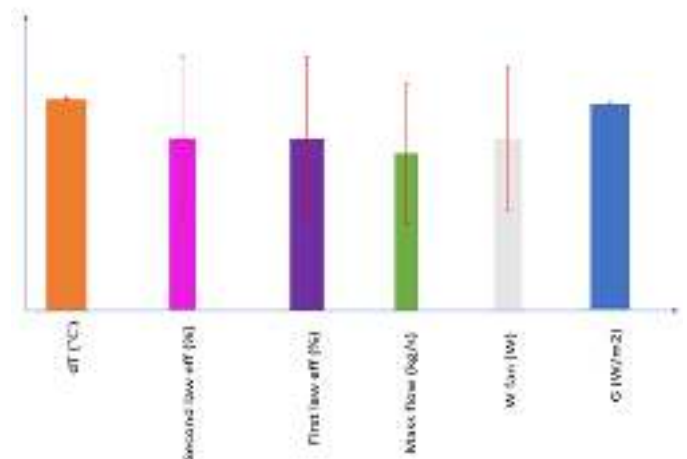


Figure 5. A graphical illustration of error bars

2.3. Thermal efficiency

To obtain the daily thermal efficiency of the collector, according to Equation (3) [15, 16], the values of inlet and outlet temperatures as well as the amount of solar radiation are needed. The amount of heat transfer into the air can be quantified by Equation (4). Due to the power consumption by the fan, this amount of electrical energy must be subtracted from the thermal energy by the fluid. For this reason, Figure shows that the temperature difference decreases with increasing flow rate, but increasing the flow rate increases the

thermal efficiency of the collector [10]. In Figure , it is clear that the maximum temperature difference is about one hour after the maximum intensity of solar radiation. Besides, the existence of temperature differences at the last hours of the day is an important result that demonstrates the ability of asphalt to store heat and to use this energy when the amount of solar radiation decreases.

$$\eta_{th,daily} = \frac{\sum \dot{q} - \sum \dot{E}_{el,fan}}{\sum G * A_C} \quad (3)$$

$$\dot{q} = \dot{m}C_p(T_{out} - T_{in}) \quad (4)$$

The pressure drop to be compensated by the fan can be calculated by Equation (5) and the consumed power by the fan can be obtained by Equation (6) [17]. The electrical power consumed by the fan is 1.1 (W) for the mass airflow rate of 0.014 (kg/s) and 0.36 (W) for 0.007 kg/s), respectively.

$$\Delta p = \frac{f\rho v^2}{2D} + \frac{k v^2}{2} \quad (5)$$

In Equation (5), f was considered 0.039 and 0.041 for mass flow rate of 0.014 (kg/s) and 0.007 (kg/s), respectively. Also, $k = 1.5$ [17].

$$\dot{E}_{el,fan} = \frac{\dot{m} * \Delta p}{\rho * \eta_{fan}} \quad (6)$$

Here, η_{fan} is fan efficiency which is 70 %.

In order to equalize the electrical energy consumed by the fan to thermal energy, an equivalence coefficient is employed. This factor is defined by Equation (7). The value of this coefficient depends on many parameters and factors such as the renewable energy market, exergy, greenhouse gas coefficients, and the number of fossil fuels in the country. According to Coventry and Lovegrove's research [18], this numerical value is between 1 and 17, such that the coefficient 1 is for energy efficiency and by increasing this value, it approaches the exergy efficiency. In Iran, according to the parameters of the renewable energy market, this amount can be considered as 4 [16].

$$r = \frac{\dot{E}_{el}}{\dot{E}_{th}} \quad (7)$$

2.4. Exergy efficiency

Due to the electrical energy consumed by the fan, the exergy loss by the fan should be subtracted from the useful exergy to the net pure exergy. The fluid entering the collector is ambient air; therefore, it has no exergy and only the input exergy to the control volume is supplied by solar radiation, which can be calculated by the patella relation given by Equation (8) as in the following [19].

$$\dot{E}_{in,sun} = GA_C \left(1 - \frac{4}{3} \frac{T_a}{T_{sun}} + \frac{1}{3} \left(\frac{T_a}{T_{sun}}\right)^4\right) \quad (8)$$

The useful exergy of the air can be calculated from Equation (9) [20].

$$\dot{E}_u = \dot{m}C_p [T_{out} - T_a - \left(T_a * \ln\left(\frac{T_a}{T_{out}}\right)\right)] \quad (9)$$

The net useful exergy is the difference between the amount of useful exergy and the fan exergy destruction. By using Equation (10), fan exergy destruction can be obtained by [17]:

$$\dot{E}_{dst,fan} = \frac{T_a}{T_F} \dot{E}_{el,fan} \quad (10)$$

In Equation (10) $\dot{E}_{el,fan}$ is the fan power, the value of which is 20 W. T_a is the ambient temperature and T_F is the temperature of the fluid, which is obtained from Equation (11) [21].

$$T_F = \frac{T_{out} - T_{in}}{\ln\left(\frac{T_{out}}{T_{in}}\right)} \quad (11)$$

The net useful exergy can be obtained by Equation (12) [22] as follows:

$$\dot{E}_{u,net} = \dot{E}_u - \dot{E}_{dst,fan} \quad (12)$$

Finally, the daily exergy efficiency of the collector can be determined by Equation 13 as follows [22]:

$$\eta_{exe} = \frac{\sum \dot{E}_{u,net}}{\sum \dot{E}_{in,sun}} \quad (13)$$

3. RESULTS AND DISCUSSION

The main purpose of this research is to investigate experimentally the performance of an asphalt solar air collector in terms of energy and exergy efficiencies. The affecting parameters can be categorized into environmental and construction ones. Environmental parameters include the amount of incident radiation on the collector surface, wind speed, and ambient temperature, which is the inlet temperature to the collector. The most important construction parameters are the materials used in the construction of the collector, pipes, and insulation. In the present study, asphalt has been used as the main material in the construction of the collector, which can absorb and store high thermal energy. Low-thickness aluminum has been selected for the pipe material, which increases the heat transfer coefficient to the airflow inside the pipes. In addition to their high heat transfer coefficient, the use of aluminum pipes is more advantageous over copper ones because it is lighter and cheaper. Figure shows the variation of ambient temperature and solar radiation intensity during a typical day.

Error! Reference source not found. shows the temperature difference between the inlet and outlet of the collector. It is seen that the temperature difference is reduced by increasing the flow rate, but increasing the flow rate increases the thermal efficiency of the collector [10]. The maximum temperature difference is about 25 K and 19 K for the mass flow rates of 0.007 kg/s and 0.014 kg/s, respectively. In Figure , it is also clear that the maximum temperature difference is about one hour after the maximum intensity of solar radiation. Besides, the existence of temperature differences at the last hours of the day is an indication of the asphalt ability to store heat.

According to the results obtained from the collector efficiency in Table , it can be seen that by increasing the flow rate, both thermal and exergy efficiencies increase.

Figure shows the variation of the surface center temperature of the collector during a typical day at two mass flow rates.

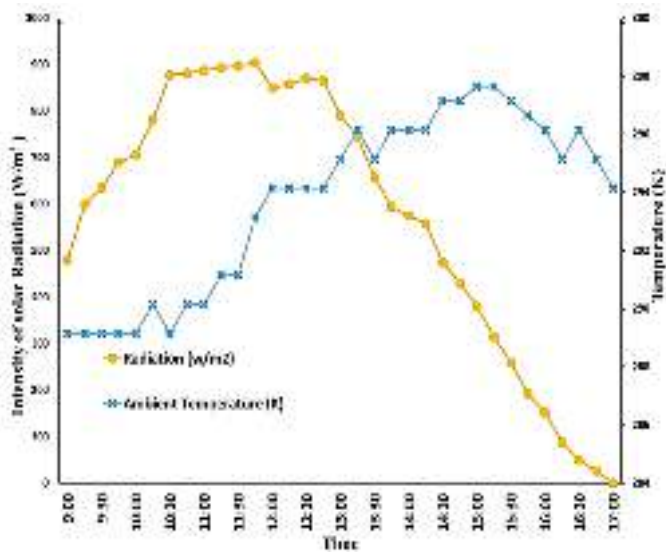


Figure 6. Ambient temperature and solar radiation intensity (2021/11/03)

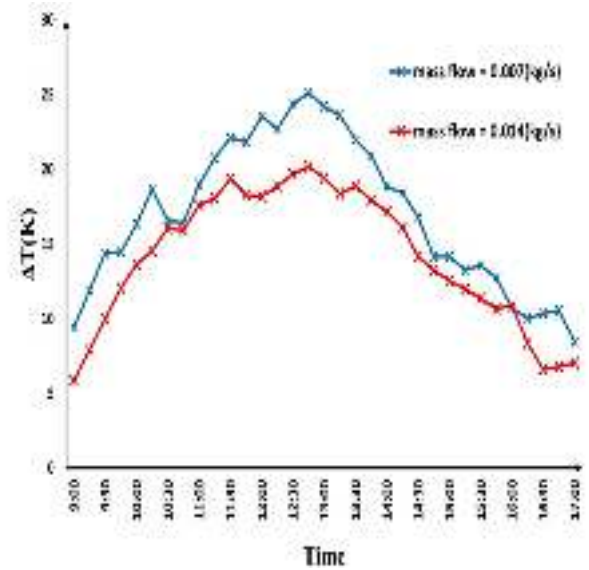


Figure 7. Variation of collector inlet and outlet temperature difference

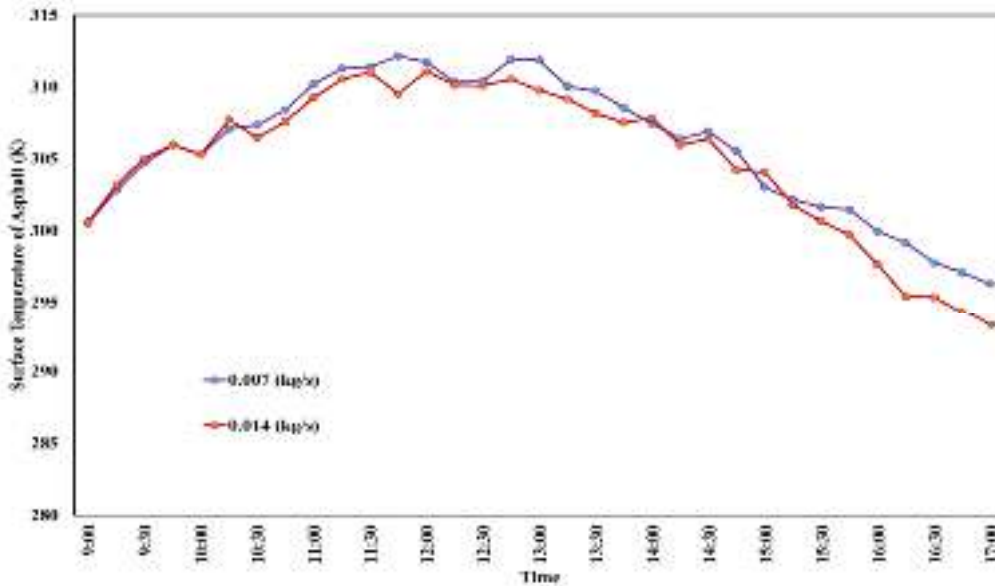


Figure 8. Variation of the surface center temperature of the collector

A better understanding of the exergy efficiency is secured by comparing the values of exergy obtained in each part. The amounts of useful exergy of the fluid and the exergy destruction of the fan are quite smaller than the amount of exergy input by the solar radiation, hence low exergy efficiency. Figure shows the input exergy from the sun. **Error! Reference source not found.** and **Error! Reference source not found.** show the comparison of useful exergy, net useful exergy, and exergy destruction of the fan at mass flow rates of 0.014 kg/s and 0.007 kg/s, respectively. According to **Error! Reference source not found.**10 and **Error!**

Reference source not found., at the final hours of the experiment, when the sun's radiant energy is low, the net useful exergy is very low. By comparing the results in **Error! Reference source not found.** and **Error! Reference source not found.**, it can be seen that lowering the flow rate reduces electricity consumption and subsequently decreases the exergy destruction, which makes the net useful exergy higher at the final hours. Since the useful exergy is dependent on the outlet temperature, its value tends to zero at the end of the day. Therefore, it can be concluded that the best hours to keep the fan on are the hours when the sun radiation is not very low.

Figure 9. Input exergy of solar radiation

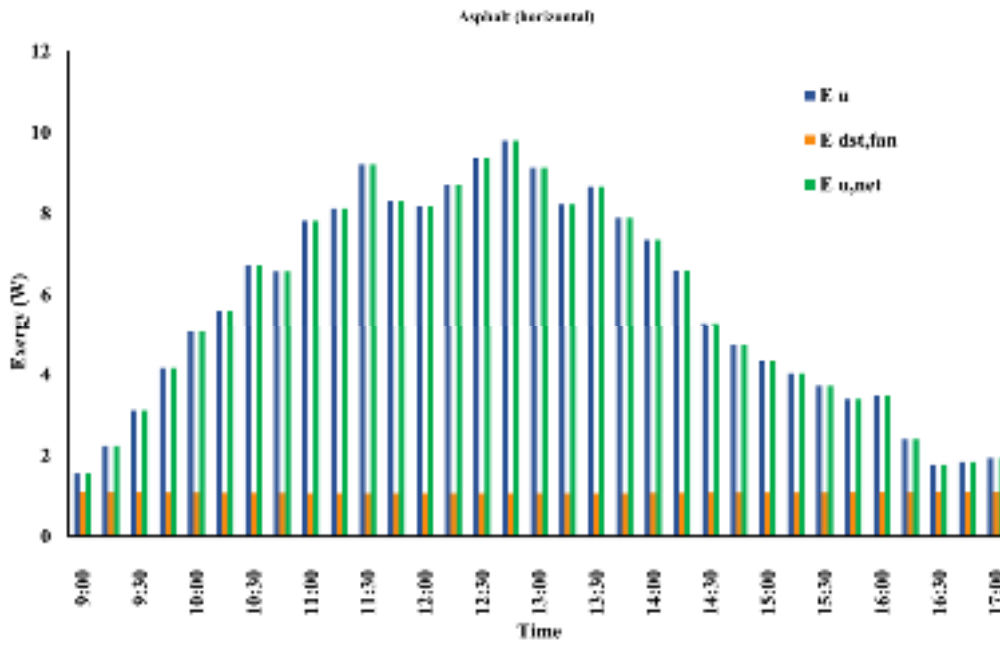
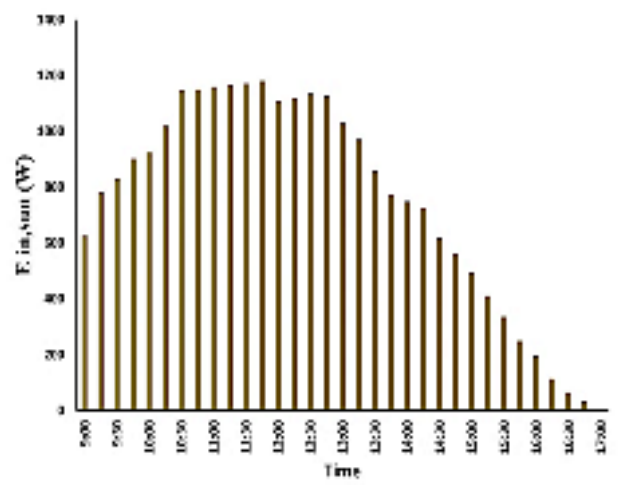


Figure 10. Comparison of useful exergy, net useful exergy, and exergy destruction of the fan for $\dot{m}=0.014$ (kg/s)

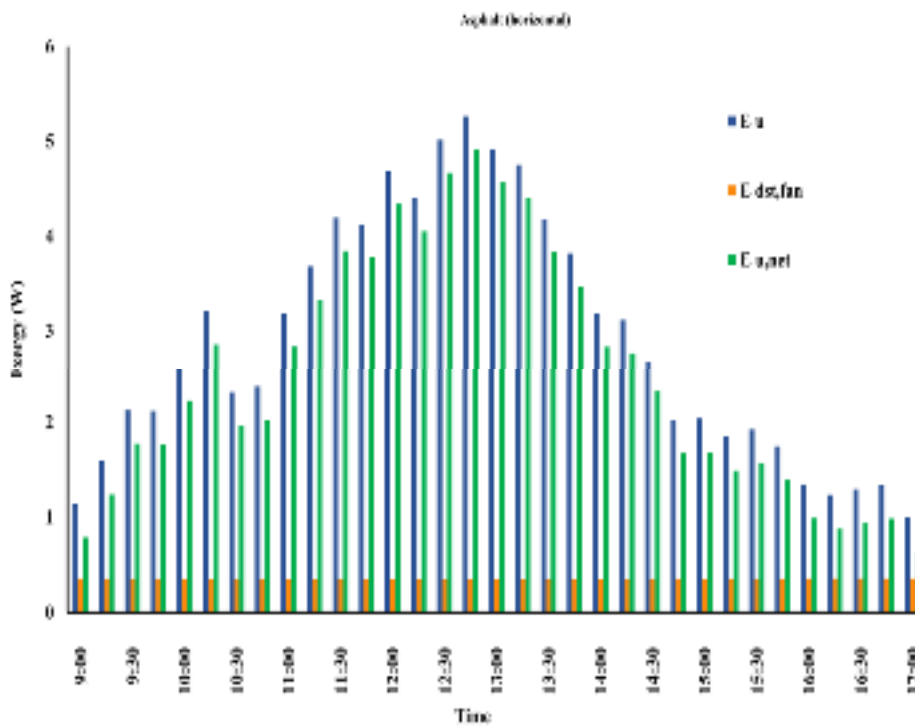


Figure 11. Comparison of useful exergy, net useful exergy, and exergy destruction of the fan for $\dot{m}=0.007$ (kg/s)

Table 4. Daily thermal and exergy efficiency of the collector

\dot{m} (kg/s)	$\eta_{th,daily(no-fan)}$ (%)	$\eta_{th,daily}$ (%)	$\eta_{th,daily,r=4}$ (%)	$\eta_{exe,daily}$ (%)
0.014	24.24	24.10	23.66	0.66
0.007	12.03	11.98	11.85	0.34

4. CONCLUSIONS

In this research, an asphalt solar air heater was tested experimentally at two different flow rates. The final results of this research included the energy and exergy efficiency on a daily basis as well as the outlet temperature of the collector. The obtained results can be listed as:

- Increasing air mass flow rate increases thermal and exergy efficiencies.
- The presence of temperature differences at the last hours of the day and even after sunset indicates the ability of asphalt in storage and releasing heat when there is no radiant energy source.
- In the process of calculating the exergy efficiency on a daily basis, to obtain the net useful exergy, we subtract the amount of exergy destruction by the fan from the useful exergy of the collector. Exergy efficiency starts to decrease when the sun radiation decreases, given the reduction of the amount of exergy entering the collector.

As a result, to design an optimal collector, both the efficiency factor and the outlet temperature must be considered simultaneously so that we can have a high outlet temperature by having a collector with proper efficiency. Also, from the results obtained from exergy calculations, two cases can be considered for improving the collector efficiency:

- Setting a time interval for the fan to be on or off
- Using variable flow rate during the day

For further research, glazing of the collector is recommended. Also, it is recommended that a simulation by CFD be conducted to investigate the effect of different parameters on the performance of the collector.

5. ACKNOWLEDGEMENT

The authors would like to thank Shahid Bahonar University of Kerman for their support.

NOMENCLATURE

A	Area (m ²)
G	The intensity of solar radiation (W/m ²)
C _p	Specific heat capacity (kJ/kg.K)
q̇	Thermal energy transferred by the fluid (kJ/s)
Ė	Exergy (W)
T	Temperature (K)
r	Equivalence coefficient
R	Non-independent parameter
x _i	Independent parameter
w	Uncertainty
f	Friction factor
l	Length of each pipe (m)
Δp	Pressure drop (Pa)
D	Outlet diameter (m)
v	Velocity (m/s)
ρ	Density (kg/m ³)
ε	Emissivity

Greek letters

η	Efficiency
---	------------

Indices

c	Collector
a	Air
in	Inlet
out	Outlet
F	Fluid
el	Electrical
th	Thermal
fan	Fan
sun	Sun
dst	Destruction
exe	Exergy
u	Useful
net	Net
daily	Daily
eq	Equivalent

REFERENCES

1. Gandjalikhan Nassab, S.A. and Moein Addini, M., "Performance augmentation of solar air heater for space heating using a flexible flapping guide wingle", *Iranian (Iranica) Journal of Energy & Environment*, Vol. 12, No. 2, (2021), 161-172. (<https://dx.doi.org/10.5829/jjee.2021.12.02.09>).
2. Daghigh, A. and Shafieian, A., "Thermal performance of a double-pass solar air heater", *Journal of Renewable Energy and Environment (JREE)*, Vol. 3, No. 2, (2016), 35-46. (<https://dx.doi.org/10.30501/jree.2016.70083>).
3. Nnamchi, S.N., Nnamchi, O.A. Sangotayo, E.O. Ismael, S.A., Nkurunziza, O.K. and Gabriel, V., "Design and simulation of air-solar preheating unit: An improved design of a flat plate solar collector", *Iranian (Iranica) Journal of Energy & Environment*, Vol. 11, No. 2, (2020), 97-108. (<https://dx.doi.org/10.5829/jjee.2020.11.02.02>).
4. O'Hegarty, R., Kinnane, O., and McCormack, S.J., "Concrete solar collectors for façade integration: An experimental and numerical investigation", *Applied Energy*, Vol. 206, (2017), 1040-1061. (<https://doi.org/10.1016/j.apenergy.2017.08.239>).
5. Larsson, O. and Thelandersson, S., "Estimating extreme values of thermal gradients in concrete structures", *Materials and structures*, Vol. 44, No. 8, (2011), 1491-1500. (<https://doi.org/10.1617/s11527-011-9714-0>).
6. Bobes-Jesus, V., Pascual-Muñoz, P., Castro-Fresno, D. and Rodriguez-Hernandez, J., "Asphalt solar collectors: A literature review", *Applied Energy*, Vol. 102, (2013), 962-970. (<https://doi.org/10.1016/j.apenergy.2012.08.050>).
7. Chiarelli, A., Al-Mohammedawi, A., Dawson, A. and Garcia, A., "Construction and configuration of convection-powered asphalt solar collectors for the reduction of urban temperatures", *International Journal of Thermal Sciences*, Vol. 112, (2017), 242-251. (<https://doi.org/10.1016/j.ijthermalsci.2016.10.012>).
8. Zaim, E.H., Farzan, H. and Ameri, M., "Assessment of pipe configurations on heat dynamics and performance of pavement solar collectors: An experimental and numerical study", *Sustainable Energy Technologies and Assessments*, Vol. 37, (2020), 100635. (<https://doi.org/10.1016/j.seta.2020.100635>).
9. Masoumi, A.P., Tajalli-Ardekani, E. and Golneshan, A.A., "Investigation on performance of an asphalt solar collector: CFD analysis, experimental validation and neural network modeling", *Solar Energy*, Vol. 207, (2020), 703-719. (<https://doi.org/10.1016/j.solener.2020.06.045>).
10. Farzan, H., Jaafarian, S.M. and Ameri M., "Experimental and theoretical investigation of flow rate effect on dynamic and efficiency of asphalt solar collector in real operating condition", *Modares Mechanical Engineering*, Vol. 20, No. 5, (2020), 1271-1282. (In Farsi). (<http://mme.modares.ac.ir/article-15-33507-en.html>).
11. Farzan, H., Zaim, E.H. and Ameri, M., "Study on effect of glazing on performance and heat dynamics of asphalt solar collectors: An

- experimental study", *Solar Energy*, Vol. 202, (2020) 429-437. (<https://doi.org/10.1016/j.solener.2020.04.003>).
12. Saad, H.E., Kaddah, K.S., Sliem, A.A., Rafat, A. and Hewhy, M.A., "The effect of the environmental parameters on the performance of asphalt solar collector", *Ain Shams Engineering Journal*, Vol. 10, No. 4, (2019), 791-800. (<https://doi.org/10.1016/j.asej.2019.04.005>).
 13. Kline, S.J., "Describing uncertainty in single sample experiments", *Mechanical Engineering*, Vol. 75, (1953), 3-8. (<https://ci.nii.ac.jp/naid/10007206317>).
 14. Kabeel, A.E., Hamed, M.H., Omara, Z.M. and Kandeal, A.W., "Influence of fin height on the performance of a glazed and bladed entrance single-pass solar air heater", *Solar Energy*, Vol. 162, (2018) 410-419. (<https://doi.org/10.1016/j.solener.2018.01.037>).
 15. Kalogirou, S.A., *Solar energy engineering: Processes and systems*, Academic press, Elsevier Science, (2013). (https://www.google.com/books/edition/Solar_Energy_Engineering/wYRqAAAAQBAJ?hl=en&gbpv=0).
 16. Ameri, M., Sardari, R. and Farzan, H., "Thermal performance of a V-corrugated serpentine solar air heater with integrated PCM: A comparative experimental study", *Renewable Energy*, Vol. 171, (2021), 391-400. (<https://doi.org/10.1016/j.renene.2021.02.113>).
 17. Pritchard, P.J. and Mitchell, J.W., *Fox and McDonald's introduction to fluid mechanics*, John Wiley & Sons, (2016). (https://www.google.com/books/edition/Fox_and_McDonald_s_Introduction_to_Fluid/v4T3DwAAQBAJ?hl=en&gbpv=0).
 18. Coventry, J.S. and Lovegrove, K., "Development of an approach to compare the 'value' of electrical and thermal output from a domestic PV/thermal system", *Solar Energy*, Vol. 75, No. 1, (2003), 63-72. ([https://doi.org/10.1016/S0038-092X\(03\)00231-7](https://doi.org/10.1016/S0038-092X(03)00231-7)).
 19. Petela, R., "Exergy of undiluted thermal radiation", *Solar Energy*, Vol. 74, No. 6, (2003), 469-488. ([https://doi.org/10.1016/S0038-092X\(03\)00226-3](https://doi.org/10.1016/S0038-092X(03)00226-3)).
 20. Kalogirou, S.A., Karellas, S., Braimakis, K., Stanciu, C. and Badescu, V., "Exergy analysis of solar thermal collectors and processes", *Progress in Energy and Combustion Science*, Vol. 56, (2016) 106-137. (<https://doi.org/10.1016/j.pecc.2016.05.002>).
 21. Holman, J.P., *Heat transfer*, McGraw-hill, (1986). (https://www.google.com/books/edition/Heat_Transfer/ksqNzgEACAAJ?hl=en).
 22. Gholampour, M. and Ameri, M., "Energy and exergy analyses of photovoltaic/thermal flat transpired collectors: Experimental and theoretical study", *Applied Energy*, Vol. 164, (2016), 837-856. (<https://doi.org/10.1016/j.apenergy.2015.12.042>).



Research Article

An Optimal Master-Slave Model for Stochastic Planning of AC-DC Hybrid Distribution Systems

Zeinab Sabzian-Molaei^a, Esmaeel Rokrok^{b*}, Meysam Doostizadeh^b

^a Department of Electrical Engineering, Khorramabad Branch, Islamic Azad University, Khorramabad, Lorestan, Iran.

^b Department of Electrical Engineering, Lorestan University, Khorramabad, Lorestan, Iran.

PAPER INFO

Paper History:

Received: 05 January 2022

Revised: 02 June 2022

Accepted: 14 June 2022

Keywords:

AC-DC Distribution Systems,
Stochastic Planning,
Graph Theory,
Converter Efficiency Curve,
Distributed Energy Resources,
Electric Vehicle Charging Stations

ABSTRACT

In this study, a novel stochastic planning method is proposed for AC-DC hybrid distribution networks. The proposed approach is based on the graph theory, and the optimal AC-DC structure of the network is selected among the system spanning trees. The presented method is a Mixed Integer Nonlinear Programming (MINLP) problem, which is solved using genetic algorithm. The buses and lines of the network can be either AC or DC to minimize the system investment costs in the master optimization problem. The location and capacity of the Distributed Energy Resources (DERs) as well as the site and size of the Electric Vehicle (EV) charging stations are optimized in the slave problem to minimize the network losses and system costs. The proposed model utilizes Monte Carlo simulation to deal with the stochastic variations of the renewable energy resources power and load demands. Besides, the converter efficiency curve in the proposed planning problem is modeled based on a function of its input current using PLECS software. The proposed approach for network design can be applied to different DG resources and AC-DC loads. The comparison between the simulation results of the proposed approach and the conventional AC planning method demonstrates the efficiency of the proposed model in reducing network losses and system costs.

<https://doi.org/10.30501/jree.2022.323167.1309>

1. INTRODUCTION

Integration of Distributed Energy Resources (DERs) with Distribution Systems (DSs) has increased the ratio of DERs operation and reduced the investment costs in DSs [1]. Green technology, such as photovoltaic (PV) generation resources, and DC loads, such as electric vehicle (EV) charging stations, are used increasingly and higher levels of reliability and power quality are demanded at the same time. Therefore, the AC power distribution system cannot continue using the traditional approach to manage and control energy effectively in this new condition. Hence, a hybrid AC-DC system is proposed as a solution to improve the network performance in terms of network losses, addressing DERs oscillations, and more flexible settings for the new network structures than the traditional AC systems [2-5].

The planning of AC-DC hybrid DSs is more complicated than the AC planning systems due to the presence of various buses, AC-DC lines, and AC-DC converters. The power electronic converters should be modeled correctly, and analysis of stochastic variations of AC-DC load demands, such as EV charging stations and DERs (PV resources and wind turbines), adds up to the complexity of the hybrid

planning problem. Also, determining the optimal size and location of some system components such as EV charging stations and DERs is another important issue that should be considered. Therefore, it is necessary to present suitable methods for AC-DC hybrid systems planning in the researches. However, the studies on hybrid DSs planning are still in the primary stages, and no comprehensive planning approach has yet been proposed to consider all the above-mentioned factors in the AC-DC DSs.

The primary studies in the field of hybrid systems planning have focused on HVDC networks. For instance, the development of Voltage Source Converter (VSC)-based transmission systems was investigated in [6], aiming at reducing investment, operation, and load shedding costs of the system. Also, a multi-objective stochastic planning model was employed in [7] in order to define the HVDC network lines so that the investment costs and the reactive power losses could be minimized. The need to deliver generated electricity by offshore wind farms led to further research on the development of a VSC-based offshore network in [8, 9]. In addition, a transmission expansion planning model was proposed in [10] by utilizing the Benders Decomposition (BD) algorithm in order to reduce system costs, including ES (energy storage) installation costs. However, the studies in [6-10] are suitable for HVDC systems, and they are not efficient

*Corresponding Author's Email: rokrok.e@lu.ac.ir (E. Rokrok)
URL: https://www.jree.ir/article_155117.html



enough to be applied to complicated DSs with cascaded AC-DC structure.

Due to the development of AC-DC hybrid DSs in recent years, the studies on the planning of these systems have increased in number. For instance, a hybrid system planning approach based on optimal location and size of Renewable Energy Systems (RESs) and ESs was proposed in [11]. Furthermore, a two-level planning technique was presented in [12] that investigated N-1 security criterion. At the first level of this model, the system investment and operation costs were minimized. Then, the second level of the planning problem (as a robust optimization problem) enhanced the system reliability. Also, a flexible multi-stage distribution expansion planning model is introduced in [13] to analyze the variations caused by the output power of DGs and loads demand. A hybrid planning model based on Benders analysis was also proposed in [14] to minimize the power losses in commercial buildings. Besides, an AC-DC planning strategy was presented in [15] for distribution network, which considered the uncertainties caused by generation resources, loads, and energy prices. This method considers the environmental concerns as well as system investment and operation costs, and it also enables network islanding to improve the system reliability.

In the microgrid connected to the main grid, a planning model was presented in [16], where the total system costs were minimized by determining bus types and optimal size of DGs. Moreover, a two-stage planning approach was proposed in [17], which defined the optimal size of power electronic converters and the microgrid type in the islanding mode.

However, the studies in [16, 17] are limited to the predefined network structures, while the configuration definition of AC-DC network among all probable network structures is one of the main concerns in the upgrading of AC network to AC-DC system.

Currently, a few studies have considered the planning of hybrid distribution systems by determining the type of network lines and buses (AC or DC). For instance, in [18], a conceptual planning model was presented for hybrid DSs which minimized the system costs by determining optimal AC-DC configuration of network buses and lines as well as optimal size of converters. However, in this method, all possible AC-DC structures of the network are not considered, and only a limited number of them are investigated. Besides, the studies in [19, 20] employed binary matrices to introduce VSC-based AC-DC networks and investigated all possible structures of the network in order to reach the optimal configuration of the AC-DC hybrid DSs. Nevertheless, the studies in [19, 20] did not cover various combinations of DG resources in terms of location and size.

On the other hand, most studies in the field of hybrid systems planning have either presented an accurate model of converter losses and approximated converter losses [8-11, 19, 20] or have completely ignored the matter for the sake of simplicity of calculations [5, 15-16, 18].

In this study, a stochastic planning method is presented for AC-DC hybrid DSs based on graph theory. The proposed model utilizes the Monte Carlo scenario generation method to investigate the stochastic variations of the renewable energy resource output and AC-DC load demand. In addition, VSC is used for power conversion. The planning problem is solved as a Mixed Integer Nonlinear Programming (MINLP) problem using Genetic Algorithm (GA) in MATLAB. The proposed method is evaluated by comparing the results of the presented

AC-DC hybrid approach with those of the traditional AC solution.

The main contributions of this paper are as follows:

- 1) A stochastic master-slave planning strategy for AC-DC DSs is presented based on the graph theory.
- 2) The optimal network configuration is determined by investigating all radial configurations of the AC-DC network. All radial structures of the system are defined as the network spanning trees, and they are generated using the Spantree program in MATLAB.
- 3) A comprehensive planning model is proposed for AC-DC hybrid DSs. The site and capacity of distributed energy resources and electric vehicle charging stations are optimized by DERs and EVs planning in the slave optimization problem.
- 4) The converter efficiency curve is modeled in the AC-DC planning formulation.

In the first step, the converter losses are modeled as a function of converter input power in PLECS (Piecewise Linear Electrical Circuit Simulation) software. In the next step, the converter efficiency curve is employed in the load flow equations in order to reach more accurate results in the planning problem solution.

The rest of the paper is organized as follows. Section 2 presents the planning problem outline. The details of the proposed planning formulation are described in Section 3. Section 4 is devoted to the analysis of simulation results. Section 5 summarize the conclusions.

2. PROBLEM OUTLINE

As shown in Figure 1, AC-DC hybrid DSs include different AC-DC loads, AC-DC generation resources, and AC-DC buses and lines. These loads and DGs are connected to the network via AC-DC converters. The AC and DC buses also use AC-DC converters to connect to each other.

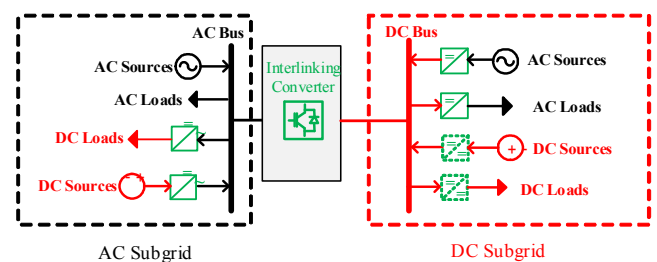


Figure 1. General structure of AC-DC hybrid DSs

In this study, the main objective of the planning problem is finding the optimal AC-DC structure for hybrid DSs. For this purpose, planning decision variables are divided into two categories as follows:

- A) The variables that determine the AC-DC radial structure of the network including 1) system bus type (AC or DC), 2) existence of the connection between two buses, and 3) network lines type (AC or DC).
- B) The variables related to DERs or EVs planning including the location and capacity of DERs and also the site and size of EV charging stations.

In this study, VSC is utilized to connect different AC-DC loads and generation resources to the network buses as well as

power conversions. In the following, the modeling procedure of the converter efficiency curve is presented in order to be employed in Load Flow (LF) calculations.

2.1. Converter model

The AC-DC systems consist of AC and DC subnetworks where AC and DC components can be connected by VSC. Equation (1) shows the relationship between the voltages of the two sides of the converter in terms of modulation index, M [19].

$$V_{dc,c}^{pu} = M^{-1} \times V_{ac,c}^{pu} \quad (1)$$

VSC is used in two operating modes, including inverter mode and rectifier mode. The relationship between the input and output power of the converter in two operating modes is determined by Equations (2) and (3), respectively, where η is the converter efficiency. The value of η can be obtained by Equation (4) in terms of input power, P_{in} , output power, P_{out} , and converter losses, $P_{loss,c}$.

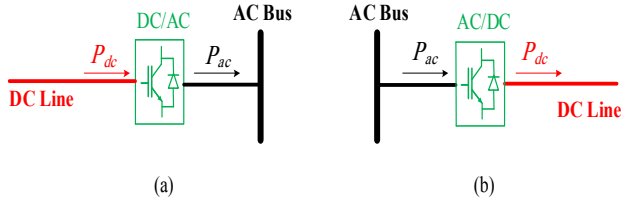


Figure 2. The operating modes of converter: (a) inverter mode and (b) rectifier mode

$$P_{out,c} = P_{ac} = \eta \times P_{dc} \quad (2)$$

$$E_{igbt/diode}^{sw} = a_{igbt/diode} i(t) e^{b_{igbt/diode}} + c_{igbt/diode} i(t) e^{d_{igbt/diode}} \quad (6)$$

where $E_{igbt/diode}^{sw}$ represents the switching losses of transistor or diode, in which $\{a, b\}$ and $\{c, d\}$ are the curve fitting constants for switching-on and switching-off losses, respectively.

The total switching losses are described as [22]:

$$P_{total}^{sw} = 6 \times f_s \times (E_{igbt}^{sw} + E_{diode}^{sw}) \quad (7)$$

In addition, fixed losses include inductor inductance losses, filters and transformers, controller circuit losses, leakage current losses, and so on. Therefore, the total converter losses are obtained as follows:

$$P_{total}^{loss} = P_{total}^{cond} + P_{total}^{sw} + P_{constnt} \quad (8)$$

In this stage, the converter losses are calculated by simulation in PLECS for different input powers of the converter. The circuit contains a heat-sink unit, and its junction temperature range is adjusted by the R_{th} resistor between 25 °C and 150 °C.

Step (2): Fitting the converter efficiency curve

According to the values of power losses calculated in Step 1, the converter efficiency is fitted as a function of the input

$$P_{out,c} = P_{dc} = \eta \times P_{ac} \quad (3)$$

$$\eta = \frac{P_{out}}{P_{in}} = \frac{P_{in} - P_{loss,c}}{P_{in}} \quad (4)$$

The amount of power losses is dependent on the converter input power. The converter efficiency is a function of the input power of the converter. Therefore, the converter efficiency is not a constant value, and can be obtained by the converter efficiency curve. Accordingly, using the application of the converter efficiency curve to model its losses in power flow equations yields more accurate results in LF solution.

In this paper, the converter efficiency curve is obtained for a typical converter that has six IGBT switches from an ABB “HiPak” module 5SNA 0650J450300, designed to be used as a single IGBT-diode pair rated for 4500 V and 650. The converter efficiency curve is used in the power flow equations according to the following steps:

Step (1): The converter loss calculation by simulation in PLECS

Total VSC loss is equals to the sum of conduction, switching and fixed losses. The VSC conduction losses includes transistor conduction losses and diode conduction losses, and they are expressed as follows [21]:

$$P_{total}^{cond} = 6 \times (P_{igbt}^{cond} + P_{diode}^{cond}) \quad (5)$$

The switching losses of the converter include the total switching losses of the diode and transistor, which is made up of two sections: switching-off losses and switching-on losses. The switching losses equal:

power to the converter in Equation (9). For the converter used in this paper, the efficiency curve is given in Figure 3.

$$\eta = f(P_{in,c}) \quad (9)$$

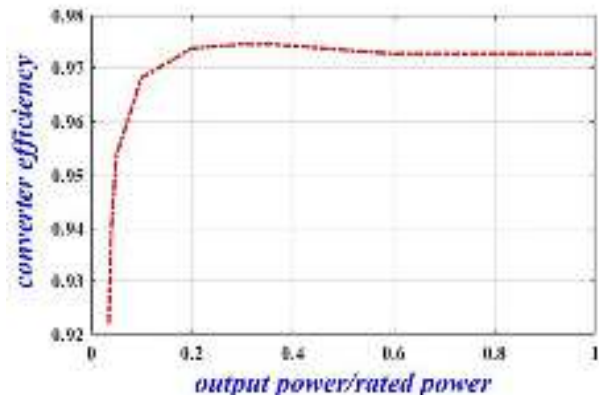


Figure 3. The converter efficiency curve for typical converter

Step (3): Modeling the converter efficiency curve in power flow equations

In this stage, the relationship between the output and input powers of the converter is obtained for both converter operating modes by combining Equations (2), (3), and (9) as:

$$P_{out,c} = f(P_{in,c}) \times P_{in,c} \quad (10)$$

The accurate value of converter losses is calculated by considering Equation (10) in load flow solution.

Figure 4 demonstrates the conducted process for modeling converter efficiency in power flow equations.

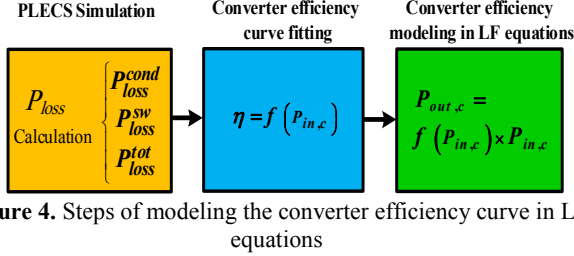


Figure 4. Steps of modeling the converter efficiency curve in LF equations

2.2. Scenarios definition

In this study, the uncertainties related to the generation of renewable resources and power demand in EV charging stations are expressed by Johnson's distribution function as Equation (11). The Pareto distribution function according to

$$\left\{ \begin{array}{l} P_{WT} = \{(\alpha_{WT,1}, \beta_{WT,1}), (\alpha_{WT,2}, \beta_{WT,2}), \dots, (\alpha_{WT,n}, \beta_{WT,n})\} \\ \sum_n \beta_{WT,n} = 1 \end{array} \right\} \quad (13)$$

$$\left\{ \begin{array}{l} P_{PV} = \{(\alpha_{PV,1}, \beta_{PV,1}), (\alpha_{PV,2}, \beta_{PV,2}), \dots, (\alpha_{PV,n}, \beta_{PV,n})\} \\ \sum_n \beta_{PV,n} = 1 \end{array} \right\} \quad (14)$$

$$\left\{ \begin{array}{l} P_L = \{(\alpha_{L,1}, \beta_{L,1}), (\alpha_{L,2}, \beta_{L,2}), \dots, (\alpha_{L,n}, \beta_{L,n})\} \\ \sum_n \beta_{L,n} = 1 \end{array} \right\} \quad (15)$$

$$\left\{ \begin{array}{l} P_{EV} = \{(\alpha_{EV,1}, \beta_{EV,1}), (\alpha_{EV,2}, \beta_{EV,2}), \dots, (\alpha_{EV,n}, \beta_{EV,n})\} \\ \sum_n \beta_{EV,n} = 1 \end{array} \right\} \quad (16)$$

where $\alpha_{WT,n}$, $\alpha_{PV,n}$, $\alpha_{L,n}$, and $\alpha_{EV,n}$ represent the n th stochastic variables for wind generation, photovoltaic generation, load consumption, and EV charging station demand, respectively. The corresponding probability with each of the mentioned variables is demonstrated as $\beta_{WT,n}$, $\beta_{PV,n}$, $\beta_{L,n}$, and $\beta_{EV,n}$, respectively.

Furthermore, all generated uncertainty sets should be combined to create an uncertainty scenario set, and the sum of the probabilities of generated scenarios must be equal to 1. Therefore, we have:

$$\left\{ \begin{array}{l} S = P_L \times P_{WT} \times P_{PV} \times P_{EV} \\ \sum_{s \in S} \beta_L \times \beta_{WT} \times \beta_{PV} \times \beta_{EV} = 1 \end{array} \right\} \quad (17)$$

Finally, the Kantorovich scenario reduction method is used to reduce the calculations of the optimization problem. More details can be found in [23].

3. PROPOSED MODEL

In this study, the planning model is an MINLP problem with discrete derivatives, which is not optimized in one optimization model because of its complexity. Hence, the proposed planning approach is formulated as a master-slave

model. The master optimization problem is a Mixed Integer Programming (MIP) problem and it defines the network AC-DC structure using the GA, while the slave optimization problem is a Non-Linear Programming (NLP) problem that defines the location and size of DERs and EV charging stations.

$$CDF(X) = \frac{1}{\sqrt{2\pi}} \int_0^{\gamma_1 + \gamma_2 \ln\left(\frac{z}{z-1}\right)} e^{-0.5t^2} dt \quad (11)$$

$$CDF(X) = 1 - \left(1 + \lambda_1 \frac{(x - \lambda_2)}{\lambda_3}\right)^{-\frac{1}{\lambda_1}}, \quad \lambda_1 \neq 0 \quad (12)$$

where $CDF(X)$ represents the cumulative distribution function of stochastic variable X ; γ_1 , γ_2 , and λ_1 are shape parameters; $z = \frac{x - \lambda_2}{\lambda_3}$; γ_4 and λ_2 are location parameters; scale parameters are γ_3 and λ_3 .

The obtained scenarios from discrete probability distribution sets for wind turbine generation, P_{WT} , photovoltaic generation, P_{PV} , load consumption, P_L , and EV charging station demand, P_{EV} , are defined as follows [23]:

model. The master optimization problem is a Mixed Integer Programming (MIP) problem and it defines the network AC-DC structure using the GA, while the slave optimization problem is a Non-Linear Programming (NLP) problem that defines the location and size of DERs and EV charging stations.

3.1. The master problem

According to the proposed framework for AC-DC hybrid DS planning, the decision for defining the network radial structure and the location and the capacity of the resources is made in the first year of the planning horizon time.

The main purpose of the proposed planning problem is to determine the optimal AC-DC network topology with the aim of minimizing system costs and network losses, by considering the constraints of the optimization problem, which is defined as:

$$\left\{ \begin{array}{l} \text{Min } F_{\text{Master}} = [C_{NP} \quad P_{\text{Loss}}] \\ C_{NP} = C_{\text{Inv}} + C_{\text{OM}} \end{array} \right\} \quad (18)$$

$$\text{s.t. } n_b \leq L_{\text{max}} \quad \forall b \in \text{NB}, s \in S \quad (19)$$

where C_{NP} is the network planning cost. Also, the system investment cost, C_{Inv} , including the investment cost of lines, C_{Line} , and the investment cost of converters, C_{Conv} .

Because the optimal structure is selected from a set of spanning trees of the network graph, the system buses are not isolated. Therefore, only the maximum bus connection limit is investigated as Equation (19). Also, the radial structure constraint of the network in this study is achieved using the Spantree program in MATLAB.

$$\text{Min } F_{\text{Slave}} = [C_{OM} \quad P_{\text{Loss}}] \quad (20)$$

$$F_{\text{Slave}} = \left[\sum_{s=1}^{N_s} \sum_{t=1}^{T_p} \sum_h \left(\frac{1}{1+D} \right)^t \times \left(\psi^s \times \sum_{j=1}^{N_{pg}} C_j \times P_{G,j}^{s,t,h} + \beta C_{\text{Inv}} \right) \quad P_{\text{Loss}} \right] \quad (21)$$

$$\text{s.t.} \quad \begin{cases} P_b^{\text{inj}} = P_b^{\text{cal}} \\ Q_b^{\text{inj}} = Q_b^{\text{cal}} \end{cases} \quad \forall b \in \text{NB} \quad (22)$$

$$\begin{cases} V_{\min} \leq V_b^s \leq V_{\max} \\ \theta_{\min} \leq \theta_b^s \leq \theta_{\max} \end{cases} \quad \forall b \in \text{NB}, s \in S \quad (23)$$

$$\begin{cases} P_{G,j,\min} \leq P_{G,j}^s \leq P_{G,j,\max} \\ Q_{G,j,\min} \leq Q_{G,j}^s \leq Q_{G,j,\max} \end{cases} \quad \forall s \in S, j \in \text{NG} \quad (24)$$

$$\begin{cases} S_{L,i}^s \leq S_{L,\max} \\ S_{C,n}^s \leq S_{C,\max} \end{cases} \quad \forall i \in \text{NL}, s \in S, n \in \text{NC} \quad (25)$$

$$M_{\min} \leq M_c^s \leq M_{\max} \quad \forall c \in \text{NC}, s \in S \quad (26)$$

$$P_{EV,k,\min} \leq P_{EV,k}^s \leq P_{EV,k,\max} \quad \forall s \in S, k \in \text{NEV} \quad (27)$$

Equation (20) calculates the system operation and maintenance cost in the planning horizon, C_{OM} , and it is formulated as an NLP problem; D is the discount rate; β shows the annual maintenance cost; ψ^s is the probability of S scenario; $P_{G,j}^{s,t,h}$ is the generation cost of unit j in scenario s ; T_p is the planning horizon; C_j is the generation cost of unit j ; and P_{Loss} is the total losses of network, including the line losses and converters losses.

Furthermore, Equations (22-26) express the constraints of the slave optimization problem. Constraint (22) ensures the power balance among the network buses, which is obtained by equalizing the calculated power to the injected pure power in each network bus. To solve (22), the AC-DC load flow method in [24] is used. The voltage stability constraint of the network buses is defined by (23). Constraint (24) investigates the limits of the power generated by DGs. The capacity limit of network lines as well as the converters capacity constraint are considered by (25). Also, (26) guarantees the modulation index of converters between upper and lower limits. Finally, the capacity constraints of EV charging stations are considered as (27).

3.3. The solution procedure of planning problem

The goal of the proposed planning is to determine the optimal AC-DC configuration by investigating all possible radial structures of the network. The presented model is defined as an MINLP problem that is solved by GA.

The master optimization problem is an MIP problem with binary decision variables. At this level of optimization, the type of buses and lines (AC or DC) as well as the type of the supplying path of the feeders are determined by GA. Radial

3.2. Optimization problem for DERs and EVs planning (the slave problem)

The objective function of slave optimization problem determines the optimal location as well as optimal capacity of DERs and EV charging stations to minimize the operation cost and network losses. Therefore, it is formulated as follows:

network structures are given as input to GA which are generated by Steps (1) to (4) as follows:

- (1) The network is modeled as a graph, G ; each bus represents a vertex and each line represents an edge. The weights of the edges represent the distance of the buses from each other.
- (2) The information of the graph, G , is given to the Spantree (spanning trees generation using the network graph) program in MATLAB.
- (3) The Spantree program generates all spanning trees of G , i.e., all possible radial structures of the network, $g = [g_1, \dots, g_r, \dots, g_R]$, where R is the number of all spanning trees of the network and g_r is the r th spanning tree of G .
- (4) The radial structures are numbered based on the total weight of the edges and given as input to the GA optimizer.

Then, the GA determines the type of buses and lines of g_r according to the planning goals. Thus, the AC-DC structure of g_r is defined. In the slave problem, the DERs and EVs planning is optimized. For the AC-DC structure of g_r , the location and size of the DERs and EV charging stations are optimized to minimize the network losses and system costs. The decision variables in the slave optimization problem include the location and size of DERs and EV charging stations. The MCS technique is utilized for addressing the stochastic variations in DERs output and load demands.

For all possible radial structures of the network (i.e., $r=1:R$), the master-slave optimization planning problem is solved.

Finally, the AC-DC structure with minimum planning cost is introduced as the optimal solution. Figure 5 shows the flowchart of the proposed planning strategy.

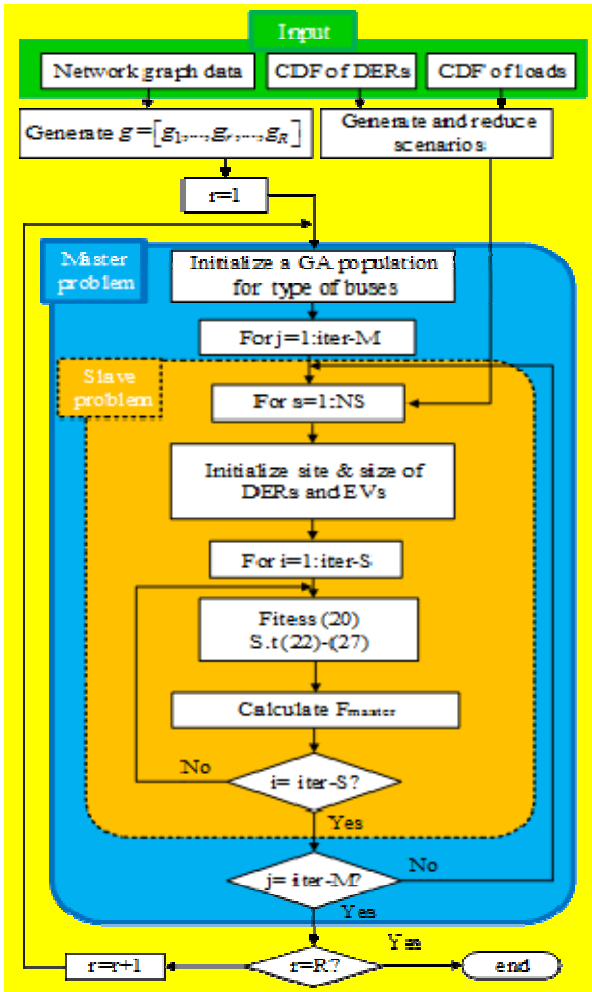


Figure 5. Flowchart of the proposed planning model

4. CASE STUDY

In this section, a test system is presented to implement and evaluate the hybrid planning method.

4.1. Test system

A 13-zone network is selected as the case study in Figure 6. The network includes different DERs and AC-DC loads, whose default locations are depicted in the Figure. The network is assumed as a directed graph, in which each zone is the node and every connection between the two zones is a weighted edge. According to the planning objectives, the lines and buses of the network can be AC or DC. Also, the location and capacity of DERs as well as the location and capacity of EV charging stations can vary. The capacity constraints of EV charging stations are $P_{EV,k,min} = 250$ kW and $P_{EV,k,max} = 1800$ kW. Figure 7 shows maximum load demand in each network bus. The maximum generated power rates of the wind generator and PV resources are 1000 kW and 2500 kW, respectively. The active and reactive power limits of other generation units and the energy price are listed in Tables 1 and 2. The distance between the network buses is the shortest possible path between two buses. Also, the effect of physical location of loads and resources on the distance of buses is considered. All possible paths between network buses are defined as the matrix arrays represented in the Appendix. The impedance for the DC and AC lines is $0.4415 \Omega/mile$ and $0.4435 + j0.726 \Omega/mile$, respectively. Besides, the line price is 28 k\$/mile [19].

The system base values include $S_b = 10$ MVA, $V_{ac}^b = 4.16$ kV, and $V_{dc}^b = 6.8$ kV. The power factor of converters is 0.95. The voltage stability limits are $V_{max} = 1.05$ p.u., $V_{min} = 0.95$ p.u., $\theta_{max} = 45$ deg, and $\theta_{min} = -45$ deg. Also, the modulation index limits are $M_{max} = 1$, and $M_{min} = 0.97$. The maximum converter capacity is 2 MVA and the converter price is 195 \$/kVA. The bus connectivity constraint is considered as $L_{max} = 4$. The planning horizon time is 10 years. The values of discount rate, D , and annual maintenance cost, β , are 0.07 and 0.06, respectively. The annual load growth is assumed to be 2%. Moreover, the presented data in [19] is used to describe the stochastic behavior of DERs, loads, and EV charging stations. To consider the uncertainty of stochastic variables in the proposed model, first, the MCS method is used to generate 1000 scenarios, including all possible network states. Then, the scenario reduction method is used to select the most probable states including probable severe network states, and the optimal power flow is performed in the planning problem considering the most probable scenarios and the probable extreme scenarios under uncertainties caused by generation resources and load demands.

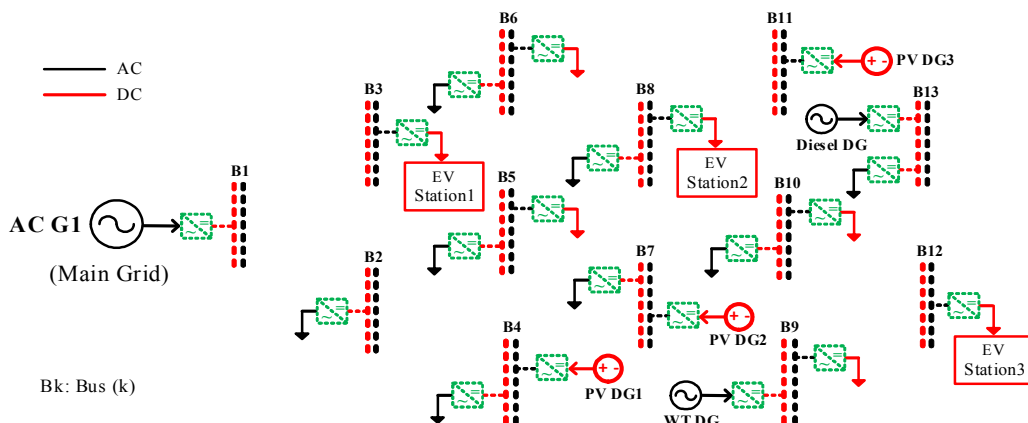


Figure 6. 13-bus test system

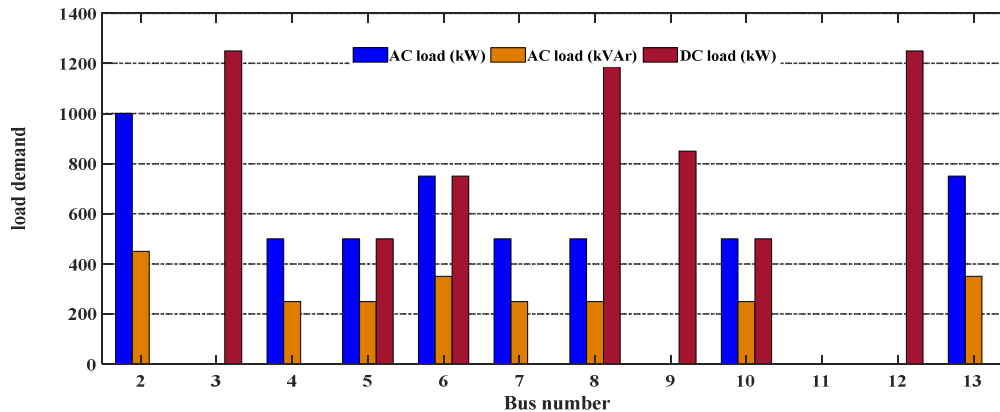


Figure 7. Maximum load demand

Table 1. Generators data

Unit	P_{\min}^{Gen} (p.u.)	P_{\max}^{Gen} (p.u.)	Q_{\min}^{Gen} (p.u.)	Q_{\max}^{Gen} (p.u.)	Energy price (\$/MWh)
AC G1	0.100	-	0.080	0.480	0.02
Diesel DG	0.100	0.200	0.010	0.096	0.20

5. RESULTS AND DISCUSSION

Four scenarios are defined in the following to evaluate the proposed approach in this work.

Scenario 1: AC planning without DERs and EVs planning

In this scenario, no binary variable exists. All buses and lines are AC. Besides, the location and the size of all DERs and EV charging stations in the AC network are defined as Figure 7 and the presented values in Table 2. The structure of the radial network is defined based on minimization of the objective function.

Scenario 2: AC planning including optimal DERs and EVs planning

For the AC system in this scenario, the radial structure of the network as well as the optimal size and location of DERs and EV charging stations are variable and are determined based on the planning objectives.

Scenario 3: AC-DC hybrid planning without DERs and EVs planning

The AC-DC structure of the network is unknown in this scenario. The system buses and lines can be AC or DC. The capacity and location of DERs and EV charging stations are considered as known parameters of the planning problem. The specified parameters are given in Figure 6 and Table 2.

Scenario 4: AC-DC hybrid planning including optimal DERs and EVs planning

In this case, the AC-DC network structure is defined according to the flowchart of Figure 5 by determining the type of buses and lines, as well as the optimal size and location of DERs and EV charging stations.

The optimal planning solution for Scenarios 1 to 4 is presented in Figures 8-11, respectively. The capacity of the converters connected to the network buses is calculated considering the annual load growth in the planning horizon, and the obtained values for the hybrid planning and AC

planning are depicted in Figures 12 and 13, respectively. In Scenario 3, the capacities of the converters installed in the network lines (C1, C2, C3) are 1500 kVA, 900 kVA, and 1000 kVA, respectively. However, in Scenario 4, the capacities of C1, C2, and C3 are 1200 kVA, 1000 kVA, and 800 kVA, respectively. The capacities of the generation units and EV charging stations for the second and fourth scenarios are presented in Table 2. Figure 14 shows the system operation cost. The network planning cost and the average value of network losses over a 10-year horizon are listed in Table 3.

The analysis of planning results in different scenarios is described as follows:

- Comparison of the first and third scenarios shows that the lower installation capacity of converters and AC lines in hybrid planning has led to the following:
 - The investment cost is significantly lower than AC traditional planning so that the investment cost in the third scenario is decreased by 785.75 k\$ in comparison with the first scenario.
 - The network loss in the hybrid structure is 63.5 kW less than its value in the AC structure.
 - The system operation cost in AC-DC planning is reduced by 1077.48 k\$ in comparison with AC planning.

Therefore, the hybrid planning has saved the total cost of planning by 4.75 % compared to traditional planning and reduced network losses by 10.5 %.

- According to the comparison of the results from the first to fourth Scenarios, planning with the definition of the optimal size and location of DERs and EV charging stations has brought about the following outcomes:
 - The investment and operation costs of the system in the fourth scenario are reduced by 199.15 k\$ and 611.51 k\$, respectively, in comparison with the third scenario. Also, in the second scenario, there

are 86.7 k\$ and 314.01 k\$ savings in the system investment cost and the system operation cost, respectively, in comparison with the first scenario.

- The planning cost and power losses of the network in the fourth scenario are decreased by 2.17 % and

8 %, respectively, in comparison with the third scenario. Besides, in the second scenario, the planning cost and power loss cost are reduced by 1.02 % and 7.6 %, respectively, in comparison with the first scenario.

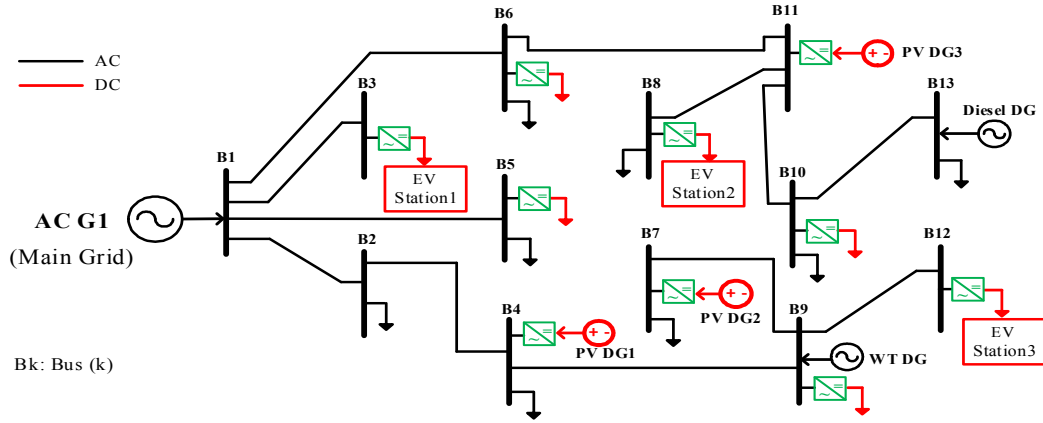


Figure 8. AC planning solution for Scenario 1

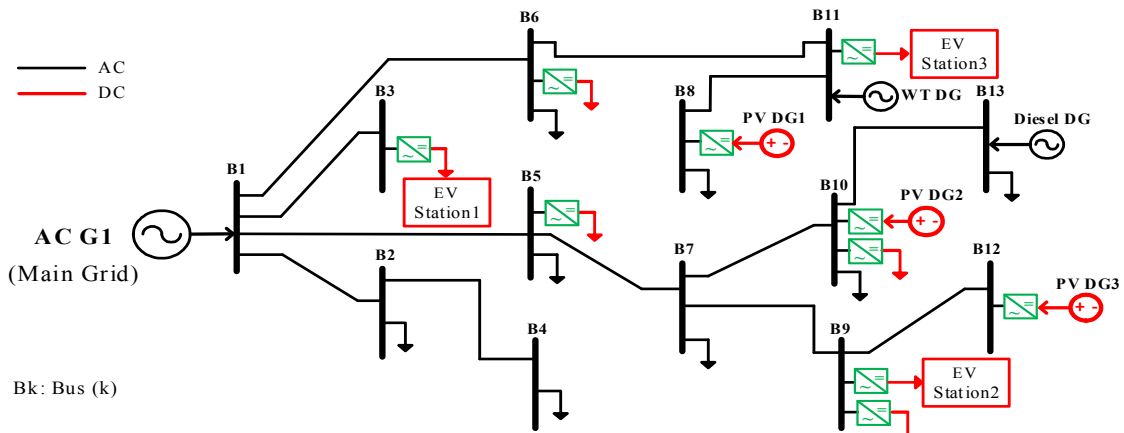


Figure 9. AC planning solution for Scenario 2

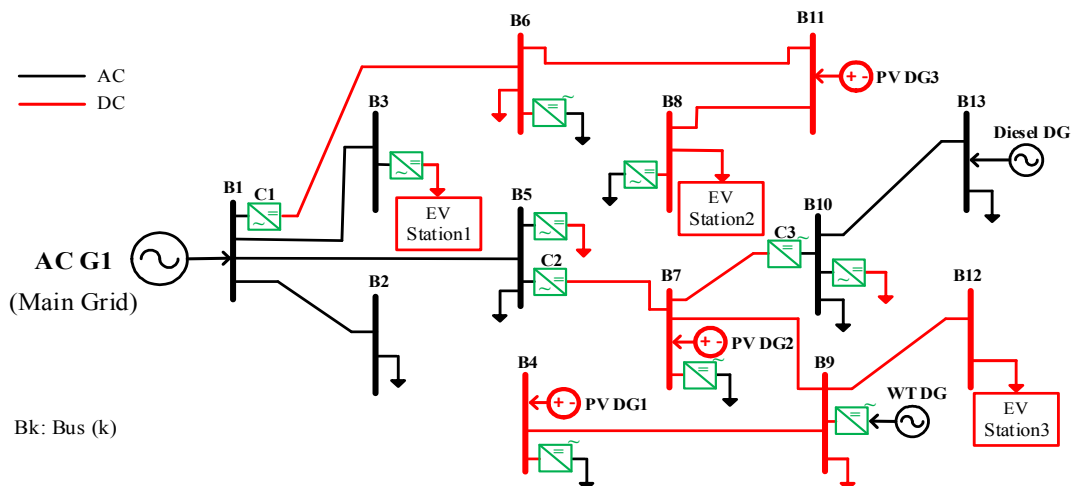


Figure 10. Hybrid planning solution for Scenario 3

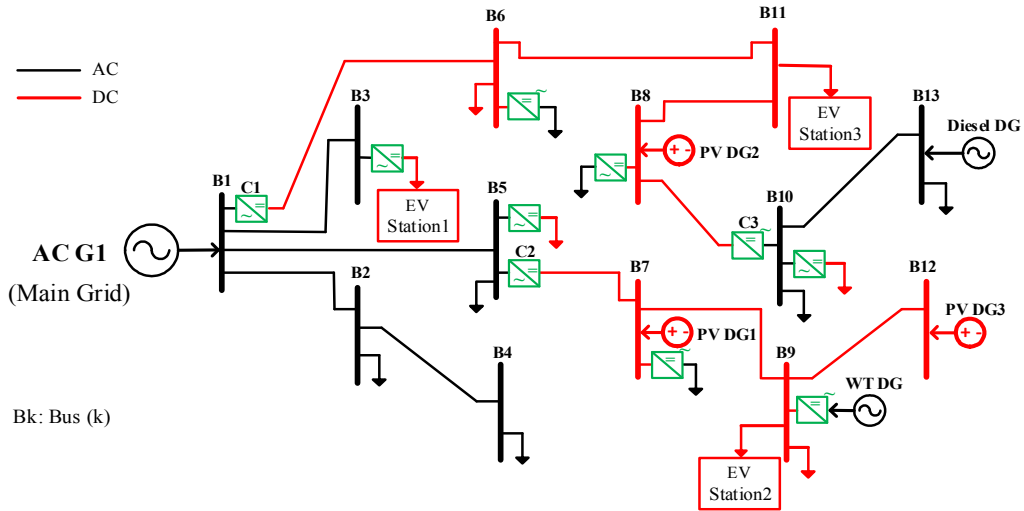


Figure 11. Hybrid planning solution for Scenario 4

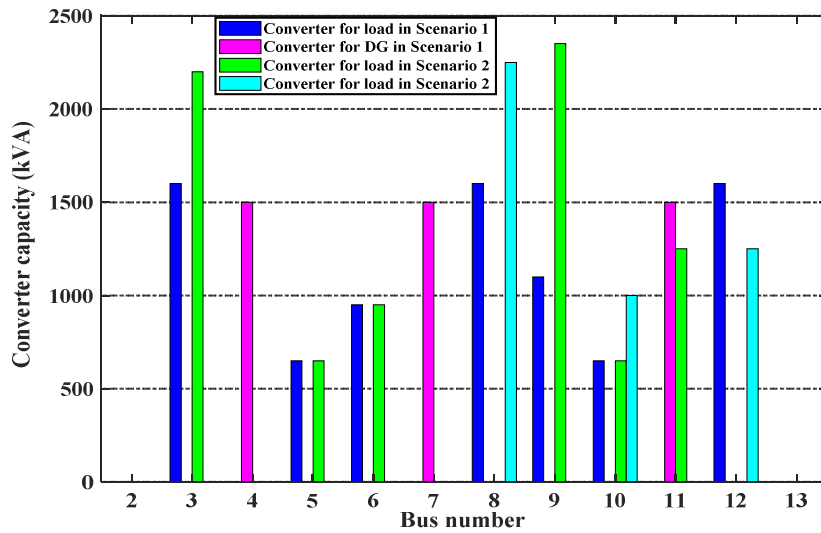


Figure 12. The capacities of converters connected to the network buses for AC planning

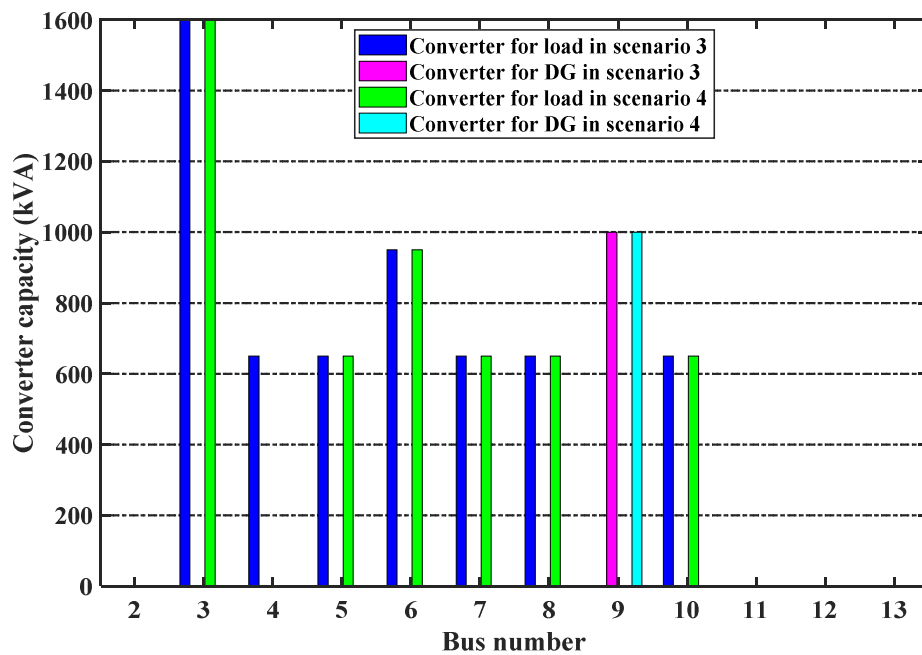
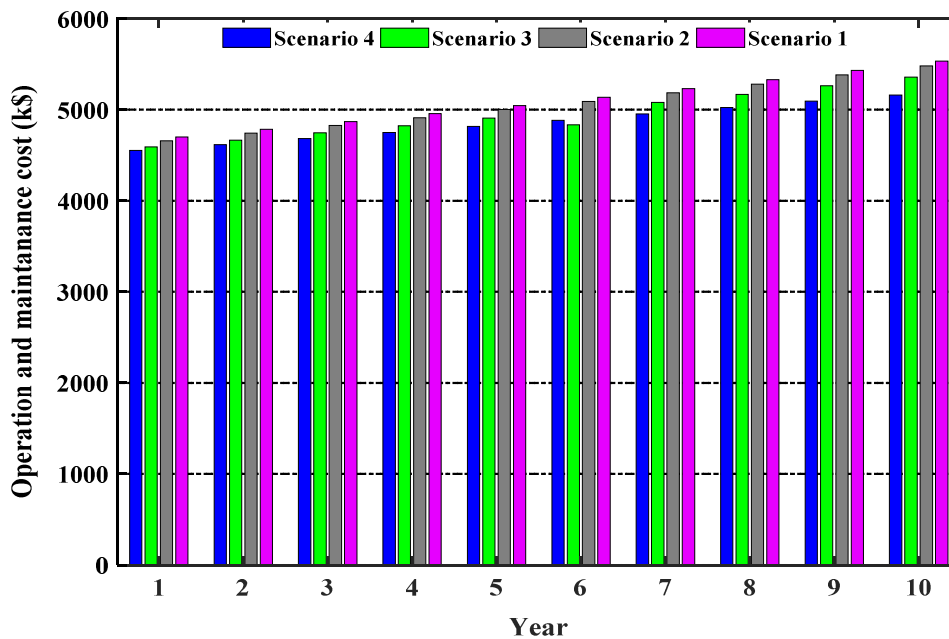


Figure 13. The capacities of converters connected to the network buses for hybrid planning

Table 2. The capacities of DGs and EV Stations (kW)

Unit	Scenario 1	Scenario 2	Scenario 3	Scenario 4
PV DG1	1500*	2250	1500**	1350
PV DG2	1500*	1000	1500**	1900
PV DG3	1500*	1250	1500**	1250
EV Station1	1250*	1750	1250**	1350
EV Station2	1250*	850	1250**	700
EV Station3	1250*	1000	1250**	1700
Diesel DG	2000*	1800	2000**	1650

* The known value for Scenario 1
** The known value for Scenario 3

**Figure 14.** The comparison of system operation cost for different scenarios**Table 3.** Planning results

Costs and values	Scenario 1	Scenario 2	Scenario 3	Scenario 4
C_{Line} (k\$)	1226.40	1159.20	918.40	924.00
C_{Conv} (k\$)	2466.75	2447.25	1989.00	1784.25
C_{Inv} (k\$)	3693.15	3606.45	2907.40	2708.25
C_{OM} (k\$)	35471.38	35157.37	34393.90	33782.39
C_{NP} (k\$)	39164.53	38763.82	37301.30	36490.65
Average of P_{Loss} (kW)	474.30	438.10	410.80	378.30

6. CONCLUSIONS

A novel stochastic planning approach for AC-DC hybrid networks was proposed in this study. The optimal network structure was defined based on investigating all possible AC-DC system configurations. The presented planning model was formulated as a master-slave optimization problem. The master optimization problem defines the type of network buses and lines in order to minimize the system investment costs. The slave problem was formulated to solve the optimal power flow equations so that the size and the location of the DERs and EV charging stations could be determined to minimize the both system operation cost and network power losses simultaneously. The stochastic variation of the loads consumption and the output of the DERs were modeled by generating scenarios with the MCS method. In the next step,

the Kantorovich scenario reduction method was applied to reduce the calculations burden of the planning problem. The efficiency curve of the converter was employed to model the converter losses accurately in the power flow equations. Finally, the proposed approach was applied to designing a 13-zone case study system, including different AC-DC loads and resources. The results showed that the presented approach could effectively reduce the system costs. The proposed method is useful for future designers of hybrid DSs due to its advantages and efficiency.

7. ACKNOWLEDGEMENT

The current study is an academic research and no assistance has been received from any organization.

NOMENCLATURE

Sets	
S	Set of scenarios
NB	Set of network buses
NL	Set of network lines
NC	Set of converters
NG	Set of generation units
NEV	Set of electric vehicle charging stations
Indices	
s	Index for scenarios
b	Index for network buses
i	Index for network lines
c	Index for converters
j	Index for generation unit
t	Index for years
k	Index for electric vehicle charging stations
Parameters	
S_b	Base value of the network power (MVA)
V_{ac}^b	AC Voltage base value (kV)
V_{dc}^b	DC Voltage base value (kV)
NS	Number of scenarios
f_s	Switching frequency (Hz)
Variables	
P_b^{inj}/Q_b^{inj}	Injected active/reactive power into bus b (kW/kVAR)
P_b^{cal}/Q_b^{cal}	Calculated active/reactive power at bus b (kW/kVAR)
$P_{G,j}/Q_{G,j}$	Active/reactive power of generation unit j (kW/kVAR)
$p_{IGBT}^{cond}/p_{diode}^{cond}$	Conduction losses in the IGBT/diode (kW)
$E_{IGBT}^{SW}/E_{diode}^{SW}$	Switching losses in the IGBT/diode (kW)
p_{total}^{cond}	The total conduction losses of the converter (kW)
p_{total}^{SW}	The total switching losses of the converter (kW)
$p_{constant}$	The fixed losses of the converter (kW)
S_L	Power passing through the network lines (kVA)
S_C	Power passing through the converters installed in network lines (kVA)
$V_{ac,c}$	Voltage at AC side of the converter (p.u.)
$V_{dc,c}$	Voltage at DC side of the converter (p.u.)
V	Voltage amplitude (p.u.)
θ	Voltage angle (deg.)
M	Modulation index of converter
X_{min}	Minimum limit of variable X
X_{max}	Maximum limit of variable X

APPENDIX

The distance between the buses of 13-bus test system used in this study is given by:

$$D(m,n)=A_m(n) \quad \forall m \in \{2,3,\dots,13\}, n \in \{1,2,\dots,12\} \quad (28)$$

where $D(m,n)$ indicates the distance between bus m and bus n of the system in miles; and values of $A_m(n)$ are defined as:

$$\begin{aligned} A_2 &= [1.0] \\ A_3 &= [1.0 \ 1.4] \\ A_4 &= [2.0 \ 1.0 \ 2.4] \\ A_5 &= [1.4 \ 1.0 \ 1.0 \ 1.4] \\ A_6 &= [2.0 \ 2.4 \ 1.0 \ 2.8 \ 1.4] \\ A_7 &= [2.4 \ 1.4 \ 2.0 \ 1.0 \ 1.0 \ 2.4] \\ A_8 &= [2.4 \ 2.0 \ 1.4 \ 2.4 \ 1.0 \ 1.0 \ 1.4] \\ A_9 &= [3.4 \ 2.4 \ 3.0 \ 1.4 \ 2.0 \ 3.4 \ 1.0 \ 2.4] \\ A_{10} &= [2.8 \ 2.4 \ 2.4 \ 2.0 \ 1.4 \ 2.0 \ 1.0 \ 1.0 \ 1.4] \\ A_{11} &= [3.4 \ 3.0 \ 2.4 \ 3.4 \ 2.0 \ 1.4 \ 2.4 \ 1.0 \ 2.8 \ 1.4] \\ A_{12} &= [3.8 \ 2.8 \ 3.4 \ 2.4 \ 2.4 \ 3.0 \ 1.4 \ 2.0 \ 1.0 \ 1.0 \ 2.4] \\ A_{13} &= [3.8 \ 3.4 \ 2.8 \ 3.0 \ 2.4 \ 2.4 \ 2.0 \ 1.4 \ 2.4 \ 1.0 \ 1.0 \ 1.4] \end{aligned}$$

REFERENCES

- Eajal, A.A., Shaaban, M.F., Ponnambalam, K. and El-Saadany, E.F., "Stochastic centralized dispatch scheme for AC/DC hybrid smart distribution systems", *IEEE Transactions on Sustainable Energy*, Vol. 7, No. 3, (2016), 1046-1059. (<https://doi.org/10.1109/TSTE.2016.2516530>).
- Peyghami, S., Mokhtari, H. and Blaabjerg, F., "Autonomous operation of a hybrid AC/DC microgrid with multiple interlinking converters", *IEEE Transactions on Smart Grid*, Vol. 9, No. 6, (2018), 6480-6488. (<https://doi.org/10.1109/TSG.2017.2713941>).
- Wang, T., Li, C., Mi, D., Wang, Z. and Xiang, Y., "Coordinated modulation strategy considering multi-HVDC emergency for enhancing transient stability of hybrid AC/DC power systems", *CSEE Journal of Power and Energy Systems*, Vol. 6, No. 4, (2020), 806-815. (<https://doi.org/10.17775/CSEEJPES.2019.02000>).
- ElNozahy, M.S. and Salama, M.M.A., "Uncertainty-based design of a bilayer distribution system for improved integration of PHEVs and PV arrays", *IEEE Transactions on Sustainable Energy*, Vol. 6, No. 3, (2015), 659-674. (<https://doi.org/10.1109/TSTE.2015.2405411>).
- Kurohane, K., Senjyu, T., Yona, A., Urasaki, N., Goya, T. and Funabashi, T., "A hybrid smart AC/DC power system", *IEEE Transactions on Smart Grid*, Vol. 1, No. 2, (2010), 199-204. (<https://doi.org/10.1109/TSG.2010.2053392>).
- Lotfjou, A., Fu, Y. and Shahidehpour, M., "Hybrid AC/DC transmission expansion planning", *IEEE Transactions on Power Delivery*, Vol. 27, No. 3, (2012), 1620-1628. (<https://doi.org/10.1109/TPWRD.2012.2194515>).
- Doagou-Mojarrad, H., Rastegar, H. and Gharehpetian, G.B., "Probabilistic multi-objective HVDC/AC transmission expansion planning considering distant wind/solar farms", *IET Science, Measurement & Technology*, Vol. 10, No. 2, (2016), 140-149. (<https://doi.org/10.1049/iet-smt.2015.0173>).
- Meng, K., Zhang, W., Qiu, J., Zheng, Y. and Dong, Z.Y., "Offshore transmission network planning for wind integration considering AC and DC transmission options", *IEEE Transactions on Power Systems*, Vol. 34, No. 6, (2019), 4258-4268. (<https://doi.org/10.1109/TPWRS.2019.2912414>).
- Torbaghan, S.S., Gibescu, M., Rawn, B.G. and Meijden, M., "A market-based transmission planning for HVDC grid-Case study of the North Sea", *IEEE Transactions on Power Systems*, Vol. 30, No. 2, (2015), 784-794. (<https://doi.org/10.1109/TPWRS.2014.2332762>).
- Moradi-Sepahvand, M. and Amraee, T., "Hybrid AC/DC transmission expansion planning considering HVAC to HVDC conversion under renewable penetration", *IEEE Transactions on Power Systems*, Vol. 36, No. 1, (2021), 579-591. (<https://doi.org/10.1109/TPWRS.2020.2988195>).
- Huang, L., Chen, Z., Cui, Q., Zhang, J., Wang, H. and Shu, J., "Optimal planning of renewable energy source and energy storage in a medium- and low-voltage distributed AC/DC system in China", *The Journal of Engineering*, Vol. 2019, No. 16, (2019), 2354-2361. (<https://doi.org/10.1049/joe.2018.8546>).
- Wu, Z., Liu, P., Gu, W., Huang, H. and Han, J., "A bi-level planning approach for hybrid AC-DC distribution system considering N-1 security criterion", *Applied Energy*, Vol. 230, (2018), 417-428. (<https://doi.org/10.1016/j.apenergy.2018.08.110>).
- Wu, Z., Sun, Q., Gu, W., Chen, Y., Xu, H. and Zhang, J., "AC/DC hybrid distribution system expansion planning under long-term uncertainty considering flexible investment", *IEEE Access*, Vol. 8, (2020), 94956-94967. (<https://doi.org/10.1109/ACCESS.2020.2990697>).
- Frank, S.M. and Rebenack, S., "Optimal design of mixed AC-DC distribution systems for commercial buildings: a nonconvex generalized benders decomposition approach", *European Journal of Operational Research*, Vol. 242, No. 3, (2015), 710-729. (<https://doi.org/10.1016/j.ejor.2014.10.008>).
- Bagheri, A., Monsef, H. and Lesani, H., "Integrated distribution network expansion planning incorporating distributed generation considering uncertainties, reliability, and operational conditions", *International Journal of Electrical Power & Energy Systems*, Vol. 73, (2015), 56-70. (<http://dx.doi.org/10.1016/j.ijepes.2015.03.010>).
- Lotfi, H. and Khodaei, A., "AC versus DC microgrid planning", *IEEE Transactions on Smart Grid*, Vol. 8, No. 1, (2017), 296-304. (<https://doi.org/10.1109/TSG.2015.2457910>).

17. Hamad, A.A., Nassar, M.E., El-Saadany, E.F. and Salama, M.M.A., "Optimal configuration of isolated hybrid AC/DC microgrids", *IEEE Transactions Smart Grid*, Vol. 10, No. 3, (2019), 2789-2798. (<https://doi.org/10.1109/TSG.2018.2810310>).
18. Ghadiri, A., Haghifam, M.R. and Larimi, S.M.M., "Comprehensive approach for hybrid AC/DC distribution network planning using genetic algorithm", *IET Generation, Transmission & Distribution*, Vol. 11, No. 16, (2017), 3892-3902. (<https://doi.org/10.1049/iet-gtd.2016.1293>).
19. Ahmed, H.M.A., Eltantawy, A.B. and Salama, M.A., "A planning approach for the network configuration of AC-DC hybrid distribution systems", *IEEE Transactions on Smart Grid*, Vol. 9, No. 3, (2018), 2203-2213. (<https://doi.org/10.1109/TSG.2016.2608508>).
20. Ahmed, H.M.A., Eltantawy, A.B. and Salama, M.M.A., "A reliability-based stochastic planning framework for AC-DC hybrid smart distribution systems", *International Journal of Electrical Power & Energy Systems*, Vol. 107, (2019), 10-18. (<https://doi.org/10.1016/j.ijepes.2018.11.003>).
21. Blaabjerg, F., Jaeger, U. and Munk-Nielsen, S., "Power losses in PWM-VSI inverter using NPT or PT IGBT devices", *IEEE Transactions on Power Electronics*, Vol. 10, No. 3, (1995), 358-367. (<https://doi.org/10.1109/63.388002>).
22. Islam, M.M., Rahman, M.A. and Islam, M.R., "Power loss and thermal impedance modeling of multilevel power converter with discontinuous modulation", *IEEE Transactions on Energy Conversion*, Vol. 36, No. 1, (2020), 36-47. (<https://doi.org/10.1109/TEC.2020.3000596>).
23. Ebrahimi, J., Abedini, M., Rezaei M.M. and Nasri M., "Optimum design of a multi-form energy in the presence of electric vehicle charging station and renewable resources considering uncertainty", *Sustainable Energy, Grids and Networks*, Vol. 23, (2020), 100375. (<https://doi.org/10.1016/j.segan.2020.100375>).
24. Sabzian Molaei, Z., Rokrok, E. and Doostizadeh M., "A unified power flow approach using VSC-efficiency for AC-DC distribution systems operating at grid connected and islanded modes", *International Journal of Electrical Power & Energy Systems*, Vol. 130, (2021), 106906. (<https://doi.org/10.1016/j.ijepes.2021.106906>).



Research Article

Biogas Production by Co-Digestion of Food Waste with Sewage Sludge and Poultry Litter: A Way Towards Sustainable Waste-to-Energy Conversion

Uttam Bista, Bhawana Rayamajhi, Bipasyana Dhungana, Sunil Prasad Lohani*

Renewable and Sustainable Energy Laboratory, Department of Mechanical Engineering, School of Engineering, Kathmandu University, P. O. Box: 6250, Dhulikhel, Nepal.

PAPER INFO

Paper History:

Received: 10 March 2022

Revised: 01 May 2022

Accepted: 21 May 2022

Keywords:

Co-Digestion,
Biogas,
Waste,
Temperature,
Sustainability

ABSTRACT

Anaerobic digestion is one of the most effective technologies for managing degradable waste, which produces renewable energy and digestate as the byproduct. In this study, sewage sludge (SS), poultry litter (PL), and food waste (FW) were co-digested at ratios (SS:PL:FW 2:1:1) with 8 % total solid content at ambient temperature (average 22 °C) and controlled temperature (35 °C) in summer. The synergistic effects of co-digesting substrates enhance the biogas production potential when digested at an optimized ratio. The maximum biogas yield was 688.7 L/kgVSa at the controlled temperature and 462.3 L/kgVSa at ambient temperature. The ambient reactor had a methane composition of 55 %, while the controlled temperature reactor had about 60 %. The results provide approaches to increase biogas production in the anaerobic digestion process through co-digestion and controlled mesophilic temperature. Biogas production from anaerobic co-digestion could significantly transform waste into energy in low-income countries to achieve the objective of clean energy production and environmental sustainability.

<https://doi.org/10.30501/jree.2022.333462.1342>

1. INTRODUCTION

Solid waste generation has been on a significant rise with the growing population and unmanaged urbanization in developing countries. However, waste management has always been a challenge for the government and municipalities, leading to environmental pollution and social threats [1]. In this context, the gaining popularity of biogas production from organic waste as part of a circular economy can give a possible way out to the government and society [2]. The circular economy mainly focuses on sustainability through the transformation of the current linear economy towards a circular approach [1]. In waste management, circularity has not yet gained adequate attention, especially in low- and middle-income countries [3]. In the era of the circular economy, waste has now become a resource for clean energy production via technologies such as Anaerobic Digestion (AD). AD process utilizes locally available organic substrates to generate biogas, thus reducing the dependency on fossil-based energy sources [4]. AD further contributes to achieving clean energy and ensuring the achievement of sustainable development goal 7: access to affordable, reliable, sustainable, and modern energy for all [5].

The waste to energy generation practice in developing countries like Nepal is still in the early stages. With more than 0.2 million tonnes of manures generation per day and an estimated theoretical potential of nearly 110 million Liquefied Petroleum Gas (LPG)² cylinders equivalent [6], Nepal reserves enough energy source (more than 4.5 times of current cooking energy supplied by LPG) to substitute cooking energy demand of the country [6]. However, the country's energy scenario shows that these resources are yet to be unrealized. Though biogas technology has existed in Nepal for more than 55 years, AD practice is still limited to mono digestion of cattle manure which in turn is restricting the country's actual bioenergy generation potential [7].

Anaerobic Digestion (AD) systems are mostly used for simultaneous treatment of waste for the production of biogas and digestate as fertilizer. However, biogas production from mono digestion is less preferred as it causes difficulties in operation through the particular inherent properties of single substrates [8]. Due to the low C/N ratio, Sewage Sludge (SS) has less bio-methane potential, resulting in low AD efficiency [8]. Similarly, food waste has low pH and high biodegradability contributing to the rapid formation and accumulation of VFAs, resulting in digester failure [9, 10]. Furthermore, AD of poultry litter alone is unfavorable due to

*Corresponding Author's Email: splohani@ku.edu.np (S.P. Lohani)

URL: https://www.jree.ir/article_156176.html

² 14.2 kg per LPG cylinder



the presence of high nitrogen concentration and is ultimately reported to have low biogas production [11].

Thus, co-digestion is being used for its additional benefits including microbial synergistic effects, potential toxic dilution, improved nutrient balance, relatively higher biogas yields, and an increased digestion rate [12, 13]. Co-digestion of the substrates not only enhances methane production potential but subsequently facilitates the management of locally available wastes [14]. The selection of a co-substrate is an important factor in co-digestion and it should complement their properties which aid both stabilization of the process and improvement of the digestion process. A limited study has been conducted with SS, PL, and FW as three co-mixed substrates for biogas production under ambient as well as controlled temperature conditions. A study on co-digestion of SS with swine manure and PL at a ratio of 7:2:1 in a semi-continuous process and cow manure with FW and SS at a ratio of 7:2:1 under mesophilic conditions reported a biogas yield of 0.336 m³/kgVS_{added} and 0.6 m³/kgVS_{added}, respectively [15]. Another study on co-digestion of rice straw with kitchen waste and pig manure in mesophilic (37 ± 1 °C) conditions (KW:PM:RS in 0.4:1.6:1) reported that the biogas yield of 674.4 L/kg VS_a was higher than that of the digestion of rice straw or pig manure alone by 71.67 % and 10.41 %, respectively [16]. A similar study by Callaghan et al. reported that the methane yield increased from 0.23 to 0.45 m³.kg⁻¹.VS_a by introducing the cattle slurry with fruit and vegetable wastes from 20 to 50 % in co-digestion at 35 °C [17]. All of these studies were carried out with substrates FW, SS, and PL in a controlled mesophilic environment, which reported a significant increase in biogas yield.

As of now, about 430,000 household biogas plants are installed in Nepal, solely operating at ambient temperature, without any digester heating provisions or feedstock pretreatments [6]. A field study conducted at the Kavre district of Nepal reported that more than 80 % of household biogas plant users (300 households surveyed) were not satisfied with the plant performance [18]. The insufficient biogas production especially during the winter was the primary concern of most users. Thus, understanding the co-digestion performance in ambient and controlled temperature conditions helps designers, bio-gas companies, and policymakers adequately assess the performance of existing biogas plants in the local context and plan for optimized performance of the plants. However, there is a dearth of literature on the performance of biogas plants practicing co-digestion of various wastes in ambient temperature conditions and their performance compared with those being operated in controlled temperature conditions or mesophilic temperature conditions. Hence, this study aims to: i) compare the biogas yield obtained from co-digestion of locally available substrates under both ambient and controlled temperature conditions and ii) explore the possibility of the use of locally available co-substrates in the household anaerobic digestion process. Moreover, this study also helps provide solutions to achieve more efficient and sustainable energy generation techniques for similar digesters operating at similar ambient temperatures in other low- and middle-income countries.

2. METHODOLOGY

In this lab-scale semi-continuous process, experiments were conducted under ambient and controlled temperature conditions. Co-digestion of SS, PL, and FW at a mixing ratio

of 2:1:1 was taken as the optimal feed co-digestion ratio since it gave the highest biogas yield during the previous experiment [19]. The overall laboratory experiment was conducted from April to July in the temperature range of 13 °C to 29 °C, which is a different temperature range from the previous experiment.

2.1. Feeding material

Sewage sludge was collected from a community wastewater treatment plant operating at ambient temperature in Dhulikhel, Nepal. Food waste was collected from the university canteen comprised of mainly cooked rice, vegetables/peels, and lentils presented in Table 1. Before feeding, FW was blended to get a finer particle size less than 10 mm in diameter and/or length as suggested by Hollinger et al. [20]. Fresh cow dung was obtained from the cattle farms of residents. A mixture of sewage sludge and cow manure at a ratio of 2:1 (wt/wt) was used as inoculum for the experiment. Poultry litter was collected from a Deep litter poultry farm in Dhulikhel. All the samples to be fed to the reactor were collected and stored at 4 °C for the entire experiment.

Table 1. Composition of food waste

Feed compositions	Percentage
Rice	60 %
Potato peels	10 %
Cucumber peels	5 %
Carrot peels	5 %
Potato cooked	3 %
Daal	10 %
Peas (Cooked vegetables)	7 %

2.2. Digester setup and operation

The experiment was carried out under ambient and controlled temperature conditions in a semi-continuous process from April to July at an average ambient temperature of 22 °C, with a maximum of 28.8 °C and a minimum of 13.5 °C recorded in the temperature logger. For the ambient temperature condition, two 5 L bottles were taken, as shown in Figure 1, with a fitted infusion set to measure the amount of gas produced during the experiment. A PVC pipe attached to plastic funnels was used to feed the substrates. Proper sealing was done to ensure an airtight setup as required for the AD process. The gas production was measured with the help of a measuring cylinder through the water displacement method.

For the experiment in ambient temperature conditions, three reactors in triplicate were set up and a co-digestion mixture of SS, PL, and FW at a mixing ratio of 2:1:1 was fed into those reactors. The mixing ratio of 2:1:1 was chosen from the previous work [19] from the Renewable and Sustainable Energy Laboratory (RSEL), Kathmandu University, which gave the highest biogas yield and maintained a stable AD process. The difference from the previous study lies in the ambient temperature range of the experiment. Moreover, this study carries out a new set of controlled temperature (35 °C) experiments so that the result can be compared with ambient temperature result, a task that was not conducted in the previous study. The organic loading rate of 1.2 g VS/L.d, HRT of 45 days, and 8 % of TS were maintained in the tests.

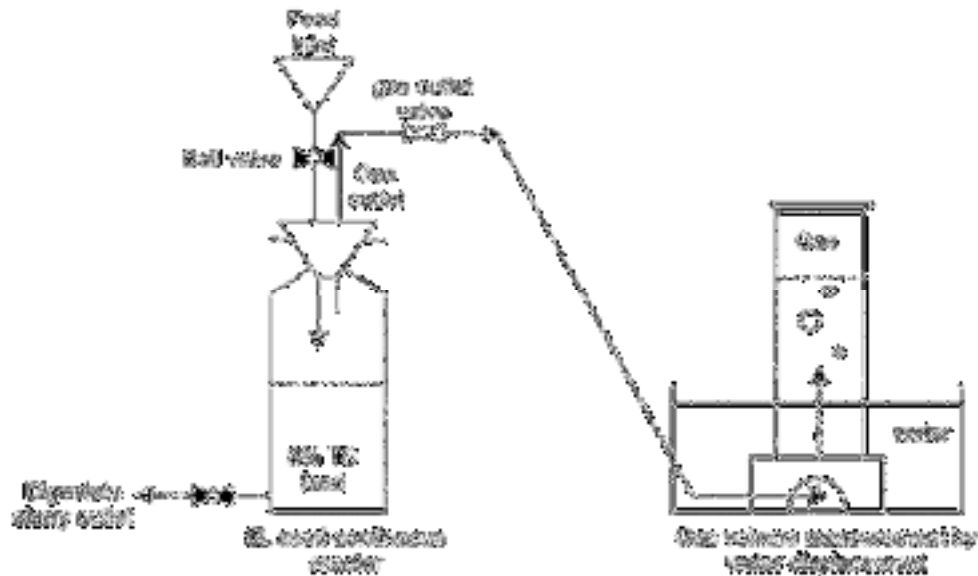


Figure 1. Schematic diagram of reactor setup for the ambient condition

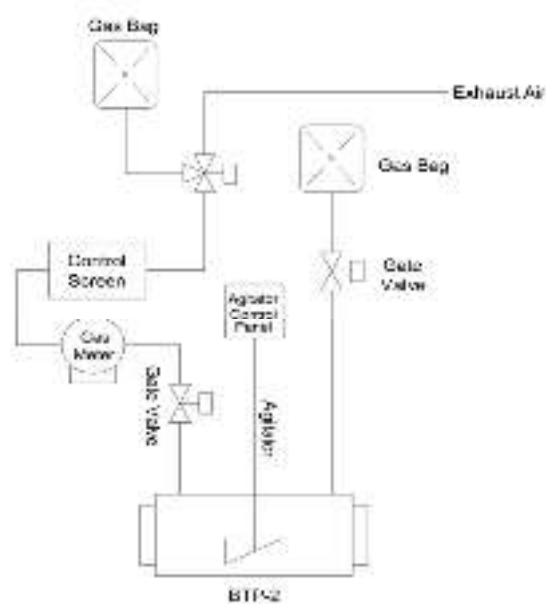


Figure 2. Schematic diagram of biogas test plant-2 (Left); biogas test plant-2 (Right)

For the controlled temperature condition, a lab-scale Biogas Test Plant (BTP 2, Umwelt-und Ingenieurtechnik GmbH Dresden) with a working volume of 15 L (Figure 2) was used. A total working volume of 8 liters was used, while 7 liters was left as the headspace. The reactor is fitted with the silicon heater band including an adjustable temperature sensor. The universal automation system SENSOcontrol is used for data acquisition applications and control of the units (pumps, agitator) in the test facility measuring pH-Value, temperature, and gas volume. An intuitive touch screen is integrated for real-time visualization of the measured data. The reactor operated at 35 °C for this study. The stirrer was programmed to start stirring at 5 rpm for 5 minutes every 2 hours. The produced biogas collected in the bag was automatically measured by wet gas meters. The substrate combinations, OLR (1.2 gVS/L/day), TS (8 %), and mixing ratio 2:1:1 were selected identical to the reactor operating at ambient

temperature; however, the BTP-2 operated for a hydraulic retention time of 30 days.

2.3. Analytical method

Total Solid and Volatile Solid content was measured with APHA, 2540 D guideline for TS, and APHA 2540 E guidelines for VS. An Exotech SOL 100 pH meter was used to monitor the pH of the substrates. The composition of the biogas was determined using a Sewerin Multitec-545 gas analyzer. To determine the C/N ratio, the TOC of all the three substrates was determined using the American Society of Agronomy and Soil Science guidelines, and their TON was determined using the APHA 4500-Norg guidelines. To account for temperature variability in the experiment of an ambient temperature condition, a temperature logger was utilized to record ambient temperature at the interval of every half an hour.

3. RESULTS AND DISCUSSION

3.1. Physiochemical properties

The physicochemical properties of a mixture of co-substrates SS, PL, and FW at a ratio of 2:1:1 are shown in Table 2. Since

the experiment was conducted at 8 % TS, the co-substrate mixture was diluted to 8 % TS. The pH of the mixture was 7.08, which is in the favorable range of 7-8 [21]. The VS % of the feeding material was 71.7 % of TS.

Table 1. Physiochemical properties of the sample

Co-substrate: SS:PL:FW		TS %	VS %	pH	C:N
		Feeding samples	Feeding samples	Feeding samples	Feeding samples
Mixing Ratio: (2:1:1)	BTP	8.2	71.7	7.08	18.3
	Ambient	8.2	71.7	7.08	18.3

3.2. Composition of biogas

Table 3 presents the composition of the elements contained in the biogas produced in the experiment from ambient and controlled temperature conditions. The composition was determined using Multitec 545 Gas Analyzer (multigas detector with infrared sensors and extended measuring range for Hydrogen Sulfide).

Table 2. Percentage composition of biogas in two different reactors

Constituents	Percentage composition	
	Ambient temperature	Controlled temperature
Methane	50-55	60-65
Carbon dioxide	35-40	30-40
Oxygen	0-5	0-5
Hydrogen sulphide	0-1	0-1
Others (Nitrogen, Hydrogen, Ammonia e.t.c.)	-	-

3.3. Co-digestion at the temperature-controlled condition

Co-digestion of SS, PL, and FW at a ratio of 2:1:1 was carried out in temperature-controlled conditions (35 °C) for about 60 days in a semi-continuous process. Since the reactor was automated, the daily production of biogas was recorded in the system. Figure 3 shows the cumulative biogas production from the BTP 2 reactor. The initial two weeks were an inoculum stabilization period during which no regular feeding was done until the biogas composition was recorded at about 50 %.

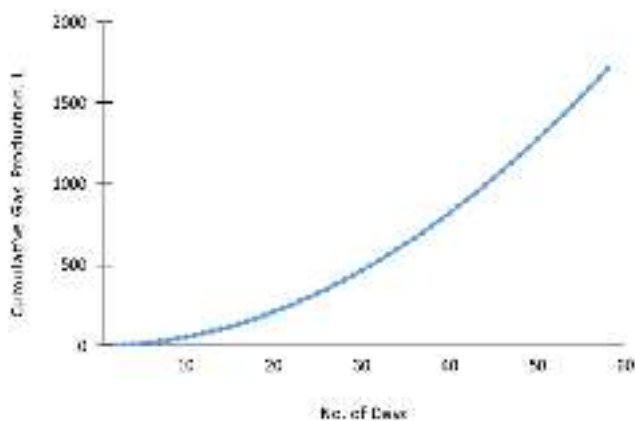


Figure 3. Cumulative biogas production at controlled temperature

The daily gas production was comparatively low in the first two weeks. After stable startup of the reactor, feeding of co-digested substrates was done every alternate day for 30 days. It is evident from Figure 3 that the biogas production exponentially increased upon the initiation of the feeding of the reactor after the 15th day of operation. The pH of the digested substrates ranged from 6.7 to 6.9 throughout the experiment and no significant drop in pH was noted. The average biogas yield was 688.7 L/kg VS_{added} with an average methane content of 60 %.

3.4. Co-digestion at the ambient temperature condition

This experiment was carried out in the daily average ambient temperature range of 13.5 °C to 28.8 °C with significant fluctuations, as shown in Figure 4. The co-substrates, mixing ratio, and other parameters (1.2 gVS/L/day OLR, 8 % TS) were identical to those in the experiment conducted in the BTP-2 reactor except for 45 days of HRT being used in this case. The digesters experienced significant fluctuation in ambient temperature as observed in Figure 4.

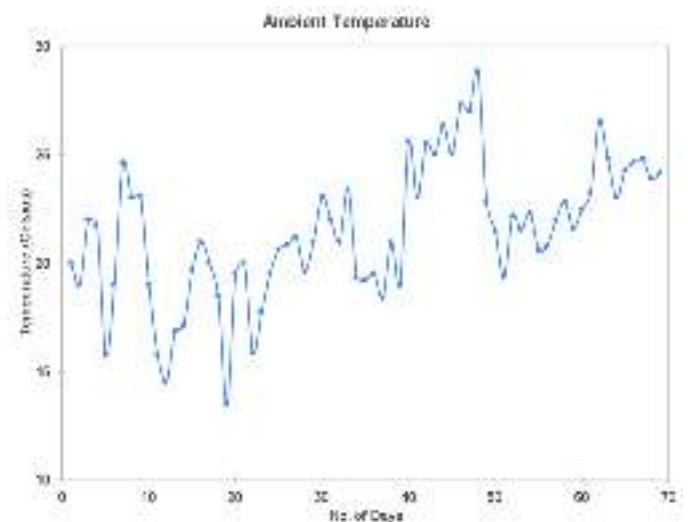


Figure 4. Ambient temperature during the experiment period

Figure 5 indicates the cumulative biogas production from the reactor fed with sewage sludge, poultry litter, and food waste at a ratio of 2:1:1 in ambient temperature conditions. The figure indicates that the reactors took about a month to effectively start up to initiate the feeding process (methane percentage about 50 %) and low gas production can be observed in that period.

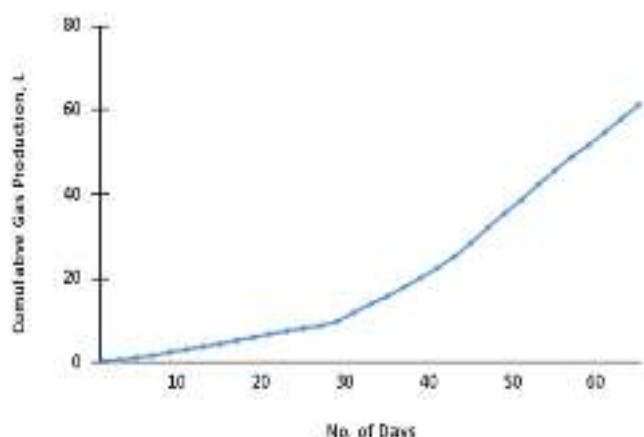


Figure 5. Cumulative Biogas Production in ambient temperature conditions

The exponential increase in biogas production could be observed after feeding was initiated from the 32nd day of operation. The average biogas yield of 462.3 L/kg VS_{added} was obtained from the experiment with average methane composition of 55 %.

It was observed that the startup time was reduced by nearly 50 % when the co-digestion experiment was performed in a temperature-controlled condition (BTP-2) in contrast to the ambient temperature condition (Figures 3 and 5). Figure 6 shows the comparison of biogas yields obtained from reactors operating in ambient conditions and temperature-controlled

conditions. Higher biogas yield was obtained from the BTP-2 reactor than that from the reactor operating at ambient temperature. Studies suggest that maintaining a constant digestion temperature is crucial to optimizing biogas production from a biogas plant [22]. If the fluctuations of digestion temperature exceed 5 °C at a short interval, then biogas production could lower considerably; therefore, a constant digestion temperature is crucial to optimizing biogas production [22]. It is apparent from this study that the temperature plays a significant role in increasing the biogas yield from a reactor as 49 % higher biogas yield is obtained in the reactor with controlled mesophilic temperature (Figure 6), which is obvious. A similar study conducted by Lohani et al. (2021) used the identical ratio of 2:1:1, 8 % TS, 1.2 gVS/L/day OLR during the summer season in the ambient temperature range of 22-26 °C, showing a biogas yield of 640 L/kgVSa. However, the same experiment conducted at winter temperatures of 11-19 °C yielded low biogas of 171 L/kgVSa, as shown in Figure 6 [19]. Based on a comparison of this study with a co-digestion experiment conducted earlier in summer in the temperature range of 22-26 °C [19], it can be found that the biogas yield was reduced by nearly 29 %. This study also suggests that biogas yield at summer ambient temperature (figure) is significant if we carefully select locally available substrates for co-digestion. As household biogas plants are serving as an important source of clean cooking energy in rural Nepal [23], their yield can be improved by co-substrate digestion.

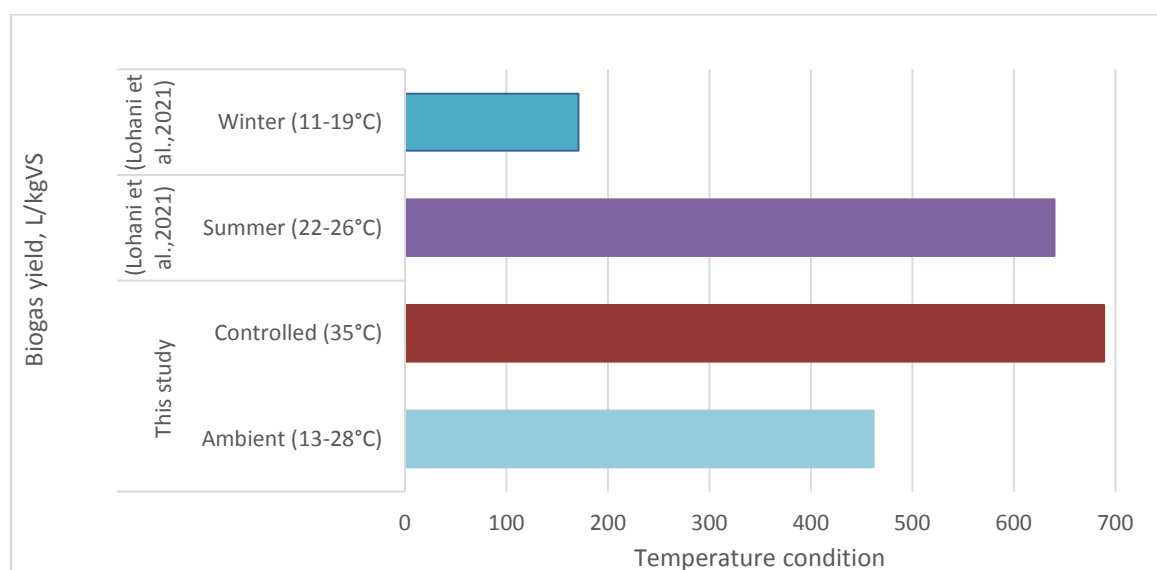


Figure 6. Biogas yields in different temperature conditions

4. CONCLUSIONS

In this study, the performance of bio-reactors co-digested with locally available substrate sewage sludge, poultry litter, and food waste at a mixing ratio of 2:1:1 was observed at both ambient summer temperature and controlled mesophilic temperature. The mixture of SS:PL:FW at a ratio of 2:1:1 had the highest biogas yield of 688.7 L/kg VS_{added} with a nearly 49 % higher value than the one operating in ambient temperature conditions at a similar mixing ratio and OLR. A reduced biogas yield of 462.3 L/kg VS_{added} was observed from the reactor operating in ambient temperature conditions. The average methane content in the controlled temperature and the

ambient temperature was 60 % and 55 %, respectively. The study suggests that temperature plays a vital role in biogas production efficiency and enhanced temperature condition and desired biogas yield can be obtained. Furthermore, the efficiency of the digester was affected by the temperature fluctuation in the ambient environment, thus reducing the biogas production by 49 % in comparison to the controlled temperature condition. From the result, it is apparent that the implementation of locally available temperature control and enhancement techniques such as canopy or greenhouse could be useful for optimized biogas production from the digesters operating under ambient conditions. Biogas production with all the locally available resources can surely be one of the best

ways to achieve sustainable waste management and it also contributes to the enhanced synergistic effect of anaerobic digestion. This study helps plan effectively towards sustainable development and circular economy by valorizing waste to energy conversion on the community and commercial scales.

5. ACKNOWLEDGEMENT

The authors would like to acknowledge the Renewable and Sustainable Energy Laboratory, Department of Mechanical Engineering, Kathmandu University.

REFERENCES

- Lohani, S.P., Keitsch, M., Shakya, S. and Fulford, D., "Waste to energy in Kathmandu Nepal-A way toward achieving sustainable development goals", *Sustainable Development*, Vol. 29, No. 5, (2021), 906-914. (<https://doi.org/10.1002/sd.2183>).
- D'Amato, D., Veijonaho, S. and Toppinen, A., "Towards sustainability? Forest-based circular bioeconomy business models in Finnish SMEs", *Forest Policy and Economics*, Vol. 110, (2020), 101848. (<https://doi.org/10.1016/j.forpol.2018.12.004>).
- Carus, M. and Dammer, L., "The circular bioeconomy-Concepts, opportunities, and limitations", *Industrial Biotechnology*, Vol. 14, No. 2, (2018), 83-91. (<https://doi.org/10.1089/ind.2018.29121.mca>).
- Sarika, J., "The contribution of anaerobic digestion and biogas towards achieving the UN sustainable development goals", *World Biogas Association*, (2016). (<https://doi.org/10.3390/su14063307>).
- Lohani, S.P., Chhetri, A. and Khanal, S.N., "A simple anaerobic system for onsite treatment of domestic wastewater", *African Journal of Environmental Science and Technology*, Vol. 9, (2015), 292-300. (<https://doi.org/10.5897/AJEST2014.1848>).
- Lohani, S.P., Dhungana, B., Horn, H. and Khatiwada, D., "Small-scale biogas technology and clean cooking fuel: Assessing the potential and links with SDGs in low-income countries-A case study of Nepal", *Sustainable Energy Technologies and Assessments*, Vol. 46, (2021), 101301. (<https://doi.org/10.1016/j.seta.2021.101301>).
- Devkota, G.P., "Renewable energy technology in Nepal: An overview and assessment", (2007). (<http://lib.icimod.org/record/6857>), (Accessed: 10 February 2022).
- Cardona, L., Levrard, C., Guenne, A., Chapleur, O. and L. Mazéas, "Co-digestion of wastewater sludge: Choosing the optimal blend", *Waste Management*, Vol. 87, (2019), 772-781. (<https://doi.org/10.1016/j.wasman.2019.03.016>).
- Akindele, A.A. and Sartaj, M., "The toxicity effects of ammonia on anaerobic digestion of organic fraction of municipal solid waste", *Waste Management*, Vol. 71, (2018), 757-766. (<https://doi.org/10.1016/j.wasman.2017.07.026>).
- Mehariya, S., Patel, A.K., Obulisamy, P.K., Punniyakotti, E. and Wong, J.W.C., "Co-digestion of food waste and sewage sludge for methane production: Current status and perspective", *Bioresource Technology*, Vol. 265, (2018), 519-531. (<https://doi.org/10.1016/j.biortech.2018.04.030>).
- Güngör-Demirci G. and Demirci, G.N., "Effect of initial COD concentration, nutrient addition, temperature and microbial acclimation on anaerobic treatability of broiler and cattle manure", *Bioresource Technology*, Vol. 93, No. 2, (2004), 109-117. (<https://doi.org/10.1016/j.biortech.2003.10.019>).
- Gómez, X., Cuertos, M.J., Cara, J., Morán, A. and García, A.I., "Anaerobic co-digestion of primary sludge and the fruit and vegetable fraction of the municipal solid wastes: Conditions for mixing and evaluation of the organic loading rate", *Renewable Energy*, Vol. 31, No. 12, (2006), 2017-2024. (<https://doi.org/10.1016/j.renene.2005.09.029>).
- Sosnowski, P., Wiczorek, A. and Ledakowicz, S., "Anaerobic co-digestion of sewage sludge and organic fraction of municipal solid wastes", *Advances in Environmental Research*, Vol. 7, No. 3, (2003), 609-616. ([https://doi.org/10.1016/S1093-0191\(02\)00049-7](https://doi.org/10.1016/S1093-0191(02)00049-7)).
- Zhang, C., Su, H., Baeyens, J. and Tan, T., "Reviewing the anaerobic digestion of food waste for biogas production", *Renewable and Sustainable Energy Reviews*, Vol. 38, (2014), 383-392. (<https://doi.org/10.1016/j.rser.2014.05.038>).
- Borowski, S., Domański, J. and Weatherley, L., "Anaerobic co-digestion of swine and poultry manure with municipal sewage sludge", *Waste Management*, Vol. 34, No. 2, (2014), 513-521. (<https://doi.org/10.1016/j.wasman.2013.10.022>).
- Ye, J., Li, D., Sun, Y., Wang, G., Yuan, Z., Zhen, F. and Wang, Y., "Improved biogas production from rice straw by co-digestion with kitchen waste and pig manure", *Waste Management*, Vol. 33, No. 12, (2013), 2653-2658. (<https://doi.org/10.1016/j.wasman.2013.05.014>).
- Kozłowski, K., Dach, J., Lewicki, A., Ciesilk, M., Czekala, W., Janczak, D. and Brzoski, M., "Laboratory simulation of an agricultural biogas plant start-up", *Chemical Engineering & Technology*, Vol. 41, No. 4, (2018), 711-716. (<https://doi.org/10.1002/ceat.201700390>).
- Lohani, S.P., Pokhrel, D., Bhattarai, S. and Pokhrel, A., "Technical assessment of installed domestic biogas plants in Kavre, Nepal", *Renewable Energy*, Vol. 181, (2021), 1250-1257. (<https://doi.org/10.1016/j.renene.2021.09.092>).
- Lohani, S.P., Shakya, S., Gurung, P., Dhungana, B., Paudel, D. and Mainali, B., "Anaerobic co-digestion of food waste, poultry litter and sewage sludge: Seasonal performance under ambient condition and model evaluation", *Energy Sources, Part A: Recovery, Utilization and Environmental Effects*, Vol. 00, No. 00, (2021), 1-16. (<https://doi.org/10.1080/15567036.2021.1887976>).
- Holliger, C., Alves, M., Andrade, D., Angelidaki, I., Astals S., Baier, U., Bougrier, C., et al., "Towards a standardization of biomethane potential tests", *Water Science and Technology*, Vol. 74, No. 11, (2016), 2515-2522. (<https://doi.org/10.2166/WST.2016.336>).
- Dobre, P., Nicolae F. and Matei, F., "Main factors affecting biogas production-An overview", *Romanian Biotechnological Letters*, Vol. 19, No. 3, (2014), 9283-9296. (https://www.rombio.eu/vol19nr3/lucr%201_Dobre%20Paul_Main%20factors%20affecting%20biogas%20production_revistaRBL_2014%20_1_.pdf).
- Sakar, S., Yetilmizsoy, K. and Kocak, E., "Anaerobic digestion technology in poultry and livestock waste treatment-A literature review", *Waste Management & Research*, Vol. 27, No. 1, (2009), 3-18. (<https://doi.org/10.1177/0734242X07079060>).
- Paudel, D., Jeuland, M. and Lohani, S.P., "Cooking-energy transition in Nepal: trend review", *Clean Energy*, Vol. 5, (2021), 1-9. (<https://doi.org/10.1093/ce/zkaa022>).



Research Article

Investigation of the Enhancement of Thermophysical Properties of New Combinations of MWCNTs with Several PCMs Consisting of a Type of Paraffin in Comparison with Some Mineral Compounds (AN-MN-6H₂O)

Seyed Amir Hassan Bathaei^a, Masoud Iranmanesh^{a*}, Hossein Amiri^a, Hajir Kourki^b

^a Department of Energy, Institute of Science and High Technology and Environmental Sciences, Graduate University of Advanced Technology, Kerman, Iran.

^b Department of Chemical Engineering, Polymer Engineering Group, Institute of Science and High Technology and Environmental Sciences, Graduate University of Advanced Technology, Kerman, Iran.

PAPER INFO

Paper History:

Received: 08 May 2022
Revised: 12 June 2022
Accepted: 28 June 2022

Keywords:

Solar Thermal Energy Storage,
Phase Change Materials,
Paraffin,
MWCNTs,
Thermophysical Properties

ABSTRACT

Thermal Energy Storage (TES) for solar thermal systems has attracted great attention because of the intermittent availability of solar energy. In the current paper, new combinations of several Phase Change Materials (PCMs) including a type of paraffin and some mineral compounds like ammonium nitrate and magnesium nitrate hexahydrate were examined and their thermophysical properties were compared. This study targets solar heating systems at different temperature intervals for the TES. Another new approach of this study is to determine the effect of Multi-Wall Carbon Nanotubes (MWCNTs) with two diameters (D) of 8 and 10-20 nm on paraffin's thermophysical property to improve these properties. An innovative method was used to measure Electrical Conductivity (EC) as it is easier to measure than thermal conductivity (K) to study the effect of nanoparticles on PCM behavior. The results showed that the highest values of improvement over paraffin properties were related to 5 % nanoparticle additive for both nanoparticle diameters among the percentages studied. The addition of 5 % nanoparticles with 10-20 nm and 8 nm to paraffin at 25 °C increased heat conductivity by 142 % and 156 %, respectively. The addition of nanoparticles to paraffin improved EC several times such that a diameter of 8 nm made a 300 % increase in EC compared to 10-20 nm.

<https://doi.org/10.30501/jree.2022.339549.1363>

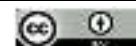
1. INTRODUCTION

The main problem associated with solar thermal energy is its storage and one of the best solutions is PCMs for storing energy by latent heat thermal energy storage (LHTES). It is considered one of the most efficient thermal energy sources. It is characterized by higher storage density (ρ) and low-temperature difference between the heat storage and release process. Due to the periodical solar energy availability, PCMs represent a proper alternative technique for storing solar energy [1]. Some criteria should be considered to select proper PCM candidates. For example, they should satisfy the operating temperature range for LHTES, high latent heat of fusion, and sizeable specific heat to ensure high storage density of the system. This material must have high thermal conductivity to increase the thermal charging and discharging rate. Besides these criteria, the material with high density is favored as it improves energy storage density and reduces the volume of the TES system. Moreover, the PCM is desired at a low price and abundant availability.

However, it is challenging to select a PCM with a perfect profile property, thermal boundaries, and operation goals for a proper application or to match the thermal conditions and requirements of LHTES design.

Considerations such as thermophysical properties, thermal stability in thermodynamic cycles, and environmental properties should be considered to find a suitable PCM for storing solar energy. Many investigations have been done on the thermophysical properties of various materials to find suitable TES materials at different temperature intervals. Using PCMs in building applications is a novel, sustainable, and efficient solution to improve the energy performance of buildings. Various PCMs such as fatty acids, paraffin, and inorganic salts have been used to improve the energy performance of buildings. The addition of Butyl Stearate (BS) enhances thermal capacity and exhibits corrosion protection of rebar by hindering penetration of chloride ions into the concrete [2]. The use of carbon fiber PCM, including paraffin, to manage the heat of lithium-ion batteries has led to the improved thermal performance of this type of battery [3-5]. PCM's TES technologies have advantages such as high energy storage density, high compactness, simple structure, and ease of maintenance. Besides, PCM can also be used as a thermal

*Corresponding Author's Email: m.iranmanesh@kgut.ac.ir (M. Iranmanesh)
URL: https://www.jree.ir/article_155110.html



control for devices that work and generate heat intermittently such as chips [6, 7]. PCMs in solar collectors like flat plates, evacuated tubes, and heat pipes are used to store energy from the collector and benefit it when solar energy is not accessible [8-11]. PCMs have a high storage density (amount of energy stored per unit mass) and a narrow temperature range for charging and discharging the storage. This range corresponds

to the phase transition temperature of the PCM. The compactness of the PCM storage system results in greater flexibility in choosing a location for the storage system [12].

Several PCMs, which many researchers have investigated and can be candidates for solar thermal applications, are presented in Table 1.

Table 1. Thermophysical properties of some appropriate materials for TES

Materials	T _m (°C)	ρ (kg/m ³)	LHM (kJ/kg)	C _p (kJ/kg.K)	K (W/m.K)	References
Formic acid	9	-	245	2.180	0.272	[13]
Polymethyl methacrylate (PMMA)	41	-	54.6-48.7	-	0.16-0.25	[14]
Paraffin wax	52	Liquid 780	210	Liquid 2.9	Liquid 0.15	[15-17]
		Solid 860		Solid 2.1	Solid 0.24	
Paraffin wax	52-54	Liquid 814	266	Liquid 2.95	Liquid 0.15	[1]
		Solid 900		Solid 2.195	Solid 0.232	
Paraffin wax	53-57	0.895	184.48	2.384	0.41	[18]
		0.867	240	3.046	0.148	
Sodium acetatetrihydrate with graphite	58	1.35	210 180-200	2.5	2-5	[19]
Palmitic acid (PA)	60.8	-	148-149	-	0.6	[20]
Mandelic acid	118-121	1300	161	-	-	[21]
Benzoic acid	121-123	1080	114-147	-	-	[21]
Phthalic anhydride	131	1530	159	-	-	[21]
Dimethyl terephthalate	142	1290	170	-	-	[21]
Adipic acid	151-155	1360	260	-	-	[21]

PCMs suffer from defects such as phase separation, slow heat transfer, leakage, and instability [22-24]. One of the significant disadvantages of PCMs is their low thermal conductivity, which is present in all pure materials except metal-based materials [25].

Hence, the low heat conductivity of PCM increases the temperature gradient and time constant, reducing the heat transfer speed [26, 27]. Low thermal conductivity reduces PCM heat storage and release [28, 29], which reduces the performance. The thermal conductivity of PCMs should be improved to enhance the heat transfer rate and the stored energy coefficient utilization [30].

It is necessary to enhance the thermal conductivity to improve the performance of the thermal energy storage system and accelerate the process of charging and discharging energy [31]. Various techniques can enhance the thermal conductivity of PCMs by incorporating fins or extended surfaces, metal matrices, electrospinning, encapsulation, dispersion of high-conductivity particles or nanomaterials in the PCM itself, employing metal foams, using multiple PCMs, and embedding heat pipes [25, 32-37].

Among all the techniques mentioned above, the addition of nanoparticles to enhance the thermal conductivity of PCMs is the topic of the present research. Nano-inclusion-assisted thermal conductivity enhancement has been used for developing nano-enhanced organic PCMs for LHTES [17, 19, 20]. The thermal conductivity increases as nanoparticle size decreases, while surface tension increases as nanoparticle size increases [38].

This study investigates the thermal conductivity effects of adding nanoparticles to paraffin. Addition of nanoparticles improves the thermophysical properties of PCM and increases the PCM's thermal performance by reducing the heat transfer time [39]. Experimental measurements showed that adding

nanoparticles to enhance thermal conductivity could bring about perfect results in optimizing the phase change temperatures and decreasing heat capacity coefficient, leading to a reduction of energy storage [18].

Due to properties of paraffin like high heat of fusion, nonpoisonous, stable properties after 1500 cycles, no phase separation, and the phase process only result in a small volume change. Meanwhile, low thermal conductivity in a solid state and supercooling (liquid state of a body when its temperature is less than the crystallization temperature) are included as the significant disadvantages of organic PCM.

The early mentioned criteria, especially melting point and latent heat, should be considered suitable for heat storage in various solar thermal energy systems [1, 40]. Thus, based on the operating temperature range for solar thermal applications like solar collectors, they are classified according to the type of concentrators listed in Table 2.

Table 2. Classification of solar collectors according to the concentration degree [41]

Category	Example	Temperature range (°C)
No concentration	Flat-plate Evacuated tube	Up to 75 Up to 200
Medium concentration	Parabolic cylinder	150-500
High concentration	Parabolic	1500 and more

Due to some unsuitable paraffin properties including thermal conductivity, two ways to increase the contact surface and add nanoparticles have received much attention [42-44].

In this research, nanoparticles are used to improve the thermal conductivity coefficient.

Past research has shown that at any temperature and concentration of nanotubes, the incorporation of some materials such as metal oxides [45], single-walled carbon nanotubes [46], MWCNTs [47], carbon nanofibers [48], nanoplatelets [49] and graphene [50] into the base fluid at a nanoscale level improves the thermal conductivity. The relative rate of improvement in thermal conductivity depended on the amount of added nanomaterials' thermal conductivity, addition ratio, and mixing quality [51]. Improvements in thermal conductivity are acceptable at limited costs [52].

According to the early mentioned criteria and the results of some reported publications in Table 1, thermophysical properties of new combinations of several PCMs for solar TES applications, especially in terms of melting point and latent heat, are studied and compared in this paper. They include a new commercial type of improved paraffin wax and three combinations of ammonium nitrate and magnesium nitrate hexahydrate (AN-MN-6H₂O).

Previous research has used solutions of PEG, PA6, and various nanoparticles (SiO₂, Al₂O₃, Fe₂O₃, and ZnO) to produce composite PCMs by electrospinning whose fiber diameter strongly depends on the electrical conductivity of the solutions. For example, the fiber diameter is reduced as the electrical conductivity increases [36, 37].

Another new approach adopted in this study is to determine the effect of the diameter of MWCNTs on the thermophysical properties of paraffin. In order to determine the appropriate weight percentage of nanoparticles, an innovative method and unique device have been implicated by measuring EC rather than thermal conductivity (K) as it is easier to measure than K to study the effect of nanoparticles on PCM behavior.

2. EXPERIMENTAL

2.1. Materials

In general, an essential specification of PCMs is to store energy through latent heat during the charging process, which justifies their ability to store heat and keep cold or hot. Considering the fact that one of the primary aims of this study is to investigate PCMs and their properties like melting point and latent heat, as mentioned earlier in the previous section, they are suitable for solar heat energy storage. Then, the measurement and comparison of the properties of four ingredients include an improved type of paraffin by MWCNTs and three mineral compounds provided by the combination of Ammonium Nitrate and Magnesium Nitrate hexahydrate (AN-MN-6H₂O). Their binary phase change diagram is displayed in Figure 1.

The eutectic is a minimum-melting composition of two or more components, as shown in Figure 1; each melts or freezes congruently, forming a mixture of the component crystals during crystallization [53]. The eutectics have a sharp melting point similar to pure substance and volumetric storage density is slightly above organic compounds.

These three selected compounds are considered:

- Eutectic (contains 61.2 % ammonium nitrate and 38.8 % magnesium nitrate hexahydrate)
- Hyper eutectic (contains 55 % ammonium nitrate and 45 % magnesium nitrate hexahydrate)
- Hypo eutectic (contains 79 % ammonium nitrate and 21 % magnesium nitrate hexahydrate)

Merck provides these minerals and Khavaran Company provides paraffin. Table 3 shows the essential characteristics of these materials. Before doing the tests, the ingredients with the specified percentages were melted and mixed with a magnetic stirrer for 15 minutes, and then they were made ready to perform the tests. The basic information about nanoparticles is listed in Table 4.

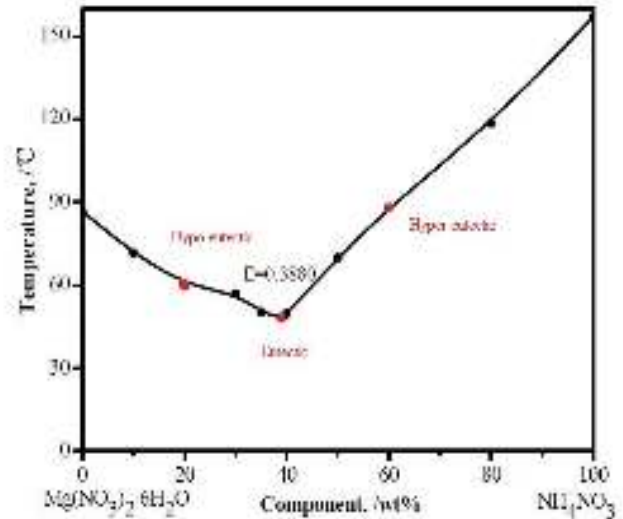


Figure 1. The binary phase change of AN-MN-6H₂O in composition

Table 3. The materials studied and the essential information including melting point and density

Materials	T _m (°C)	ρ (kg/m ³)
Paraffin	59	931
Eutectic	44.8	1561.4
Hypo eutectic	60	1577
Hyper eutectic	118	1665.4

Table 4. Specification of nanoparticles

Material	Paraffin	MWCNTs (8 nm)	MWCNTs (10-20 nm)
Purity (%)	95	> 95	> 95
-COOH content (wt %)	-	3.86	2.00
OD (nm)	-	< 8	10-20
ID (nm)	-	2-5	5-10
Length (μm)	-	10-30	10-30
Special surface area (m ² /g)	-	> 500	> 200
ρ (g/cm ³)	0.931	2.1	2.1
EC (S/cm)	-	> 100	> 100

2.2. Nanocomposite preparation

Nanofluid is generally prepared in two ways. In the one-step method, nanoparticles are prepared and dispersed directly into the fluid. The nanoparticles are provided in powder form and then added to the base fluid by the two-stage method. On the other hand, the suspension, surfactants, diffusers' pH controls, and ultrasonic oscillations are used to stabilize the

nanoparticles and prevent agglomeration and particle deposition. The second method has been used to prepare the nanocomposite in this research. Ultrasonic agitator, mechanical agitator, and toluene as a solvent have been used to disperse and homogenize the compound. After weighing the material with 5 grams of paraffin and the desired percentage of nanoparticles, it is dissolved in 50 ml of toluene and stirred for 15 minutes with an ultrasonic stirrer (three times, each time for five minutes with one-minute intervals for device rest and mixing). The solution is mixed with a mechanical stirrer for 20 minutes (twice for ten minutes at one-minute intervals to rest the device and mix). To improve the paraffin's thermal storage properties and find the optimal combination of nanoparticles with the PCM, different percentages of MWCNT such as 0.5 wt %, 1 wt %, 2.5 wt %, and 5 wt % were selected to add the PCM. Each ingredient was mixed with the base material (as mentioned) in a cylindrical glass container with a 52 mm diameter. Due to the accumulation of electric charge at sharp points and the negative impact on measuring electrical conductivity, a cylindrical container was used, as displayed in Figure 2. An electrical circuit setup was arranged to test the electrical resistance of all the samples, as displayed in Figure 3. The specific resistance of the nanoscale compound was measured, with a voltage range of 200 v to 200 kV.



Figure 2. Picture of the cylindrical glass container for electrical resistance testing



Figure 3. Picture of the electrical circuit setup

Determination of the thermo-physical properties of PCM is the basic required information for the research and applications. The properties mainly include density, melting point, fusion latent heat, thermal conductivity, specific heat capacity (C_p), viscosity, and thermal expansion coefficient. Generally, the phase change properties such as melting point, fusion latent heat, and specific heat capacity can be measured by Differential Scanning Calorimetry (DSC) [54]. A DSC was used to determine the thermos-physical properties of the binary system. Depending on the DSC settings throughout the measurements, varying results were obtained. In this research, a heating rate of 5 °C per minute was used.

Furthermore, the correct phase transition temperature range was almost impossible to obtain simply from DSC measurement. Combining phase equilibrium considerations with DSC measurements presents a reliable design method to incorporate phase-change heat and temperature range [12]. Various thermo-physical properties of the mentioned materials like density, viscosity of liquid phase, thermal conductivity, heat capacity, and heat release rate (HR) were measured by standard methods described in detail. Materials' density was measured by the Immersion method at different temperatures in the liquid and solid phases with the accuracy of 10 %. The experiments for thermal analysis of materials were carried out by the DSC1 model, with a heating/cooling rate of 5 °C/min. The neutral atmosphere in this device is nitrogen gas and the atmosphere is reactive with oxygen gas. This device monitors the sample's thermal behavior with Topem software and in the form of modulating. This device is based on measuring the heat flux between the sample and the reference, measured by temperature changes and sinusoidally. This device is capable of operating in the temperature range of -130 to 600 °C (if this temperature does not destroy the sample). The DSC tests were performed as melting-solidification-melting. The conductivity of PCM samples was measured by the KD2 Pro thermal properties analyzer based on the transient hotwire method.

The materials' thermophysical properties such as specific heat capacity, latent heat (L), and thermal conductivity (K) for the temperature range of 25-55 °C were measured based on their standard code. The instruments for measuring the properties are shown in Figure 4 and their specifications and standard methods are listed in Table 5.

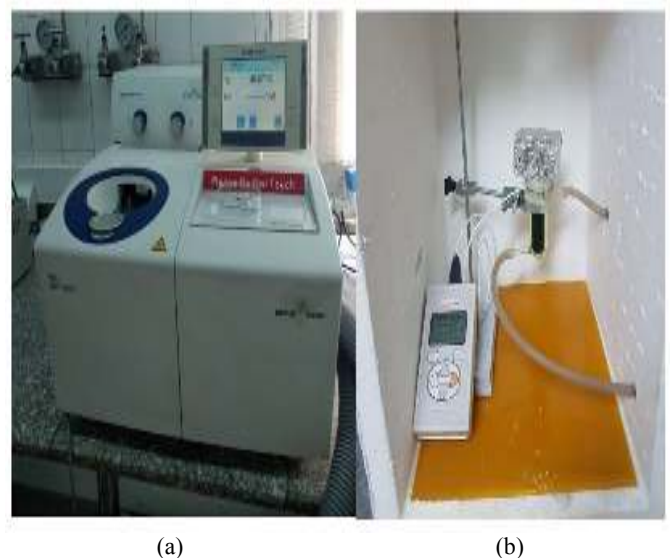


Figure 4. Picture of the DSC testing machine manufactured by (a) Mettler toledo and (b) KD2 testing device from Decagon company

3. METHOD

3.1. Measurement of properties

Table 5. The measurement tools and their specifications

Properties	Producer and model	Standard	Accuracy (%)
Latent heat	Mettler toledo DSC 1	ASTM D3418	0.52
Specific heat	Mettler toledo DSC 1	ASTM E1269:2018	0.52
Thermal conductivity	Decagon KD2	EN55022:1987	5
Density	-	-	5

An insulated flask was used to measure the materials' heat release rate (the flask was insulated up to 6 cm thickness of polyurethane foam), as shown in Figure 5. The insulated flask container was filled with 200ml water and PCM was filled in a 10 ml spherical glass container and immersed in the water. Two thermocouples (K type) were used to measure the temperatures and were recorded by the data logger, one in the glass container for PCM and one in the water flask. After melting the PCM entirely in the glass container at a constant temperature, it was placed inside the flask and the temperature changes were recorded. Due to the flask insulation, all the heat released from the PCM was absorbed by the water and finally, it reached the equilibrium temperature.

**Figure 5.** Picture of the insulated flask and measuring heat release rate test setup

4. RESULTS AND DISCUSSION

4.1. Comparison of mineral PCMs

One of the desirable features of PCM is the low volume expansion coefficient (α_L), which is obtained here by examining PCM volume in both liquid and solid states. This value was 1 % for paraffin and is 5.08 and 1.2 % for the combination of eutectic and hypo, respectively. Table 6 shows the density values and volumetric expansion coefficients of the test materials.

Table 6. Density and thermal expansion coefficient of materials

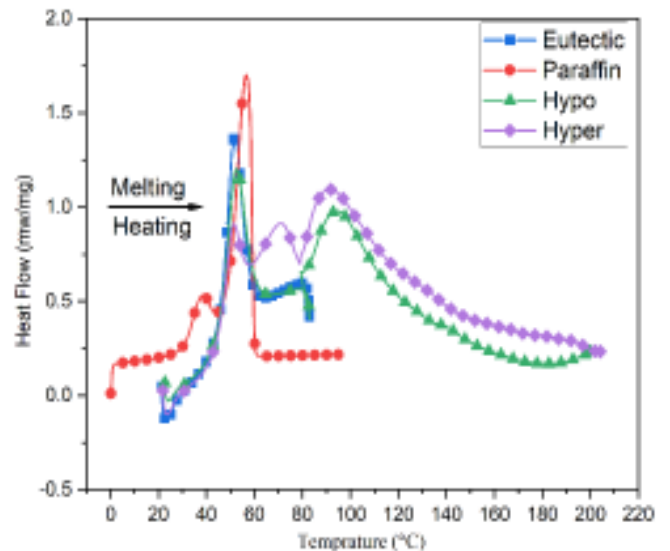
Material	T_m (°C)	ρ_{solid} (kg/m ³)	ρ_{liquid} (kg/m ³)	α_L (%)
Paraffin	59	931	911	1
Eutectic	44.8	1596	1515	5.08
Hyper	118	1665	-	-
Hypo	60	1577	1558	1.2

The DSC test results for the materials have been reviewed, as shown in Figure 6, and compared with each other considering the importance of latent heat and specific heat capacity in selecting PCMs. The amount of Latent Heat during the Melting (LHM) process or the enthalpy change of phase transition (storage density) is possible to estimate by using the area under the peak level of the DSC diagram [12]. The Origin software automatically calculates the total peak area, i.e., the total enthalpy change (Q_{PC}) phase transition. It can be calculated theoretically using the following equation:

$$Q_{pc} = \int_{t_1}^{t_2} \left(\frac{\delta Q}{dt} \right)_{pc} dt \quad (1)$$

As per Figure 6, it is seen that the peak of each curve is near the melting point of the corresponding material. For the paraffin, the amount of LHM obtained was 187.78 kJ/kg in the temperature range of 48.01 to 59.82 °C. Alternatively, for the eutectic, hypo, and hyper composition, the amount of latent heat content obtained was 152.2 kJ/kg, 416 kJ/kg, and 559 kJ/kg, respectively, for the temperature range of 28-58 °C, 50-120 °C, and 75-150 °C.

The higher the amount of latent heat, the more the ability of PCM's TES. As demonstrated by the results, the highest amount of latent heat was obtained for the hyper eutectic composition, but due to its high melting point (118 °C), it could be applied to the solar collectors rather than flat plate ones. The lowest amount of latent heat was for the eutectic composition. The comparative layout of the DSC results of all the investigated materials in a single diagram is shown in Figure 6.

**Figure 6.** Comparative diagram of DSC analysis of the materials

DSC tests were employed to measure the variations of specific heat capacity corresponding to the temperature obtained from materials' three states (solids, liquid, and phase changes). The comparative results of the materials' specific heat capacity in a single diagram are shown in Figure 7. This figure indicates that the most remarkable value of all these materials is obtained during the phase change period and the most significant value is for the eutectic compound.

The test results of obtaining the heat release of a particular volume of material during the solidification process (discharging PCM) in an insulated flask within 1000 Sec are shown in Figure 8. The results show that the hypereutectic

compound has the highest discharge time and the most extended duration related to heat release; after that, paraffin, hypo, and eutectic compounds are in the following order.

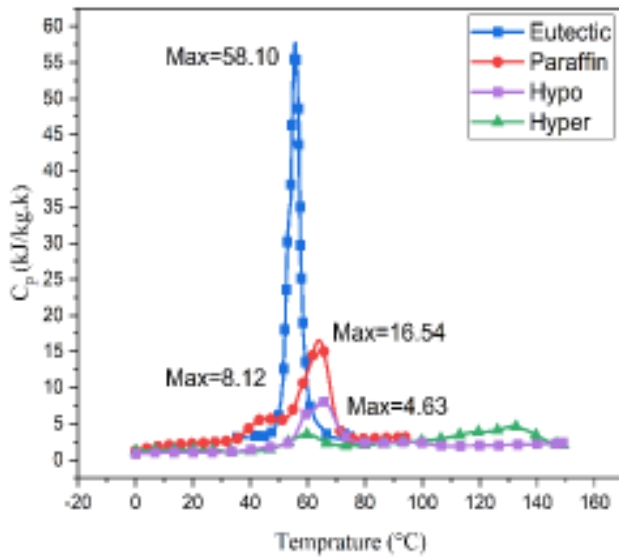


Figure 7. Comparative diagram of specific heat capacity variations versus the temperature of the materials

The heat released rate values for a given volume of 10 ml of the substance in 200 ml of water are given in Table 7. The results are compared with the amount of DSC calculation of the total enthalpy change of phase transition (latent heat) (Q_{PC}) using Equation 1. The results indicate that the higher the heat release rate, the higher the material's latent heat and the greater the melting point. In addition, it is clear that the hyper composition is suitable for higher-temperature applications of solar thermal energy. Others including hypo composition, paraffin, and eutectic composition have the capability to be used for the lower temperature of solar thermal energy applications. Moreover, the amounts of specific heat capacity in each state in Table 7 show that this

Table 7. The values of specific heat capacity (C_p) in different states and the latent heat content of materials

Materials	L (kJ/kg)	HR (J/s)	$C_{p,Liquid}$ (kJ/kg.K)	$C_{p,Max}$ (kJ/kg.K)
Paraffin	187.78	0.7954	3.23	16.5409
Eutectic	152.2	0.5775	3.5564	58.102
Hypo	416	1.419	2.02898	8.12041
Hyper	559	2.3119	2.05435	4.63736

The hyper composition shows the highest amount of K factor at 0.727 while paraffin content shows the lowest value of 0.328 w/m.K. They are almost identical to the values reported in the references [55].

Table 8. The results for the conduction heat transfer coefficient of the materials

Materials	$K_{55^\circ C}$ (w/m.K)
Paraffin	0.328
Eutectic	0.635
Hypo	0.532
Hyper	0.727

In summary, the variation of all the tested materials' measured properties including density, latent heat, and

property is not proportional to the material's latent heat. It could not be the only proper criterion for selecting PCM.

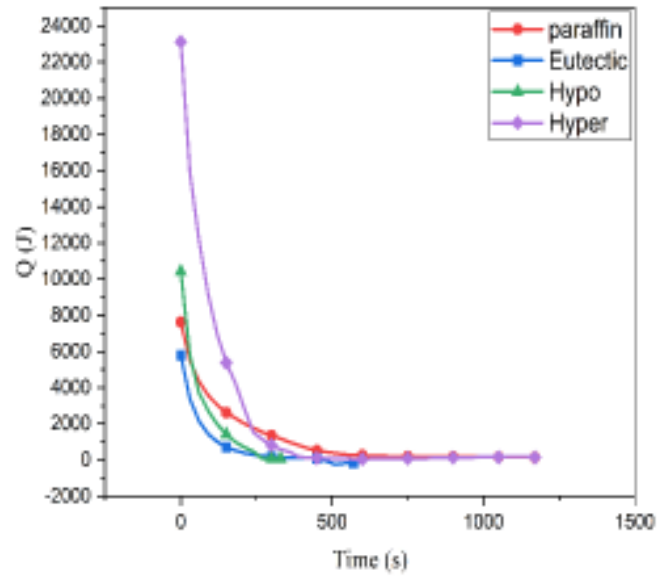


Figure 8. Comparative diagram of the heat released within 1000 seconds for materials

A cylindrical mold with an outer diameter of 10 mm, a length of 6.5 cm, and an inner diameter of 2 mm was prepared to measure the conduction heat transfer coefficient (K factor) of solid-state PCMs for the Hyper and Hypo composition tests. In the liquid state of paraffin and eutectic composition, a quantity of 50 ml of the substance is placed inside the container and the probe measures the K factor. The thermal conductivity values measured at 55 °C for the materials can be seen in Table 8. The excellent value of this factor accelerates the heat transfer rate and shorter melting time to absorb energy storage. The lower heat transfer coefficient helps longer solidification time and provides thermal stability for designing a TES system.

thermal conductivity corresponding to the melting point is illustrated in Figure 9. It is vital to notice that the properties of all the PCMs consisting of density, latent heat, and thermal conductivity proportionally change with the melting point except for the eutectic compound. Finally, it is worth mentioning that the eutectic composition shows the minimum melting point.

4.2. Effect of adding nanoparticles to paraffin

This part of the study examines the effect of adding MWCNTs with two different diameters and different weight percentages on the properties of paraffin which aims to determine the optimal percentage of nanoparticles based on the output current through nanocomposite with increasing voltage at the ambient temperature of about 25 °C. The results shown in

Figure 10 are for output currents through paraffin nanocomposites versus the input voltages with different weight percentages of 0.5, 1, 2.5, and 5 for the two size nanocomposites 8 and 10-20 nm. The applied voltage changes from 0 to 12000 volts and the output current changes from 0 to 20 mA. It is observed that the electrical conductivity increases with the percentage of adding nanoparticles for both sizes, 8 and 10-20 nm. It shows excellent electrical conductivity even at low voltages of about 15 volts. The currents that passed through the 8 and 10-20 nm nanocomposites are 20 mA and 0.52 mA, respectively.

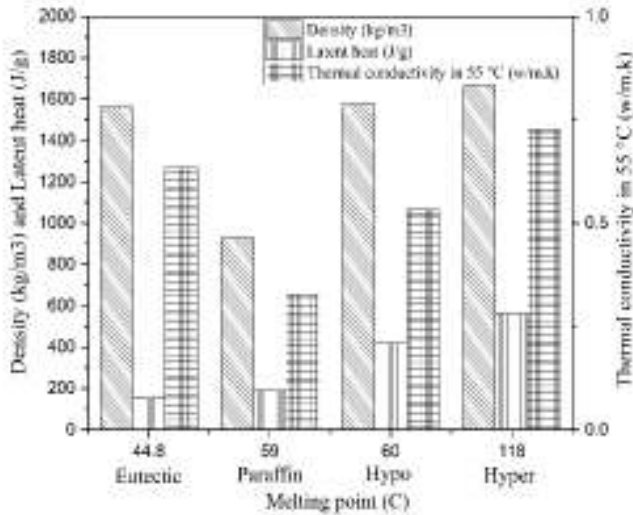


Figure 9. Comparative diagram of density, latent heat, and thermal conductivity of tested materials

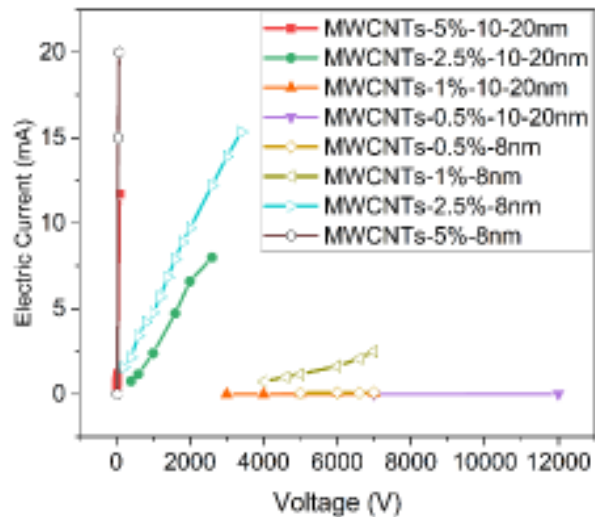


Figure 10. Comparative diagram of changes in electrical current through nanocomposites with increasing voltage

In Figure 11, nanocomposites' electric conductivity with different percentages is visible for both nanoparticles 10-20 and 8 nm, indicating an increase in its value from zero to 0.12721 and 0.38121 S/cm, respectively, as per Figure 12. Among the four different percentages nominated for review, 5 % addition of each of the nanoparticles shows the best behavior based on the electrical conductivity. This weight percentage addition (5 %) has been used for further experiments due to the highest electrical conductivity in nanocomposites shown in Table 9.

Table 9. Specifications of nanocomposites

Base material	Nano particle	Particle diameter r (nm)	Particle weight percentage (wt %)	Nano-paraffin composite symbol
Paraffin	MWCNTs	< 8	5	A
Paraffin	MWCNTs	10-20	5	B

Moreover, the higher conductance rate for Nanoparticles 8 is higher than 10-20 nm due to their higher specific surface.

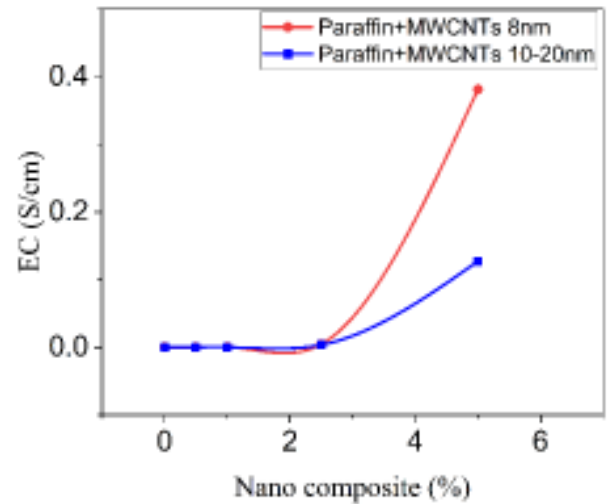


Figure 11. Comparative diagram of changes in electrical conductivity of compounds with different percentages of nanoparticles

As shown in Figure 12, adding nanoparticles to paraffin does not change the shape of the DSC diagram. However, it reduces the maximum value, which leads to a decrease in the subsurface area of the diagram, thus reducing the amount of latent heat. For the paraffin, the amount of LHM obtained was 187.78 kJ/kg in the temperature range of 48.01 to 59.82 °C. In comparison, addition of nanoparticles with diameters of 10-20 and 8 nm reduces the LHM to 162.02 and 168.58 kJ/kg in the same temperature range, respectively.

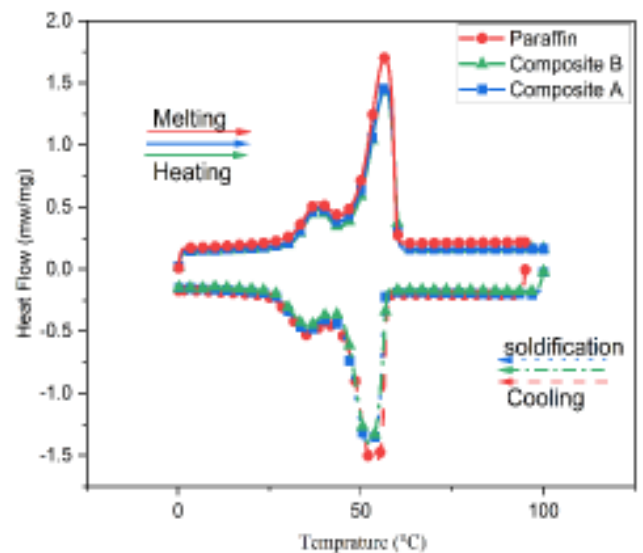


Figure 12. Comparative diagram of DSC analysis of the paraffin and nano-paraffin composites

Due to the uniformity of C_p as per Figure 13, the diagram shows that in the case of paraffin and its nanocomposite, the maximum specific heat value is selected as a suitable criterion for comparative analysis of their behavior. Adding 8 nm diameter nanoparticles reduces the maximum amount of specific heat to 13.9379 kJ/kg.K. In comparison, adding nanoparticles with 10-20 nm diameter increases this amount to 17.5034 kJ/kg.K.

values of K , ρ , and C_p at 55 °C in Equation 2, α values are obtained for paraffin and nanocomposites.

$$\alpha = \frac{K}{\rho C_p} \tag{2}$$

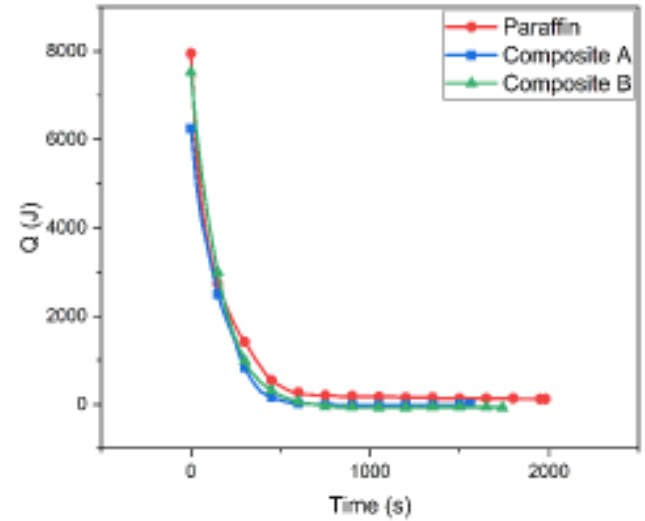
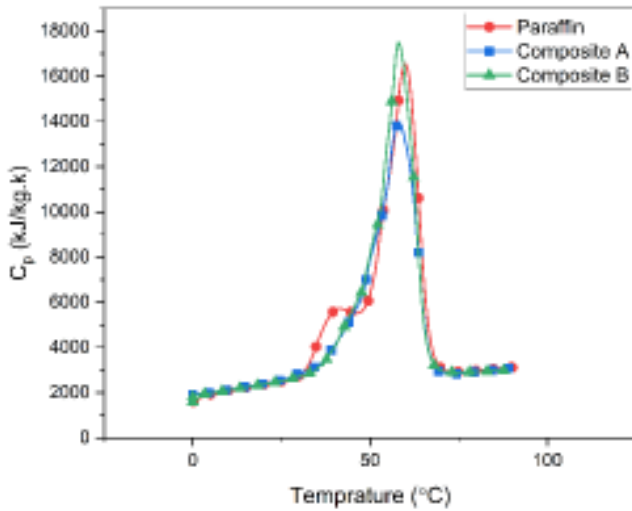


Figure 13. Comparative diagram of specific heat capacity variations versus the temperature of paraffin and nano-paraffin composites

Figure 14. Comparative diagram of heat released within 1000 seconds for paraffin and nano-paraffin composites

A decrease in heat release in 1000s was observed by adding nanoparticles to paraffin and 0.7525 and 0.6253 (J/s) for nanoparticles with diameters of 10-20 and 8 nm, respectively. These changes are observed in Figure 14.

The addition of nanoparticles with diameters of 8 and 10-20 nm shows an increase in the thermal diffusivity by 35.68 % and 4.88 %, respectively, as displayed in Table 10.

Thermal diffusivity shows the heat transfer rate of material from the hot end to the cold end. By placing the measured

Table 11 shows the obtained results achieved by some other researchers where the elements affect thermal conductivity and the percentages of different nanoparticles were added with different diameters. It can be concluded that the results are superbly similar to the present study findings.

Table 10. Thermal properties of paraffin and nano-paraffin composites

Materials	L (kJ/kg)	$C_{p,Max}$ (kJ/kg.K)	$K_{25^\circ C}$ (w/m.K)	$K_{55^\circ C}$ (w/m.K)	$EC_{25^\circ C}$ (S/cm)	$\alpha_{L, 55^\circ C}$ (mm ² /s)	HR (J/s)
Paraffin	187.78	16.5409	0.088	0.328	-	0.021719	0.7954
Composite A	168.58	13.9379	0.138	0.375	0.38121	0.029469	0.6253
Composite B	162.02	17.5034	0.125	0.364	0.12721	0.022778	0.7525

Table 11. Improvement in thermal conductivity of different nanocomposites with specified weight percentage by the researchers

Nanoparticle	MWCNTs	MWCNTs	nano-Al ₂ O ₃ nano-ZnO ₂ nano-SiC
Base material	Myristic acid (MA)	Paraffin	Paraffin
OD (nm)	< 8	20 50	
length (µm)	10-30	0.52 515	
fraction (vol %)	1 2 3	5	1
K (w/m.K)	0.1913 0.2026 0.2083	0.324 0.309	0.2
K Improvement (%)	3.63 9.75 12.84	23 17	3.3 1.8 4.2
References	[56]	[57]	[51]

According to Figure 15, Both composites have improved thermal and electrical conductivity. On the other hand, adding nanoparticles to paraffin has reduced the amount of latent heat, which is not desirable for energy storage systems. Furthermore, it is obvious that composite A has shown the highest value of $EC_{25^{\circ}C}$, $K_{25^{\circ}C}$ and $C_{P,Max}$.

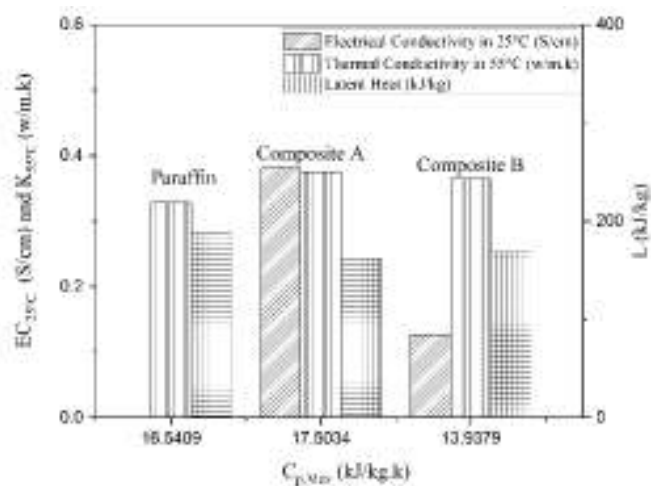


Figure 15. Comparative diagram of latent heat, electrical and thermal conductivity of nanocomposite and paraffin in maximum specific heat capacity

In summary, the investigation on adding nanoparticles to paraffin on its thermophysical properties reduces the LHM. However, it is deduced that adding nanoparticles to paraffin improves the base material's thermal conductivity, electrical conductivity, and thermal diffusivity. Adding nanoparticles with diameters of 10-20 and 8 nm, decreases latent heat by 10.22 % and 13.71 %, increasing thermal conductivity by 10.975 % and 14.329 % at 55 °C, relatively. Adding nanoparticles with a diameter of 8 nm reduces the maximum amount of specific heat by 15.77 %. In comparison, adding nanoparticles with a diameter of 10-20 nm is 5.8 %. An increase in this amount was detected.

5. CONCLUSIONS

Several PCMs have been studied in this experimental investigation based on thermophysical properties to introduce proper TES materials for solar heating systems applications.

To select the proper PCM candidates, a set of criteria that are supposed to be followed for storing energy includes; Phase change temperature in the desired range, fusion's latent heat, thermal conductivity, specific heat, and density, which is considered and tested, and the obtained results can be deduced from this research as follows:

- The operating temperature range of applications based on melting temperature is between 44.8 °C and 118 °C for paraffin wax, eutectic, hypo, and hyper eutectic combination AN-MN-6H₂O. The results indicate that all tested materials' melting points and latent heat proportionally increase or decrease. The rational conclusion would express that the higher the latent heat of the material, the greater the melting point.
- The properties of all the PCMs, like density, latent heat, and thermal conductivity, proportionally change with the melting point except for the eutectic compound. The eutectic composition has a minimum melting point among all the tested materials.

- All the materials investigated in this research have almost a low thermal conductivity coefficient, slowing down the conduction heat transfer, which is advantageous in many TES areas.
- The other criterion was the latent heat of fusion, in which the amount should be high enough to ensure the system's high storage density. The DSC analysis showed that the highest latent heat was obtained for the hyper eutectic composition (118 kJ/kg). The smallest one was obtained for the eutectic composition (44.8 kJ/kg).
- Comparing the amounts of latent heat with the specific heat capacity for three states (solids, liquid, and phase changes) of materials shows that this property is not proportioned to the material's latent heat. It could not be the only criterion for selecting PCM.
- According to the properties such as; high heat release rate, high thermal capacity, and high latent heat, paraffin would be suitable for storing thermal energy in applications below 60 °C, as in solar thermal heating systems. Its low thermal conductivity helps longer solidification time and provides thermal stability for its design's TES system. However, the low density of this type of paraffin reduces its potential for heat storage capability.
- By adding nanoparticles to paraffin, a latent heat reduction has been observed for both nanoparticle diameters, notably lesser in 8 nm-diameter nanoparticles. On the other hand, increasing the amount of thermal and electrical conductivity in 8 nm diameter nanoparticles is more. Suppose latent heat and a reduction in specific heat capacity are not considered. In that case, adding 8 nm-diameter nanoparticles is a better choice between the two diameters of nanoparticles nominated to improve paraffin's performance.
- By reducing the nanoparticle diameter from 10-20 to 8 nm, PCM's proper properties improved even further, one of the reasons being the increase in the surface area of the nanocomposite.
- Finally, since none of the PCMs has a perfect property profile, each application has unique thermal boundaries. Operation goals and the excellent variety of PCMs make it challenging to select one to match the thermal conditions and LHTES design requirements.

Nanoparticles' effect on electrical conductivity has been much more significant than thermal conductivity and other thermophysical materials' properties.

6. ACKNOWLEDGEMENT

The authors appreciatively acknowledge the Research Council of the Graduate University of Advanced Technology.

NOMENCLATURE

TES	Thermal Energy Storage
ASTM	American Society for Testing and Materials
DSC	Differential Scanning Calorimetry
LHM	Latent Heat During the Melting
LHTES	Latent Heat Thermal Energy Storage
PCMs	Phase Change Materials
MWCNTs	Multi-Wall Carbon Nanotubes
SEM	Scanning Electron Microscopy
T_c	The temperature that the PCM start to phase change (°C)
T	Temperature (°C)

T_m	Melting point temperature (°C)
C_p	Specific heat capacity (kJ/kg.K)
C_{max}	Maximum specific heat capacity (kJ/kg.K)
Q	Heat release (kJ)
HR	Heat release rate (J/s)
m_{pcm}	Mass of PCM (g)
m_{water}	Mass of water (g)
C_{PCM}	Specific heat of PCM (kJ/kg.K)
C_{water}	Specific heat of water (kJ/kg.K)
T_{PCM}	The temperature of PCM (°C)
T_{water}	The temperature of water (°C)
t	Time (s)
EC	Electrical Conductivity (S/cm)
K	Thermal conductivity (w/m.k)
L	Specific latent heat (kJ/kg)
ρ	Density (kg/ m ³)
α	Thermal diffusivity (m ² /s)
α_L	Thermal expansion coefficient

REFERENCES

- Khyad, A., Samrani, H., Bargach, M. and Tadili, R., "Energy storage with pcms: Experimental analysis of paraffin's phase change phenomenon & improvement of its properties", *Journal of Materials and Environmental Sciences*, Vol. 7, No. 7, (2016), 2551. (https://www.jmaterenvironsci.com/Document/vol7/vol7_N7/271-MES-2362-Khyad.pdf).
- Cellat, K., Tezcan, F., Kardaş, G. and Paksoy, H., "Comprehensive investigation of butyl stearate as a multifunctional smart concrete additive for energy-efficient buildings", *International Journal of Energy Research*, Vol. 43, No. 13, (2019), 7146-7158. (<https://doi.org/10.1002/er.4740>).
- Babapoor, A., Azizi, M. and Karimi, G., "Thermal management of a Li-ion battery using carbon fiber-PCM composites", *Applied Thermal Engineering*, Vol. 82, (2015), 281-290. (<https://doi.org/10.1016/j.applthermaleng.2015.02.068>).
- Karimi, G., Azizi, M. and Babapoor, A., "Experimental study of a cylindrical lithium ion battery thermal management using phase change material composites", *Journal of Energy Storage*, Vol. 8, (2016), 168-174. (<https://doi.org/10.1016/j.est.2016.08.005>).
- Samimi, F., Babapoor, A., Azizi, M. and Karimi, G., "Thermal management analysis of a Li-ion battery cell using phase change material loaded with carbon fibers", *Energy*, Vol. 96, (2016), 355-371. (<https://doi.org/10.1016/j.energy.2015.12.064>).
- Kinkelin, C., Lips, S., Soupremanien, U., Remondière, V., Dijon, J., Le Poche, H., Ollier, E., Zegaoui, M., Rolland, N., Rolland, P.-A., Lhostis, S., Descouts, B., Kaplan, Y. and Lefèvre, F., "Theoretical and experimental study of a thermal damper based on a CNT/PCM composite structure for transient electronic cooling", *Energy Conversion and Management*, Vol. 142, (2017), 257-271. (<https://doi.org/10.1016/j.enconman.2017.03.034>).
- Ali, H.M., Ashraf, M.J., Giovannelli, A., Irfan, M., Irshad, T.B., Hamid, H.M., Hassan, F. and Arshad, A., "Thermal management of electronics: An experimental analysis of triangular, rectangular and circular pin-fin heat sinks for various PCMs", *International Journal of Heat and Mass Transfer*, Vol. 123, (2018), 272-284. (<https://doi.org/10.1016/j.ijheatmasstransfer.2018.02.044>).
- Khan, M.M.A., Ibrahim, N.I., Mahbulul, I.M., Muhammad Ali, H., Saidur, R. and Al-Sulaiman, F.A., "Evaluation of solar collector designs with integrated latent heat thermal energy storage: A review", *Solar Energy*, Vol. 166, (2018), 334-350. (<https://doi.org/10.1016/j.solener.2018.03.014>).
- Shafieian, A., Khiadani, M. and Nosrati, A., "A review of latest developments, progress, and applications of heat pipe solar collectors", *Renewable and Sustainable Energy Reviews*, Vol. 95, (2018), 273-304. (<https://doi.org/10.1016/j.rser.2018.07.014>).
- Zhou, F., Ji, J., Yuan, W., Zhao, X. and Huang, S., "Study on the PCM flat-plate solar collector system with antifreeze characteristics", *International Journal of Heat and Mass Transfer*, Vol. 129, (2019), 357-366. (<https://doi.org/10.1016/j.ijheatmasstransfer.2018.09.114>).
- Essa, M.A., Mostafa, N.H. and Ibrahim, M.M., "An experimental investigation of the phase change process effects on the system performance for the evacuated tube solar collectors integrated with PCMs", *Energy Conversion and Management*, Vol. 177, (2018), 1-10. (<https://doi.org/10.1016/j.enconman.2018.09.045>).
- He, B., Martin, V. and Setterwall, F., "Phase transition temperature ranges and storage density of paraffin wax phase change materials", *Energy*, Vol. 29, No. 11, (2004), 1785-1804. (<https://doi.org/10.1016/j.energy.2004.03.002>).
- Shima, P.D. and Philip, J., "Role of thermal conductivity of dispersed nanoparticles on heat transfer properties of nanofluid", *Industrial & Engineering Chemistry Research*, Vol. 53, No. 2, (2014), 980-988. (<https://doi.org/10.1021/ie403086g>).
- Das, P.K., "A review based on the effect and mechanism of thermal conductivity of normal nanofluids and hybrid nanofluids", *Journal of Molecular Liquids*, Vol. 240, (2017), 420-446. (<https://doi.org/10.1016/j.molliq.2017.05.071>).
- Zerradi, H., Mizani, S., Loulijat, H., Dezaïri, A. and Ouaskit, S., "Population balance equation model to predict the effects of aggregation kinetics on the thermal conductivity of nanofluids", *Journal of Molecular Liquids*, Vol. 218, (2016), 373-383. (<https://doi.org/10.1016/j.molliq.2016.02.064>).
- Guo, H. and Zhao, N., "Interfacial layer simulation and effect on Cu-Ar nanofluids thermal conductivity using molecular dynamics method", *Journal of Molecular Liquids*, Vol. 259, (2018), 40-47. (<https://doi.org/10.1016/j.molliq.2018.03.001>).
- Sheikholeslami, M., "Solidification of NEPCM under the effect of magnetic field in a porous thermal energy storage enclosure using CuO nanoparticles", *Journal of Molecular Liquids*, Vol. 263, (2018), 303-315. (<https://doi.org/10.1016/j.molliq.2018.04.144>).
- Babapoor, A., Karimi, G. and Sabbaghi, S., "Thermal characteristic of nanocomposite phase change materials during solidification process", *Journal of Energy Storage*, Vol. 7, (2016), 74-81. (<https://doi.org/10.1016/j.est.2016.05.006>).
- Sheikholeslami, M., "Numerical modeling of nano enhanced PCM solidification in an enclosure with metallic fin", *Journal of Molecular Liquids*, Vol. 259, (2018), 424-438. (<https://doi.org/10.1016/j.molliq.2018.03.006>).
- Lohrasbi, S., Sheikholeslami, M. and Ganji, D.D., "Discharging process expedition of NEPCM in fin-assisted latent heat thermal energy storage system", *Journal of Molecular Liquids*, Vol. 221, (2016), 833-841. (<https://doi.org/10.1016/j.molliq.2016.06.044>).
- Yan, S.-R., Kalbasi, R., Nguyen, Q. and Karimipour, A., "Sensitivity of adhesive and cohesive intermolecular forces to the incorporation of MWCNTs into liquid paraffin: Experimental study and modeling of surface tension", *Journal of Molecular Liquids*, Vol. 310, (2020), 113235. (<https://doi.org/10.1016/j.molliq.2020.113235>).
- Sharif, M.K.A., Al-Abidi, A.A., Mat, S., Sopian, K., Ruslan, M.H., Sulaiman, M.Y. and Rosli, M.A.M., "Review of the application of phase change material for heating and domestic hot water systems", *Renewable and Sustainable Energy Reviews*, Vol. 42, (2015), 557-568. (<https://doi.org/10.1016/j.rser.2014.09.034>).
- Giro-Paloma, J., Martínez, M., Cabeza, L.F. and Fernández, A.I., "Types, methods, techniques, and applications for microencapsulated phase change materials (MPCM): A review", *Renewable and Sustainable Energy Reviews*, Vol. 53, (2016), 1059-1075. (<https://doi.org/10.1016/j.rser.2015.09.040>).
- Jamekhorshid, A., Sadrameli, S.M. and Farid, M., "A review of microencapsulation methods of phase change materials (PCMs) as a thermal energy storage (TES) medium", *Renewable and Sustainable Energy Reviews*, Vol. 31, (2014), 531-542. (<https://doi.org/10.1016/j.rser.2013.12.033>).
- Ibrahim, N.I., Al-Sulaiman, F.A., Rahman, S., Yilbas, B.S. and Sahin, A.Z., "Heat transfer enhancement of phase change materials for thermal energy storage applications: A critical review", *Renewable and Sustainable Energy Reviews*, Vol. 74, (2017), 26-50. (<https://doi.org/10.1016/j.rser.2017.01.169>).
- Tao, Z., Wang, H., Liu, J., Zhao, W., Liu, Z. and Guo, Q., "Dual-level packaged phase change materials – thermal conductivity and mechanical properties", *Solar Energy Materials and Solar Cells*, Vol. 169, (2017), 222-225. (<https://doi.org/10.1016/j.solmat.2017.05.030>).
- Yang, J., Tang, L.-S., Bao, R.-Y., Bai, L., Liu, Z.-Y., Yang, W., Xie, B.-H. and Yang, M.-B., "Largely enhanced thermal conductivity of poly (ethylene glycol)/boron nitride composite phase change materials for solar-thermal-electric energy conversion and storage with very low content of graphene nanoplatelets", *Chemical Engineering Journal*, Vol. 315, (2017), 481-490. (<https://doi.org/10.1016/j.cej.2017.01.045>).

28. Jegadheeswaran, S., Pohekar, S.D. and Kousksou, T., "Conductivity particles dispersed organic and inorganic phase change materials for solar energy storage—an exergy based comparative evaluation", *Energy Procedia*, Vol. 14, (2012), 643-648. (<https://doi.org/10.1016/j.egypro.2011.12.989>).
29. Shukla, A., Buddhi, D. and Sawhney, R.L., "Thermal cycling test of few selected inorganic and organic phase change materials", *Renewable Energy*, Vol. 33, No. 12, (2008), 2606-2614. (<https://doi.org/10.1016/j.renene.2008.02.026>).
30. Qureshi, Z.A., Ali, H.M. and Khushnood, S., "Recent advances on thermal conductivity enhancement of phase change materials for energy storage system: A review", *International Journal of Heat and Mass Transfer*, Vol. 127, (2018), 838-856. (<https://doi.org/10.1016/j.ijheatmasstransfer.2018.08.049>).
31. Karaipekli, A., Biçer, A., Sarı, A. and Tyagi, V.V., "Thermal characteristics of expanded perlite/paraffin composite phase change material with enhanced thermal conductivity using carbon nanotubes", *Energy Conversion and Management*, Vol. 134, (2017), 373-381. (<https://doi.org/10.1016/j.enconman.2016.12.053>).
32. Cárdenas, B. and León, N., "High temperature latent heat thermal energy storage: Phase change materials, design considerations and performance enhancement techniques", *Renewable and Sustainable Energy Reviews*, Vol. 27, (2013), 724-737. (<https://doi.org/10.1016/j.rser.2013.07.028>).
33. Fan, L. and Khodadadi, J.M., "An experimental investigation of enhanced thermal conductivity and expedited unidirectional freezing of cyclohexane-based nanoparticle suspensions utilized as nano-enhanced phase change materials (NEPCM)", *International Journal of Thermal Sciences*, Vol. 62, (2012), 120-126. (<https://doi.org/10.1016/j.ijthermalsci.2011.11.005>).
34. Liu, L., Su, D., Tang, Y. and Fang, G., "Thermal conductivity enhancement of phase change materials for thermal energy storage: A review", *Renewable and Sustainable Energy Reviews*, Vol. 62, (2016), 305-317. (<https://doi.org/10.1016/j.rser.2016.04.057>).
35. Liu, M., Saman, W. and Bruno, F., "Review on storage materials and thermal performance enhancement techniques for high temperature phase change thermal storage systems", *Renewable and Sustainable Energy Reviews*, Vol. 16, No. 4, (2012), 2118-2132. (<https://doi.org/10.1016/j.rser.2012.01.020>).
36. Babapoor, A., Karimi, G., Golestaneh, S.I. and Mezzin, M.A., "Coaxial electro-spun PEG/PA6 composite fibers: Fabrication and characterization", *Applied Thermal Engineering*, Vol. 118, (2017), 398-407. (<https://doi.org/10.1016/j.applthermaleng.2017.02.119>).
37. Babapoor, A., Karimi, G. and Khorram, M., "Fabrication and characterization of nanofiber-nanoparticle-composites with phase change materials by electrospinning", *Applied Thermal Engineering*, Vol. 99, (2016), 1225-1235. (<https://doi.org/10.1016/j.applthermaleng.2016.02.026>).
38. Munyalo, J.M. and Zhang, X., "Particle size effect on thermophysical properties of nanofluid and nanofluid based phase change materials: A review", *Journal of Molecular Liquids*, Vol. 265, (2018), 77-87. (<https://doi.org/10.1016/j.molliq.2018.05.129>).
39. Nitsas, M. and Koronaki, I.P., "Performance analysis of nanoparticles-enhanced PCM: An experimental approach", *Thermal Science and Engineering Progress*, Vol. 25, (2021), 100963. (<https://doi.org/10.1016/j.tsep.2021.100963>).
40. Xu, B., Li, P. and Chan, C., "Application of phase change materials for thermal energy storage in concentrated solar thermal power plants: A review to recent developments", *Applied Energy*, Vol. 160, (2015), 286-307. (<https://doi.org/10.1016/j.apenergy.2015.09.016>).
41. Olfián, H., Ajarostaghi, S.S.M. and Ebrahimataj, M., "Development on evacuated tube solar collectors: A review of the last decade results of using nanofluids", *Solar Energy*, Vol. 211, (2020), 265-282. (<https://doi.org/10.1016/j.solener.2020.09.056>).
42. Raam Dheep, G. and Sreekumar, A., "Influence of nanomaterials on properties of latent heat solar thermal energy storage materials – A review", *Energy Conversion and Management*, Vol. 83, (2014), 133-148. (<https://doi.org/10.1016/j.enconman.2014.03.058>).
43. Kibria, M.A., Anisur, M.R., Mahfuz, M.H., Saidur, R. and Metselaar, I.H.S.C., "A review on thermophysical properties of nanoparticle dispersed phase change materials", *Energy Conversion and Management*, Vol. 95, (2015), 69-89. (<https://doi.org/10.1016/j.enconman.2015.02.028>).
44. Nazir, H., Batoool, M., Bolivar Osorio, F.J., Isaza-Ruiz, M., Xu, X., Vignarooban, K., Phelan, P., Inamuddin and Kannan, A.M., "Recent developments in phase change materials for energy storage applications: A review", *International Journal of Heat and Mass Transfer*, Vol. 129, (2019), 491-523. (<https://doi.org/10.1016/j.ijheatmasstransfer.2018.09.126>).
45. Veerakumar, C. and Sreekumar, A., "Phase change material based cold thermal energy storage: Materials, techniques and applications – A review", *International Journal of Refrigeration*, Vol. 67, (2016), 271-289. (<https://doi.org/10.1016/j.ijrefrig.2015.12.005>).
46. Zeng, J.L., Cao, Z., Yang, D.W., Xu, F., Sun, L.X., Zhang, X.F. and Zhang, L., "Effects of MWNTs on phase change enthalpy and thermal conductivity of a solid-liquid organic PCM", *Journal of Thermal Analysis and Calorimetry*, Vol. 95, No. 2, (2009), 507-512. (<https://doi.org/10.1007/s10973-008-9275-9>).
47. Yu, Z.-T., Fang, X., Fan, L.-W., Wang, X., Xiao, Y.-Q., Zeng, Y., Xu, X., Hu, Y.-C. and Cen, K.-F., "Increased thermal conductivity of liquid paraffin-based suspensions in the presence of carbon nano-additives of various sizes and shapes", *Carbon*, Vol. 53, (2013), 277-285. (<https://doi.org/10.1016/j.carbon.2012.10.059>).
48. Cui, Y., Liu, C., Hu, S. and Yu, X., "The experimental exploration of carbon nanofiber and carbon nanotube additives on thermal behavior of phase change materials", *Solar Energy Materials and Solar Cells*, Vol. 95, No. 4, (2011), 1208-1212. (<https://doi.org/10.1016/j.solmat.2011.01.021>).
49. Kim, S. and Drzal, L.T., "High latent heat storage and high thermal conductive phase change materials using exfoliated graphite nanoplatelets", *Solar Energy Materials and Solar Cells*, Vol. 93, No. 1, (2009), 136-142. (<https://doi.org/10.1016/j.solmat.2008.09.010>).
50. Fan, L.-W., Zhu, Z.-Q., Zeng, Y., Lu, Q. and Yu, Z.-T., "Heat transfer during melting of graphene-based composite phase change materials heated from below", *International Journal of Heat and Mass Transfer*, Vol. 79, (2014), 94-104. (<https://doi.org/10.1016/j.ijheatmasstransfer.2014.08.001>).
51. Ali, A.H., Ibrahim, S.I., Jawad, Q.A., Jawad, R.S. and Chaichan, M.T., "Effect of nanomaterial addition on the thermophysical properties of Iraqi paraffin wax", *Case Studies in Thermal Engineering*, Vol. 15, (2019), 100537. (<https://doi.org/10.1016/j.csite.2019.100537>).
52. Jawad, Q.A., Mahdy, A.M.J., Khuder, A.H. and Chaichan, M.T., "Improve the performance of a solar air heater by adding aluminum chip, paraffin wax, and nano-SiC", *Case Studies in Thermal Engineering*, Vol. 19, (2020), 100622. (<https://doi.org/10.1016/j.csite.2020.100622>).
53. Sharma, S.D. and Sagara, K., "Latent heat storage materials and systems: A review", *International Journal of Green Energy*, Vol. 2, No. 1, (2005), 1-56. (<https://www.tandfonline.com/doi/abs/10.1081/GE-200051299>).
54. Sedov, I.A., Muhametzyanov, T.A. and Solomonov, B.N., "A procedure for calibration of differential scanning calorimeters", *Thermochimica Acta*, Vol. 639, (2016), 10-13. (<https://doi.org/10.1016/j.tca.2016.07.010>).
55. Souayfane, F., Fardoun, F. and Biwole, P.-H., "Phase change materials (PCM) for cooling applications in buildings: A review", *Energy and Buildings*, Vol. 129, (2016), 396-431. (<https://doi.org/10.1016/j.enbuild.2016.04.006>).
56. He, M., Yang, L., Lin, W., Chen, J., Mao, X. and Ma, Z., "Preparation, thermal characterization and examination of phase change materials (PCMs) enhanced by carbon-based nanoparticles for solar thermal energy storage", *Journal of Energy Storage*, Vol. 25, (2019), 100874. (<https://doi.org/10.1016/j.est.2019.100874>).
57. Fan, L.-W., Fang, X., Wang, X., Zeng, Y., Xiao, Y.-Q., Yu, Z.-T., Xu, X., Hu, Y.-C. and Cen, K.-F., "Effects of various carbon nanofillers on the thermal conductivity and energy storage properties of paraffin-based nanocomposite phase change materials", *Applied Energy*, Vol. 110, (2013), 163-172. (<https://doi.org/10.1016/j.apenergy.2013.04.043>).



Research Article

Residential Consumer's Willingness to Pay for Renewable Energy: Evidence from a Double-Bounded Dichotomous Choice Survey from India

Vasundhara Sen*

Department of Infrastructure, Symbiosis Centre for Management and Human Resource Development, Symbiosis International (Deemed University), Pune, India.

PAPER INFO

Paper History:

Received: 03 January 2022

Revised: 21 June 2022

Accepted: 06 July 2022

Keywords:

Green Energy Contracts,
Contingent Valuation,
Renewable Energy,
Willingness to Pay

ABSTRACT

Despite the falling costs of Renewable Energy (RE), RE adoption in Indian residential households is still at tepid growth rates. With the onset of retail electricity market deregulation in India, the introduction of “green tariffs” for residential households can be effective in resolving the issue of low RE adoption. This study investigates the willingness to pay for green tariffs/renewable energy-based electricity contracts using the contingent valuation method. Data collected from 476 Indian residential households are analyzed by the Double-Bounded Dichotomous Choice technique. The results of the conducted maximum Likelihood Estimation (MLE) method reveal the mean willingness to pay 308.52 Rs per household/month for consumption of green power in a premium-paying setting. Results indicate that although households hold positive perception of renewable energy, the willingness to pay is not commensurately high, indicating an attitude-action gap. The study recommends green energy defaults in residential energy contracts, direct marketing of non-use value of RE use (altruistic and bequest) by power supplying utilities, and promoting RE use through RE opinion champions/influencers as measures to enhance RE adoption amongst Indian residential energy consumers.

<https://doi.org/10.30501/jree.2022.314713.1302>

1. INTRODUCTION

The adoption of Renewable Energy (RE) in Indian residences does not feature prominently in India's clean energy transition journey. For Indian households, RE adoption is most plausible through investments in on-site solar rooftop systems – a sector with many subsidies and monetary incentives [1]. Economic savings on energy costs, pursuit of pro-environmental objectives, energy independence, and the opportunity to generate power closer to the point of consumption are all factors that encourage solar rooftop adoption at homes [2]. Above all, the net metering mechanism (where energy generated from the solar rooftop system is netted against monthly consumption) has been a key motivator [1]. However, available data point to dismal achievement of residential installation of solar rooftops in India, reaching only 1.1 Giga-Watt of capacities as of 2020 [3]. Adoption has been disappointing due to incentive roll-backs as power-supplying utilities face high revenue losses on account of consumer migration to green energy [1]. As a result, solar rooftops and RE-powered mini/microgrids capacity additions have much to achieve [4]. Subsidized cost of electricity consumption in comparison to other consumer categories [5], lack of technical knowledge of owning and maintaining RE systems [4],

ownership of premises (rented vs. owned), place of residence (rural/urban), and other financial concerns [6] act as major adoption barriers amongst residences. Third-party project developers who bridge the awareness gap of owning and maintaining onsite rooftop systems for residents have also played an inadequate role [7], thus exacerbating adoption worries. Much remains to be done before residential consumers can transition to “cleaner and renewable” energy consumption.

One strategy to increase RE consumption amongst residences is to use “Green tariffs”. Green tariffs are energy supply contracts between electricity consumers and incumbent power supply utilities. Consumers who opt for green tariffs pay a premium to source renewable energy-based electricity supply, facilitated by the local power supplier. With green tariffs, end consumers can consume RE-based power without making capital investments in RE systems, but they merely pay a premium over existing retail tariffs. Green tariffs are either voluntary or default in nature. “Green defaults”, as popularly known, have been more successful in nudging green energy consumption [8, 9] as it slows down the switch back to grey power due to consumer inertia [10], thereby helping countries meet RE objectives efficiently [11].

Green Tariffs have been introduced in India recently (in 3 states) [12]. With this introduction, all end consumers of electricity (in applicable states) can opt for a 100 % renewable energy-based electricity supply by paying a premium per unit

*Corresponding Author's Email: vasundhara_sen@scmhrd.edu (V. Sen)
URL: https://www.jree.ir/article_155034.html



of electricity consumed [13]. India has thus enabled choice-based energy supply contracts for electricity end users, much like many of the European economies [14]. However, existence of green tariffs does not guarantee adoption due to large attitude-action gaps in adoption [15, 16]. The willingness to pay for green tariffs (thereby for renewable energy) and factors driving higher enrollment rates in green tariffs are important considerations in the energy transition success. Focus on the same issue is sufficiently evident in developed economies [17-19]; yet, studies from India are few. This study aims to close this research gap by investigating the Willingness To Pay (WTP) for Green Tariffs (GT) for domestic consumers of electricity and to identify factors affecting the same.

In this study, WTP for GT is estimated using a Double-Bounded Dichotomous Choice Contingent Valuation (DBDC CV) experiment conducted with data collected from 476 residential households in the state of Maharashtra in western India. Responses were collected using a 4-part CV questionnaire from urban residences located in the cities of Pune and Mumbai, which are two major urban concentrations in the state. Maharashtra was chosen as the study area given its highest residential energy costs in the country [20] and in the state, cities of Pune and Mumbai are predicted to exhibit the highest growth rate in domestic energy consumption between 2019-2029 [21]. The DBDC model results are compared with Single-Bounded Dichotomous Choice (SBDC) model results to establish the robustness and efficiency gains in DBDC estimates. DBDC estimates indicate that households are willing to pay a mean monthly premium of 310.84 Rs for green energy contracts. Age exerts a negative influence, whereas higher education and income positively re-enforce the WTP. In addition, attitudinal, perceptual, and behavioral traits of an individual impact the WTP. Based on these findings, this study presents policy recommendations to close the attitude-action gap in RE adoption amongst residences.

This paper is structured in 7 sections. Section 1 introduces the study background and rationale. Section 2 presents a comprehensive literature review of studies investigating WTP for RE. Section 3 details the research methodology. Section 4 then presents data analysis and results, followed by Section 5 that discusses key conclusions. Section 6 contains policy recommendations and finally, Section 7 highlights the study limitations.

2. LITERATURE REVIEW

Studies on willingness to pay for renewable energy, published between 2009 and 2020, were analyzed to better understand the existing literature on the subject. The following keywords were used to retrieve most relevant studies: “Willingness to pay for renewable energy”; “Paying for green energy”; “Willingness to pay for green energy”; “Contingent valuation and renewable energy”; “Discrete choice experiments and renewable energy”; “Choice experiments and renewable energy”; “Willingness to accept for renewable energy”, and “Grounded theory and renewable energy”. A concept-centric literature analysis approach was used to identify the many concepts/meanings associated with willingness to pay for renewable energy [22].

Literature analysis suggests that Willingness To Pay (WTP) for RE can be interpreted in one of the three ways. First, the end consumer’s WTP for renewable energy is a signal of green energy’s market acceptance [23], with higher WTP

reflecting higher social acceptance of RE. Second, it encapsulates non-use values of RE to consumers such as existence, bequest, and option values [24-27]. Finally, in the context of this study, WTP for RE portrays the preferred attributes of electricity supply, with content of supply (green power /thermal power) being one of them [28-31], especially in competitive retail electricity markets.

Competitive retail electricity markets enable end consumers to choose preferred power supplier and content of power [14]. In such markets, “consumer switching/consumer shopping” is encouraged, where end consumers can switch from one supplier to another based on power supply attributes [32]. High rates of consumer switching reflect the effectiveness and success of competition in retail markets [33]. In consumer switching decisions, many non-price attributes gain significance in the consumer decision-making process such as the type of RE supply [31, 34]. Consumers differ in RE preferences, which translate into differences in consumer’s WTP for RE. As can be seen in the literature, solar energy has higher public acceptance than other RE forms, so much so that solar energy-based “defaults” are preferred over voluntary signups for wind and biomass-based energy supply contracts [29, 30]. Preference for hydro is noted over wind energy-based supply [28]; however, wind is the supply of choice over natural gas and nuclear power due to its wider social and health benefits [35, 36].

Other than the type of RE source, nature of power supplying entity and geographical orientation of power supplier also influence WTP for RE significantly. Publicly owned power supplying companies gather a higher WTP for green electricity than energy co-operatives [37]. Transparency in power pricing strategies, a seamless communication strategy, and a more democratic decision-making process followed by power utilities also encourage consumers to pay a premium for RE contracts [38]. Locally procured RE and RE powers supplied by regional power suppliers are preferred over power suppliers with foreign ties [39].

Consumer heterogeneity in green energy preferences can be masked with the introduction of green energy defaults. Evidence suggests that once RE-based energy supply is established as default, consumers seek compensation to move to grey power [15] owing to inertia. Introduction of green energy defaults for residential consumers in India can be a powerful tool to ensure higher RE adoption. However, as a premium paying model, it can put the poor at a disadvantage [40]. Given that India is still a developing country and more than 20 % of the population is below the poverty line (as of last census in 2011) [41], voluntary green energy contracts are more suitable. This study explores the willingness to pay for voluntary green electricity supply contracts. Studies estimating WTP for RE have emanated in plenty from other developing economies. Developing countries report low rates of RE penetration and widespread rural energy poverty. The role of renewable electricity in ending energy poverty and willingness to pay for it has thus been at focus, especially in the South African sub-continent [42-46]. WTP for RE has also been studied to understand social acceptance of RE in Asian countries, where RE adoption is in nascent stages [47]. Indian studies published so far have focused either on WTP for RE among large consumers of electricity where green energy transition has accelerated [48, 49], or for distributed RE in rural areas to increase energy access [50-52] or for better power quality [53, 54]. In contrast to previous Indian studies, this paper estimates WTP for RE in the case of domestic

consumers in the context of increased competition in retail electricity supply.

India introduced competition in retail electricity supply via green tariffs [55]. Under Green Tariffs (GTs), consumers can opt to consume RE power by paying a premium over existing retail tariff applicable. Even though GT in India have largely been opted by commercial and industrial consumers [48], domestic consumers can opt for it too and green their own energy consumption. In the Indian market, GTs are available at a premium and the willingness to pay for it remains unknown, especially amongst domestic consumers. This study aims to close this research gap by estimating the Willingness To Pay for renewable energy-based green tariffs amongst domestic consumers and to add to the existing body of literature valuably.

3. METHOD

This section is structured in 3 sub-sections. Section 3.1 contains the survey questionnaire design. Section 3.2 then explains choice of study areas and data collection methods. Finally, Section 3.3 elaborates the statistical model chosen for the study.

3.1. Survey questionnaire design

Since electricity is an “invisible” commodity for households [56], assessment of WTP for RE requires the use of non-market valuation methods. For this study, WTP was estimated using both Single-Bounded Dichotomous Choice Contingent Valuation (SBDC CV) and then, was compared with Double-Bounded Dichotomous Choice Contingent Valuation estimates (DBDC CV) [57-59] to choose the most efficient model [60]. A four-part questionnaire was designed to arrive at an optimal design for the CV survey instrument, suitable for a developing country setup [61].

Part 1 of the instrument included questions testing respondent’s perception of renewable energy, generic environmental concerns/environmental responsibility, and presence of altruistic tendencies through 21 questions asked based on a 1-to-5-point Likert scale. Environmental and other

socio-economic benefits of RE use shape positive RE perception and motivate consumers to pay [62-65], but social negative externalities and risks associated with RE depressed consumers’ WTP for it [66]. Impact of environmental concerns on WTP for RE use remains mixed, while some studies point to its high positive influence on green electricity contract enrollment rates [67, 68]. In other studies, no such impact could be found [69]. Environmental responsibility—the act of feeling responsible to take pro-environmental actions has spurred the willingness to pay a premium for green energy, acting as an internal variable [67]. Finally, individual altruistic tendencies often dominate respondent’s willingness to pay for an environment friendly product. Consumers state their willing to pay for a “green” product since it helps them purchase moral satisfaction [70-77]. Questions included in Part-1 were thus chosen basis extensive literature evidence, suggesting possible influence on WTP for RE.

Part 2 then presented information on renewable energy in India, international best practices adopted to promote RE, and introduced the concept of green tariffs. Guidelines were followed to make information presentation as effective as possible [78]. 2 pilot studies were conducted (n=94) to test for response fatigue with the information presented. Based on pilot study feedback, information was converted to graphs and other visual aids from text, to improve cognitive ease and interpretation.

Next in part 3, the WTP question was asked in the DBDC format. 3 bid values (WTP values) were selected (from here on referred to as B^1 , B^{higher} and B^{lower}), so as to bind respondent’s valuation [60]. A split sample technique with 3 bid combinations/designs was used to avoid starting point bias [79]. As per design, a typical respondent was presented with 1 of 3 bid combinations, where bid values represented premiums to be paid over and above monthly electricity bill amounts. Different bid values were chosen after conducting secondary research on domestic consumer’s monthly electricity bill. Bid values chosen constituted a 2-12 % premium over currently monthly electricity bills in the state. A summary of the bid values appear in Table 1.

Table 1. Selection of bid values

	B^1 (Starting Bid) (Rs./month)	B^{higher} (Higher bid) (Rs./month)	B^{lower} (Lower bid) (Rs./month)
Sub-sample 1	100	150	50
Bid as a % of monthly electricity bills	4 %	6 %	2 %
Sub-sample 2	200	300	100
Bid as a % of monthly electricity bills	8 %	12 %	4 %
Sub-sample 3	300	450	150
Bid as a % of monthly electricity bills	12 %	18 %	6 %
Note: the monthly electricity bill is assumed to be the same in all samples, based on average residential consumer’s consumption patterns in the state of Maharashtra [80].			

Contingent valuation studies are known to suffer from hypothetical bias, where consumers tend to overstate their WTP due to the hypothetical nature of product/program being valued [81]. Cheap talk scripts are an effective way to reduce this hypothetical bias [82]. It refers to inclusion of body of text within the survey, that reminds the respondent that they

may be suffering from hypothetical bias and hence may overstate their actual WTP. Accordingly, a brief cheap talk was also included, to correct for any hypothetical biases.

Finally, part 4 of the instrument contained follow up questions to the WTP valuation questions along with socio-demographic variables. Variables captured respondent’s age,

gender, income, occupation, education, location of residence, type of utility/power suppliers supply electricity to the household (public Vs private) and number of appliances at home. Data was also collected on monthly hours of electricity consumption, monthly electricity bills and back-up arrangement for power supply (such as generator sets, battery/invertors and use of solar RTPV), with the intention to understand possible influences of prior use of renewable energy on WTP, if any.

3.2. Study area and data collection methods

Responses were collected from 476 residential households from the cities of Pune and Mumbai. Of the total 476 observations, 70 % of the residents belonged to Pune and 30 % resided in Mumbai. The final survey instrument was administered using both offline methods (face to face interviews) as well as online tools, since mixed methods for data collection do not compromise the quality of data in large sample studies [83], but help by reducing time and costs [84].

Data was collected by a team of trained enumerators, trained to conduct CV studies in a developing country setting as per best practices guidelines [85]. The 2 urban centers chosen for the study were divided in zones of electricity supply and samples were collected from each supply zone. A sample inclusion criterion defined a typical respondent to be a resident of either Pune/Mumbai, connected on domestic connection of electricity, and is the head of the household. Stratified purposive sampling was then used to reach more than 1200 respondents, but usable data amounted to only 476 responses. Sample size considered for this study resonates with literature [86, 87], and hence was deemed sufficient.

3.3. Model specification

Latent factors impacting WTP for RE were identified using Exploratory Factor Analysis (EFA). Next, statistical estimation of mean WTP values using the DBDC format was done using parametric methods. Under parametric estimation, the sample data collected is assumed to follow a particular distribution, and the parameter estimates confirm the probability distribution that the observed data belongs to the referenced study [88]. Nonparametric methods, on the other hand, make no apriori assumption about the data distribution. Parametric estimation can be done using either the Least Squares Estimation (LSE) method or the Maximum Likelihood Estimation (MLE); however, MLE has the advantage of estimating the distribution parameters with narrower confidence intervals, thereby rendering this estimation method with higher sufficiency, consistency, and efficiency [88]. For this study, the MLE method of parametric estimation of DBDC CV model was adopted. In the model, a typical respondent can be denoted by “i” and the maximum Willingness To Pay (WTP) for renewable energy-based electricity be denoted by y_i^* . Since a DBDC CV method was used, a typical response could be one of the following four possible responses to the bid values presented (B^1 = Initial Bid, B^{higher} = Higher Bid and B^{lower} = Lower bid):

- 1) “Yes” to B^1 and a “Yes” to B^{higher} =Yes-Yes (YY)
- 2) “Yes” to B^1 and a “No” to B^{higher} =Yes-No (YN)
- 3) “No” to B^1 and a “Yes” to B^{lower} =No-Yes (NY)

- 4) “No” to B^1 and a “No” to B^{lower} =No-No (NN)

while respondents falling in categories (i), (ii), and (iii) carry a positive WTP, those falling in category (iv) are known as protest respondents. Respondents can reveal zero WTP as either they truly carry zero willingness to pay for the good in question, or the bid values presented are unable to capture the true WTP [89]. Since there is a probability assigned to each answer format, the likelihood functions need to be estimated. The likelihood function helps understand how likely it is for the sample data to come from the assumed probability distribution.

Let “ Π ” define the likelihood function; then, the 4 answer formats in the DBDC CV experiment can be written as follows [60]:

$$\Pi_i^{YY}(B^1; B^{\text{higher}}) = \Pr(y_i^* > B^1 \text{ and } y_i^* \geq B^{\text{higher}}) = 1 - G(B^{\text{higher}}, \theta) \quad (1)$$

where Π_i^{YY} represents a consumer i, with a “Yes-Yes” response in the bid values presented.

Further, G (Bid value, θ) is a statistical distribution function with associated parameter estimates vector “ θ ”, and $1 - G(B^{\text{higher}}, \theta)$ represents the cumulative density function (cdf) of the respondent’s true maximum WTP. Similarly:

$$\Pi_i^{YN}(B^1; B^{\text{higher}}) = \Pr(y_i^* \geq B^1 \text{ but } y_i^* < B^{\text{higher}}) = G(B^{\text{higher}}, \theta) - G(B^1, \theta) \quad (2)$$

$$\Pi_i^{NY}(B^1; B^{\text{lower}}) = \Pr(y_i^* < B^1 \text{ but } y_i^* \geq B^{\text{lower}}) = G(B^1, \theta) - G(B^{\text{lower}}, \theta) \quad (3)$$

$$\Pi_i^{NN}(B^1; B^{\text{lower}}) = \Pr(y_i^* < B^1 \text{ and } y_i^* < B^{\text{lower}}) = G(B^{\text{lower}}, \theta) \quad (4)$$

Functions (1) to (4) the total likelihood function (L), representing the joint probability distribution of the sample, can be constructed as follows:

$$L(\theta) = \Pi_i^{YY} + \Pi_i^{YN} + \Pi_i^{NY} + \ln \Pi_i^{NN} \quad (5)$$

The best parameter estimates can be achieved when the Log-Likelihood function is maximized [88]. By maximizing the log likelihood function, the probability that the observed data comes from the assumed distribution is maximized. Thus, the log (denoted as “ln”) of Equation (5) that must be considered for computational purposes is constructed as follows:

$$\ln L(\theta) = \ln \Pi_i^{YY} + \ln \Pi_i^{YN} + \ln \Pi_i^{NY} + \ln \Pi_i^{NN} \quad (6)$$

For a single respondent i, the response will be any one from YY, YN, NY, or NN formats. Therefore, a dummy binary variable which can take a value of 0 or 1 in the log-likelihood function (based on the respondent’s i’s response) is necessary. If “d” indicates the dummy variable, then the final Log-Likelihood function will be constructed as follows:

$$\ln L(\theta) = \sum_{i=1}^N \{d_i^{YY} \ln \Pi_i^{YY} + d_i^{YN} \ln \Pi_i^{YN} + d_i^{NY} \ln \Pi_i^{NY} + d_i^{NN} \ln \Pi_i^{NN}\} \quad (7)$$

where i represents a sample respondents and can range from 1, 2, 3,....., N and d_i^{YY} , d_i^{YN} , d_i^{NY} and d_i^{NN} are binary

variables with values assigned as either 0 or 1, depending on the i^{th} sample response.

4. RESULTS AND DISCUSSION

This section contains details of the sample statistics in Section 4.1, followed by results from exploratory factor analysis contained in section 4.2. Finally, section 4.3 presents quantitative estimates of WTP for RE.

4.1. Respondent profile

Data for this study was collected in split samples (3 sub-samples) to avoid the starting point bias [79]. Each split sample had a near equal sample size, ensuring that no split sample suffered from over or under representation. Table 2 appends the following summary of the key socio-demographic variables by the split sample.

Table 2. Sample statistics

Socio-demographic variables	Split sample 1 (n = 159)	Split sample 2 (n = 152)	Split sample 3 (n = 165)
Average age (years)	27.9	31.2	29.1
Average annual income (Rs. INR)			
Less than Rs. 10 lacs	111 (69.8)	85 (55.9)	98 (59.4)
Rs. 11 Lacs – Rs. 21 Lacs	20 (12.6)	26 (17.1)	42 (25.5)
More than Rs. 21 Lacs	12 (7.5)	13 (8.6)	19 (11.5)
Did not report	16 (10.1)	28 (18.4)	6 (3.6)
Educational attainment			
Less than school degree			
School degree	4 (2.5)	1 (0.7)	3 (1.8)
Under graduation	65 (40.9)	73 (48.0)	80 (48.5)
Post-graduation	80 (50.3)	71 (46.7)	66 (40.0)
Higher education	10 (6.3)	7 (4.6)	16 (9.7)
Gender			
Male	107 (0.70)	86 (0.60)	109 (0.70)
Female	52 (0.30)	66 (0.40)	56 (0.30)
Average family size (number of members)	2.9	2.8	2.8
Past use of solar (% users)	8.18 %	8.55 %	5.45 %
Alternate sources of electricity (% of yes respondents)	11.32 %	15.13 %	7.88 %

Numbers in parenthesis represent column percentages.
 Split sample 1: (B^1 , B^{higher} and B^{lower}) = (100_150_50); Split sample 2: (B^1 , B^{higher} and B^{lower}) = (200_300_100); Split sample 3: (B^1 , B^{higher} and B^{lower}) = (300_450_150)

A typical respondent was 30 years of age on average, completed either an under-graduate or a post-graduate degree, did not exceed annual family income Rs. 10 Lacs, and came from a family of less than 3 members. The majority of the

respondents in each split sample were found willing to pay for RE with a share of protest respondents (respondent not willing to pay) limited to 14.7 % (data in Table 3 below).

Table 3. Response to bid values

Response	Split sample 1 (n = 159)	Split sample 2 (n = 152)	Split sample 3 (n = 165)	Total
Yes - Yes	78	71	79	228 (47.8%)
Yes - No	48	39	49	136 (28.5%)
No - Yes	11	17	14	42 (8.8%)
No – No (Protest)	22	25	23	70 (14.7%)
Total	159	152	165	476

Split sample 1: (B^1 , B^{higher} and B^{lower}) = (100_150_50); Split sample 2: (B^1 , B^{higher} and B^{lower}) = (200_300_100), Split sample 3: (B^1 , B^{higher} and B^{lower}) = (300_450_150)

Only 5-8 % of the households (in each split sample) had used solar energy in the past (total 35 out of 476 households: 7, 19, and 9 in split samples 1, 2, and 3, respectively). This finding is in agreement with the literature, pointing to lower RE adoption amongst households [90]. The limited adopters

of solar rooftops in the sample (35 of 476) installed battery backups or generator systems as well, indicating the lack of reliability of solar rooftops due to intermittency of the power supply. While the falling costs of solar RTPV have encouraged adoption, conventional backup options are still the

mainstay [91]. A near-complete reliance on grid supplied electricity is also evident since only 8-11 % of respondents maintained alternate sources of electricity to fall back upon. Further, more than 60 % of the respondents preferred to switch off appliances while not in use while only 37 % purchased Energy Efficient Appliances (EEAs). This mirrors energy behavior in residential households in other parts of Asia as well [92] and corroborates the results with the literature, suggesting the lagging adoption of EEAs in India due to concerns other than appliance cost [93], and it also confirms the slower pace of energy transition in households [94].

4.2. Exploratory factor analysis and latent factors identification

Reliability and validity of 21 questions captured on Likert scale data were checked based on the Cronbach's alpha statistic. A high alpha value of .740 reflects internal consistency of the instrument [95]. To ensure validity, content validity was used. Content validity refers to expert reviews of questions for establishing validity and verifying the extent to which questions capture the research objectives. Content validity was established by conducting expert interviews with

academic and industry experts from the fields of environmental economics and renewable energy. Survey feedback from pilot studies also helped refine the final survey instrument.

Exploratory Factor Analysis (EFA) was conducted on Likert-scale data variables to discover latent variables with possible impact on WTP for renewable energy. EFA was conducted using the Principal Component Analysis (PCA) procedure in SPSS. The Kaiser-Meyer-Olkin (KMO) test and Bartlett's test of Sphericity confirmed the need and applicability of factor analysis [96]. The KMO test returned a high value of 0.772 justifying sample adequacy. Bartlett's test for sphericity was also significant ($\chi^2(210) = 1701.342, p = 0.00$), indicating the presence of latent factors. Finally, variable communalities above 0.3 confirmed that latent factors explained a significant amount of variation in the variables [97]. EFA used the varimax rotation and 5 latent factors were discovered, each with an eigenvalue of > 1 . The 5 latent factors explained 46.57 % of the total variance. No variables reported cross factor loadings, and all variables with factor loadings less than 0.50 were suppressed. Final factor loading, latent factor identification, and variable communalities are reproduced below in Table 4.

Table 4. Results from exploratory factor analysis

Sample No.	Variable name	Rotated component matrix						Communalities
		1	2	3	4	5	6	
1	Green is as reliable as conventional energy					0.767		0.598
2	Everyone should pay extra to contribute to the generation of Green Electricity					0.649		0.455
3	I believe the generation of electricity from coal contributes to pollution in the country	0.391						0.453
4	The effects of pollution on public health are worse than we realize	0.690						0.518
5	I believe human activities are major contributors to pollution	0.715						0.533
6	I believe that electricity generation from renewable energy will clean the environment	0.557						0.478
7	I feel partly responsible for the environmental problems on our planet				0.648			0.557
8	I recycle what I can (paper, glass, or other recyclables)						-.666	0.608
9	Every citizen must take responsibility for the environment	0.774						0.646
10	I feel that pollution from electricity generation should be taxed				0.692			0.551
11	I feel a moral obligation to protect the environment				0.586			0.507
12	I have given directions to a stranger			0.514				0.533
13	I have given money to charity			0.742				0.575
14	I have donated goods or clothes to a charity			0.765				0.606
15	I have done voluntary work for charity			0.659				0.579
16	I have donated blood		0.472					0.353
17	I have helped carry a stranger's belonging		0.708					0.577

18	I have delayed an elevator so that someone else can come in		0.499					0.456
19	I have allowed someone else to go ahead of me in a line (Xerox line/ supermarket etc)		0.523					0.463
20	I have given a stranger lift in my car		0.728					0.533
21	I have helped a handicap cross the street		0.625					0.519

The 5 latent factors discovered can be interpreted as follows:

- **Perception of RES-E/green energy:** Two variables load on this factor that reflect how respondents perceive RES-E or green energy (Variable 1 and Variable 2). This factor was also identified as a major effect on the consumer's WTP by the researchers in [98] and hence, aligned with the previous literature.
- **Environmental consciousness:** Four variables load on to this factor (Variables 4, 5, 6, and 9), each of which captures the respondent's environmental consciousness and awareness of the impacts from use of green energy. This latent factor was also found to be of significance in influencing pro-environmental behavior in previous studies; hence, it validates the variable grouping [99].
- **Environmental responsibility:** Three variables that captured a sense of environmental responsibility

amongst respondents constructed these latent factors (Variables 7, 10, and 11).

- **Tangible altruism:** This factor encapsulated altruistic traits tangible in nature and was constructed out of Variables 12, 13, 14, and 15.
- **Intangible altruism:** Five variables loaded on to this factor that captured altruistic behaviors with intangible nature, namely Variables 17, 18, 19, 20, and 21.

Three variables could not be grouped under any latent factor, each having factor loading of less than 0.50. Hence, they were dropped (Variables 3, 8, and 16).

4.3. Estimates of willingness to pay for renewable energy

The statistical SBDC and DBDC CV model development was done in R software. Table 5 below lists the statistical summary of the considered variables for analysis.

Table 5. List and nature of variables considered for model development

Sample No.	Variable	Mean	Standard deviation
1	Gender (1 if Male, 2 otherwise)	1.37	.482
2	Age of the respondent (years)	29.32	8.72
3	Annual income of the household (1 if < 5 lacs per annum, 5 if > 21 lacs per annum (ordinal variable))	2.29	1.24
4	Level of education of respondent (1 if < school degree, 5 if >= higher education (ordinal variable))	3.58	0.64
5	City of residence (1 if Pune, 0 if Mumbai)	0.69	0.46
6	Household monthly electricity bill (Rs.)	1742.84	1611.15
7	Household size (1 if single, 5 if > 10 members (ordinal variable))	2.83	0.67
8	Past use of solar (1 if yes, 0 otherwise)	0.56	0.50
9	Alternate sources of electricity (1=yes, 0=no)	0.11	.32
10	Factor 1: Perception of RES (PER = V1+V2)	7.34	1.56
11	Factor 2: Environmental Consciousness (EC) = V4+V5+V6+V9	17.56	2.15
12	Factor 3: Environmental Responsibility (ER) = V7+V10+V11	12.00	1.87
13	Factor 4: Tangible Altruism (A1) = V12+V13+V14+V15	13.99	3.64
14	Factor 5: In tangible Altruism (A2) = V17+V18+V19+V20+V21	14.41	4.53
15	Answer to bids presented in YY-YN-NY-YY format (dependent variable)	-	-

For the Single-Bounded Dichotomous Choice (SBDC) model estimation, only the starting bid value for each split sample was considered [100]. Due to the categorical/dichotomous nature of the dependent variable (answer to bid values), Ordinary Least Squares (OLS) method of regression could not be applied since the error distribution violated normality assumption. Hence, Generalized Linear Models (GLM) were chosen [100]. For GLM models where parametric estimations are undertaken, error terms can follow any of the following probability distribution functions:

Logistic, Log-normal, Log-logistic, and Weibull distributions [100]. For this study, the Maximum Likelihood Estimator (MLE) method is used to estimate the distribution parameters. The model fit was adjudged by the Akaike Information Criterion (AIC) and Bayesian Information Criterion (BIC) derived from the Kullback–Liebler distance [101]. Parametric models using multiple distributional assumptions namely Logistic, Log-Logistic, and Weibull distributions were analyzed, as reported in Table 6 below.

Table 6. Single-Bounded Dichotomous Choice (SBDC) parametric estimation results

Variable	Logistic	Log-Logistic	Weibull
(Intercept)	-2.67	-0.35	-0.14
Log(bid)	0.00	-0.55*	-0.32
Age	-0.04***	-0.04***	-0.04***
Gender	-0.07	-0.06	-0.06
Income (cat.5)	1.16***	1.17***	0.90***
Income (cat.4)	-0.10	-0.11	-0.01
Income (cat.3)	0.68**	0.68*	0.70**
Income (cat.2)	0.52	0.53	0.50
Education (cat.4)	0.96	0.98	0.84*
Education (cat.3)	-0.12	-0.14	-0.03
Education (cat.2)	0.10	0.11	0.07
Awareness of consequences	0.03	0.03	0.01
Tangible altruism	-0.01	-0.01	-0.02
Intangible altruism	0.02	0.02	0.02
Perception of RES	0.34***	0.34***	0.29***
Ascription of responsibility	0.15**	0.15**	0.10**
Average monthly electricity bill	0.00	0.00	0.00032***
City of residence (Pune)	-0.02	-0.02	0.17
Awareness of RES	0.01	0.01	-0.01
Number of family members	0.03	0.02	-0.06
Past usage of solar	-0.24	-0.24	-0.30
Use of alternate sources of electricity	0.46	0.45	0.40
P-value	0.00	0.00	0.00
AIC	432.5	431.9	438.9
BIC	521.4	520.8	527.7
Mean WTP in Rs. - Truncated at maximum bid value (Figures in brackets represent upper and lower values of the WTP estimate)	250 (233 – 262)	254 (235-265)	249 (232-261)
* Significant at 90 % CI; ** significant at 95 % CI; *** significant at 99 %			
Lower and upper bounds of WTP estimated using Krinsky & Robb simulation method			
Income and education variables are on the ordinal scale. Results omit the 1 st category for estimation.			

The SBDC mean WTP value for the given observations ranges from Rs. 249 to Rs. 254/household/month, indicating that the mean values are not sensitive to parametric distributional assumptions. AIC and BIC values for all models were also in similar ranges, indicating that no model was strongly superior to the rest. Four variables emerged to have a common impact on consumers' WTP for RES-E irrespective of the distribution specification. First, age exerts a negative influence on WTP. This indicates that younger consumers are more likely to accept higher bid values. Second, higher income positively influences the willingness to pay, suggesting that RE adoption is more likely amongst high-income households. Third, respondents holding higher RE perception are more welcoming of RE-based electricity contracts and are willing to pay more for it than respondents with lower perception. This suggested a direct correlation

between RE perceptions and willingness to pay for it, as has also been documented in the literature [63]. Fourth, respondents who ascribe higher self-responsibilities to undertake pro-environmental actions are more likely to pay more for RE-based electricity supply. Higher education and higher monthly electricity bills also nudge consumers to pay more for renewable electricity; however, these variables were only found significant in the Weibull distribution, but not for the logistic and log-logistic models.

Next, DBDC estimation was conducted next with the same distributional specifications (logistic, log-logistic, and Weibull). However, of the 3 models, Weibull estimation did not converge to a true solution. The variable coefficients, mean WTP values, and model fit values of the Logistic and Log-Logistic distributions are reproduced below in Table 7.

Table 7. Double-Bounded Dichotomous Choice (DBDC) parametric estimation results

Variable	Logistic	Log-Logistic
(Intercept)	-0.53	9.04***
Log(bid)	-0.01***	-1.92***
Age	-0.05***	-0.05***
Gender	0.10	-0.09
Income (cat.5)	0.89***	0.93***
Income (cat.4)	-0.17	-0.44
Income (cat.3)	0.73	0.61
Income (cat.2)	0.29	0.33
Education (cat.4)	1.11**	1.22***
Education (cat.3)	0.28	0.14
Education (cat.2)	0.53	0.55
Awareness of consequences	0.04	0.00
Tangible altruism	-0.03	0.05**
Intangible altruism	0.05*	0.02
Perception of RES	0.34***	0.33***
Ascription of responsibility	0.07	0.11*
Average monthly electricity bill	0.0006***	0.001***
City of residence (Pune)	-0.12	-0.01
Awareness of RES	0.02	0.02
Number of family members	-0.41***	-0.42***
Past usage of solar	-0.38	-0.78**
Use of alternate sources of electricity	0.34	0.05
P-value	0.00	0.00
AIC	1094.25	1079.7
BIC	1183.14	1168.5
Mean WTP in Rs. - Truncated at maximum bid value (Figures in brackets represent upper and lower values of the WTP estimate)	316.5 (299 – 332.5)	310.8 (283.9 - 317.5)
* Significant at 90 % CI; ** significant at 95 % CI; *** significant at 99 %		
Lower and upper bounds of WTP estimated using Krinsky & Robb simulation method		
Income and education variables are on the ordinal scale. Results omit the 1 st category for estimation.		

The DBDC mean WTP values for the set of observations range between Rs. 310.8 – Rs. 316.5. This again suggests no large impact of the distribution assumption on mean value estimation. While the AIC and BIC values for DBDC models are inflated as compared to the SBDC models, a larger number of significant variables are realized for the DBDC models. Between the 2 models, the log-logistic model had the lowest AIC values and was, hence, considered a better model. First, a positive intercept value ($\beta = 9.04$; p-value = 0.00) suggests an inherent willingness to pay for RE, irrespective of other independent variables. This indicates a general positive attitude towards green electricity. Second, a negative Log(Bid) estimate ($\beta = -1.92$; p-value = 0.00) indicates that the higher the bid value, the lower the probability of bid acceptance. This result is in alignment with standard economic theory that prescribes the higher the price, the lower the willingness to consume the product. Third, younger

respondents exhibit a higher probability accepting the presented bid values ($\beta = -0.05$, p-value = 0.00). This could be due to a greater awareness of RES-E and rising environmental consciousness amongst the youth. Fourth, higher income households are willing to pay more for RE ($\beta = .93$, p-value = 0.00) presumably due to higher affordability. Fifth, higher education levels spur willingness to pay ($\beta = 1.22$, p-value = 0.04). This finding aligns with the literature, as highly educated consumers are found to be more eco-conscious and hence, they support RES. Sixth, consumers engaged in altruistic activities before are found more willing to pay (Altruistic traits (tangible, $\beta = .05$, p-value = 0.04)). This finding again is in line with the literature, whereby paying for RES is considered to satisfy altruistic considerations [76]. Seventh, respondents holding positive perception of RES are seen as willing to pay more ($\beta = 0.33$, p-value = 0.00). Eighth, consumers who hold a high ascribed responsibility (ascription

of responsibility) for themselves to undertake pro-environmental actions feel more obliged to adopt RES-E and are hence willing to pay more ($\beta = 0.11$; p -value = 0.07). Ninth, counter-intuitively consumers with higher monthly bills are willing to pay more. This could be due to the belief that the application of RESs helps save them on monthly electricity bills. However, due to the small value of the estimate, compelling conclusions cannot be drawn ($\beta = 0.001$; p -value = 0.000). Next, it is observed that larger families do not support paying more for RES (Number of family members: $\beta = -0.42$; p -value = 0.01). This could be attributed to a higher value of electricity consumption that may result in higher monthly bills, thereby discouraging the willingness to pay more. Finally, existing consumers of solar energy (through solar RTPV solutions) appear to be more reluctant to pay for RES than the non-users ($\beta = -0.78$; p -value = 0.04).

This is counter-intuitive as users of solar should be pro RE, having reaped savings in monthly electricity bill amounts. This result indicates that necessary policy interventions are required to improve user satisfaction.

Efficiency gains from the estimates of SBDC and DBDC models were then checked to choose the best model. Efficiency gains in estimation can be established by considering the variance in confidence interval of mean WTP values as a percentage of the mean values (difference in confidence intervals/mean WTP), with lower variances indicating higher efficiency [102]. Contingent valuation studies in the past also used this ratio to establish the model efficiency of DBDC estimation [103]. Efficiency ratios for this study for both SBDC and DBDC computations are reported and compared below in Table 8.

Table 6. Efficiency ratio estimation of SBDC and DBDC models

Variable	SBDC - Logistic	DBDC - Logistic	SBDC - Log logistic	DBDC - Log logistic
Mean WTP	250.4	316.5	253.8	310.8
Lower Bound (LB)	233.2	299.1	235	283.9
Upper Bound (UB)	261.9	332.5	265	317.5
Difference in UB & LB	28.6	33.5	30	33.6
Efficiency Ratio (UB-LB/Mean WTP)	0.116	0.105	0.118	0.108

Efficiency ratio estimates report two key observations. First, the DBDC estimates from both the logistic and log-logistic model report lower efficiency ratios than the respective SBDC models, suggesting econometric superiority of DBDC estimation. Hence, it is clear that DBDC models gain inefficiency. Second, between the logistic and log-logistic DBDC estimates, the log-logistic model is weakly inferior (.108) over the logistic model (.105). However, for the purpose of this study and based on the set of observations, the DBDC log-logistic model is considered final due to the lower AIC and BIC values and 11 significant variables influencing WTP for RES-E, thus fitting standard economic theory. Thus, in conclusion, it can be reported that the mean WTP for RES-E rests at Rs. 310.8/household/month when charged as a premium over existing monthly electricity bills for residential households.

Given the WTP achieved as a monthly charge, it was of interest to study the WTP per unit of electricity consumed. To this end, the average residential consumption patterns in the state of Maharashtra were studied. An average residential household in Maharashtra does not consume more than 300 units of electricity (measured in kWh terms) [20]. This number increases exponentially in near future due to higher incomes, affordability, and urbanization in the state, but is currently contained within 300 units per month. Accordingly, the average WTP for GT is calculated at Rs. 1.03/unit/month. Although this number looks sufficiently small, CV studies in developing economies (especially, for pro-environmental products/programs) often report low WTP values. Table 9 appended below compares WTP for RE from other countries with the findings of this study.

Table 7. WTP for RE in other economies

Year of study	Country of study	WTP for RE *	Finding	Authors
2014	China	USD 2.35 – 2.82	Mandatory payment vehicle prompts higher WTP	[104]
2015	Lebanon	USD 20 – 50	For replacement of generator sets with solar PV (lumpsum payment)	[105]
2016	South Korea	USD 3.21	For bequest value of RE	[106]
2017	Hong Kong	USD 16.12	For natural gas based deep decarbonization	[107]

*: WTP per household per month, unless specified otherwise

In comparison, this study reports a WTP for RE at USD 4.97/household/month (78.05 INR = 1 USD). This finding aligns with the literature pieces as low willingness to pay for pro-environmental products in developing nations is attributed to the higher value assigned to real consumption than to environmental quality [108].

5. KEY FINDINGS AND CONCLUSIONS

This study was undertaken to investigate household willingness to pay for green energy-based electricity contracts. Data was collected from 476 residential households from the twin urban cities of Pune and Mumbai in the western state of

Maharashtra. A DBDC CV experiment was conducted with sample respondents to estimate the WTP for RE-based electricity supply and to identify the factors influencing the same. Analysis reveals that residential consumers carry a monthly mean WTP of Rs. 310.83 per household per month when charged as a premium over and above current monthly electricity bills. Higher age influences negatively, whereas higher education and income positively re-enforce this willingness to pay. Perceptions of green energy are positive and widespread. While 71 % of the respondents held positive perceptions of RE and perceived it to be as reliable as conventional energy forms, only 68 % agreed that people

should pay a premium for it. Thus, an attitude-action gap appears, which is a phenomena observed in other economies as well [109, 15, 16, 64]. This gap can hinder consumer switching to green energy in deregulated retail energy markets. Other behavioral factors that positively and significantly spur WTP include a high sense of responsibility to undertake pro-environmental actions and past altruistic behavior (tangible altruism).

6. RECOMMENDATIONS

Based on the above findings, this study proposes 4 recommendations for policy consideration.

First, to address the attitude-action gap in RE adoption, it is recommended that “green energy defaults” are introduced for residential consumers, initially. While green defaults are undesirable due to affordability and welfare concerns [19], they are also successful in eliminating lethargy in “consumer switching” from grey contracts to green contracts [110]. Green defaults can be a temporary introduction in the market and slow transition to voluntary contracts can be made following the expedition of RE adoption amongst residences. The feasibility, acceptability, design and welfare impacts of green energy tariffs and contracts need further exploring and are recommended for future research.

Second, marketing of voluntary sign-ups to green tariffs should be based on altruistic and bequest values of RE. Power suppliers would be of benefit by showcasing the non-use values of RE such as altruistic pleasures arising out of green consumption and leaving a greener environment for future generations (bequest values). Targeted consumer awareness campaigns towards this task can be conducted by sharing information passed through monthly electricity bills and other social media campaigns undertaken by power supplying utilities.

Third, since households with higher income, higher education, and lower age profiles exhibit higher acceptability and willingness to pay for RE, it is recommended that a sub-set of households meeting this socio-demographic profile should be identified as “influencers”. “Influencers” should be equipped with complete knowledge of benefits of green energy and can be incentivized to conduct awareness campaigns amongst residential societies. Local nodal agencies/state energy development boards can be entrusted to both identify the influencing agents, as well as conduct of awareness campaigns. This will positively fine tune the perception of RE, which also emerged as a key influencing factor of WTP for RE.

Fourth and finally, research design followed in this study can also be replicated to elicit green tariffs amongst Micro Small and Medium Enterprises (MSMEs) in India. Self-financing RE systems have become more challenging for Indian MSMEs in the post COVID-19 times, since MSMEs are unable to justify the cost benefit analysis of high RE system costs vis-à-vis low energy demand. Added business uncertainties on account of COVID-19-related slowdowns are also making financial lenders cautious of lending to SMEs, exacerbating RE financing bottlenecks [111, 112]. Given this, incumbent power suppliers would benefit from marketing green tariffs, especially MSME clusters in the state. By paying the green tariff premium, MSMEs can meet RE procurement targets (voluntary targets or as mandated by business partners, as applicable) without making capital expenditures in RE systems.

7. LIMITATIONS

This study was undertaken in two urban concentrations in the state of Maharashtra. Since the sample was collected from only one Indian state, the willingness to pay estimates are not generalizable to the entire India. However, the research design used in this study could be replicated in other Indian states to elicit WTP for that state, since WTP estimates are sensitive to state-wise social, economic, and individual attributes of respondents.

8. ACKNOWLEDGEMENT

The author thanks Symbiosis International (Deemed University) for providing access to resources and research guidance throughout the conducting of this study.

REFERENCES

1. Sarangi, G.K. and Taghizadeh-Hesary, F., "Rooftop solar development in India: Measuring policies and mapping business models", *Asian Development Bank Institute*, (2021). (<https://www.adb.org/publications/rooftop-solar-development-india-policies-mapping-business-models>).
2. Parsad, C., Mittal, S. and Krishnankutty, R., "A study on the factors affecting household solar adoption in Kerala, India", *International Journal of Productivity and Performance Management*, (2020), 1695-1720. (<https://doi.org/10.1108/IJPPM-11-2019-0544>).
3. Bridge to India, "India solar rooftop map 2020", (21 September 2021). (<https://bridgetoindia.com/report/india-solar-rooftop-map-december-2020/>).
4. Bhati, P., Sreenivasan, P., Singh, M., Koshy, S.M., Jhavar, P. and Sambyal, S., "The state of renewable energy in India 2019 - A citizen's report", *Centre for Science and Environment*, New Delhi, (2019). (<https://shaktifoundation.in/wp-content/uploads/2019/04/State-of-Renewable-Energy-in-India.pdf>).
5. Parag, Y. and Sovacool, B.K., "Electricity market design for the prosumer era", *Nature Energy*, (2016). (<https://doi.org/10.1038/NENERGY.2016.32>).
6. Jeyapaul, P.P., "A mathematical approach to analyze factors influencing adoption of solar based power production in residential buildings in tamilnadu state of India", *International Journal of Renewable Energy Research*, Vol. 10, No. 2, (2020), 537-548. (https://www.researchgate.net/profile/Praveen-Jeyapaul/publication/357793707_A_Mathematical_Approach_to_Analyze_Factors_Influencing_Adoption_of_Solar_Based_Power_Production_in_Residential_Buildings_in_Tamilnadu_State_of_India/links/61dfcfc034dda1b9ef3506d/A-Mathematical-Approach-to-Analyze-Factors-Influencing-Adoption-of-Solar-Based-Power-Production-in-Residential-Buildings-in-Tamilnadu-State-of-India.pdf).
7. Quraishi, K.S. and Ahmed, S., "Analysis of purchase behaviour of residential solar rooftop pv adopters", *International Journal of Management*, Vol. 10, No. 5, (2019), 28-37. (<https://ssrn.com/abstract=3508704>).
8. Sauthoff, S., Danne, M. and Mußhoff, O., "To switch or not to switch? Understanding German consumers' willingness to pay for green electricity tariff attributes", *Georg-August-Universität Göttingen, Department für Agrarökonomie und Rurale Entwicklung (DARE)*, Göttingen, Diskussionsbeitrag No. 1707, (2017). (<https://www.econstor.eu/handle/10419/161433>).
9. Chassot, S., Wüstenhagen, R., Fahr, N. and Graf, P., "Introducing green electricity as the default option", *Marketing Renewable Energy - Concepts, Business Models and Cases*, (2017), 109-122. (https://doi.org/10.1007/978-3-319-46427-5_6).
10. Meran, G. and Schwarze, R., "A theory of optimal green defaults", *Sustainability*, Vol. 10, No. 8, (2018). (<https://doi.org/10.3390/su10082902>).
11. Ebeling, F. and Lotz, S., "Domestic uptake of green energy promoted by opt-out tariffs", *Nature Climate Change*, Vol. 5, No. 9, (2015), 868-871. (<https://doi.org/10.1038/nclimate2681>).
12. Bridge to India, "India corporate renewable brief", Bridge to India, (2021). (<https://india-re-navigator.com/public/uploads/1628144382-BRIDGE-TO-INDIA-India-Corporate-Renewable-Brief.pdf>).

13. M. E. R. Commission, "Green power tariff order", MERC, Mumbai, (2021). (<https://www.mahaurja.com/meda/data/rporec/reports/MERCOrder134of2020.pdf>).
14. Defeuilley, C., "Retail competition in electricity markets", *Energy Policy*, Vol. 37, No. 2, (2009), 377-386. (<https://doi.org/10.1016/j.enpol.2008.07.025>).
15. Pichert, D. and Katsikopoulos, K.V., "Green defaults: Information presentation and pro-environmental behaviour", *Journal of Environmental Psychology*, Vol. 28, No. 1, (2008), 63-73. (<https://doi.org/10.1016/j.jenvp.2007.09.004>).
16. Litvine, D. and Wüstenhagen, R., "Helping "light green" consumers walk the talk: Results of a behavioural intervention survey in the swiss electricity market", *Ecological Economics*, Vol. 70, No. 3, (2011), 462-474. (<https://doi.org/10.1016/j.ecolecon.2010.10.005>).
17. Koto, P.S. and Yiridoe, E.K., "Expected willingness to pay for wind energy in Atlantic Canada", *Energy Policy*, Vol. 129, (2019), 80-88. (<https://doi.org/10.1016/j.enpol.2019.02.009>).
18. Xie, B.C. and Zhao, W., "Willingness to pay for green electricity in Tianjin, China: Based on the contingent valuation method", *Energy Policy*, Vol. 114, (2018), 98-107. (<https://doi.org/10.1016/j.enpol.2017.11.067>).
19. Schubert, R., Schmitz, J., Grieder, M. and Ghesla, C., "Green by default-Welfare effects of green default electricity contracts: Final report", *ETH Zurich Research Collection*, Zurich, (2017). (<https://doi.org/10.3929/ethz-b-000230116>).
20. Prayas, A.C., "Residential electricity consumption in India: what do we know", Prayas, Energy Group, Pune, (2016). (<https://energy.prayaspune.org/our-work/research-report/residential-electricity-consumption-in-india-what-do-we-know>).
21. Authority, C.E., "Report on nineteenth electric power survey of India", Ministry of Power, New Delhi, India, (2020). (https://cea.nic.in/wp-content/uploads/2020/04/summary_19th_eps.pdf).
22. Webster, J. and Watson, R.T., "Analyzing the past to prepare for the future: Writing a literature review", *MIS Quarterly*, Vol. 26, No. 2, (2002), 13-23. (<http://www.jstor.org/stable/4132319>).
23. Wüstenhagen, R., Wolsink, M. and Bürer, M.J., "Social acceptance of renewable energy innovation: An introduction to the concept", *Energy Policy*, Vol. 35, No. 5, (2007), 2863-2691. (<https://doi.org/10.1016/j.enpol.2006.12.001>).
24. Yoo, S.H. and Kwak, S.Y., "Willingness to pay for green electricity in Korea: A contingent valuation study", *Energy Policy*, Vol. 37, No. 12, (2009), 5408-5416. (<https://doi.org/10.1016/j.enpol.2009.07.062>).
25. Kwak, S.Y. and Yoo, S.H., "The public's value for developing ocean energy technology in the Republic of Korea: A contingent valuation study", *Renewable and Sustainable Energy Reviews*, Vol. 43, (2015), 432-439. (<https://doi.org/10.1016/j.rser.2014.11.036>).
26. Lee, C.Y., Lee, M.K. and Yoo, S.H., "Willingness to pay for replacing traditional energies with renewable energy in South Korea", *Energy*, Vol. 128, (2017), 284-290. (<https://doi.org/10.1016/j.energy.2017.04.037>).
27. Nakano, R., Miwa, T. and Morikawa, T., "Comparative analysis on citizen's subjective responses related to their willingness to pay for renewable energy in Japan using latent variables", *Sustainability*, Vol. 10, No. 7, (2018), 1-14. (<https://doi.org/10.3390/su10072423>).
28. Goett, A.A., Hudson, K. and Train, K.E., "Customers' choice among retail energy suppliers: The willingness-to-pay for service attributes", *The Energy Journal*, Vol. 21, No. 4, (2000) 1-28. (<https://www.jstor.org/stable/41322898>).
29. Borchers, A.M., Duke, J.M. and Parsons, G.R., "Does willingness to pay for green energy differ by source?", *Energy Policy*, Vol. 35, No. 6, (2007), 3327-3334. (<https://doi.org/10.1016/j.enpol.2006.12.009>).
30. Cicia, G., Cembalo, L., Del Giudice, T. and Palladino, A., "Fossil energy versus nuclear, wind, solar and agricultural biomass: Insights from an Italian national survey", *Energy Policy*, Vol. 42, (2009), 59-66. (<https://doi.org/10.1016/j.enpol.2011.11.030>).
31. Yang, Y., Solgaard, H.S. and Haider, W., "Value seeking, price sensitive, or green? Analyzing preference heterogeneity among residential energy consumers in Denmark", *Energy Research and Social Science*, Vol. 6, (2015), 15-28. (<https://doi.org/10.1016/j.erss.2014.11.001>).
32. Shin, K.J. and Managi, S., "Liberalization of a retail electricity market: Consumer satisfaction and household switching behavior in Japan", *Energy Policy*, Vol. 110, (2017), 675-685. (<http://dx.doi.org/10.1016/j.enpol.2017.07.048>).
33. Yang, Y., "Understanding household switching behavior in the retail electricity market", *Energy Policy*, Vol. 69, (2014), 406-414. (<https://doi.org/10.1016/j.enpol.2014.03.009>).
34. Ndebele, T., Marsh, D. and Scarpa, R., "Consumer switching in retail electricity markets: Is price all that matters?", *Energy Economics*, Vol. 83, (2019), 88-103. (<https://doi.org/10.1016/j.eneco.2019.06.012>).
35. Nkansah, K. and Collins, A.R., "Willingness to pay for wind versus natural gas generation of electricity", *Agricultural and Resource Economics Review*, Vol. 48, No. 1, (2019), 44-70. (<https://doi.org/10.1017/age.2017.40>).
36. Koto, P.S. and Yiridoe, E.K., "Expected willingness to pay for wind energy in Atlantic Canada", *Energy Policy*, (2019), 80-88. (<https://doi.org/10.1016/j.enpol.2019.02.009>).
37. Rommel, J., Sagebiel, J. and Müller, J.R., "Quality uncertainty and the market for renewable energy: Evidence from German consumers", *Renewable Energy*, Vol. 94, (2016), 106-113. (<https://doi.org/10.1016/j.renene.2016.03.049>).
38. Sagebiel, J., Müller, J.R. and Rommel, J., "Are consumers willing to pay more for electricity from cooperatives? Results from an online choice experiment in Germany", *Energy Research & Social Science*, Vol. 2, (2014), 90-101. (<https://doi.org/10.1016/j.erss.2014.04.003>).
39. Kalkbrenner, B.J., Yonezawa, K. and Roosen, J., "Consumer preferences for electricity tariffs: Does proximity matter?", *Energy Policy*, Vol. 107, (2017), 413-424. (<https://doi.org/10.1016/j.enpol.2017.04.009>).
40. Ghesla, C., Grieder, M. and Schubert, R., "Nudging the poor and the rich—A field study on the distributional effects of green electricity defaults", *Energy Economics*, Vol. 86, (2020), 104616. (<https://doi.org/10.1016/j.eneco.2019.104616>).
41. M. o. S. a. P. Implementation, "India in Figures", Central Statistical Organisation, Delhi, (2018). (http://mospi.nic.in/sites/default/files/publication_reports/India_in_figures-2018_rev.pdf).
42. Entele, B.R., "Analysis of households' willingness to pay for a renewable source of electricity service connection: Evidence from a double-bounded dichotomous choice survey in rural Ethiopia", *Heliyon*, Vol. 6, No. 2, (2020), 03332. (<https://doi.org/10.1016/j.heliyon.2020.e03332>).
43. Ugulu, A.I. and Aigbavboa, C., "Assessing urban households' willingness to pay for standalone solar photovoltaic systems: A case study of Lagos, Nigeria", *Journal of Sustainable Development of Energy, Water and Environment Systems*, Vol. 7, No. 3, (2019), 553-566. (<https://doi.org/10.13044/j.sdewes.d7.0274>).
44. Ayodele, T.R., Ogunjuyigbe, A.S.O., Ajayi, O.D., Yusuff, A.A. and Mosethe, T.C., "Willingness to pay for green electricity derived from renewable energy sources in Nigeria", *Renewable and Sustainable Energy Reviews*, Vol. 148, (2021), 111279. (<https://doi.org/10.1016/j.rser.2021.111279>).
45. Nduka, E., "How to get rural households out of energy poverty in Nigeria: A contingent valuation study", *Energy Policy*, Vol. 149, (2021), 112072. (<https://doi.org/10.1016/j.enpol.2020.112072>).
46. Oluoch, S., Lal, P., Susaeta, A. and Wolde, B., "Public preferences for renewable energy options: A choice experiment in Kenya", *Energy Economics*, Vol. 98, (2021), 105256. (<https://doi.org/10.1016/j.eneco.2021.105256>).
47. Numata, M., Sugiyama, M., Swe, W. and del Barrio Alvarez, D., "Willingness to pay for renewable energy in Myanmar: Energy source preference", *Energies*, Vol. 45, No. 4, (2021), 1505. (<https://doi.org/10.3390/en14051505>).
48. Krishnan, D.S., Thanikonda, A.K., Kumar, P. and Mandal, T., "How electricity distribution companies in India can work with commercial and industrial consumers for renewable energy procurement", Delhi, (2020). (<https://wri-india.org/sites/default/files/uploads/how-electricity-distribution-companies-india-can-work-commercial-industrial-consumers-renewable-energy-procurement.pdf>).
49. Mandal, T., Sen, V. and Anirudh, S., "Renewable energy procurement perceptions among commercial and industrial consumers: Current practices and future possibilities", World Resources Institute, (2022). (<https://www.wri.org/research/renewable-energy-procurement-perceptions-among-commercial-and-industrial-consumers>).
50. Lahiri, D. and Acharjee, G., "Biomass gasifier electricity and study of willingness to pay", *International Journal of Renewable Energy*

- Resources*, Vol. 3, No. 1, (2013), 16-18. (<https://doi.org/10.1109/CET.2011.6041471>).
51. Dossani, R. and Ranganathan, V., "Farmers willingness to pay for power in India: Conceptual issues, survey results and implication for pricing", *Energy Economics*, Vol. 26, No. 3, (2004), 359-369. (<http://dx.doi.org/10.1016%2Fj.eneco.2004.04.004>).
 52. Urpelainen, J. and Yoon, S., "Solar home systems for rural India: Survey evidence on awareness and willingness to pay from Uttar Pradesh", *Energy for Sustainable Development*, Vol. 24, (2015), 70-78. (<https://doi.org/10.1016/j.esd.2014.10.005>).
 53. Gunatilake, H., Patail, S. and Yang, J.C., "Valuing electricity service attributes: A choice experiment study in Madhya Pradesh, India", *Asian Development Bank*, Philippines, (2012). (<http://hdl.handle.net/10419/109432>).
 54. Gill, B., Saluja, S. and Palit, D., "Charging power: Understanding electricity pricing and willingness to pay for electricity in India", Delhi, (2017). (https://www.teriin.org/sites/default/files/2019-03/Charging%20Power_Policy%20Note_270217-FINAL.pdf).
 55. Bridge To India, "India corporate renewable energy brief", Bridge to India, (2021). (https://www.fin.awsassets.panda.org/downloads/india_corporate_renewable_brief_q3_2021.pdf).
 56. Buckley, P., "Prices, information and nudges for residential electricity conservation: A meta analysis", *Ecological Economics*, Vol. 172, (2020), 106635. (<https://doi.org/10.1016/j.ecolecon.2020.106635>).
 57. Abdullah, S. and Jeanty, P.W., "Willingness to pay for renewable energy: Evidence from a contingent valuation survey in Kenya", *Renewable and Sustainable Energy Reviews*, Vol. 15, No. 6, (2011), 2974-2983. (<https://doi.org/10.1016/j.rser.2011.03.016>).
 58. Kim, J., Park, J., Kim, H. and Heo, E., "Assessment of Korean customers' willingness to pay with RPS", *Renewable and Sustainable Energy Reviews*, Vol. 16, No. 1, (2012), 695-703. (<https://doi.org/10.1016/j.rser.2011.08.034>).
 59. Andor, M.A., Frondel, M. and Vance, C., "Germany's energiewende: A tale of increasing costs and decreasing willingness to pay", *ECONSTOR*, Vol. 645, (2017). (<http://dx.doi.org/10.4419/86788750>).
 60. Hanemann, M., Loomis, J. and Kanninen, B., "Statistical efficiency of double-bounded dichotomous choice contingent valuation", *American Journal of Agricultural Economics*, Vol. 73, No. 4, (1991), 1255-1263. (<https://doi.org/10.2307/1242453>).
 61. Whittington, D., "Administering contingent valuation surveys in developing countries", *World Development*, Vol. 26, No. 1, (1998), 21-30. ([https://doi.org/10.1016/S0305-750X\(97\)00125-3](https://doi.org/10.1016/S0305-750X(97)00125-3)).
 62. Bigerna, S. and Polinori, P., "Italian households' willingness to pay for green electricity", *Renewable and Sustainable Energy Reviews*, Vol. 34, (2014), 110-121. (<https://doi.org/10.1016/j.rser.2014.03.002>).
 63. Ntanos, S., Kyriakopoulos, G., Chalikias, M., Arabatzis, G. and Skordoulis, M., "Public perceptions and willingness to pay for renewable energy: A case study from Greece", *Sustainability*, Vol. 10, No. 3, (2018). (<https://doi.org/10.3390/su10030687>).
 64. Hobman, E.V. and Frederiks, E.R., "Barriers to green electricity subscription in Australia: Love the environment, love renewable energy, but why should I pay more?", *Energy Research & Social Science*, Vol. 3, (2014), 78-88. (<https://doi.org/10.1016/j.erss.2014.07.009>).
 65. Li, H., Jenkins-Smith, H.C., Silva, C.L., Berrens, R.P. and Herron, K.G., "Public support for reducing US reliance on fossil fuels: Investigating household willingness-to-pay for energy research and development", *Ecological Economics*, Vol. 68, No. 3, (2009), 731-742. (<https://doi.org/10.1016/j.ecolecon.2008.06.005>).
 66. Sun, C., Ouyang, X. and Meng, X., "Public acceptance towards waste-to-energy power plants: A new quantified assessment based on willingness to pay", *Journal of Environmental Planning and Management*, Vol. 62, No. 14, (2019). (<https://doi.org/10.1080/09640568.2018.1560930>).
 67. Clark, C.F., Kotchen, M.J. and Moore, M.R., "Internal and external influences on pro-environmental behavior: Participation in a green electricity program", *Journal of Environmental Psychology*, Vol. 23, No. 3, (2003), 237-246. ([https://doi.org/10.1016/S0272-4944\(02\)00105-6](https://doi.org/10.1016/S0272-4944(02)00105-6)).
 68. Hansla, A., Gamble, A., Juliusson, A. and Garling, T., "Psychological determinants of attitude towards and willingness to pay for green electricity", *Energy Policy*, Vol. 36, No. 2, (2008), 768-774. (<https://doi.org/10.1016/j.enpol.2007.10.027>).
 69. Ozaki, R., "Adopting sustainable innovation: What makes consumers sign up to green electricity?", *Business Strategy and the Environment*, Vol. 20, No. 1, (2011), 1-17. (<https://doi.org/10.1002/bse.650>).
 70. Kahneman, D. and Knetsch, J., "Valuing public goods: The purchase of moral satisfaction", *Journal of Environmental Economics and Management*, Vol. 22, No. 1, (1992), 57-70. ([https://doi.org/10.1016/0095-0696\(92\)90019-S](https://doi.org/10.1016/0095-0696(92)90019-S)).
 71. Guagnano, G.A., "Altruism and market-like behavior: An analysis of willingness to pay for recycled paper products", *Population and Environment: A Journal of Interdisciplinary Studies*, Vol. 22, (2001), 425-438. (<https://doi.org/10.1023/A:1006753823611>).
 72. Araña, J.E. and León, C.J., "Willingness to pay for health risk reduction in the context of altruism", *Health Economics*, Vol. 11, No. 7, (2002), 623-635. (<https://doi.org/10.1002/hec.687>).
 73. Onwujekwe, O., Chima, R., Shu, E., Nwagbo, D., Akpala, C. and Okonkwo, P., "Altruistic willingness to pay in community-based sales of insecticide-treated nets exists in Nigeria", *Social Science & Medicine*, Vol. 54, No. 4, (2002), 519-527. ([https://doi.org/10.1016/S0277-9536\(01\)0000](https://doi.org/10.1016/S0277-9536(01)0000)).
 74. Ojea, E. and Loureiro, M., "Altruistic, egoistic and biospheric values in willingness to pay for wildlife", *Ecological Economics*, Vol. 63, No. 4, (2007), 807-814. (<https://doi.org/10.1016/j.ecolecon.2007.02.003>).
 75. Umberger, W.J., Thilmany McFadden, D.D. and Smith, A.R., "Does altruism play a role in determining U.S. consumer preferences and willingness to pay for natural and regionally produced beef?", *Agribusiness: An International Journal*, Vol. 25, No. 2, (2009), 268-285. (<https://doi.org/10.1002/agr.20194>).
 76. Herbes, C., Friege, C., Baldo, D. and Mueller, K.M., "Willingness to pay for green electricity? Applying a neuroscience-based method to WTP for green electricity", *Energy Policy*, Vol. 87, (2015), 562-572. (<https://doi.org/10.1016/j.enpol.2015.10.001>).
 77. Hansla, A., "Value orientation and framing as determinants of stated willingness to pay for eco-labeled electricity", *Energy Efficiency*, Vol. 4, (2010), 185-192. (<https://doi.org/10.1007/s12053-010-9096-0>).
 78. Champ, P.A., Boyle, K.J. and Brown, T.C., A primer on nonmarket valuation, Springer, (2017). (<https://doi.org/10.1007/978-94-007-0826-6>).
 79. Boyle, K.J., Bishop, R.C. and Welsh, M.P., "Starting point bias in contingent valuation bidding games", *Land Economics*, Vol. 61, No. 2, (1985), 188-194. (<https://doi.org/10.2307/3145811>).
 80. Chunekar, A., Varshney, S. and Dixit, S., "Residential electricity consumption in India", Prayas Energy Group, Pune, (2016). (<https://energy.prayasgroup.org/our-work/research-report/residential-electricity-consumption-in-india-what-do-we-know>).
 81. Loomis, J., "Whats to know about hypothetical bias in stated preference valuation studies", *Journal of Economic Surveys*, Vol. 25, No. 2, (2011) 363-370. (<https://doi.org/10.1111/j.1467-6419.2010.00675.x>).
 82. Özdemir, S., Johnson, F.R. and Hauber, A.B., "Hypothetical bias, cheap talk, and stated willingness to pay for health care", *Journal of Health Economics*, Vol. 28, No. 4, (2009), 894-901. (<https://doi.org/10.1016/j.jhealeco.2009.04.004>).
 83. Ethier, R.G., Poe, G.L., Schulze, W.D. and Clark, J., "A comparison of hypothetical phone and mail contingent valuation responses for green-pricing electricity programs", *Land Economics*, (2000), 54-67. (<https://doi.org/10.2307/3147257>).
 84. Carson, R.T., "Contingent valuation: A user's guide", *Environmental Science and Technology*, (2000), 1413-1418. (<https://ageconsearch.umn.edu/record/7245/files/wp970025.pdf>).
 85. Whittington, D., "Improving the performance of contingent valuation studies in developing countries", *Environmental and Resource Economics*, Vol. 22, (2002), 323-367. (<https://doi.org/10.1023/A:1015575517927>).
 86. Arega, T. and Tadesse, T., "Household willingness to pay for green electricity in urban and peri-urban Tigray, Northern Ethiopia: Determinants and welfare effects", *Energy Policy*, Vol. 100, (2017), 292-300. (<https://doi.org/10.1016/j.enpol.2016.10.022>).
 87. Cook, D., Davíðsdóttir, B. and Kristofersson, D.M., "Willingness to pay for the preservation of geothermal areas in Iceland-The contingent valuation studies of Eldvörp and Hverahlíð", *Renewable Energy*, Vol. 116, (2018), 97-108. (<https://doi.org/10.1016/j.renene.2017.09.072>).
 88. Myung, I.J., "Tutorial on maximum likelihood estimation", *Journal of Mathematical Psychology*, Vol. 47, (2003), 90-100. ([https://doi.org/10.1016/S0022-2496\(02\)00028-7](https://doi.org/10.1016/S0022-2496(02)00028-7)).

89. Kristrom, B., "Spike models in contingent valuation", *Journal of Agricultural Economics*, Vol. 79, No. 3, (1997), 1013-1023. (<https://doi.org/10.2307/1244440>).
90. Dutt, D., "Understanding the barriers to the diffusion of rooftop solar: A case study of Delhi (India)", *Energy Policy*, Vol. 144, (2020). (<https://doi.org/10.1016/j.enpol.2020.111674>).
91. Bhati, P. and Kalsotra, R., "Solar rooftop: Replacing diesel generators in residential societies", Centre for Science and Environment, New Delhi, (2017). (<http://cdn.cseindia.org/userfiles/Policy-Brief-Solar-Rooftop-Replacing-Diesel-Generators-in-Residential-Societies.pdf>).
92. Jareemit, D. and Limmeechokchai, B., "Understanding resident's perception of energy saving habits in households in Bangkok", *Energy Procedia*, (2017), Vol. 138, 247-252. (<https://doi.org/10.1016/j.egypro.2017.10.048>).
93. Sen, V., Joshi, G. and Kunte, M., "Purchasing energy efficient appliances: A qualitative investigation using text analysis", *Test Engineering and Management*, Vol. 82, (2020), 13230-13241. (<https://www.testmagazine.biz/index.php/testmagazine/article/view/2958/2595>).
94. Berkhout, F., Marcotullio, P. and Hanaoka, T., "Understanding energy transitions", *Sustainable Science*, (2012), 109-111. (<https://doi.org/10.1007/s11625-012-0173-5>).
95. Taber, K.S., "The use of Cronbach's Alpha when developing and reporting research instruments in science education", *Research in Science Education*, Vol. 48, (2018), 1273-1296. (<https://link.springer.com/article/10.1007/s11165-016-9602-2>).
96. Taherdoost, H., Sahibuddin, S. and Jalaliyoon, N., "Exploratory factor analysis; concepts and theory", *Advances in Applied and Pure Mathematics*, (2014), 375-382. (<https://hal.archives-ouvertes.fr/hal-02557344/document>).
97. Neill, J., "Writing up a factor analysis", University of Canberra, Canberra, (2008). (https://www.academia.edu/2831918/Writing_up_a_factor_analysis).
98. Chan, K.Y.A., Oerlemans, L.A., Volschenk, J. and Oliver, H., "Objective and subjective willingness to pay for green electricity, Do they measure the same? Evidence from South African case", *Proceedings of PICMET '11: Technology Management in the Energy Smart World (PICMET)*, Portland, USA., (2011). (<https://ieeexplore.ieee.org/document/6017886/authors#authors>).
99. Onwezen, M.C., Antonides, G. and Bartels, J., "The norm activation model: An exploration of the functions of anticipated pride and guilt in pro-environmental behaviour", *Journal of Economic Psychology*, Vol. 39, (2013), 141-153. (<https://doi.org/10.1016/j.joep.2013.07.005>).
100. Aizaki, H., Nakatani, T. and Sato, Z., Stated preference methods using R, Taylor and Francis, (2015). (<https://doi.org/10.1201/b17292>).
101. Kuha, J., "AIC and BIC: Comparisons of assumptions and performance", *Sociological Methods and Research*, Vol. 33, No. 2, (2004), 188-229. (<https://doi.org/10.1177/0049124103262065>).
102. Loomis, J. and Ekstrand, E., "Alternative approaches for incorporating respondent uncertainty when estimating", *Ecological Economics*, Vol. 27, No. 1, (1998), 29-41. ([https://doi.org/10.1016/S0921-8009\(97\)00126-2](https://doi.org/10.1016/S0921-8009(97)00126-2)).
103. Donfouet, H.P.P., Jeanty, P.W. and Mahieu, P.-A., "Dealing with internal inconsistency in double-bounded dichotomous choice: An application to community-based health insurance", *Empirical Economics*, Vol. 46, (2014), 317-328. (<https://doi.org/10.1007/s00181-012-0665-2>).
104. Guo, X., Liu, H., Mao, X., Jin, J., Chen, D. and Cheng, S., "Willingness to pay for renewable electricity: A contingent valuation study in Beijing, China", *Energy Policy*, Vol. 68, (2014), 340-347. (<https://doi.org/10.1016/j.enpol.2013.11.032>).
105. Dagher, L. and Harajli, H., "Willingness to pay for green power in an unreliable electricity sector: Part I. The case of the Lebanese residential sector", *Renewable and Sustainable Energy Reviews*, Vol. 50, (2015), 1634-1642. (<https://doi.org/10.1016/j.rser.2015.04.162>).
106. Lee, C.-Y. and Heo, H., "Estimating willingness to pay for renewable energy in South Korea using the contingent valuation method", *Energy Policy*, Vol. 94, (2016), 150-156. (<https://doi.org/10.1016/j.enpol.2016.03.051>).
107. Cheng, Y., Cao, K., Woo, C. and Yatchew, A., "Residential willingness to pay for deep decarbonization of electricity supply: Contingent valuation evidence from Hong Kong", *Energy Policy*, Vol. 109, (2017), 218-227. (<https://doi.org/10.1016/j.enpol.2017.07.006>).
108. Oliva, P., Alexianu, M. and Nasir, R., "Suffocating prosperity: Air pollution and economic growth in developing countries", (2019). (<https://www.theigc.org/publications/suffocating-prosperity-air-pollution-and-economic-growth-developing-countries>).
109. Hansla, A., Gamble, A., Juliusson, A. and Garling, T., "Psychological determinants of attitude towards and willingness to pay for green electricity", *Energy Policy*, Vol. 36, No. 2, (2008), 768-774. (<https://doi.org/10.1016/j.enpol.2007.10.027>).
110. Ebeling, F. and Lotz, S., "Domestic uptake of green energy promoted by opt put tariffs", *Natural Climate Change Letters*, Vol. 5, (2015), 868-871. (<https://doi.org/10.1038/nclimate2681>).
111. Gulia, J., Jadhav, A., Garg, V. and Kuiper, D. G., "Financing trends in the rooftop solar commercial and industrial segment (C&I) in India: Scaling up rooftop solar finance in untapped markets", IEEFA and JMK Research, New Delhi, (2021). (http://ieefa.org/wp-content/uploads/2021/09/Financing-Trends-in-the-Rooftop-Solar-Consumer-and-Industrial-Segment-in-India_September-2021.pdf).
112. Shekhar, J., Suri, D., Somani, P., Lee, S.J. and Arora, M., "Reduced renewable energy stability in India following COVID-19: Insights and key policy recommendations", *Renewable and Sustainable Energy Reviews*, Vol. 144, (2021). (<https://doi.org/10.1016/j.rser.2021.111015>).



Research Article

Assessing the Environmental Impacts of Biomass Energy Production in Loka Abaya District, Sidama Region, Southern Ethiopia

Ararsa Derese Seboka^{a*}, Fiseha Bekele Teshome^b, Motuma Tolera Feyissa^a

^a Department of General Forestry, Wondo Genet College of Forestry and Natural Resources, Hawassa University, P. O. Box: 128, Shashemene, Ethiopia.

^b Department of Environmental Science, Wondo Genet College of Forestry and Natural Resources, Hawassa University, P. O. Box: 128, Shashemene, Ethiopia.

PAPER INFO

Paper History:

Received: 15 March 2022

Revised: 18 June 2022

Accepted: 23 June 2022

Keywords:

Biomass Energy,
Wood Fuel,
Charcoal,
Firewood,
Greenhouse Gases,
Environment Impacts

ABSTRACT

This study was conducted in the Loka Abaya District of Sidama Region, Southern Ethiopia to assess the environmental impacts of biomass energy production with particular emphasis on charcoal and firewood. The data collection was undertaken using the questionnaire survey administered to 186 randomly selected households. This task was followed by key informant interviews and an analysis of the literature. The sampled households produced 208 432.9 kg firewood yr⁻¹ for domestic consumption and 261 039.8 kg charcoal yr⁻¹ for sale in town. 2.3 × 10⁶ km² of the forest is cleared to produce a single sack of charcoal. Charcoal and firewood production is totally responsible for the degradation of 39.4 ha of forest per year. The associated emissions of CO₂, CO, N₂O, CH₄, and TNMHC (total non-methane hydrocarbon) during the production and consumption of firewood and charcoal were calculated based on the emission factors indicated by previous studies. The results demonstrated that the trace gases produced during charcoal making were higher than that of charcoal burning. Further, the amounts of greenhouse gases generated during firewood burning were higher than the ones generated during charcoal burning. In order to minimize the challenges of deforestation and greenhouse gas emissions caused by charcoal and firewood consumption, a strategy of promoting the utilization of alternative clean energy sources such as solar and biogas should be implemented in parallel to the effort of adoption of improved biomass energy-saving cook stoves.

<https://doi.org/10.30501/jree.2022.334270.1346>

1. INTRODUCTION

Global wood removal for wood fuel production is estimated to be 61 per cent [1]; over the last 50 years, global charcoal production increased from 17.3 million tons in 1964 to 53.1 million tons in 2014 [2]. In Sub-Saharan Africa (SSA), the vast majority of households depend on wood energy -comprising firewood and charcoal- for their daily energy requirement; the projection done by International Energy Agency reported that the number of wood-based biomass energy consumers in Sub-Saharan Africa would reach almost one billion by 2030. This indicates that reliance on wood-based biomass energy from firewood and charcoal is far greater in Sub-Saharan Africa (SSA) than in any other region in the world. In 34 countries worldwide, wood-based biomass energy satisfies more than 70 percent of energy needs, and it satisfies more than 90 percent in 13 countries. The majority of these countries are located in SSA [7]. Statistically, Africa accounts for 63 % of the global charcoal production [8]. About 94 % of the African rural population and 73 % of the urban population use wood fuels as their primary energy

source with the urban and rural areas heavily dependent on charcoal and firewood, respectively [9].

The Ethiopian total rural household consumption of wood (including the charcoal equivalent of wood) is estimated to be 91.2 million per year with 4.2 million tons per year of charcoal. Total consumption of residues and dung is estimated to be 19.3 million tons per year and 20.7 million tons per year respectively [10]. Biomass energy is highly consumed in rural and urban areas for cooking and heating [11]. Both urban and rural households have upgraded their biomass use from low-quality residues and dung to firewood and charcoal [12]. The availability of these fuels at low cost and the lack of available alternative energy sources are causes for the high dependence of the communities on firewood and charcoal across the country. In urban areas, firewood as the primary fuel varies according to factors such as differences in price and availability of alternatives. Firewood is often burned in open stoves resulting in low energy density and low total energy efficiency during combustion, often between 10 % and 20 %. Furthermore, the difficulty of controlling heat levels in an open stove implies that large masses of fuel must be burned.

Concerning the combustion of firewood and charcoal, the cooking stoves and kitchens are majorly unvented in the study area and this is true for rural households in developing

*Corresponding Author's Email: 20aro201@gmail.com (A.D. Seboka)
URL: https://www.jree.ir/article_160919.html



countries. Consequently, Particulate Matter (PM) and gases such as carbon monoxide (CO), carbon dioxide (CO₂), oxides of nitrogen (NO_x), volatile organic compounds (VOCs), sulphur oxides (SO_x), and a range of trace species including polyaromatic hydrocarbons affect the health of household members directly involved in cooking and heating activities. Furthermore, most of these compounds have a much higher global warming potential than carbon dioxide [13].

The lack of clean alternative energy services in the study areas caused social and economic impacts as well as serious environmental and health problems. The main environmental challenge of the study area was excessive deforestation, which led to the depletion of tree stock, and caused what is known as the household energy crisis in Ethiopia. For the great majority of the population, wood and other biomass fuels are the only sources of energy that have negative environmental, ecological, economic, and health impacts on the lives of the rural poor.

This study was conducted in Loka Abaya district, Sidama Region, Southern Ethiopia. In rural households of Loka Abaya, the inefficient and unsustainable energy production and consumption practices have serious implications for the environment, such as forest resource degradation, land degradation, and tree species diversity loss. In the area, nearly all of the rural households depend on firewood for their cooking requirements, which has led to high deforestation. Furthermore, consumed and produced biomass fuels use smoky and inefficient traditional stoves and kilns. The current study mainly focuses on quantifying the amount of wood removed for fuel in the form of charcoal and firewood as well as assessing their environmental impacts. Specifically, this study is intended to i) estimate the amount of firewood and charcoal produced in the area, ii) analyse the implications of firewood and charcoal production on forest resources, and iii) estimate the number of greenhouse gases emitted during production and consumption.

The study area is the hot spot of firewood and charcoal production mainly for commercial purposes. The environmental consequences of massive wood extraction in the district have not been studied; as a result, there was no meaningful data regarding the amount of wood removed from the area for firewood and charcoal production. Both researchers and development agents have not taken into account the issues of forest resource degradation, biodiversity loss, and emission of pollutants from firewood and charcoal production and consumption. However, the current study mainly (a) focused on generating reliable data that indicate the magnitude of deforestation and forest resource degradation caused by firewood and charcoal production and (b) carried out the estimation of the trace gases emitted during firewood and charcoal combustion.

2. RESEARCH METHODS

2.1. Study area

Loka Abaya District is found in the Sidama region of Southern Ethiopia with a total area of 119,000 ha, at about 325 km south of Addis Ababa. The district is geographically situated between 60 46' N and 380, 04'E. The study area has bimodal rainfall: July to September (heavy rains) and February to April (light rains), the remaining months of the year are fairly dry. The mean annual rainfall and temperature in the area are 1,001-1,400 mm and 17.6-25 °C, respectively [14]. The district is endowed with forest vegetation that is dominated by species such as *Acacia species*, *Erythrina brucei*, *Commiphora africana*, *Albizia gummifera*, *Balanite egyptiaca*, *Ficus species*, *Cordia africana*, *Calpurnia aurea*, *Croton macrostachyus*, and others. Exotic plant species such as *Grevillea robusta*, *Pinus patula*, and *Eucalyptus* and *Cupressus lusitanica* occupy the plantation forest of the district.

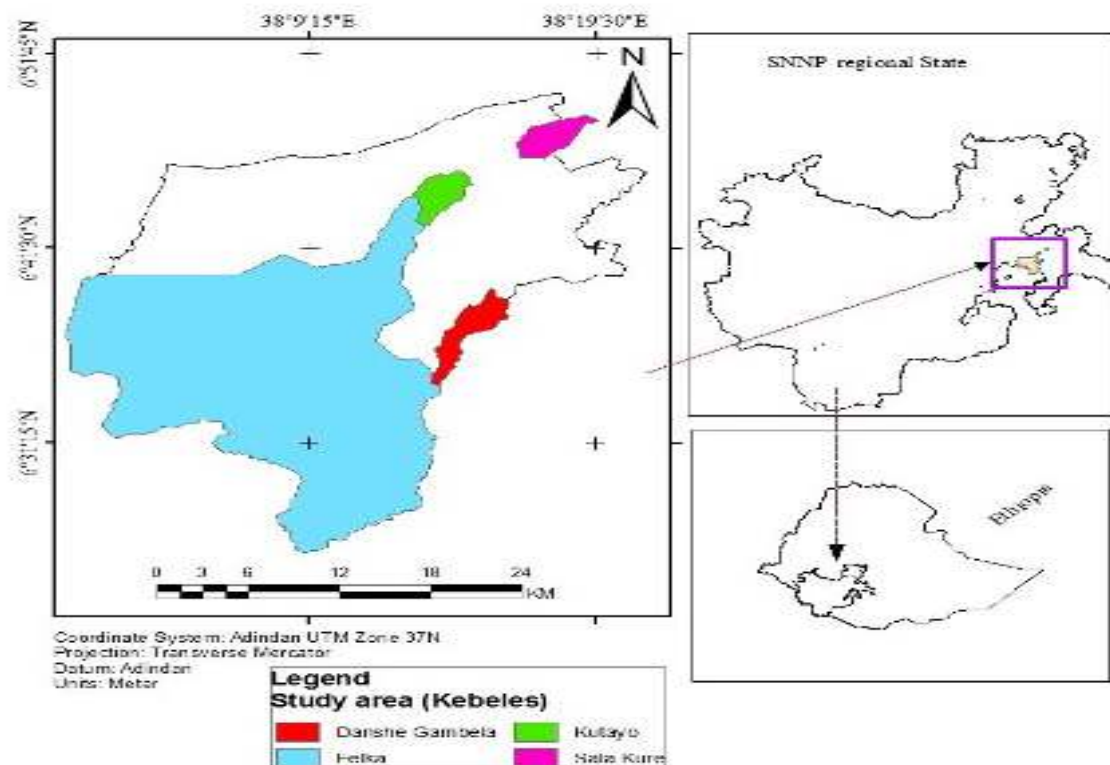


Figure 1. The map of study area

2.2. Data collection and sampling

In sampling, the population of the study multistage sampling was used. The target district was purposively selected based on its potential for charcoal and firewood production. In this study, 5 % of the study populations were randomly sampled for the household surveys. Moreover, the key informants from the energy and agricultural sectors were interviewed to gather general information regarding charcoal and firewood production in the area.

The data of various aspects of charcoal and firewood production were collected through the techniques such as questionnaire surveys, key informant interviews, and literature-based surveys. The questionnaires of different contents were designed and administered to 186 households to gather reliable information from households that use charcoal and firewood at the household level and for sale. Because the amount of wood used to produce these fuels for sale and household level consumption are unquestionably different. Besides, the key informant interview was used to collect qualitative information from government officials, experts, charcoal and firewood sellers, and users.

2.3. Estimation of wood fuel

The estimation of the amount of fuelwood consumed for different household activities such as cooking, heating, and other uses has been undertaken during fieldwork. This was conducted at both the household level and sellers of charcoal and firewood to the nearby towns. The estimation was based on the common weight of a sack of charcoal and a bundle of fuelwood used and sold in the market of the area. The number of households administered in this study was not manageable to carry out the measurements of wood fuels in each household. Thus, a sub-sample of 60 households was selected for wood fuel estimation. Hence, initially, the households were stratified based on family size and wealth categories. Practically, the measurement of charcoal and firewood was carried out by listing the types of meals cooked in the selected households; then, the repetition of each meal cooked per week was recorded and the respondents classified the amount of wood fuel they consume per activity. The data collectors were hired to measure the amount of wood fuel using weight balance. In this work, females are entirely engaged in the

estimation of wood fuel as the household activities are mainly accomplished by them.

3. RESULTS AND DISCUSSION

3.1. Wood estimation for firewood and charcoal production

The Loka Abaya district is a hot spot for charcoal and firewood production in the Sidama zone. The charcoal and firewood produced in the district are transported to the nearby towns such as Boricha, Dilla, Yirgalem, Hawassa, AletaWondo, and Hantate. This aggravates the environmental degradation in the area. Moreover, the use of inefficient charcoal production kilns and illegal cutting of trees for fuel results in excessive deforestation, land degradation, and emission of green house gases to the environment. This study mainly addressed the environmental impacts of biomass energy production, specifically the problems posed during charcoal and firewood production.

The amount of annual firewood and charcoal produced for household consumption and the market sale was assessed and estimated in kilograms per household. Accordingly, the annual average consumption of firewood and charcoal is estimated to be 1126.6 kg and 702.4 kg, respectively. On the other hand, the amount of firewood and charcoal produced in the district is estimated to be 208432.9 kilograms/year and 261039.8 kilograms/year, respectively (See Table 1). The study conducted in Western Ethiopia estimated that the amount of charcoal production was about 4514400 kg of charcoal used annually in the area [15], which is much higher than the current study. Likewise, the annual firewood consumption presented by [16] is 3635.3 kg of firewood used per household in western Ethiopia, which is higher than the current study. Although there is a difference across the districts, the amount of charcoal and firewood consumed at the district level is an indicator of increased national consumption, which is estimated to be 260,000 tons, all of which was produced by traditional kilns needing at least 2.3 million tons of wood [17]. The household survey revealed that the amount of firewood and charcoal produced in Falka kebele was higher than that in the rest of the target villages, whereas there are no charcoal production activities except firewood in Tula Gorbe kebele.

Table 1. Summary of the monthly production of firewood and charcoal across the study kebeles

Kebeles	Fuel types	Mean	Median	Sum	St. deviation	SE
Kutayo	Charcoal	2308.7	2217.2	48483.1	1856.2	405.05
	firewood	864.7	630	34587.4	1176.9	186.09
Falka	Charcoal	12661.2	3433.7	189918.7	24750.4	6390.5
	firewood	1822.8	630	118485.4	3492.6	433.21
Danshe Gambela	Charcoal	3234	3332	22638	668.87	252.8
	Firewood	644.8	630	25149.4	192.15	30.77
Tula Gorbe	Charcoal	-	-	-	-	-
	Firewood	736.8	750	30210.6	162.9	25.44

3.2. Household's woodfuel consumption and production

In the study area, the household energy sources for cooking and heating include firewood, charcoal, agricultural residues,

and animal manure. However, more frequently firewood and agricultural residues are the principal energy sources consumed by the majority of the households. In rare cases, households use animal manure for cooking as it is easily accessible. Charcoal is produced by the households and used as a source of income rather than domestic consumption. As a result, firewood is the dominant household energy source compared to charcoal. The study conducted in the other parts of Ethiopia indicates that almost 100 % of the households subjected to the sampling of their study use firewood as a primary energy source [16].

According to the respondents, firewood is preferred for cooking and heating than other fuels due to its accessibility and affordability. Charcoal is not affordable and needs a lengthy process for production. Nevertheless, the community extensively participates in charcoal production to generate income for their livelihood. This is realized by other studies such that the sale and trading of charcoal and firewood provide an income for the rural communities; particularly, landless and very poor households gather and sell wood for fuel [4].

3.3. Impacts on forest resources

In Ethiopia, wood extraction for domestic firewood or charcoal production constitutes one of the major threats to forests in Ethiopia. The key factors in the increase in fuel

production and consumption are mainly urbanization and population growth; as a result, these fuels are highly demanded by urban household markets and other businesses. In the study area, the production and consumption of charcoal and firewood have enormous consequences on the forest resources since the mode of production and consumption of these fuels still remain traditional. This leads to an important waste of wood resulting in the clearance of a large number of trees, as previous studies revealed that 90 % of forest removal was associated with firewood and the production of 3.2 million tons of charcoal in Ethiopia, leading to the overall deforestation rates of 141,000 hectares per year [17]. Consequently, excessive exploitation of forest resources for firewood and charcoal puts pressure on the ecosystem and is ultimately harmful to the environment and biodiversity.

The traditional earth-mound kilns and traditional earth pit-kiln are the two most dominant types of technologies used for charcoal production in the study area, which are similar with kilns used in other African countries such as Mozambique, Malawi, Tanzania Kenya Zambia, and others [15, 18]. Consequently, the wood-to-charcoal conversion efficiency of these technologies is very low. According to Chudimayo and Gumbo [19], average wood-to-charcoal conversion rates of commonly used kilns in tropical regions range from 0.118 to 0.257. Hence, the efficiency of charcoal production in Loka Abaya district of Southern Ethiopia also lies in the same range

Table 2. the forest areas in the study village and their potential of charcoal and firewood production

No.	Kebeles	Name of forest in the locality	Amount of wood fuel produced in Kg per year in each village	
			Charcoal	Firewood
1	Falka	Erbe, wachano, huluto, lukito, shigasha Loka-Merera, sucha, Adama Woda kao, Tulula, Hadho, Dudda Lafa lixa, Mokona, Gado, Kalala	189918.70	118485.40
2	Danshe Gambela	Bukito, Wochano, Erbe, Bikka, Shombicha Shanashno, Dalacha, Sinto, Sinto Molalogn, Argada, Tulo, Chala, Kute Olano, Qararcho, Gado, Gambela, Ogolo Edola, Hogano	22638.00	25149.45
3	Kutayo	Wachano, Lukkito, Chafa, Aga Darba, Chafa, Gada, Gagagsa Dubbisa, Sache, Mereera Lukume, Solosa, Wayicho, Hates, Ogolo She-gasha	48483.10	34587.40
4	Tula Gorbe	Duda, Adama, Gada Mokona, Hadhosa, Etano Gale, Matigola, Lukkito	--	30210.62

3.4. Estimation of forest needed for charcoal and firewood

In this research, the forest area needed to produce firewood and charcoal was estimated, although the amount of wood used to produce a kilogram of charcoal varies depending on the type of woody species and efficiency of conversion methods used for charcoal making and the amount of wood contained in a hectare of forest used for wood fuel production.

The total forest area (ha) that can be deforested each year due to charcoal production in the district was estimated using the model suggested by Chidumayo and Gumbo [19].

$$\text{Deforestation}_{\text{year}} (\text{ha}) = \frac{\text{Charcoal}_{\text{produced}} (1/0.19)}{\text{Biomass}_{\text{density}}} \quad (1)$$

The wood-to-charcoal conversion efficiency for the traditional earth mound kilns (0.19) was adopted from Chidumayo et al. [19], and the wood biomass stocking rate for woodland was estimated at 40 ton/ha/yr by FAO [20]. Accordingly, the forest areas cleared due to charcoal production are estimated to be 34.35 ha year⁻¹. Besides, the area of forest needed for firewood is also calculated based on the stock density of the area; thus, the area of forest needed for firewood consumed in the area is 5.2 ha year⁻¹. This study showed that in the Loka Abaya district, charcoal and firewood production was totally responsible for the degradation of 39.4 ha year⁻¹ of forest resources each year. The area needed for charcoal production calculated in this research was smaller than the result of the study conducted in Ambo town of Ethiopia, in which 21.2 and 254 hectares of forest were destructed per month and year, respectively [15]. In collective

terms, charcoal and firewood based energy demands were identified as a mechanism of forest cover change in Africa [21].

More specifically, it is important to calculate the amount of forest needed to produce one sack of charcoal [22], which is given by:

$$F_s = M_s * E_k * 1/S \quad (2)$$

where M_s is the mass of a single sack of charcoal in tons, E_k is the kiln efficiency (tons of charcoal per tons of wood), and S is the stock density (tons of wood/ha of forest).

According to the sample weight taken in the charcoal market in the area, the average weight of a sack of charcoal is ranging from 45 to 50 kg; hence, the weight of a single sack used in this calculation is 47.5 kg. The calculated area of forest needed to produce a single sack of charcoal in the district is, therefore, estimated to be 2.3×10^{-6} km² of forest per year. On the other hand, charcoal and firewood produced from a hectare of forest are estimated to be 5.6 m³ ha⁻¹yr⁻¹ and 29.6 m³ ha⁻¹ yr⁻¹, respectively. This is calculated based on the stock density of the forest of the area. According to Moges et al. [23], the mean annual increment of the woodlands of Ethiopia is 0.79 m³ ha⁻¹ yr⁻¹. Hence, the amount of forest removed for charcoal and firewood production is by far greater than the mean annual increment of the forest. This is an indicator that charcoal firewood production is the major driver of deforestation and forest degradation in the district. A study conducted in the Western part of Ethiopia also realized that the rate of deforestation and forest degradation increased due to the heavy demand for forest products, mainly firewood and charcoal [24].

The result of this study indicates that charcoal production and firewood collection are the main drivers of deforestation and forest degradation in the study area. Because the wood for wood fuel production is most of the time obtained by illegal cutting of wood from the nearby forest areas. According to the key informants, there was high commercialization of charcoal, which is the major cause of deforestation and forest resource degradation in the study area. Studies conducted in this area also realized that commercial charcoal production was linked to forest deforestation and degradation [25]. There is a definite link between wood fuel (charcoal and firewood) use and deforestation [26]. Devendra et al. [27] pinpointed this issue as fuelwood from the forest which is a common source of domestic energy supply in rural and urban areas of developing countries. The experience of African countries also showed that wood for charcoal and firewood production derived from the woodlands, although an insignificant amount also came from plantations and trees outside the forests. The potential for woodland to produce charcoal mainly hinges on the ability of the woody species to regenerate and grow [4].

In the areas where the households depend on biomass energy both for their basic energy requirement and livelihood, there will be continued forest degradation from the legal and illegal use of the forest for firewood and charcoal, despite the protection of the forest. This is the reality in most of the African countries; firewood collection and charcoal production are the main components of this forest degradation in most of the African woodlands [19].

3.5. Long term effect of wood fuel production on forest resources

The forest resources of Ethiopia play significant roles in provisions of energy, construction wood, poles, and timber and non-timber forest products (NTFPs) [28]. There is a significant rate of deforestation in Ethiopia. The main drivers are small-scale farmland expansion and unsustainable fuelwood consumption. The reports indicated that 22.7 % of the African land area was covered by forests, estimated to be 674,419,000 ha. Likewise, the Ethiopian land area that was covered by forest was 11.2 %; this is estimated to be 12,296,000 ha [8]. To be specific, 10,105.2 ha of the land area of the study area (Loka Abaya district) was covered by forest resources [29].

The finding of the current study indicates that the total of 39.4 ha of forest is degraded due to charcoal and firewood production and consumption in the study area. This is evidence that a large area of forest was cleared for the primary energy requirement of the rural and urban communities of the developing countries.

3.6. Greenhouse gas emission estimation

In the study area, charcoal is produced more dominantly using traditional earth mound kilns and traditional earth pit kilns. Consequently, the production is carried out in an oxygen-poor environment, leading to the emission of greenhouse gases such as Carbon dioxide (CO₂), Carbon Monoxide (CO), Nitrous Oxide (N₂O), and Methane (CH₄) and Non-Methane Hydrocarbon (NMHC). In this study, the amount of greenhouse gases emitted from charcoal and firewood production and consumption is calculated based on certain baseline emission factors indicated by the previous studies (Table 3).

The amounts of estimated charcoal and firewood were obtained through the household survey. Accordingly, the estimation for firewood and charcoal is 208432.9 kg yr⁻¹ and 261039.8 kg yr⁻¹, respectively. Based on the previously estimated emission factors, the amount of pollutants emitted during charcoal and firewood production and consumption is calculated and presented in Table 4. The presented emission factors of the pollutants are displayed in range; however, the average values of maximum and minimum figures were used in the current study.

Table 3. Emission factors of the greenhouse gases as stated in several studies

Types of fuel	Emission factors					References
	CO ₂	CO	N ₂ O	CH ₄	NMHC	
Fuel wood burning	450	43	0.52	1.5	0.125	[5, 21]
Charcoal Burning	170	25	0.29	0.5	-	[6, 2]
Charcoal Production	500	550	0.22	700	355	[2, 7]

Table 4. the estimate of the amount of pollutants emitted during charcoal and firewood production and combustion

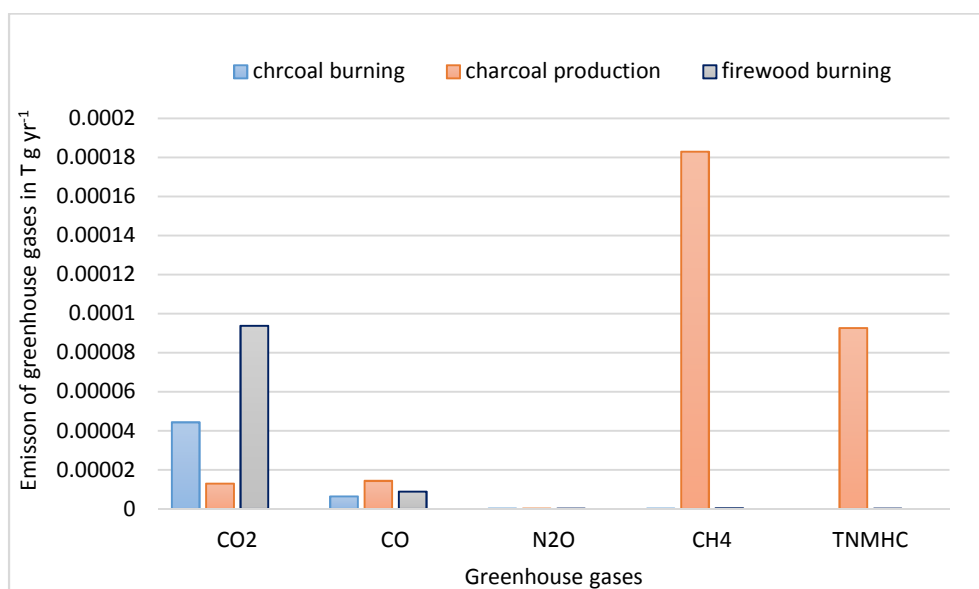
Trace gases	Charcoal		Emission during firewood combustion in(T g year ⁻¹)**
	Emission during production in (T g year ⁻¹)**	Emission during combustion in (T g year ⁻¹)**	
Carbon dioxide (CO ₂)	1.3×10^{-5}	4.44×10^{-5}	1.3×10^{-4}
Carbon monoxide (CO)	8.96×10^{-6}	6.5×10^{-6}	1.44×10^{-4}
Nitrous oxide (N ₂ O)	1.084×10^{-7}	7.57×10^{-8}	5.74×10^{-8}
Methane (CH ₄)	3.13×10^{-17}	1.3×10^{-7}	1.83×10^{-4}
Total non-methane hydrocarbon (TNMHC)*	2.6×10^{-8}	---	9.27×10^{-5}

* Total non-methane hydrocarbons (TNMHC) are defined as organic compounds excluding methane (CH₄) that contain only C and H; examples include alkanes, alkenes, alkynes, aromatics, and terpenes.
 ** (T g year⁻¹): Tera gram of greenhouse gases per year.

In this study, we have drawn a conclusion that the emission of trace gases produced during charcoal making is higher than that of charcoal burning. Other studies also agree with this result; for example, Kammen and Lew [30] presented that the emission during charcoal production had a greater global warming contribution than emissions from charcoal combustion.

Domestic biomass burning for energy generation constitutes a continuous input of trace compounds into the atmosphere, unlike vegetation fires that represent a seasonal phenomenon

[31]. In this study, the amount of greenhouse gases generated during firewood burning exceeds the one generated during charcoal burning (see Figure 2). The study conducted in Zambia by Bertschi et al. [32] is in accordance with the result of the current study; they indicated that fuelwood was used more than charcoal with wood combustion producing 9.8 T g C yr⁻¹ as CO₂ and charcoal producing 3.3 T g C yr⁻¹. NO_x was emitted in the lowest quantities from both wood and charcoal.

**Figure 2.** Emission of GHGs during domestic fuel combustion

According to Akagi et al. [33], biomass burning is the second largest source of greenhouse gases and the largest source of primary fine carbonaceous particles in the global troposphere. The emission of trace gases from biomass combustion is one of the important factors for global climate change in developing countries. Firewood and charcoal, animal dung, and agricultural residues account for more than 30 % of the global sources of atmospheric NO_x and NMHC, about 40 % of CO emissions, and about 15 % of CH₄ emission [35]. This indicates that the emissions associated with charcoal and firewood production and burning represent a key component of large CO₂ emissions and emission uncertainties on a global scale [34].

3.7. Impact of wood fuel production and consumption on habitat, economy, and society

Forests and woodlands provide not only wood, livestock feed, other non-timber products, and environmental goods and services but also serve as a habitat of biodiversity including endemic birds and wild animals. Forests provide fuelwood that is serving as the major source of energy for rural areas, enhancing the role of the forestry sector in Ethiopia for rural and urban households. The national fuelwood demand was estimated as 20 % higher than the combined demand of all other forest products, which was assessed at 109 million m³yr⁻¹ [36].

The high degree of dependence on wood fuels and agricultural residues for fuel has an impact on the social, economic, and environmental well-being of society. Demand for wood fuels contributes significantly to forest losses and demand for agricultural residues as fuel reduces what is available as livestock feed and what can be left for soil

fertility. This could have a direct impact on the economy and the livelihood of the society despite the loss of productivity of land and deficiency of fodder for livestock production. The district is rich in tree and shrub species such as *Comberetum spp.*, *Acacia drepanolobium*, *A. mellifera*, *A. seyal*, *A. tortilies*, *A. senegal*, *A. albida*, *A. nilotica*, *A. olifera*, *A. nubica*, *Aloe vera*, *Euophorbia tirucalli*, *Ricinus communes*, *Caparis tomoentosa*, *Balanites aegyptica* and *Balanites routindifolia Ficus sur*, *Ficus vasta*, *Petrolatum stelatum*, *Trechlea sp.*, *Zizihpusspina-christi*, and *Tamarindus indica*.

The Loka Abaya National Park is found in the study area and the district is home to wildlife such as Lesser Kudu (*Tragelaghus imberbis*), Defassa Waterbuck (*Kobus defassa*), Common Bushbuck (*Tragelaghus scriptus*), Lion (*Panthera leo*), Leopard (*Pantera pardus*), and African wild dog (*Lycaon pictus*) [37]. The finding of the current study indicated that the total of 39.5 ha of forest was cleared every year for wood fuel production and consumption in the area. The uncontrolled firewood collection and logging for charcoal production resulted in the migration of wildlife from the area to other places for survival as their habitat was continuously disturbed for firewood and charcoal purposes. Undeniably, these have a direct implication on the economy of the society and the country at large.

3.8. Alternative and sustainable options

In Ethiopia, biomass energy is not sustainably produced and used in general, and it thus is not yet carbon neutral. There is a huge loss of biomass energy during production, transportation, and utilization. Mostly women and girls are involved in the process and are considerably impacted by it. Based on the realities explored in the current study, the authors suggested sustainable options for biomass energy utilization and production for rural and urban households' energy requirements. Accordingly, the key stakeholders in charge of household energy developments raise public awareness of the costs of existing energy losses and associated energy efficiency and conservation benefits and practices. Additionally, it is crucial to enhance the transfer and adoption of efficient and cleaner energy technologies that are appropriate for the socio-economic needs of the society. Lastly, the clean and renewable energy technologies should be based on the local condition and available resources in the study area. The viable alternative clean energy source could be solar energy. Biogas and fuel-saving cookstoves are used to reduce the rate of clearance of forest resources for firewood and charcoal.

3.9. Policy perspectives

The Ethiopian energy policy enacted in 2012 was a set of objectives to promote improved bio-energy conversion technologies including agro-industrial waste for thermal and power applications and biogas from urban, livestock, and poultry waste. These directions were focused on building local capacity in production and generation techniques. The policy also enacted and enforced appropriate charcoal and firewood regulations and recommended a strategy to reduce the rate of deforestation and promote clean energy technology in place. The establishment and enforcement of standard and quality control of different energy technologies was stated in the energy policy of the country [38]. However, the issues depicted in the energy direction were not properly executed.

In the current study context, the promotion of clean energy development from locally available feedstock is deemed to be important. Besides, awareness creation and dissemination of fuel-efficient cookstoves through specifying their standard and quality should be implemented and clearly supported by policy and strategy.

4. CONCLUSIONS

As in many African countries, the majority of rural and urban households in Ethiopia depend on charcoal and firewood for their daily energy needs. The expansion of urban areas and population growth have increased the demand for these fuels in the country. In addition to household consumption, the rural households produce charcoal and firewood as means of livelihood; particularly, landless and poor households entirely rely on this business. In the study area, the estimation for firewood and charcoal is 208432.9 kg yr⁻¹ and 261039.8 kg yr⁻¹, respectively. Charcoal and firewood production has far-reaching impacts extending across a range of social and environmental and economic aspects of human life. These include health problems resulting from pollutant gases that specifically affect charcoal producers, women and children; environmental impacts are greenhouse gas emissions and depletion of forest resources.

In the Loka Abaya district, the firewood collection and charcoal production were becoming attractive businesses and the farmers are shifting their livelihood from agricultural activities to firewood and charcoal businesses. The finding of the current study indicated that the total of 39.4 ha of forest was degraded due to charcoal and firewood production and consumption in the study area. This implies deforestation is overwhelmingly high in the area as a result of the traditional and inefficient mode of production and consumption of fuels. Consequently, the estimated amount of wood needed for charcoal and firewood production has a major contribution to the deforestation, loss of important native species, and emission of greenhouse gases. Therefore, immediate intervention is needed to retard the rate of vegetation clearance, loss of tree species diversity, and greenhouse gas emissions. Depending on the results of this research, options to produce environmentally viable household energy sources should be deemed important. In order to tackle the problem, priority should be given to adopting improved charcoal production technologies and efficient utilities, developing alternative energy sources (biogas, solar), enhancing wood lots plantation, and promoting incentives that encourage investments in sustainable forest management recommended on the basis of the present study.

5. ACKNOWLEDGEMENT

This research was funded by Hawassa University, Wondo Genet College of Forestry and Natural Resources. Special thanks to the Research and Technology Transfer of the Office of Wondo Genet College of Forestry and Natural Resources for the encouragement and facilitation of our fieldwork. Finally, our acknowledgement goes to the Loka Abaya District Irrigation and Energy office experts for their assistance during data collection.

NOMENCLATURE

CH ₄	Methane
CO	Carbon monoxide

CO ₂	Carbon dioxide	PM	Particulate Matter
FAO	Food and Agriculture Organization	SO _x	Sulphur oxides
ha	Hactare	SSA	Sub Saharan Africa
Kg	Kilogram	T g year ⁻¹	Tera gram of greenhouse gases per year
km ²	Kilometer square	TNMHC	Total non-methane hydrocarbon
N ₂ O	Nitrous oxide	VOCs	Volatile organic compounds
NTFPs	Non-timber forest products		

APPENDIX

Questionnaire survey

Name of Enumerator: _____ Date: _____ Signature: _____
 Location: X _____ Y _____

I: The socio economic characteristics of the respondents

- Kebele: _____
- Sex of respondent (household head) (1=Female, 2= Male): _____
- Age of respondent: _____
- Marital status (1=single, 2=married, 3=divorced, 4=widowed, 5=widower): _____
- Education level (1=Illiterate, 2=Able to read and write, 3=Lower primary (1-4), 4=Upper primary (5-8), 5=High school (9-10), 6=Preparatory(11-12), 7=Diploma, 8=Degree and above): _____
- Family size of the household: _____
- Average landholding size of the household (in ha): _____
- Annual Income sources of the households:

No.	Livelihood activity	Annual estimated yield	Estimated annual revenue in ETB
1	Annual mono crop production		
2	Agroforestry		
3	Monoculture perennial crop production		
4	Wood lot		

- Do you have access to credit services (1=No, 2=Yes): _____ please list credit institutions in your locality and the type of service you are able to access: _____

10. Is there any social safety net programs in your locality? (1=No, 2=Yes): _____ if your answer is yes please indicate the amount of cash income you received in the last two years 2008-2010 E.C if any _____

- Do any of your household member had involved on any non-farm activities? (1=No, 2=Yes) _____ If your answer is "yes" please complete the table below:

No.	Non-farm activity	Number of household members involved	Annual estimated earned income
1	Beekeeping		
2	Poultry		
3	Charcoal production and marketing		
4	Firewood collection and marketing		
5	Carpentry		
6	Labor market participation		
7	Pity trade		
8	If other please specify?		

II. Production and consumption of woodfuels

- Which type of fuel is dominantly used in your household? Please give a rank from 1 to 4

No.	Sources	Rank	Remark
1	Firewood		
2	Charcoal		
3	Crop residues		
4	Animal dung		

- If your household use both firewood and charcoal, please complete the table below:

No.	List of activities	Firewood		Charcoal	
		Bundle (kg) of firewood consumed per activity	Frequency of activities/week	Kg of charcoal consumed per activity	Frequency of activities/week
1	'Injera' baking				
2	Bread baking				
3	Coffee preparation				
4	'Wot' making				
5	Room heating				
6	If other please specify				

14. What are the methods commonly you use to produce charcoal?

(1=Earth mound kiln, 2=Earth pit kiln, 3= Cassamance kiln, 4=Metal kiln, 5=if other please specify) (Multiple answer is possible)

Other: _____

III. The species and sources of wood for charcoal and firewood production

15. What are the names of forest areas found around your locality?

- a) _____
 b) _____
 c) _____
 d) _____

16. Are there areas of forest that degraded due to charcoal and firewood production? a) Yes b) No

17. What class of vegetation used for charcoal production? a) Bushes b) Shrubs c) Trees

18. What class of vegetations used for firewood production? a) Herbs b) Bushes c) Shrubs d) Trees

19. What are the most preferred trees you commonly used to produce charcoal?

- a) _____ e) _____
 b) _____ f) _____
 c) _____ g) _____
 d) _____ h) _____

Criteria of preference:

20. What are the most preferred trees you commonly used to produce firewood?

- a) _____ e) _____
 b) _____ f) _____
 c) _____ g) _____
 d) _____ h) _____

Criteria of preference:

21. Where do you access these trees for charcoal production?

a) Private wood lots b) Communal forest c) State forest d) Clan forest f) All g) Specify if there is another sources

22. Where do you access these trees for firewood?

a) Private wood lots b) Communal forest c) State forest d) Clan forest f) All g) Specify if there is another sources

REFERENCES

- FAOSTAT, Food and Agriculture Organization of the United Nations, Statistics Division, Economic and Social Development Department, Rome, Italy, (2016). (<https://www.fao.org/faostat/en/#home>), (Accessed on 31 December 2016).
- FAO, "Criteria and indicators for sustainable woodfuels: Case studies from Brazil, Guyana, Nepal, Philippines and Tanzania", Rome, Italy, (2009). (<https://www.fao.org/3/i1321e/i1321e01.pdf>).
- Seyoum, Y., Birhane, E., Hagazi, N., Esmael, N., Mengistu, T. and Kassa, H., "Enhancing the role of forestry in building climate resilient green economy in Ethiopia", Center for International Forestry Research Ethiopia Office, Ministry of Environment, Forest and Climate Change, The Federal Democratic Republic of Ethiopia, Addis Ababa, Ethiopia, (2015). (https://www.cifor.org/publications/pdf_files/Books/BKassa1503.pdf).
- Msuya, N., Masanya, E. and Temu, A.K., "Environmental burden of charcoal production and use in Dar es Salaam, Tanzania", *Journal of Environmental Protection*, Vol. 2, No. 10, (2011). (<https://doi.org/10.4236/jep.2011.210158>).
- Geissler, S., Hagauer, D., Horst, A., Krause, M. and Sutcliffe, P., "Biomass energy strategy for Ethiopia", AMBERO Consulting Gesellschaft mbH, (2013), 61476. (<https://ambero.de/projekte-slug/biomass-energy-strategy-for-ethiopia/>).

6. Sitoe, A., Remane, I., Ribeiro, R., Falcão, M.P., Mate, R., Nhamirre, J., Walker, S., Murray, L. and Joana Melo, J., "Identificação e análise dos agentes e causas directas e indirectas de desmatamento e degradação florestal em Moçambique", (2016). (<https://www.fnds.gov.mz/index.php/pt/documentos/relatorios/identificacao-e-analise-dos-agentes-e-causas-directas-e-indirectas-de-desmatamento-e-degradacao-florestal-em-mocambique>).
7. Akagi, S.K., Yokelson, R.J., Wiedinmyer, C., Alvarado, M.J., Reid, J.S., Karl, T., Crouse, J.D. and Wennberg, P.O., "Emission factors for open and domestic biomass burning for use in atmospheric models", *Atmospheric Chemistry and Physics*, Vol. 11, No. 9, (2011), 4039-4072. (<https://doi.org/10.5194/acp-11-4039-2011>).
8. Nike, D. and Meshack, C., "The marginalization of sustainable charcoal production in the policies of a modernizing African nation", *Frontiers in Environmental Science*, Vol. 5, (2017), 27. (<https://doi.org/10.3389/fenvs.2017.00027>).
9. FAO Forestry Paper, "Global Forest Resource Assessment, Progress towards sustainable forest management", 147, (2005). (<http://www.env-edu.gr/Documents/Global%20Forest%20Resources%20Assessment%202005.pdf>).
10. Malimbwi, R.E. and Zahabu, E.M., "The analysis of sustainable charcoal production systems in Tanzania", Criteria and indicators for sustainable woodfuels: Case studies from Brazil, Guyana, Nepal, Philippines and Tanzania, FAO, Rome, (2008), 229-258.
11. Ludwig, J., Marufu, L.T., Huber, B., Andrae, M.O. and Helas, G., "Domestic combustion of biomass fuels in developing countries: A major source of atmospheric pollutants", *Journal of Atmospheric Chemistry*, Vol. 44, No. 1, (2003), 23-37. (<https://doi.org/10.1023/A:1022159910667>).
12. Demeke, A., Sintayehu, T., Ermias, K. and Girma, M., "Diversity and relative abundance of birds in Loka Abaya National Park, Sidama Zone, Southern Ethiopia", *International Journal of Biodiversity and Conservation*, Vol. 11, No. 8, (2019), 230-240. (<https://doi.org/10.5897/IJBC2019.1306>).
13. Global Forest Resource Assessment, "Main report", *Food and Agriculture Organization of the United Nations*, Rome, (2010).
14. Abaynesh, K., Chimdi A. and Akhila S.N., "Effect of firewood energy consumption of households on deforestation in Debis watershed, Ambo District, Oromia Regional State, Ethiopia", *World Applied Sciences Journal*, Vol. 33, No. 7, (2015), 1154-1163. (<https://doi.org/10.4314/star.v4i1.26>).
15. Fekadu, G., "Floristic composition and structural analysis of Komto Afromontane Rainforest, East Wollega Zone of Oromia Region, West Ethiopia", Ph. D. Thesis, Addis Ababa University, (2010). (<http://thesisbank.jhia.ac.ke/6804/>).
16. Esayas, A. and Woldegiorgis, M., "The impacts of charcoal and firewood production and consumption on natural forests surrounding Ambo Town, ISSN, Vol. 6, (2017), 1-20.
17. Kammen, D.M. and Lew, D.J., "Review of Technologies for the production and Use of charcoal", *Renewable and Appropriate Energy Laboratory Report*, Vol. 1, (2005). (https://www.researchgate.net/profile/Debra-Lew/publication/237577160_Review_of_Technologies_for_the_Production_and_Use_of_Charcoal/links/00463528265a28ccda00000/Review-of-Technologies-for-the-Production-and-Use-of-Charcoal.pdf).
18. Abebe, D., Koch, S.F. and Mekonnen, A., "Coping with fuelwood scarcity: Household responses in rural Ethiopia", *Environment for Development Initiative*, (2012). (https://www.researchgate.net/profile/Steve-Koch/publication/254446194_Coping_with_Fuel_Wood_Scarcity_Household_Responses_in_Rural_Ethiopia/links/55a6173008aef604aa047498/Coping-with-Fuel-Wood-Scarcity-Household-Responses-in-Rural-Ethiopia.pdf).
19. Devendra, L.P., Kiran Kumar, M. and Pandey, A., "Evaluation of hydrotropic pretreatment on lignocellulosic biomass", *Bioresource Technology*, Vol. 213, (2016), 350-358. (<https://doi.org/10.1016/j.biortech.2016.03.059>).
20. Dewees, P.A., "The woodfuel crisis reconsidered: Observations on the dynamics of abundance and scarcity", *World Development*, Vol. 17, No. 8, (1989), 1159-1172. (https://www.researchgate.net/profile/Peter-Dewees/publication/222238813_The_woodfuel_crisis_reconsidered_Observations_on_the_dynamics_of_abundance_and_scarcity/links/5a2956454585155dd428feb1/The-woodfuel-crisis-reconsidered-Observations-on-the-dynamics-of-abundance-and-scarcity.pdf).
21. Ciaia, P., Bombelli, A., Williams, M., Piao, S.L., Chave, J., Ryan, C.M., Henry, M., Brender, P. and Valentini, R., "The carbon balance of Africa: Synthesis of recent research studies", *Philosophical Transactions of the Royal Society A: Mathematical, Physical and Engineering Sciences*, Vol. 369, No. 1943, (2011), 2038-2057. (<https://doi.org/10.1098/rsta.2010.0328>).
22. Falcão, M.P., "Charcoal production and use in Mozambique, Malawi, Tanzania, and Zambia: Historical overview, present situation and outlook", *Proceedings of The Conference on Charcoal and Communities in Africa*, International Bamboo and Rattan Organization (INBAR), (2008). (https://www.inbar.int/resources/inbar_publications/charcoal-and-communities-in-africa/).
23. Feyisa, B.N., Feyssa, D.H. and Jiru, D.B., "Fuel wood utilization impacts on forest resources of Gechi District, South Western Ethiopia", *Journal of Ecology and the Natural Environment*, Vol. 9, No. 8, (2017), 140-150. (<https://doi.org/10.5897/JENE2017.0642>).
24. MoWIE, "Ethiopian National Energy Policy (2nd Draft)", Federal Democratic Republic of Ethiopia, Ministry of Water, Irrigation and Energy (MoWIE), Addis Ababa, (2012). (<https://www.devex.com/organizations/ministry-of-water-irrigation-and-energy-mowie-ethiopia-124251>).
25. SZBCT (Sidama Zone Bureau of Culture and Tourism), "A report on the boundary demarcation and biological survey of the proposed Loka Abaya National Park in the Sidama Zone, Sidama, Hawassa", Unpublished Report, (2009), 24.
26. MoWIE, "Environmental impact assessment report for Gidabo irrigation project", Federal Democratic Republic of Ethiopia, Ministry of Water, Irrigation and Energy (MoWIE), Addis Ababa, (2019).
27. Bertschi, I.T., Yokelson, R.J., Ward, D.E., Christian, T.J. and Hao, W.M., "Trace gas emissions from the production and use of domestic biofuels in Zambia measured by open-path Fourier Transform Infrared Spectroscopy", *Journal of Geophysical Research: Atmospheres*, Vol. 108, No. D13, (2003), 8469. (<https://doi.org/10.1029/2002JD002158>).
28. Lindsay, J.A., "African savanna fires, global atmospheric chemistry and the southern tropical Atlantic regional experiment", *Fire in the Southern African Savanna: Ecological and Environmental Perspectives*, Witwatersrand University Press, (1997), 1-15.
29. Jargstorf, B., "Introduction to renewable energy/rural energy: Technology overview and the Ethiopian situation", *Proceedings of Symposium on Renewable Energies in Ethiopia (Mobile Exhibition)*, Addis Abeba, Ethiopia, German Technical Cooperation, (2004). (<https://agris.fao.org/agris-search/search.do?recordID=ET2006000014>).
30. United Nations (UN), "World population prospects: The 2015 revision, key findings and advance tables", United Nations (UN), Department of Economic and Social Affairs, Population Division, Working Paper No. ESA/P/WP.241, (2015). (https://esa.un.org/unpd/wpp/publications/files/key_findings_wpp_2015.pdf).
31. Moges, Y., Eshetu, Z. and Nune, S., "Ethiopian forest resources: Current status and future management options in view of access to carbon finances", Final Report, Federal Democratic Republic of Ethiopia, Ministry of Water, Irrigation and Energy (MoWIE), Addis Ababa, (2010). (<https://www.un-redd.org/sites/default/files/2021-10/ETHIOPIAN%20FOREST%20RESOURCES-%20%20CURRENT%20STATUS%20AND%20FUTURE%20MANAGEMENT%20OPTIONS%20%20IN%20VIEW%20OF%20ACCESS%20TO%20CARBON%20FINANCES%20.pdf>).
32. Intergovernmental Panel on Climate Change (IPCC), "Mitigation of climate change-Summary for policymakers", Working Group III: Contributions to the Intergovernmental Panel on Climate Change, Bangkok, Thailand, (2018). (https://www.ipcc.ch/site/assets/uploads/2018/03/ar4_wg3_full_report-1.pdf).
33. Modi, V., McDade, S., Lallement, D. and Saghir, J., "Energy services for the millennium development goals", (2005). (<https://qsel.columbia.edu/assets/uploads/blog/2016/publications/energy-services-for-the-millennium-development-goals.pdf>).
34. Hansen, M.C., Potapov, P.V., Moore, R., Hancher, M., Turubanova, S.A., Tyukavina, A., Thau, D., Stehman, S.V., Goetz, S.J., Loveland, T.R. and Kommareddy, A., "High-resolution global maps of 21st century forest cover change", *Science*, Vol. 342, No. 6160, (2013), 850-853. (<https://doi.org/10.1126/science.1244693>).

35. Trefon, T., Hendriks, T., Kabuyaya, N. and Ngoy, B., "L'économie politique de la filière du charbon de bois à Kinshasa et à Lubumbashi", (2010). (<https://irias.kuleuven.be/retrieve/173858>).
36. Lemenih, M., Bongers, F., Wiersum, K.F. and Art, B., "What the future holds for forestry development in Ethiopia? Foresight through scenarios construction", *Ethiopia*, (2011), 101.
37. D'Agostino, A.L., Urpelainen, J. and Xu, A., "Socio-economic determinants of charcoal expenditures in Tanzania: Evidence from panel data", *Energy Economics*, Vol. 49, (2015), 472-481. (<https://doi.org/10.1016/j.eneco.2015.03.007>).
38. Chidumayo, E.N. and Gumbo, D.J., "The environmental impacts of charcoal production in tropical ecosystems of the world: A synthesis", *Energy for Sustainable Development*, Vol. 17, No. 2, (2013), 86-94. (<https://doi.org/10.1016/j.esd.2012.07.004>).



Research Article

Impact of Organic Hydrocarbons on Fuel Properties and Engine Characteristics of Thermally Cracked Cashew Nut Shell Liquid

Gokul Raghavendra Srinivasan*, Aditya Mahajan, Rajiv Seth, Rakesh Mahajan

Research and Development Department, Steamax Envirocare India Private Limited, Janak Puri, Delhi-110058, India.

PAPER INFO

Paper History:

Received: 26 March 2022

Revised: 06 July 2022

Accepted: 07 July 2022

Keywords:

Cashew Nut Wastes,
Thermal Cracking,
Screw Press Extraction,
Anacardic Acid,
Cresol

ABSTRACT

The present study aims to explore the role of characterized hydrocarbons in thermally cracked shell liquid in determining its overall fuel properties and combustion characteristics in a CI engine. For this purpose, waste shell liquid was extracted from waste cashew nut shell by means of cold extraction technique using a simple electrically operated mechanical screw press, which reported maximum extractable oil content as 17.7 %. In addition, it was thermally cracked at 350–400 °C using conventional heating for both lab-scale and pilot-scale extraction. Based on its chemical composition, raw shell liquid contained anacardic acid and cardol, while thermally cracked shell liquid had cresol and methyl oleate as their dominant hydrocarbon compounds. Their composition was found to be 51.84 %, 33.68 %, 43.87 %, and 28.49 %, respectively. According to their contribution, both cyclic and aromatic as well as linear-chained hydrocarbons exhibited significant effect on the fuel properties of the cracked shell liquid, with carbon atoms contributing to its physical and thermal properties, whereas cyclic and aromatic hydrocarbons enhance its flow characteristics. Next, neat and blend samples of this cracked shell liquid with petro diesel reported higher peak in-cylinder pressure by 5.6 % (on average) due to the presence of fatty acid esters, which induced early ignition and provided sufficient time for combustion. Meanwhile, higher emission levels were attributed by both cyclic and aromatic and linear-chained hydrocarbons, citing aromaticity and unsaturation in their molecules, which also resulted in reduced thermal efficiencies by 12.5 % (on average), upon accounting for their inferior calorific content. In conclusion, it is evident that hydrocarbons in these treated shell liquids play a significant role in their fuel properties and engine characteristics.

<https://doi.org/10.30501/jree.2022.335041.1349>

1. INTRODUCTION

Rise in environmental concerns and energy demand has increased the necessity to rely on renewable energy resources even for large-scale and industrial applications. These industrial applications include even food and food processing, which uses a large volume of biomass and helps reduce serious pollution threats and climate change issues [1]. One such biofuel is Cashew Nut Shell Liquid (CNSL) that enjoys a good potential in serving as an effective alternative fuel for supplying necessary energy [2].

To begin with, CNSL is a pericarp fluid of cashew nut, present inside the soft honey comb structure of its shell. Usually, it appears as a reddish brown liquid with high viscosity and is regarded as a cheap, yet effective, source for unsaturated phenols [3]. Although the thickness of these honey comb structures is about 1/8th of an inch, the availability/concentration of this CNSL-based oil content ranges between 30–35 wt % and varies from the nature of plant growth, cultivation technique, and geography [4].

Besides, this CNSL comprises 4 most dominant chemical compounds, namely anacardic acid, cardanol, cardol, and 2-methyl cardol and their distribution in the CNSL is entirely based on the extraction technique used for extracting this liquid from the shell [5]. By acknowledging this, variation of the distribution of these chemical compounds in the raw CNSL extracted by different rendering techniques is summarized in Table 1 and for different operating parameters in Table 2 [3, 6, 7]. In fact, numerous researchers reported the chemical composition and physicochemical properties of these CNSLs in addition to their extraction techniques in the past studies and considered them as the most predominantly found chemical compounds.

Drawing on the above findings, Kyei and Onyewuchi Akaranta (2019) studied the extraction technique and physicochemical properties of CNSL extracted from CNS upon synthesizing resin from these CNS-based liquids. Here, accelerated solvent extraction was identified as the most efficient technique and an average yield of 31 % of CNSL was reported. In terms of fuel properties, CNSL exhibited very high density ($> 950 \text{ kg/m}^3$) and acidity with slightly increased FFA content and very high saponification value (255.26 mg

*Corresponding Author's Email: gokusrinivasan@gmail.com (G.R. Srinivasan)
URL: https://www.jree.ir/article_155097.html

Please cite this article as: Srinivasan, G.R., Mahajan, A., Seth, R. and Mahajan, R., "Impact of organic hydrocarbons on fuel properties and engine characteristics of thermally cracked cashew nut shell liquid", *Journal of Renewable Energy and Environment (JREE)*, Vol. 10, No. 2, (2023), 81-94. (<https://doi.org/10.30501/jree.2022.335041.1349>).



KOH/g). Moreover, spectral analysis of extracted CNSL revealed its chemical nature as polymeric with a higher concentration of phenolic compounds [8].

Looking into the extraction techniques, Rodrigues et al. (2011) studied the effectiveness of different extraction methods in extracting CNSL and investigated their significance. Next, CNSLs extracted by roasting the waste cashew nut shells at slightly higher temperatures (180 and 200 °C) were considered as technical CNSL (T-CNSL) and were compared with the CNSL extracted at room temperature using screw press (CNSL-NP) and hexane-based solvent extraction

(CNSL-NS). Based on the characterization of chemical compounds, both CNSL-NP and -NS were reported to have a higher concentration of Anacardic acid and cardol and a lower concentration of cardanol than T-CNSL; however, natural extraction techniques were discriminated in terms of cardanol concentration variation. Besides, these naturally extracted liquids exhibited poor performance as a result of increased viscosity and impurity content and lower thermo-oxidative stabilities and ebullition temperature. Yet, CNSL extracted using cold solvent extraction retained their actual fuel properties as compared to other methods [9].

Table 1. Chemical composition (in %) of raw CNSLs extracted by various rendering techniques [3, 6]

Constituents	Pyrolysis	Decarboxylation	Soxhlet's extraction		SCW extraction	SC-CO ₂ extraction	Two-step extraction	
			Hexane	Methanol			Hexane-SCW	Methanol-SCW
Cardanol								
Saturated Cardanol			1.22	1.45	2.4	1.52	1.04	1.84
Monounsaturated Cardanol	54	65	26.64	27.19	68.93	1.09	48.84	49.22
Anacardic Acid								
Monounsaturated Anacardic Acid	5	2	27.9	19.06	9.47	52.24	18.64	11.4
Cardol								
Saturated Cardol	27	31	20.31	34.88	1.85	29.58	9.76	12.64
Monounsaturated Cardol	–	–	1.05	–	–	–	0.57	–
Di-unsaturated Cardol	–	–	7.62	10.39	–	6.72	4.13	6.07
Known Hydrocarbons								
Octacosene	–	–	–	–	4.91	–	2.25	2.04
Stigmasterol	–	–	–	–	3.44	–	1.57	1.43
Triacotene	–	–	3.33	3.41	–	4.31	1.85	5.45
β-Sitosterol	–	–	1.38	1.86	1.63	1.63	0.75	1.76
Unknown Hydrocarbons								
Hydrocarbon 1	–	–	5.7	–	–	–	–	3.33
Hydrocarbon 2	–	–	–	–	3.42	–	1.57	1.42
Hydrocarbon 3	–	–	–	–	3.29	–	1.51	1.37
Others	14	2	4.85	1.76	0.66	2.91	7.52	2.03

* SC: Supercritical; SCW: Supercritical Water; SC CO₂: Supercritical Carbondioxide

Table 2. Variation in chemical composition of CNSL with varying rendering techniques and operating parameters [3, 7]

Operating parameter (P bar/T °C)	SC-CNSL from CNS		SC-CNSL from CNS obtained through heat exchanger unit		SC-CNSL from Pyrolysis CNSL	
	Compound	Comp. %	Compound	Comp. %	Compound	Comp. %
200/60	Cardanol-C15	84.2	Cardanol	62.31	Cardanol diene	48.61
	Methyl Cardanol	2.83	Cardanol diene	31.24	2-methyl benzaldehyde	20.51
	Hexadecanoic acid	0.71	Heptadecane	0.77	3-ethyl phenol	7.64
	Cardanol-C13	0.69	8-methyl heptadecane	0.7	3-butyl phenol	1.39
	Oleic acid	0.62	Hexadecane	0.67		
			Pentadecane	0.67		
225/60	Cardanol-C15	86.26	2,6,10,14 tetra methyl pentadecane	0.65	Cardanol diene	66.82
	Methyl Cardanol	3.11	Hexadecanoic acid	0.61	Ethoxybenzene	11.21
	Oleic acid	0.684	Elicosane	0.47	Acenaphthylene	7.12
	Cardanol-C13	0.65			3-ethyl phenol	3.31
	Hexadecanoic acid	0.56			3-butyl phenol	2.28
					Azulene	1.89

250/60	Cardanol-C15	64.89	Cardanol	81.54	Cardanol	64.91
	Diethyl Phthalate	12.34	2-methyl Cardanol diene	2.97	Propyl benzene	11.96
	Cardanol-C13	7.42	Tetradecanal	1.99	4-ethyl phenol	5.01
	Methyl Cardanol	3.03	Cardanol-C13	1.62	3-pentyl phenol	3.18
	Hexadecanoic acid	0.58	Hexadecanoic acid	1.27	Acenaphthylene	2.83
			Heptadecane	0.08	3-butyl phenol	1.35
		Pentadecane	0.04			
300/60	Cardanol-C15	61.34	Cardanol diene	81.94	Cardanol	80.5
	Diethyl Phthalate	13.35	2-methyl Cardanol diene	2.97	2-methyl benzaldehyde	8.73
	Cardanol-C13	2.32	Hexadecanoic acid	1.01	2-ethyl phenol	4.89
	Cardanol-C17	2.06	Oleic acid	0.98		
	Hexadecanoic acid	0.8				
	Oleic acid	0.67				

On account of their industrial significance, these CNSLs are used as raw materials for manufacturing paints and varnishes, polyurethane-based polymers, friction linings, foundry chemicals, surfactants, epoxy resins, laminating, and rubber compounding resins; and they even include intermediates for chemical industry [10, 11]. Although CNSL has its significance across the diversified industrial domain, it cannot be used directly for manufacturing or production process as each end product uses this CNSL in their respective processed manner. For this purpose, these CNSL are treated using numerous chemical treatment techniques; and the most commonly preferred technique uses chemical reactions such as transfer hydrogenation reactions, isomerization reactions, metathesis reactions, carbonylation reactions, polymerization reactions, isomerizing metathesis reaction, and isomerizing carbonylation reactions [12].

Although these techniques make CNSL as a highly efficient raw material or even more a suitable candidate for industrial applications, it fails to be processed into an ideal fuel compatible with combustion-based applications. Hence, any CNSL must be cracked or degraded into its smallest stable molecular form, and this must be achieved easily with minimal resource utilization. As a result, thermal and chemical cracking techniques can be identified as effective measures for cracking the macro molecules into simple aromatic and linear hydrocarbons. Specifically, thermal cracking is widely preferred for processing these CNSLs on industrial and large scales. Supporting this, Velmurugan et al. (2014) cracked the raw CNSL by heating it at slightly higher temperatures (200-400 °C) [13].

Furthermore, Vedharaj et al. (2016) reported the catalyst-assisted thermal cracking of CNSL before being subjected to evaluation in a Compression Ignition (CI) engine. Accordingly, the raw CNSL was preheated at 200 °C using an electric heater, followed by heating at 400 °C inside the main reactor. The vapor of CNSL was condensed using a water cooled condenser before passing the condensed cracked CNSL into the storage tank. Finally, the utilization of zeolite catalyst enhanced the rate of cracking of CNSL and overall yield [14].

These processed CNSLs serve as effective supplements or alternatives for existing biodiesel and neat diesel and can be used for wide varieties of combustion-based applications. However, in order to understand its effectiveness as fuel, it must be evaluated for its combustion and emission characteristics. Accordingly, Velmurugan et al. (2014) studied the performance of Thermally Cracked CNSL (TC-CNSL) in CI using a single-cylinder, water-cooled, diesel Direct Injection (DI), Kirloskar AV-1 diesel engine and reported that its characteristics was slightly identical to neat diesel.

Accordingly, TC-CNSL reported reduced CO and HC mission and increased NO_x and CO₂ emission on account of its fuel bound oxygen content. On the other hand, TC-CNSL exhibited increased rate of fuel consumption, which resulted in lower thermal efficiency. Interestingly, TC-CNSL exhibited a prolonged ignition delay followed by a longer combustion duration due to its aromatic compounds [13].

Next, Loganathan et al. (2020) tested the TC-CNSL in a CI engine by blending it with neat diesel and enriched the combustion products with hydrogen, which was administered into the engine in order to reduce the HC and CO emissions. In order to achieve a stable emission level, Exhaust Gas Recirculation (EGR) technique was employed on the engine with the circulation administered at 10 % of exhaust gas, while the flow rate of hydrogen was maintained at 6 LPM. The test results reported a simultaneous rise in the thermal efficiency up to 36.5 % and a reduction in HC and CO emission concentrations by 20 % and 10 %, respectively, while running at full load. On the contrary, these supplementary enrichments increased the NO_x emission by 40 %; however, reduced it upon introducing 30 % of EGR. In short, this study recommended using supplementary enrichment techniques for improving the engine properties of both ordinary and thermally cracked CNSLs [15].

Although numerous pieces of relevant literature report the availability, chemical composition, fuel properties, and engine characteristics of these CNSLs, the results obtained from these studies vary accordingly with rendering and processing techniques used. Hence, it is highly recommended that the molecular effect of various chemical compounds available in these raw and processed shell liquids be investigated so as to determine the parameters mentioned earlier. However, no previous studies have been focused or reported in relevance to the molecular impact on fuel properties and engine characteristics of CNSLs, though being reported for biodiesel fuels [16]. Considering this as an abridged research gap and an attempt to understand the molecular contribution, this present study exclusively focused on the role of characterized hydrocarbons in thermally cracked CNSLs in determining its fuel properties and engine characteristics. To be specific, this study used thermally cracked CNSLs extracted from waste CNS using mechanical screw press at lower temperatures, characterized them using GC and FT-IR spectroscopy, evaluated them for their fuel properties based on IS standards, and assessed them for the engine properties in single-cylinder CI engine.

2. MATERIALS AND METHODOLOGY

2.1. Proximate composition of cashew nut shell

Waste Cashew Nut shells (CNSs) used in the study were procured from local cashew processing units and were stored in air-tight containers to avoid any contamination. To begin with, proximate analysis of waste cashew nut shells to estimate their fraction mass of moisture and fixed carbon content, volatile matter, and ash residues was carried out by following the standard analytical methods, ASTM D 3173-3175. The fraction of moisture content in these shells was determined using ASTM D 3173 method in a drying oven. Then, the fraction of volatile matter was estimated as per ASTM D 3175 method, while the quantity of residual ash content was determined according to ASTM D 3174 method. Furthermore, the fixed carbon content in these shells was calculated by difference, accounting for the other calculated proximate compositions. Finally, the higher heating value of the waste shells was determined using a bomb calorimeter following the ASTM E 711 method, wherein the combustion was carried out in an environment with high pressure of oxygen (to ensure complete combustion) saturated with steam of water (to ensure that the whole water was converted into its liquid form).

2.2. Extraction of CNSL using mechanical extraction

Both lab-scale and Pilot-scale extraction of CNSL from CNS was executed by means of mechanical extraction method using a customized mechanical screw press. Here, the screw press was comprised of tapered compression screws mounted inside a cylindrical casing and was operated using an electric motor. The CNSs were fed into cylindrical casing using a feeding hopper attached transversely, and they were fed in the batch process. Furthermore, the compression screw was operated at a spindle speed of 7-13 rpm, while the maximum feeding and extraction rate were found to be 54-95 kg/hr and 11.93-14.90 kg/hr, respectively [17, 18]. It may be noted that

the waste CNS residues were re-fed into the screw press to extract the leftover CNSL from it.

2.3. Thermal cracking of CNSL

The extracted CNSL was thermally cracked using the high-temperature distillation technique on both lab and pilot scales. Accordingly, a simple distillation setup was used for cracking CNSL on a lab scale and it comprised a 500 mL flat bottomed flask mounted on a tripod stand and was fitted with a water jacketed condenser to cool the vapor collected post cracking. Here, a simple LPG fuelled gas burner was used for the purpose of heating and the temperature was maintained at 350-400 °C. In case of pilot-scale extraction, a stainless steel container was mounted on a customized LPG fuelled gas stove, which was used as the prime source for heating the CNSL inside it and was fitted to a water cooling jacket. The gas stove was capable of producing heat up to 550 °C, while the temperature was maintained at 410 °C throughout the cracking process. In the case of both of these setups, the condensates (TC-CNSL) were collected in the storage tanks and used for further analytical purposes.

2.4. Characterization of raw oil and TC CNSL

Both raw oil and TC CNSL were characterized for their chemical compounds using GC-MS and evaluation of function group using FT-IR spectroscopy, respectively. Tables 3 and 4 summarize the technical specifications of GC-MS and FT-IR spectroscopy [19, 20]. All the samples were prepared as per the standard sample preparation technique and obtained results were compared with those in standard library search databases to identify the suitable component and their activities.

Table 3. Technical specifications of gas chromatograph – mass spectrometer [19, 20]

Gas chromatograph		Mass spectrometer	
Equipment	Agilent 6890 chromatograph	Equipment	JOEL GC mate II bench top
Injector liner	direct/2 mm	Type	Double focusing magnetic sector MS
Column	15 m all tech ec-5 (25 µm ID, 0.25 µm thickness)	Operation mode	Electron ionization (EI) mode
Split ratio	10:01	Software	TSS-2001
Oven temperature	35 °C/2 min	Resolving power	1000 (20 % height definition)
Ramp	20 °C/min @ 300 °C for 5 min	Scanning feature	25 m/z to 700 m/z @ 0.3 s/scan
Helium carrier gas	2 ml/min (constant flow mode)	Inter scan delay	0.2 s

Table 4. Technical specifications of FT-IR spectrometer

JASCO	FTIR-4700
Standard wavenumber measurement range	7800 to 350 cm ⁻¹
Wavenumber range	15,000 to 0 cm ⁻¹
Detector	deuterated L-alanine doped triglycene sulphate-attenuated total reflectance (DLATGS.ATR)
Crystals	Zinc selenide (ZnSe)
Optical system	Single beam

2.5. Fuel properties evaluation for raw oil and TC CNSL

The necessary fuel properties and other physicochemical parameters were evaluated for both raw oil and TC CNSL as per Indian standards (IS: 1448). Accordingly, properties like density and kinematic viscosity were evaluated as per IS

standards using relative density balance method (IS:1448(P-32) 1992) and viscometer (IS:1448(P-25) 1976), respectively. Then, properties like flash and fire, ignition point, pour point, and calorific value were evaluated as per IS:1448(P-69) 2013 (Cleveland Open Cup Method), IS:1448(P-10/Sec-2) 2013, and IS:1448(P-6) 1984 (Bomb Calorimeter Method) testing

methods, respectively. Next, IS:1448(P-15) 2004 was followed to study the corrosiveness induced by the test samples on a copper strip, while the carbon residue content in these samples was evaluated using Conradson method as per IS:1448(P-122) 2013 testing standard.

2.6. Assessment of engine characteristics of TC-CNSL

Effects of identified hydrocarbons on combustion and emission characteristics of TC-CNSL were studied from their engine data and reported based on their testing in a single-cylinder CI engine, whose technical specifications are tabulated in Table 5 [16, 19]. For this purpose, three different samples of TC-CNSL, namely (i) TC-CNSL 20 blend, (ii) TC-CNSL 50 blend, and (iii) neat TC-CNSL or TC-CNSL 100 blend were prepared by blending with neat diesel in varying

proportions, in addition to comparing it as the reference sample. Here, TC-CNSL 20 sample represented the cracked biofuel at their minimal blending ratios and was considered as the globally accepted high-performance blend for any biofuel with neat diesel on global and commercial scales, whereas the TC-CNSL 50 sample signified the equivalent contribution of both cracked CNSLs and neat diesel. Moreover, the parameters studied from the engine characteristics include the peak pressure recorded, total delay period taken by fuel to initiate its combustion, rate of fuel consumed for unit power and their convertible efficiency, harmful emission gases like carbon monoxide (CO) and unburnt hydrocarbon (HC), and completely combusted carbon dioxide (CO₂) and nitrogen oxide (NO_x) emission.

Table 5. Technical specifications of Kirloskar TV1 Engine and AVL DI GAS 444 N Flue gas analyzer [19]

Kirloskar engine TV 1 specifications		AVL DI GAS 444 N (five gas analyzer)	
Type: Four-Stroke, Single-Cylinder Water Cooled		Measurement	Resolution
Rated power	5.2 KW	CO [0-15 Vol. %]	0.0001 Vol. %
Rated speed	1500 rpm	HC [0-20000 ppm Vol.]	1 ppm/10 ppm
Bore diameter (D)	87.5 mm	CO ₂ [0-20 Vol. %]	0.1 Vol. %
Stroke (L)	110 mm	O ₂ [0-25 Vol. %]	0.01 Vol. %
Compression ratio	17.5:1	NO _x [0-6000 ppm Vol.]	1 ppm Vol.

2.7. Error analysis

To ensure increased accuracy of the results, all the experiments were carried out in triplicates and results were reported in the form of mean \pm standard deviation. This deviation was taken into account as the variation results from the mean value and can be originated from different means, including human error and instrumental error. Equation 1 was used to calculate the standard deviation of each measured entity, where σ is the deviation from the mean value, x_i is the reported result, μ is the average mean of the reported results, and N is the number of times experiments were repeated ($N=3$, in this case) [20].

$$\sigma = \sqrt{\frac{\sum(x_i - \mu)^2}{N}} \quad (1)$$

3. RESULTS AND DISCUSSION

3.1. Proximate analysis of CNS

From the results of proximate analysis on cashew nut shell, it was clearly evident that the collected wastes were highly suitable for gasification. Table 6 summarizes the proximate composition of waste CNS estimated as per ASTM standards. It was observed that the average moisture content of cashew nut shell waste was 5.9 % and was well within the acceptable limit (below 15 %), as prescribed for any fuel [21], and this ensured its free flow and ability to produce good quality gas. Next, the average volatile matter content in cashew nut shell was estimated to be 74.83 %, and the higher amount of volatile matter was encouraged for its gasification. Then, the analysis of the suggested their average ash content at 0.9 % points to its suitability for gasification with minimum blocking of flow of air and fuel and formation of clinkers. Moreover, as the most desirable component for stating the volume of non-volatile carbon in the biomass, the average fixed carbon content in these waste shellst was calculated as 18.4 %.

Again, heating value of the biomass also decides its suitability for their gasification and the results present the average higher heating value of these cashew nut shells as 5036.8 Kcal/m³ (21.09 MJ/kg).

Table 6. Proximate composition of waste CNS

Proximate composition	CNS	Standard
Moisture (%)	5.9	ASTM D 3173
Volatile matter (%)	74.83	ASTM D 3175
Ash content (%)	0.9	ASTM D 3174
Fixed carbon (%)	18.4	By difference
Higher heating value (MJ/kg)	21.09	ASTM E 711

3.2. Extraction of raw CNSL

CNS, in this present study, had a maximum pericarp liquid (lipid) content of 23.8 % and this liquid played a significant role in protecting the seed kernel from harmful pests and moisture content entering into it [22, 23]. In general, maximum renderable oil content was found to be between 21.5 % and 22.9 %; however, extraction of CNSL using mechanical screw press yielded only up to 17.7 %. The reduction of oil content resulted from the lack of chemical interaction, wastage, and evaporation of highly volatile chemical compounds due to high compression force exerted by the mechanical components in the screw press. Eventually, slightly increased rendering yield was explained by the re-feeding of CNS residues into the press, which helped extract the leftover CNSL (upto 5.7 %) from the waste residues. Moreover, CNSL obtained by this method was highly viscous with increased concentration of impurities (CNSL purity: 83.2 wt %), in addition to lower boiling temperature and poor thermal oxidation stability [9].

3.3. GC and FT-IR characterization of raw CNSL

cm^{-1} , related to the stretching of carbon and hydrogen, was found only in the aromatic compounds (anacardic acid, cardol, and cardanol). Likewise, peaks corresponding to unsaturation in hydrocarbon moieties of anacardic acid, cardol, and cardanol were reported at 3016 cm^{-1} . In addition, the asymmetric and symmetric stretching of alkyl C-H bond was considered based on the peaks reported at 2912 and 2859 cm^{-1} , respectively. The stretching of unsaturated carbon bonds ($\text{C}=\text{C}$) in the aromatic rings of anacardic acid, cardol, and cardanol were noted at two distinct peaks reported at 1637 cm^{-1} . Peak at 1444 cm^{-1} represented the C-H bending between the phenolic ring and hydrocarbon chain in the characterized

compounds. Meanwhile, the peak at 1373.4 cm^{-1} signified the O-H bending corresponding to the -OH bonded with aromatic rings of cardol and cardanol. Next, the peaks at 988 and 907 cm^{-1} corresponded to the $\text{C}=\text{C}$ bending in the polycardanol structure, which were reported at the conjugated cis-trans double bond and the terminal vinyl group. Moreover, the peak at 687 cm^{-1} corresponded to the $\text{C}=\text{C}$ bending of the vinyl group which is formed as the polyaromatic structure. Summing up, it was clearly evident that CNSL existed in polymeric form, with carboxylic and hydroxyl groups bonding to aromatic (phenolic) compounds. The same finding was achieved in the existing literature [24-26].

Table 8. Peaks and chemical compounds contributing to various bond activities in raw CNSL

Peak (cm^{-1})	Bond activity	Contributing chemical compound
3348.19	O-H stretching	Anacardic acid; cardol; cardanol
3074	Aromatic C-H stretching	Anacardic acid; cardol; cardanol
3016	Vinylic C-H stretching	Double bonds in hydrocarbons and aromatic rings
2912	Asymmetric C-H stretching	Alkyl groups in hydrocarbon chains
2859	Symmetric C-H stretching	Alkyl groups in hydrocarbon chains
1637	Aromatic $\text{C}=\text{C}$ stretching	Anacardic acid; cardol; cardanol
1444	Methyl group C-H bending	Anacardic acid; cardol; cardanol
1373.4	O-H bending	Anacardic acid; cardol; cardanol
1291.7	Ester group C-O stretching	Anacardic acid
988 and 907	$\text{C}=\text{C}$ bending (vinyl group)	Polyaromatic structure
687	$\text{C}=\text{C}$ bending (vinyl group)	Polyaromatic structure

3.4. Properties of raw CNSL bio oil

Based on the characterization data, CNSL is distributed at a higher concentration of anacardic acid and cardol followed by cardanol and it comprises aromatic hydrocarbons attached to long aliphatic carbon chains ranging up to 18 carbon atoms [27]. Owing to these aromatic rings and long carbon chains, raw CNSL displayed higher density and kinematic viscosity, which were 15.8% and $73.45 \text{ mm}^2/\text{s}$ higher than the permissible range for neat diesel, respectively [28]. Furthermore, increased molecular integrity in view of these phenolic ring structures provided the lowest pour point for CNSL ($-21 \text{ }^\circ\text{C}$) and ensured its functioning even at very low temperatures and in cold weather conditions. In addition, these anacardic acid and cardol contributed to the higher flash point

for CNSL, which made it safe for handling and transportation, besides increasing its auto ignition temperature slightly higher than neat diesel. The higher acidic pH value (4.1) for CNSL was accounted by the higher concentration of anacardic acid (51.84%), which was the result of controlled low-temperature extraction of CNSL. Upon investigating the proximate elemental composition, raw CNSL exhibited high carbon content of 81.02% , hydrogen content by 8.5% , and oxygen content by 8.6% . Besides, raw CNSL reported mild traces of nitrogen and sulphur content, which reduced its overall caloric value compared to its counter petro products. Table 9 summarizes the fuel properties of the raw CNSL evaluated as per IS and ASTM standards.

Table 9. Fuel properties of raw CNSL evaluated as per IS and ASTM standards

Parameters	Raw CNSL	Standards
Gross calorific value, kcal/kg	9061 ± 17	IS:1448(P-6) 1984
Kinematic viscosity @ $40 \text{ }^\circ\text{C}$, cSt	77.05 ± 1.14	IS:1448(P-25) 1976
Density @ $15 \text{ }^\circ\text{C}$, g/ml	0.9611 ± 0.01	IS:1448(P-32) 1992
Ash content, % by mass	1.3 ± 0.2	IS:1448(P-4) 1984
Flash point, $^\circ\text{C}$	206 ± 5	IS:1448(P-69) 2013
Pour point, $^\circ\text{C}$	-21 ± 2	IS:1448(P-10/Sec-2) 2013
Carbon residue (CCR), % by mass	6.45 ± 0.45	IS:1448(P-122) 2013
pH value	4.1 ± 0.4	By pH meter
Copper strip corrosion at $100 \text{ }^\circ\text{C}$ for 3 hours	1 No.	IS:1448(P-15) 2004
Ignition temperature, $^\circ\text{C}$	230 ± 8	IS:1448(P-69) 2013
Ultimate analysis		
Carbon, % by mass	81.02 ± 0.84	By CH analyzer

Hydrogen, % by mass	8.50 ± 0.12	By CH analyzer
Nitrogen, % by mass	0.30 ± 0.015	ASTM D3228
Sulphur, % by mass	0.09 ± 0.001	IS:1448(P-33) 1991
Ash, % by mass	1.31 ± 0.1	IS:1448(P-4) 1984
Moisture, % by mass	0.16 ± 0.03	ASTM D 6304
Oxygen, % by mass	8.62 ± 0.67	By difference

3.5. Thermally cracked CNSL (TC-CNSL)

3.5.1. GC characterization of TC-CNSL

Based on GC characterization on TC-CNSL (Table 10), methyl phenol (cresol), methyl oleate, methyl tetradecenoate, isopropyl cyclohexanedione, and 1-butyl-2-ethyl cyclobutane were identified as the dominant chemical compounds present in the thermally cracked CNSL (TC-CNSL). Eventually, the formation of linear chained and aromatic ring-shaped hydrocarbons is altogether justified by the thermal cracking of polymeric macro molecules available in raw CNSL [29], which induced cracking of linear HC from the aromatic ring in their carboxylic functional group. Further, TC-CNSL reported

a significant concentration of FAEs (upto 31.49 %), which made it suitable for combustion-based applications; in particular, methyl oleate played a major role in exhibiting fuel properties slightly similar to biodiesel. Interestingly, thermal cracking of CNSL also resulted in the formation of octadecane, sulfurous acid up to a concentration of 3.48 % and was found to be a source of sulphur in the resulting product. Figure 5 illustrates the GC spectra of TC-CNSL, whereas Figures 6-8 illustrate the optimized 3D molecular structure of cresol, methyl oleate, and methyl tetradecenoate designed using Avogadro tool.

Table 10. Chemical compounds characterized in the TC-CNSL using GC

Chemical compound	Composition (in %)	Chemical formula	Linearity/aromaticity
Phenol, 2-methyl	43.87	C ₇ H ₈ O	Aromatic
8-Octadecenoic acid, methyl ester	28.49	C ₁₉ H ₃₆ O ₂	Linear
Methyl 9-tetradecenoate	7.63	C ₁₅ H ₂₈ O ₂	Linear
Octadecane, sulfurous acid	3.48	C ₁₈ H ₃₆ SO ₃	linear
Ethanone, 1-cyclopentyl-cyclopentane	1.34	C ₉ H ₁₄ O ₂	Aromatic
4-Isopropyl-1, 3-cyclohexanedione	7.12	C ₉ H ₁₄ O ₂	aromatic
Cyclobutane, 1-butyl-2-ethyl	6.89	C ₁₀ H ₂₀	Aromatic
1-Dodecene, cyclododecane	1.18	C ₂₄ H ₄₇	aromatic

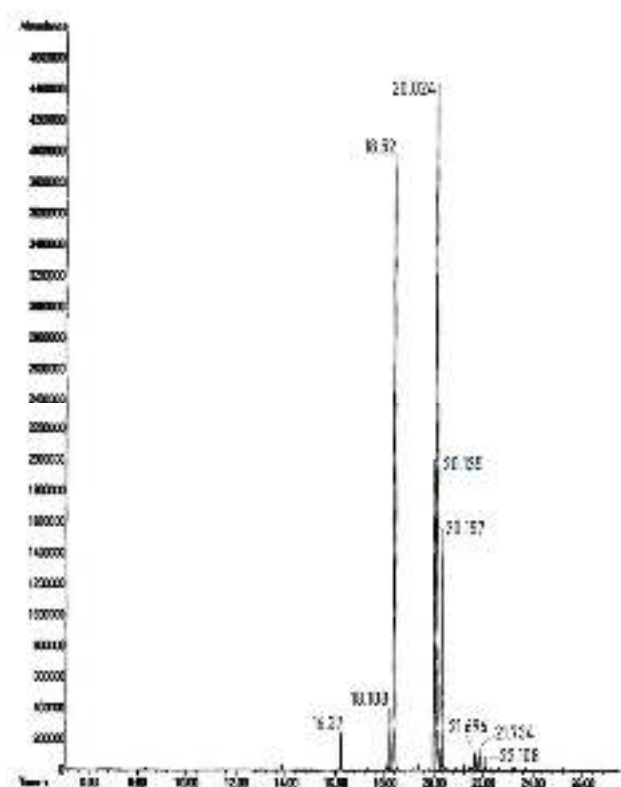


Figure 5. GC Spectra of TC-CNSL



Figure 6. Optimized 3D molecular structure of cresol developed using Avogadro tool (molecular formula: C₇H₈O; molecular weight: 108.14 g/mol)



Figure 7. Optimized 3D molecular structure of methyl oleate developed using Avogadro tool (molecular formula: C₁₉H₃₆O₂; molecular weight: 296.5 g/mol)

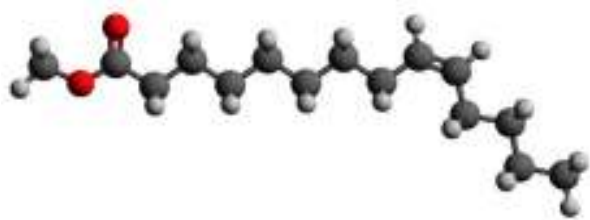


Figure 8. Optimized 3D molecular structure of methyl tetradecenoate developed using Avogadro tool (molecular formula: $C_{15}H_{28}O_2$; molecular weight: 240.4 g/mol)

3.5.2. FT-IR characterization of TC-CNSL

Based on the FT-IR spectral curve, a significant peak was reported at 3274 cm^{-1} , which signified the stretching of hydroxyl functional group (-OH) of methyl phenol (Cresol). Then, another peak between 2769 and 2934 cm^{-1} reported the asymmetric and symmetric stretching of C-H bonds in the alkyl chains of hydrocarbons. In the following, two significant

peaks at 1197 and 1738 cm^{-1} signified the presence of ester-based compounds (methyl oleate and methyl 9-tetradecenoate) [16] and played a significant role in improving the fuel properties of the resulting TC-CNSL and cresol. Moreover, another distinct peak at 1434 cm^{-1} signified the -OH bending and was related with the bending activities noted, exclusively, for any acidic compounds (cresol, octadecane, and sulphurous acid in this case). Furthermore, another distinct peak was reported at 1288 cm^{-1} , which corresponded to the stretching between carbon and oxygen molecule present in any aromatic esters. In addition, it contributed to the cyclic hydrocarbons available in it. Most importantly, the presence of octadecane and sulphurous acid was confirmed based on the peak reported at 1056 cm^{-1} , which was dedicated exclusively to the sulfoxide (S=O) stretching [30]. Table 11 consolidates the dominant peaks in the FT-IR spectra and chemical compounds contributing to these based on their corresponding bond activities in raw CNSL.

Table 11. Peaks and chemical compounds contributing to various bond activities in TC-CNSL

Peak (in cm^{-1})	Bond activity	Contributing chemical compound
3274	Phenols -OH stretching	Methyl phenol (Cresol)
1738	Ester C-O stretching	Methyl oleate, methyl 9-tetradecenoate
2769	Alkane C-H stretching	Hydrocarbon compounds
1434	Carboxylic (-OH) bending	Methyl phenol; octadecane, sulphurous acid
1288	Aromatic ester C-O stretching	Ethanone, 1-cyclopentyl-cyclopentane
1197	Ester C-O stretching	Methyl oleate, methyl 9-tetradecenoate
1056	Sulfoxide S=O stretching	Octadecane, sulphurous acid

3.6. Fuel Properties of TC-CNSL

According to the fuel properties of TC-CNSL, a drastic reduction in density and kinematic viscosity was reported and was estimated to be reduced by 8.75 % and 96 %, respectively, as compared to raw CNSL. Yet, higher density and viscosity than neat diesel (density: 830 kg/m^3 and kinematic viscosity: $2.47\text{ mm}^2/\text{s}$) were reported by 5.7 % and 21.5 %, respectively. Eventually, variation in density and kinematic viscosity was accounted for the formation of thermally cracked chemical compounds like cresol, FAEs, and cyclic hydrocarbons. In addition, the flash point of TC-CNSL was reduced by 46.6 % and was justified by the presence of FAEs in it, whereas its pour point was reduced by $24\text{ }^\circ\text{C}$ due to its aromatic and cyclic hydrocarbons, whose molecular

structure resembled the molecular structure of neat diesel. Furthermore, the formation of chemical compounds like cresol and Octadecane and sulphurous acid simply increased the pH by 43.2 % than compared to raw CNSL. Besides, high gross calorific value of TC-CNSL was explained by the presence of hydrocarbons, including long carbon chained molecules and combustible sulphur content; however, mild traces of nitrogen and sulphur content produced a slightly lower calorific value than neat diesel. The proximate elemental composition of TC-CNSL reported high carbon content of 84.16 %, hydrogen content of 11.45 %, and oxygen content of 4.01 %. Table 12 summarizes the fuel properties of TC-CNSL evaluated as per IS and ASTM standards.

Table 12. Fuel properties of TC-CNSL evaluated as per IS and ASTM standards

Parameters	TC-CNSL	Standards
Kinematic viscosity @ $40\text{ }^\circ\text{C}$, cSt	3.0 ± 0.62	IS:1448 (Pt-25) 2013, RA-2018
Gross calorific value, kcal/kg	10530 ± 23	IS:1448(Pt-6)1984, RA-2018
Density @ $15\text{ }^\circ\text{C}$, g/ml	0.877 ± 0.01	IS:1448 (Pt-32) 2019
Flash point (Abel), $^\circ\text{C}$	110 ± 5	IS:1448 (Pt-20) 2019
Copper strip corrosion at $100\text{ }^\circ\text{C}$ for 3 hours	1a	IS:1448 (Pt-15) 2004, RA-2016
Pour point, $^\circ\text{C}$	-45 ± 2.5	IS:1448 (Pt-10/Sec-2) 2013, RA-2018
pH	5.9 ± 0.6	By pH meter
Ultimate analysis, % by mass (IS:1448 (Pt-4) 1974, RA-2012)		
Ash content	0.001	IS:1448 (Pt-4) 1974, RA-2017
Carbon content	84.16 ± 0.75	ASTM D 5373-14, Guidelines
Hydrogen content	11.45 ± 0.5	ASTM D 5373-14, Guidelines

Nitrogen content	0.33 ± 0.025	ASTM D 5373-14, Guidelines
Sulphur content	0.05 ± 0.001	ASTM D 4239-17, (method B), guidelines
Oxygen content	4.01 ± 0.72	By calculation
Moisture (water) content, % by mass	Less than 0.05	IS:1448 (Pt-40) 2015

3.7. Combustion analysis

The stoichiometric air-to-fuel ratio required for combusting the TC-CNSL was calculated from the quantity of air needed for completely combusting its one mol. For this purpose, the quantity of air (N_{AIR}) was calculated using Equation 2, with numbers of carbon (N_C), hydrogen (N_H), and oxygen (N_O) molecules determined using the molecular formula of TC-CNSL, which was found to be $C_{12}H_{21}O$ [19]. As can be seen in this formulated molecular formula, the volume of air required for combusting one mol of TC-CNSL was calculated as 16.75 mols and the stoichiometric air-fuel ratio was 12.74:1. However, an excess amount of air is always needed to completely combust these TC-CNSLs; hence, the actual stoichiometric air to fuel ratio was adjusted to 19.12:1; thus, extra requirement for air was 1.5 times the calculated amount [31].

$$N_{AIR} = \frac{4N_C + N_H - 2N_O}{4} \quad (2)$$

Table 13. Engine characteristics of neat diesel and variation of engine data for TC-CNSL blends

Parameters	Unit	Diesel	TC-CNSL 20	TC-CNSL 50	TC-CNSL 100
Peak in-cylinder pressure	Bar	56.7	2.01 % ↑	4.74 % ↑	10.15 % ↑
Ignition delay	°CA	11.8	10.17 % ↑	15.25 % ↑	27.12 % ↑
Specific fuel consumption	Kg/kW-hr	0.37	5.46 % ↑	12.82 % ↑	24.91 % ↑
Brake thermal efficiencies	%	27.8	5.33 % ↓	11.89 % ↓	20.40 % ↓
Carbon monoxide emission	%	0.06	48.33 % ↑	196.41 % ↑	361.59 % ↑
Carbon dioxide emission	%	5.09	19.72 % ↑	41.67 % ↑	97.96 % ↑
Nitrogen oxide emission	PPM	405.9	15.59 % ↑	45.92 % ↑	89.35 % ↑
Unburnt hydrocarbon emission	PPM	52.6	15.21 % ↑	37.45 % ↑	74.90 % ↑
Exhaust gas temperature	°C	198.8	7.34 % ↑	22.69 % ↑	50.50 % ↑

To begin with, TC-CNSL had higher cylinder pressure than neat diesel (Figure 9) and it increased along with the concentration. This finding is justified by the early start and prolonged durations of their complete combustion, attributed by their higher cetane number, and fuel bound oxygen content [33]. Here, the higher concentration of oxygen molecules in TC-CNSL samples, especially from cresol, methyl oleate, methyl 9-tetradecenoate and 4-isopropyl-1, 3-cyclohexanedione, ensured their early ignition upon injection, followed by administering a complete oxidation, which resulted in liberation of a large amount of heat and pressure inside the cylinder. Accordingly, ignition delay was reduced at 100 % for neat TC-CNSL sample, citing the increased availability of fuel bound oxygen content from the injected fuel mass, which also helped meet the energy demand. However, ID of TC-CNSL samples remained higher than the neat diesel throughout the experimental runs (Figure 10) and were caused by physical and chemical delay raised due to the linear FAEs, followed by cyclic and aromatic hydrocarbons [34]. As a result of prolonged combustion duration and availability of surplus oxygen content, these TC-CNSL samples underwent complete combustion and generated significant heat, which resulted in higher EGTs and NO_x emission than neat diesel (Figures 11 and 12). In particular,

3.8. Engine characteristics of TC-CNSL

As can be seen from their engine characteristics (from Table 13), both neat TC-CNSL (TC-CNSL 100) and TC-CNSL blend samples reported superior combustion characteristics and mixed emission characteristics, besides reporting slightly poor performance characteristics. In fact, the increased combustion behavior of the biofuel samples was justified by their enhanced cetane number, which prolonged the duration of their combustion, whilst fuel-bound oxygen content ensured their complete oxidation [16, 32]. On the other hand, mixed emission concentrations and poor fuel performance were measured based on their increased density and viscosity, cyclic structure, aromaticity, unsaturation, and inferior calorific value. Here, this aromaticity and cyclic structure were predominantly contributed by cresol and 4-Isopropyl-1,3-cyclohexanedione, respectively, while unsaturation was affected by both long linear carbon chained (8-Octadecenoic acid, methyl ester and methyl 9-tetradecenoate) and aromatic hydrocarbons.

the oxidation of long-chain hydrocarbons like FAEs and cyclic hydrocarbons liberated a large amount of heat, fairly enough for nitrogen in the intake air to react with oxygen molecules to recombine into nitrogen oxides (NO_x) [35]. Here, both EGT and NO_x emissions increased proportionally with increase in concentration of TC-CNSL in the blended samples.

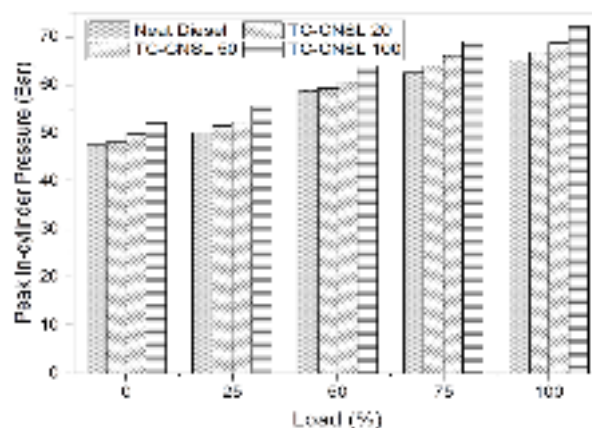


Figure 9. Peak in-cylinder pressure of neat diesel and TC-CNSL blends for varying engine loads

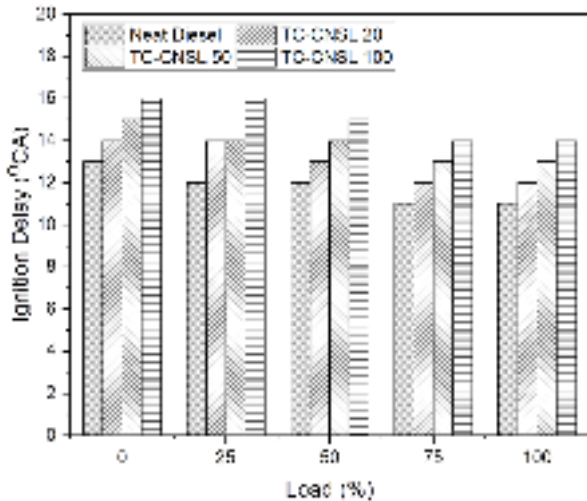


Figure 10. Ignition delay of neat diesel and TC-CNSL blends for varying engine loads

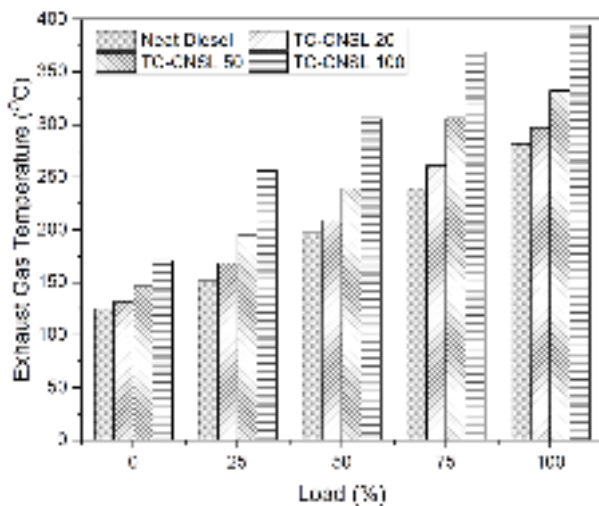


Figure 11. Exhaust gas temperature of neat diesel and TC-CNSL blends for varying engine loads

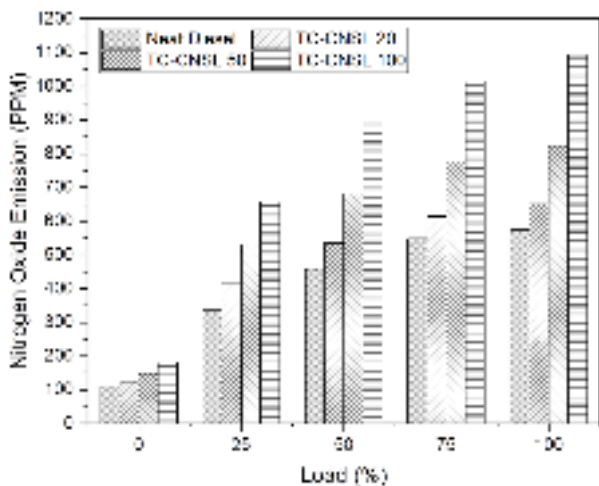


Figure 12. Nitrogen oxide emission of neat diesel and TC-CNSL blends for varying engine loads

the fuel bound oxygen content from the hydrocarbons, which helped oxidize a large amount of hydrocarbon molecules in CO_2 and water, leaving behind a part of incomplete combustion and uncombusted by-products [36]. In this regard, carbon monoxide (CO) was produced as the incomplete by-product during the combustion and increased significantly with TC-CNSL concentration owing to their higher degree of unsaturated double bonds [19] (Figure 14). Unfortunately, these bonds failed to undergo complete combustion due to the need for high bond disassociation energy, which increased further at higher loads, citing the increased injection of fuel mass. On the other hand, from Figure 15, TC-CNSL samples reported a notable amount of unburnt hydrocarbon emission due to the lower adiabatic flame temperature near the wall surfaces and area surrounding large fuel droplets. Here, increased density and viscosity from both linear and cyclic hydrocarbons failed to atomize effectively, thus forming large droplets of fuel during injection and quenching the flame temperature inside the cylinder, thereby leaving behind a significant amount of unburnt hydrocarbon. Besides, unsaturation played a crucial role in contributing to this unburnt HC emission, as these unsaturated hydrocarbons needed more energy and heat for initiating combustion [31, 37].

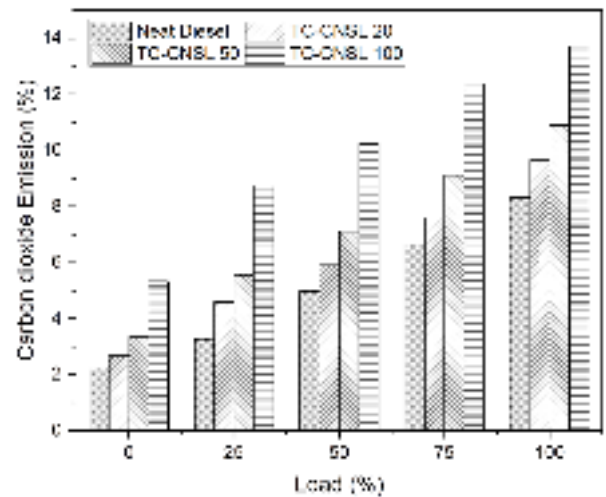


Figure 13. Carbon dioxide emission of neat diesel and TC-CNSL blends for varying engine loads

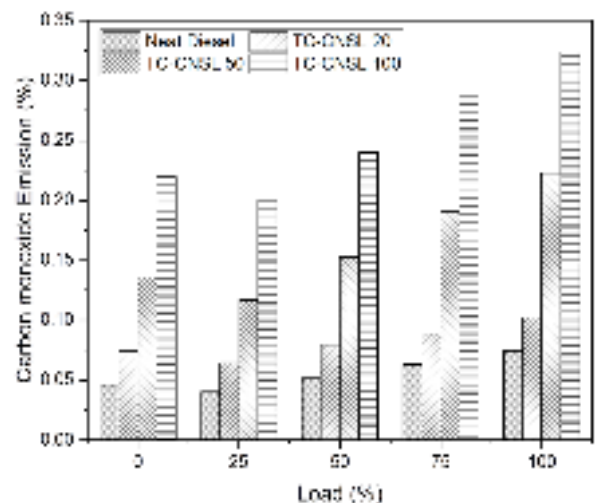


Figure 14. Carbon monoxide emission of neat diesel and TC-CNSL blends for varying engine loads

In view of their complete oxidation, these TC-CNSL samples reportedly had a higher concentration of CO_2 emission than neat diesel (Figure 13) and remained higher for equivalent and neat TC-CNSL blend. This was accounted by

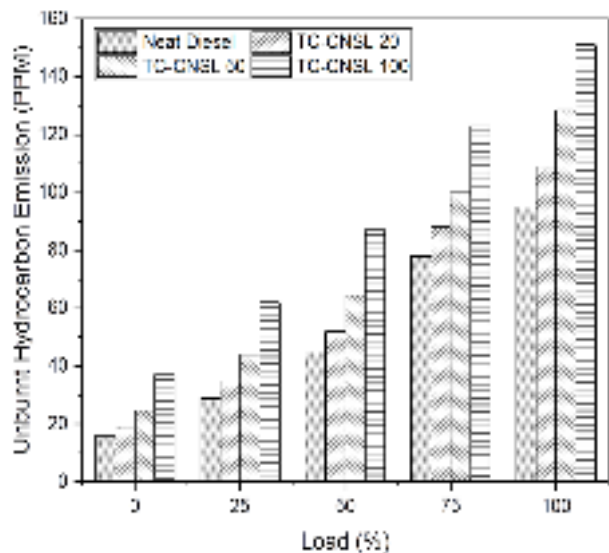


Figure 15. Unburnt hydrocarbon emission of neat diesel and TC-CNSL blends for varying engine loads

Based on their performance characteristics (Figures 16 and 17), TC-CNSL samples reportedly had a higher rate of fuel consumption and slightly reduced brake thermal efficiencies, citing their lower calorific content and higher density and viscosity than neat diesel. Here, the higher rates of density and viscosity for TC-CNSL samples were predominantly contributed by cresol, followed by FAEs and cyclic hydrocarbons, thus causing certain setbacks like increased quantity of injected fuel and poor atomization [16]. On the other hand, the absence of oxidizable molecules like nitrogen and small portion of sulphur content failed to report higher calorific value for TC-CNSL samples, thus requiring a greater amount of fuel for combustion to deliver equivalent energy as delivered by neat diesel [33, 38]. Moreover, their efficiency increased with engine load to maintain the engine speed all the time; however, it decreased with increasing TC-CNSL concentration, citing reduced calorific value due to the reduction of neat diesel concentration. Eventually, no knocking activities were reported for any test samples throughout the experimental runs; hence, this fuel is recommended given its compatibility with commercial applications.

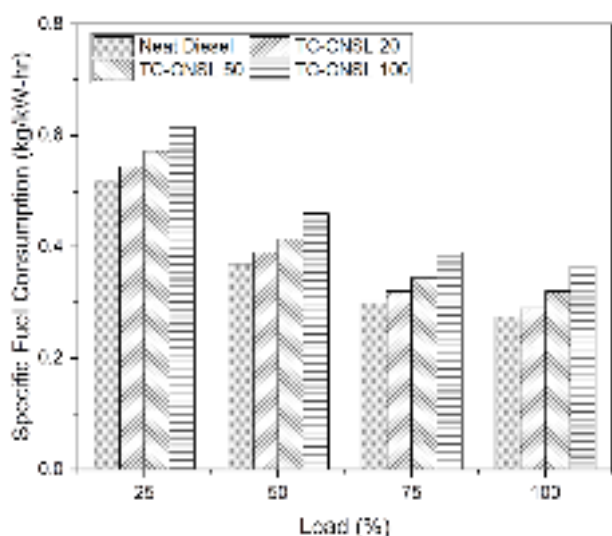


Figure 16. Specific fuel consumption of neat diesel and TC-CNSL blends for varying engine loads

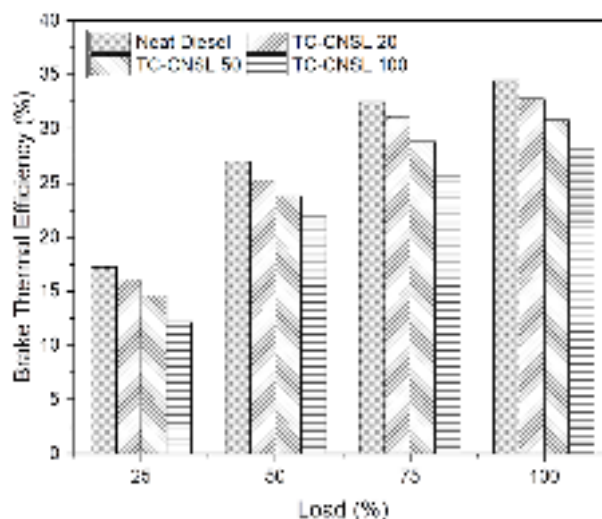


Figure 17. Brake thermal efficiencies of neat diesel and TC-CNSL blends for varying engine loads

4. CONCLUSIONS

Aimed at developing a suitable alternative to existing petrodiesel, this study achieved a sustainable biofuel from renewable biomass by thermally cracking the CNSL extracted from waste cashew nut shell by means of cold extraction technique. Effective utilization of this biofuel could be achieved upon evaluating its fuel properties and performance in CI engine, which in turn were determined by the chemical compounds available in it. Hence, it is of priority to understand the contribution of these chemical compounds on these entities. Thus, the impact of characterized hydrocarbons on deciding the overall fuel properties and engine characteristics of thermally cracked shell liquid was studied and the following were the major conclusions drawn from this study:

- (i) Both waste cashew nut shell and its liquid were identified as potential biomass feedstocks, which could be used as energy sources for both domestic and industrial purposes, accounting for their technical aspects.
- (ii) Waste CNS reported its maximum pericarp lipid content as 23.84 %; yet, the amount of CNSL rendered depends on the type of rendering technique. Next, the concentration of organic hydrocarbons in raw CNSL varied with respect to rendering technique; accordingly, the higher concentration of anacardic acid was reported in raw CNSL extracted using cold extraction technique.
- (iii) Thermal cracking of raw CNSL extracted using cold rendering was effective in the temperature range of 300-400 °C and it produced a higher concentration of cresol, methyl oleate, and tetradecenoate as the most dominant aromatic and linear chained hydrocarbons, respectively. It was also evident that thermal cracking of macromolecules was seen as an alternative means of synthesizing FAEs, besides transesterification.
- (iv) Fuel properties of TC-CNSL were deeply affected by the characterized hydrocarbons, with a large number of carbon atoms and long carbon chained molecules contributing to its physical and thermal properties, especially its calorific content. To be specific, cyclic and aromatic hydrocarbons facilitated enhancing their flow characteristics, whereas the presence of oxygen

molecules in the cracked shell liquid improved its cetane number.

- (v) Combustion of TC-CNSL in the CI engine presented a higher combustion rate and emission levels owing to the early start and prolonged duration of complete combustion contributed by both cyclic and aromatic and linear chained hydrocarbons including FAEs. Besides, aromaticity and unsaturation in these molecules increased their density and viscosity and reduced their calorific content, thereby resulting in reduced thermal efficiencies.

To sum up, it can be strongly concluded that the entire molecular composition of any CNSL is dependent on its rendering technique and thermal cracking of these liquids induces changes in their molecular structures, which has made a significant contribution to deciding its fuel properties and engine characteristics. Ultimately, understanding the impact of these molecules will facilitate (a) using this biofuel more effectively depending upon its end applications and (b) easily predicting its behavior during its life cycle, thereby ensuring sustainability and renewability throughout.

5. ACKNOWLEDGEMENT

Authors wish to thank the Management of Steamax Envirocare Private Limited for providing their support and facility to carry out this present work.

REFERENCES

- Sisco, M.R., Pianta, S., Weber, E.U. and Bosetti, V., "Global climate marches sharply raise attention to climate change: Analysis of climate search behavior in 46 countries", *Journal of Environmental Psychology*, Vol. 75, (2021), 101596. (<https://doi.org/10.1016/j.jenvp.2021.101596>).
- Lomonaco, D., Mele, G. and Mazzetto, S.E., "Cashew nutshell liquid (CNSL): From an agro-industrial waste to a sustainable alternative to petrochemical resources", *Cashew nut shell liquid*, Springer, Cham, (2017), 19-38. (https://doi.org/10.1007/978-3-319-47455-7_2).
- Taiwo, E.A., "Cashew nut shell oil—A renewable and reliable petrochemical feedstock", *Advances in Petrochemicals*, Vol. 1, (2015), 13. (<https://www.intechopen.com/chapters/48869>).
- Viswalingam, K. and Emerson Solomon, F., "A process for selective extraction of cardanol from Cashew Nut Shell Liquid (CNSL) and its useful applications", *International Journal of Scientific & Engineering Research*, Vol. 4, No. 3. (<https://citeseerx.ist.psu.edu/document?repid=rep1&type=pdf&doi=1403141c531df86831c96b16626232c7641097fb>).
- Oliveira, M.S.C., de Moraes, S.M., Magalhães, D.V., Batista, W.P., Vieira, Í.G.P., Craveiro, A.A., de Maneses, J.E.S.A., Carvalho, A.F.U. and de Lima, G.P.G., "Antioxidant, larvicidal and anti acetylcholinesterase activities of cashew nut shell liquid constituents", *Acta Tropic*, Vol. 117, No. 3, (2011), 165-170. (<https://doi.org/10.1016/j.actatropica.2010.08.003>).
- Yuliana, M., Tran-Thi, N.Y. and Ju, Y.H., "Effect of extraction methods on characteristic and composition of Indonesian cashew nut shell liquid", *Industrial Crops and Products*, Vol. 35, No. 1, (2012), 230-236. (<https://doi.org/10.1016/j.indcrop.2011.07.007>).
- Patela, R.N., Bandyopadhyay, S. and Ganesh, A., "Selective extraction of cardanol and phenols from cashew nut shell liquid obtained through pyrolysis of cashew nut shells", *Proceedings of the Indian Chemical Engineering Congress, Novel Separation Processes Session (CHEMCON-2005)*, 14-17.
- Kyei, S.K. and Onyewuchi Akaranta, G.D., "Extraction, characterization, and application of cashew nut shell liquid from cashew nut shells", *Proceeding of China-Africa Urban Development Forum (CAUDF)*, University of Cape Coast, Cape Coast, Ghana, (2019), 104. (https://uiispace.unilorin.edu.ng/bitstream/handle/20.500.12484/7918/FI_NALCAUDF_2020_July_2020.pdf?sequence=1&isAllowed=y#page=113).
- Rodrigues, F.H., França, F.C., Souza, J.R., Ricardo, N.M. and Feitosa, J., "Comparison between physico-chemical properties of the technical Cashew Nut Shell Liquid (CNSL) and those natural extracted from solvent and pressing", *Polímeros*, Vol. 21, (2011), 156-160. (<https://doi.org/10.1590/S0104-14282011005000028>).
- Lubi, M.C. and Thachil, E.T., "Cashew Nut Shell Liquid (CNSL)-A versatile monomer for polymer synthesis", *Designed Monomers and Polymers*, Vol. 3, No. 2, (2000), 123-153. (<https://doi.org/10.1163/156855500300142834>).
- Sharma, P., Gaur, V.K., Sirohi, R., Larroche, C., Kim, S.H. and Pandey, A., "Valorization of cashew nut processing residues for industrial applications", *Industrial Crops and Products*, Vol. 152, (2020), 112550. (<https://doi.org/10.1016/j.indcrop.2020.112550>).
- Mubofu, E.B. and Mgaya, J.E., "Chemical valorization of cashew nut shell waste", *Topics in Current Chemistry*, Vol. 376, No. 2, (2018), 1-15. (<https://doi.org/10.1007/s41061-017-0177-9>).
- Velmurugan, A., Loganathan, M. and Gunasekaran, E.J., "Experimental investigations on combustion, performance and emission characteristics of thermal cracked cashew nut shell liquid (TC-CNSL)-diesel blends in a diesel engine", *Fuel*, Vol. 132, (2014), 236-245. (<https://doi.org/10.1016/j.fuel.2014.04.060>).
- Vedharaj, S., Vallinayagam, R., Yang, W.M., Saravanan, C.G. and Roberts, W.L., "Synthesis and utilization of catalytically cracked cashew nut shell liquid in a diesel engine", *Experimental Thermal and Fluid Science*, Vol. 70, (2016), 316-324. (<https://doi.org/10.1016/j.expthermflusci.2015.09.026>).
- Loganathan, M., Thanigaivelan, V., Madhavan, V.M., Anbarasu, A. and Velmurugan, A., "The synergetic effect between hydrogen addition and EGR on cashew nut shell liquid biofuel-diesel operated engine", *Fuel*, Vol. 266, (2020), 117004. (<https://doi.org/10.1016/j.fuel.2019.117004>).
- Srinivasan, G.R., Shankar, V., Chandra Sekharan, S., Munir, M., Balakrishnan, D., Mohanam, A. and Jambulingam, R., "Influence of fatty acid composition on process optimization and characteristics assessment of biodiesel produced from waste animal fat", *Energy Sources, Part A: Recovery, Utilization, and Environmental Effects*, (2020), 1-19. (<https://doi.org/10.1080/15567036.2020.1771477>).
- Garkal, D.J. and Bhande, R.S., "Review on extraction and isolation of cashew nut shell liquid", *International Journal of Innovations in Engineering Research and Technology*, Vol. 1, No. 1, (2014). (<https://repo.ijert.org/index.php/ijert/article/download/192/180/357>).
- Sivakumar, S., Venkatachalam, R., Nedunchezian, N., Sivakumar, P. and Rajendran, P., "Processing of cashew nut shell and feasibility of its oil as bio fuel in compression ignition engine", *Journal of Chemical and Pharmaceutical Sciences*, (Special Issue), Vol. 4, (2014), 133-135. (<https://jchps.com/specialissues/Special%20issue4/jchps%2047%20siva%20kumar%20s%20133-135.pdf>).
- Srinivasan, G.R., Shankar, V. and Jambulingam, R., "Experimental study on influence of dominant fatty acid esters in engine characteristics of waste beef tallow biodiesel", *Energy Exploration & Exploitation*, Vol. 37, No. 3, (2019), 1098-1124. (<https://doi.org/10.1177/0144598718821791>).
- Jambulingam, R., Srinivasan, G.R., Palani, S., Munir, M., Saeed, M. and Mohanam, A., "Process optimization of biodiesel production from waste beef tallow using ethanol as co-solvent", *SN Applied Sciences*, Vol. 2, No. 8, (2020), 1-18. (<https://doi.org/10.1007/s42452-020-03243-7>).
- Motta, I.L., Miranda, N.T., Maciel Filho, R. and Maciel, M.R.W., "Biomass gasification in fluidized beds: A review of biomass moisture content and operating pressure effects", *Renewable and Sustainable Energy Reviews*, Vol. 94, (2018), 998-1023. (<https://doi.org/10.1016/j.rser.2018.06.042>).
- Pandiyan, C.V., Shylaja, G., Srinivasan, G.R. and Saravanan, S., "Studies on use of Cashew Nut Shell Liquid (CNSL) in biopesticide and biofertilizer", *Nature Environment & Pollution Technology*, Vol. 19, No. 1, (2020), 103-111. ([https://neptjournal.com/upload-images/9\)B-3614.pdf](https://neptjournal.com/upload-images/9)B-3614.pdf)).
- Liu, W., Yue, Y., Tang, F., Qin, D., Hua, R. and Cao, H., "Fungicidal and insecticidal activities of CNSL", *Journal of Anhui Agricultural University*, Vol. 37, No. 4, (2010), 753-756.
- Achi, S.S. and Myina, O.M., "Preliminary investigation of Kaduna-Grown cashew nutshell liquid as a natural precursor for dyestuffs, pigments and binders for leather finishing", *Nigerian Journal of Chemical Research*, Vol. 16, (2011), 9-14. (https://www.researchgate.net/publication/281319361_Preliminary_Invstigation_of_Kaduna-

- [Grown Cashew Nutshell Liquid as a Natural Precursor for Dyestuffs Pigments and Binders for Leather Finishing](#)).
25. Balgude, D. and Sabnis, A.S., "CNSL: An environment friendly alternative for the modern coating industry", *Journal of Coatings Technology and Research*, Vol. 11, No. 2, (2014), 169-183. (<https://doi.org/10.1007/s11998-013-9521-3>).
 26. Srivastava, R. and Srivastava, D., "Mechanical, chemical, and curing characteristics of cardanol–furfural-based novolac resin for application in green coatings", *Journal of Coatings Technology and Research*, Vol. 12, No. 2, (2015), 303-311. (<https://doi.org/10.1007/s11998-014-9630-7>).
 27. Morais, S.M., Silva, K.A., Araujo, H., Vieira, I.G., Alves, D.R., Fontenelle, R.O. and Silva, A., "Anacardic acid constituents from cashew nut shell liquid: NMR characterization and the effect of unsaturation on its biological activities", *Pharmaceuticals*, Vol. 10, No. 1, (2017), 31. (<https://doi.org/10.3390/ph10010031>).
 28. Ike, D.C., Ibezim-Ezeani, M.U. and Akaranta, O., "Cashew nutshell liquid and its derivatives in oil field applications: An update", *Green Chemistry Letters and Reviews*, Vol. 14, No. 4, (2021), 620-633. (<https://doi.org/10.1080/17518253.2021.1991485>).
 29. Lomonaco, D., Maia, F.J.N., Clemente, C.S., Mota, J.P.F., Junior, A.E.C. and Mazzetto, S.E., "Thermal studies of new biodiesel antioxidants synthesized from a natural occurring phenolic lipid", *Fuel*, Vol. 97, (2012), 552-559. (<https://doi.org/10.1016/j.fuel.2012.01.059>).
 30. Keating, C.S., McClure, B.A., Rack, J.J. and Rubtsov, I.V., "Sulfoxide stretching mode as a structural reporter via dual-frequency two-dimensional infrared spectroscopy", *The Journal of Chemical Physics*, Vol. 133, No. 14, (2010), 144513. (<https://doi.org/10.1063/1.3482708>).
 31. Raman, L.A., Deepanraj, B., Rajakumar, S. and Sivasubramanian, V., "Experimental investigation on performance, combustion and emission analysis of a direct injection diesel engine fuelled with rapeseed oil biodiesel", *Fuel*, Vol. 246, (2019), 69-74. (<https://doi.org/10.1016/j.fuel.2019.02.106>).
 32. Srinivasan, G.R., Palani, S., Munir, M., Saeed, M., Thangavelu, L., Mohanam, A. and Jambulingam, R., "Engine characteristics study on beef tallow biodiesel produced by ethanol based co-solvent transesterification", *Energy Sources, Part A: Recovery, Utilization, and Environmental Effects*, (2020), 1-21. (<https://doi.org/10.1080/15567036.2020.1826014>).
 33. Miron, L., Chiriac, R., Brabec, M. and Bădescu, V., "Ignition delay and its influence on the performance of a diesel engine operating with different diesel–biodiesel fuels", *Energy Reports*, Vol. 7, (2021), 5483-5494. (<https://doi.org/10.1016/j.egy.2021.08.123>).
 34. Brezinsky, K., "The high-temperature oxidation of aromatic hydrocarbons", *Progress in Energy and Combustion Science*, Vol. 12, No. 1, (1986), 1-24. ([https://doi.org/10.1016/0360-1285\(86\)90011-0](https://doi.org/10.1016/0360-1285(86)90011-0)).
 35. Talibi, M., Hellier, P. and Ladommatos, N., "Impact of increasing methyl branches in aromatic hydrocarbons on diesel engine combustion and emissions", *Fuel*, Vol. 216, (2018), 579-588. (<https://doi.org/10.1016/j.fuel.2017.12.045>).
 36. Siegl, W.O., McCabe, R.W., Chun, W., Kaiser, E.W., Perry, J., Henig, Y.I., Trinker, F.H. and Anderson, R.W., "Speciated hydrocarbon emissions from the combustion of single component fuels, I. Effect of fuel structure", *Journal of the Air & Waste Management Association*, Vol. 42, No. 7, (1992), 912-920. (<https://doi.org/10.1080/10473289.1992.10467041>).
 37. Jambulingam, R., Shankar, V., Palani, S. and Srinivasan, G.R., "Effect of dominant fatty acid esters on emission characteristics of waste animal fat biodiesel in CI engine", *Frontiers in Energy Research*, Vol. 7, (2019), 63. (<https://doi.org/10.3389/fenrg.2019.00063>).
 38. Hellier, P., Talibi, M., Eveleigh, A. and Ladommatos, N., "An overview of the effects of fuel molecular structure on the combustion and emissions characteristics of compression ignition engines", *Proceedings of the Institution of Mechanical Engineers, Part D: Journal of Automobile Engineering*, Vol. 232, No. 1, (2017), 90-105. (<https://doi.org/10.1177/0954407016687453>).



Research Article

Energy Management of Multi-Microgrids in Joint Energy and Ancillary Service Market Considering Uncertainties of Renewables

Ritu Jain, Vasundhara Mahajan *

Department of Electrical Engineering, Sardar Vallabhbhai National Institute of Technology, P. O. Box: 395007, Surat, Gujarat, India.

PAPER INFO

Paper History:

Received: 14 February 2022

Revised: 05 August 2022

Accepted: 07 August 2022

Keywords:

Renewable Energy Sources,
Energy Management,
Multi-Microgrid,
Energy Market,
Ancillary Service Market

ABSTRACT

In this study, energy management of grid-connected Multi-Microgrid (MMG) is performed through joint optimization of the energy and ancillary service market. The test system comprises the IEEE 30 bus system as the main grid and the 16-bus system as an MMG. The MMG is comprised of dispatchable and non-dispatchable generation and loads. The non-dispatchable generators are based on renewable energy sources (RES) such as solar and wind. The uncertainty modeling for wind and solar is performed by Weibull and beta probability distribution function. The strategic integration of RES helps MMG deliver both energy and ancillary services to the utility grid. This research aims to reduce the total energy cost while reducing reserve cost by maximizing the use of RES under normal operation and during contingency conditions. It is observed that if MMG is incorporated into the system, then the total generation cost, reserve cost, and power losses are reduced to 0.11 %, 0.325 %, and 1.201 %, respectively, in normal operating conditions. Under contingency, when Generator 5 is out of service and the main grid is operating alone, the total generation cost increased significantly from 22118.92 \$ day⁻¹ to 22435.68 \$ day⁻¹ and the real power loss increased from 233.35 MW day⁻¹ to 245.11 MW day⁻¹. However, by interconnecting MMG with the main grid, generation cost and power loss get reduced to 22375.60 \$ day⁻¹ and 243.35 MW day⁻¹, respectively. It is analyzed that participation of MMG provides techno-economic benefits during normal operation and contingency conditions.

<https://doi.org/10.30501/jree.2022.329343.1334>

1. INTRODUCTION

Competition in the restructured power market is a driving force for price minimization and social benefit maximization. Co-optimization of energy and reserve markets is used by several independent system operators (ISO), including Pennsylvania–Jersey–Maryland (PJM), California ISO, New York ISO (NYISO), New England ISO (ISO-NE), Australian, and New Zealand markets [1, 2]. The ISO coordinates energy and reserve dispatch to reduce total operating costs while meeting load demand and reserve requirements as well as staying within network limits [3]. In this paradigm, ISO considers the overall offered cost to be the market cost, and determine payments for clearing energy and reserve bids using a settlement process. Three price resolution procedures are employed in energy markets: uniform pricing system, pay-as-bid, and LMP-based scheme (Locational Marginal Price). All accepted offers/bids are paid at the uniform market clearing price (MCP) in a uniform pricing scheme. Each accepted offer is paid according to the offer price rather than the MCP in pay-as-bid. Accepted offers are paid based on locational marginal price in the LMP-based technique [4].

*Corresponding Author's Email: vmahajan@eed.svnit.ac.in (V. Mahajan)
URL: https://www.jree.ir/article_156095.html

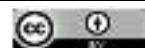
In this paper, LMP-based pricing scheme is used for market price settlement. There are different methods used by ISO for clearing Energy Market (EM) and Ancillary Services Market (ASM) [5]. These are explained below:

Merit Order Dispatch (MOD): This is the basic form of dispatch where the independent stacks of the quantity of the energy and offers are considered for the EM and ASM. The bid blocks are then arranged based on merit. The energy market is then dispatched until the supply is equal to the demand. The same process is repeated for the AS market. This approach is simple and easy to understand when there is a coupling between EM and AS markets. However, this will lead to infeasible results when there is no coupling between products. The coupling means that the sum of energy and reserve dispatch is less than the unit limit.

Sequential dispatch optimization: This is the extension for MOD. Herein, both the energy market and the ASM have the same generation capacity. The EM and ASM are dispatched separately and sequentially. The EM is cleared first, followed by the clearing of the ASM. It is easy to determine the winner because both markets are dispatched separately.

Joint or simultaneous optimization: The goal of this technique is to distribute several indivisible items to a group of bidders while minimizing the collective bid cost of

Please cite this article as: Jain, R. and Mahajan, V., "Energy management of multi-microgrids in joint energy and ancillary service market considering uncertainties of renewables", *Journal of Renewable Energy and Environment (JREE)*, Vol. 10, No. 2, (2023), 95-107. (<https://doi.org/10.30501/jree.2022.329343.1334>).



delivering energy and ancillary services. It is difficult to justify the schedule and pricing with this mechanism. As compared to MOD and sequential techniques, this technique has a strong coupling between the products.

Authors in [2, 6-10] presented several models for market clearing of joint energy and reserve auctions in which the energy and reserve offer costs were minimized while static and dynamic security criteria, such as the voltage drop and overloading indices, as well as corrected transient energy and voltage stability margins (VSMs) were also taken into account. In Ref. [2], the joint energy and reserve market clearance was performed considering the proposed multi-objective optimization problem, i.e., the payment cost minimization and voltage stability maximization. However, the stochastic nature of RES is not considered in this paper. In Ref. [6], a multi-market paradigm is proposed to facilitate the trading of energy and ancillary services across nano-grids in an islanded microgrid (MG). However, energy management in the grid interconnected mode is not considered in this work. In Ref. [10], simultaneous optimization of energy and reserve market is performed for IEEE 39 bus test system. In this study, wind and solar plant with PSP-based energy storage is integrated with the system, but uncertainty modeling for RES is not performed.

The primary factor contributing to the fast depletion of fossil fuels and rise of the green-house gas (GHG) emissions is the rapid rise in load demand. In order to overcome these issues, the world is moving towards the deployment of renewable-based distributed generation. The integration of these distributed generations (DG) with grid introduces the concept of microgrid [11]. A microgrid is a group of micro sources, loads, and batteries that represents itself as a single entity which can reciprocate the control signals sent by the central control center. MG is a low-voltage intelligent distributed network that is composed of micro sources or distributed generations, energy storage devices (ESD), and loads [12, 13]. In the case of the grid, it is termed as the controlled entity which can be operated as the aggregated load and as a micro source for power and ancillary services. From the consumer side, it is termed as the low-voltage distribution system [14]. Microgrids have a self-healing ability, thus improving the reliability of the distribution network by minimizing the chances of load shedding [15, 16], increasing the power quality, reducing carbon emissions [17, 18], and decreasing the price by optimally scheduling the renewable energy sources [19]. In addition, it supplies energy to remote areas [20]. Though the MG enjoys numerous benefits, the major issue faced by the microgrid central controller (MGCC) is to deal with the uncertainty of Renewable Energy Sources (RES) and to predict the generation from these sources accurately. The inaccuracy in prediction will result in failure of components and blackouts. The authors in [21] maintained that wind and solar were the fastest growing and most attractive RESs for electricity production. They identified wind and solar energy potentiality for four cities of Iran including Ahvaz, Sirjan, Neyshabur, and Tabriz. The results show the comparative analysis of wind and solar power generation potential for four cities. The wind turbine type and solar photovoltaic (PV) panel should be compatible with the geographical location and environmental conditions of the selected site for installation. In [22], the Technique of Order Preference by Similarity to Ideal Solution (TOPSIS) approach was used to determine the most compatible turbine with

respect to the geographical and topological characteristics of the location under consideration. In [23], the effect of environmental and turbine parameters on the energy gains from wind farm was investigated. The Artificial Neural Network (ANN) model was developed, which demonstrated how energy gain increased with increase in annual mean wind speed. In [24], multi-group grey wolf optimizer (MG-GWO) was used to retrieve the parameters of a single-diode photovoltaic solar cell module. According to their results, the MG-GWO exhibited its superiority over classical GWO. There are various factors that affect the performance of wind turbine generator and solar PV panel. The output of solar panel depends on the ambient conditions, intensity of solar irradiance falling on it, and module temperature [25, 26]. Solar insolation is affected by the dust accumulating on the panel [27] or by partial shading of solar panel [28]. The performance of a solar PV plant can be improved by cooling technology [29] or shade dispersion technique explained in [30].

The main feature of MG is that it can be operated in the grid-connected and islanded modes. The decision on the mode of operation is taken by MGCC considering the economic and security constraints. The MG usually operates in the grid-connected mode for the economic operation of the power system. However, if it is operating in the standalone mode, then it should have sufficient capacity to supply its load during emergency conditions. The MG is isolated from the main grid through switches at the point of common coupling [31]. In the grid-connected mode, MG provides the reserved energy to the main grid in cases of (a) a sudden increase in load demand, (b) reduction in energy generation from Conventional Generators (CGs), or (c) inaccurate load forecast [32]. There is an extensive scope of literature available on optimal scheduling of MG in the grid-connected mode [33-35], but quite a limited literature is available on the islanded operation of MG. The optimal energy management of MG can be done in a centralized or decentralized manner. In the centralized method, all the information regarding the available generation and load is collected for centralized operation and control [36], whereas in the decentralized method, every entity is considered as an agent which is free to take decisions [37]. For the systematic operation of MG in the interconnected mode, it is required that MGCC be coordinated with grid operations. Four different control strategies for energy management in MMGs were explained in Ref. [38]. First is the centralized control, in which all the generation and consumption devices are controlled by the central controller, but it fails to protect the customer privacy. Its main objective is to maximize profit of the whole MMG system. The MMG in this case operates at a very high risk given that the whole system will get affected if the centralized control fails. In decentralized control, individual MG is an autonomous entity that has a local controller (LC) to maximize its profit. The LC manages the MG and determines the operating point of generation and loads. Failure of one LC will not result in the failure of the operation of MMG. However, this method will introduce a competitive environment between the MGs to maximize their profit. In hybrid control, the central controller is at the MMG level and the local controller at the MG level. The LC performs local energy management and informs the central controller about the surplus/deficit of energy. Then, the central controller negotiates with multi-MG for its reliable operation. Thus, it is a two-level controlled strategy. The last one is the nested multi-microgrid energy management system

(MMGEMS). It is a hierarchical structure with multiple levels, and each microgrid constitutes a level of the whole MMG system. The privacy of customers with this control scheme can be preserved due to the multiple-layered privacy structure. The functionalities and operations of MGs were explained in [39]. In this study, the multi-agent system for the operation of the integrated MG was explained. A hierarchical control scheme was utilized for maximizing the production of DG and optimizing the power exchange between MGs and the grid. A novel double-layer coordinated control approach to MG was proposed in [40]. The schedule layer operates on the forecasted data and the dispatch layer provides power for controllable units in real time. The error between the two layers is resolved by their coordinated control.

According to the literature review, it is observed that much of the literature is focused on the islanded operation of the MG. However, a limited scope of the literature has focused on the joint optimization of the energy and ancillary services market of MMG in interconnected operation with the main grid considering the uncertainty of wind and solar. In this study, the uncertainty modeling for wind speed and solar irradiance is done through beta-Weibull probability distribution function (pdf). Also, this work considered the (N-1) contingency analysis. The contingency considered is generator and line outage. The energy management of MMG in the grid interconnected mode is performed by joint optimization of the EM and Reserve Market (RM). Generally, the RES is thought of as the consumer of ramping services due to their variability and intermittent nature. However, when these sources are integrated with fast ramping generators (micro-turbine and energy storage system), they can support the grid by providing reserves in the ASM. Thus, MMG considered in this work is composed of dispatchable and non-dispatchable generators as well as loads.

The rest of the paper is organized as follows. Section II shows the problem formulation and modeling of wind and solar power. Section III outlines the results and discussion. Section IV concludes the paper.

2. PROBLEM FORMULATION AND UNCERTAINTY MODELING

2.1. Objective function

The aim of this study is to minimize the energy and reserve costs by utilizing the energy available with RES in the MMG system. The market model considered in this paper is based on a joint dispatch mechanism. The simplicity and transparency of this mechanism are the main reasons behind the widespread use of this approach. In simultaneous or joint optimization, the ISO task is to match consumer demand with power plant capability in the most cost-effective manner while maintaining system stability and security. The goal is to achieve the following criteria by procuring energy and reserves at the lowest possible cost. In the deregulated power market, generating companies (GenCo) and distribution company (DisCo) submit their bids for the energy and reserve market in day-ahead of actual schedule. In this work, only the generator side bidding for energy is considered. There is no bidding from the consumer side. The cost minimization problem was given in [10], which was modified in this study. The proposed objective function is shown in Eq. 1. The proposed approach and its flowchart are shown in Figure 1 and Figure 2, respectively.

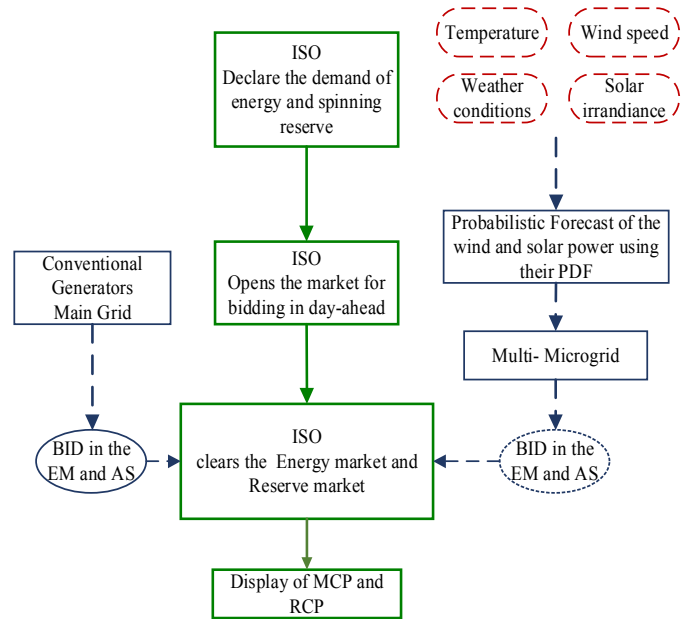


Figure 1. Proposed approach for joint optimization of energy and ancillary market

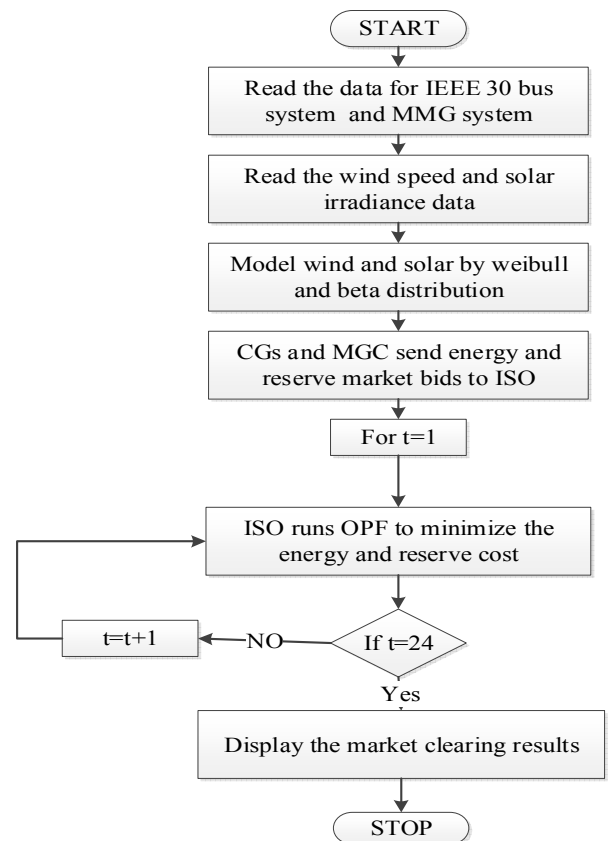


Figure 2. Flowchart of the proposed approach

$$\min TC = \sum_{h=1}^{24} \left(\sum_{i=1}^{N_G} \{CE_i(P_i) + CR_i(R_i)\} + \sum_{j=1}^{N_{MMG}} \{CE_j(P_j) + CR_j(R_j)\} \right) \quad (1)$$

The above objective is subjected to equality and inequality constraints. The equality constraints are binding constraints, whereas inequality constraints may or may not be binding. Here, P_i and R_i are the generations of the i^{th} unit of the main grid in the energy and reserve market, respectively. However, P_j and R_j are the generation of the j^{th} unit of MMG in energy

and reserve market, respectively. RR_i is the ramp rate of the i^{th} conventional generator (CG) at the main grid, h is the number of hours, and N_G and N_{MMG} represent the number of generators in the grid and MMG, respectively. Here, $(P_{i,\max}-P_i)$ represents the maximum reserve available for CG.

$$\sum P_{G,k} = P_{\text{loss}} + P_{D,k} \quad (2)$$

$$\sum Q_{G,k} = Q_{D,k} + Q_{\text{loss}} \quad (3)$$

$$P_i + R_i \leq P_i \text{ max} \quad (4)$$

$$R_i = \min\{(P_{i,\max} - P_i), RR_i\} \quad (5)$$

$$P_j + R_j \leq P_j \text{ max} \quad (6)$$

$$P_{j\min} \leq P_j \leq P_{j\max} \quad (7)$$

$$P_{i\min} \leq P_i \leq P_{i\max} \quad (8)$$

$$P_{ij} \leq P_{ij\max} \quad (9)$$

$$V_{i\min} \leq V_i \leq V_{i\max} \quad (10)$$

2.2. Uncertainty modeling of RES

2.2.1. Wind speed modeling

The power output of a Wind Turbine Generator (WTG) depends on the wind speed [41]. As the wind speed increases, the power output of the wind energy increases approximately as the cube of the wind speed is shown in Eq. 11 as follows:

$$P_w = \frac{1}{2} \times \rho \times A \times v^3 \quad (11)$$

where P_w is the power generated from WTG, ρ the density of air in kg m^{-3} , A the area of blades in m^2 , and v the wind speed in m s^{-1} . Thus, the power generated from WTG is defined as in Eq. 12.

$$P_{WT} = \begin{cases} 0, v < v_{in}, v > v_{out} \\ P_r \times \frac{(v - v_{in})}{v_r - v_{in}}, v_{in} < v < v_r \\ P_r, v_r < v < v_{out} \end{cases} \quad (12)$$

Wind speed is variable and follows a Weibull PDF shown in Eq. 13 [42]:

$$f(v) = \frac{k}{c} \left(\frac{v}{c}\right)^{k-1} e^{-\left(\frac{v}{c}\right)^k} \quad (13)$$

For Rayleigh PDF, the value of k is 2. This is the preferred PDF as it has periods of both low and high wind speeds. Hourly mean wind speed and standard deviation of wind are used as the input data to create the pdf for wind speed.

2.2.2. Solar PV modeling

The generated power of the PV module is determined by the site's ambient temperature, solar irradiation, and module features. The beta distribution is used to model the solar irradiations. The solar irradiation follows the bimodal distribution, which is, combination of two unimodal distributions [43].

$$f_{pv}(ir) = \begin{cases} \left(\frac{\Gamma(\alpha+\beta)}{\Gamma(\beta)\Gamma(\alpha)}\right) \times ir^{\alpha-1} \times (1-ir)^{\beta-1}, & \text{for } 0 \leq ir \leq 1, \alpha \geq 0, \beta \geq 0 \\ 0, & \text{otherwise} \end{cases} \quad (14)$$

The values of alpha and beta can be calculated using Eq. 15:

$$\beta = (1 - \mu) \times \left(\frac{\mu \times (1 + \mu)}{\sigma^2} - 1\right) \quad (15)$$

$$\alpha = \frac{\mu \times \beta}{1 - \mu}$$

From the generated PDF, the output power of the solar is modeled, as shown in Eq. 16 to Eq. 20.

$$P_{pv}(h) = N \times FF \times V(h) \times I(h) \quad (16)$$

$$FF = \frac{V_{MPP} \times I_{MPP}}{V_{oc} \times I_{sc}} \quad (17)$$

$$V(h) = V_{oc} - k_v \times T_c \quad (18)$$

$$I(h) = S_a \times [I_{sc} + k_i(T_c - 25)] \quad (19)$$

$$T_c = T_a + S_a \times \left(\frac{N_{OT} - 20}{0.8}\right) \quad (20)$$

3. RESULTS AND DISCUSSION

In this study, IEEE 30 bus system is considered as the main grid, whereas the 16 bus test system is taken as the MMG system. The IEEE 30 bus system is composed of 6 generators, 41 transmission lines, and 21 loads [44, 45]. The MMG system is comprised of MG1, MG2, and MG3. The MG1 contains 1 wind turbine (WT), 1 micro turbine, 1 photovoltaic (PV), and 1 fuel cell and 5 loads. The MG2 is composed of 1 diesel generator, 1 PV, 1 WT, and 1 load. The MG3 has 2 WT, 1 PV, 1 CHP, and 7 loads. The MMG system data is taken from [46]. Figure 3 shows the system under study, and Figure 4 shows the architecture of the main grid. The data of solar irradiation and wind speed is taken from [47, 48]. The wind and solar power available for a day is shown in Figure 5 and Figure 6, respectively. The load data of MMG shown in Figure 7 is taken from [49] and scaled for the considered test system. The load data for the main grid in the energy market and reserve market are shown in Figure 8, which were taken from [50], and normalized according to the system data. The demand of the reserve market is taken as 10 % of the demand in EM. Table 1 and Table 2 show the generator data and its cost coefficients for the main grid and MMG. The ramp rate is measured at almost 10 % of the maximum power.

Table 1. Generator data in the main grid

No.	Pmax (MW)	Energy price			Reserve price (\$ MW ⁻¹)	RR
		α	β	γ		
G1	200	0.00375	2	0	2.25	15
G2	80	0.0175	1.75	0	2	8
G3	50	0.0625	1	0	1.5	5
G4	35	0.00834	3.25	0	3.5	3
G5	30	0.025	3	0	3.25	3
G6	40	0.025	3	0	3.35	4

Table 2. Dispatchable and non-dispatchable units in MMG

No.	Gen	Pmax (MW)	Energy price (\$ MW ⁻¹)	Reserve price (\$ MW ⁻¹)
MG1	WT1	2	1.5	1.5
	PV1	1	1.5	1.5
	FC	1	2	2.25
	MT	1.5	2.25	2.5
MG2	PV2	1.2	1.5	1.5
	DG	0.8	2.5	2.75
	WT2	1	1.5	1.5
MG3	WT3	1	1.5	1.5
	PV3	1.1	1.5	1.5
	CHP	0.4	2	2.25
	WT4	1	1.5	1.5

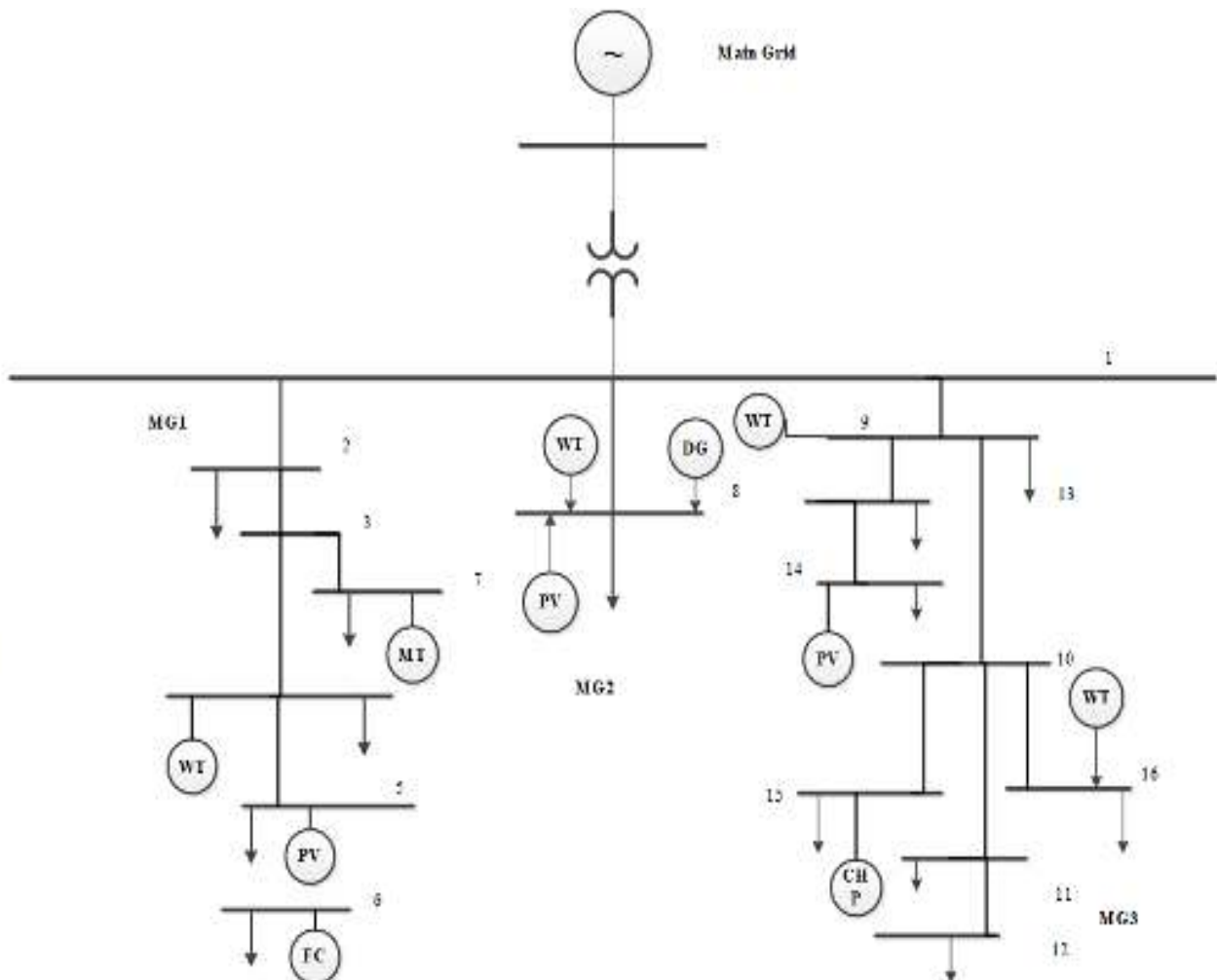


Figure 3. Test system



Figure 4. Main Grid (IEEE 30 bus system)

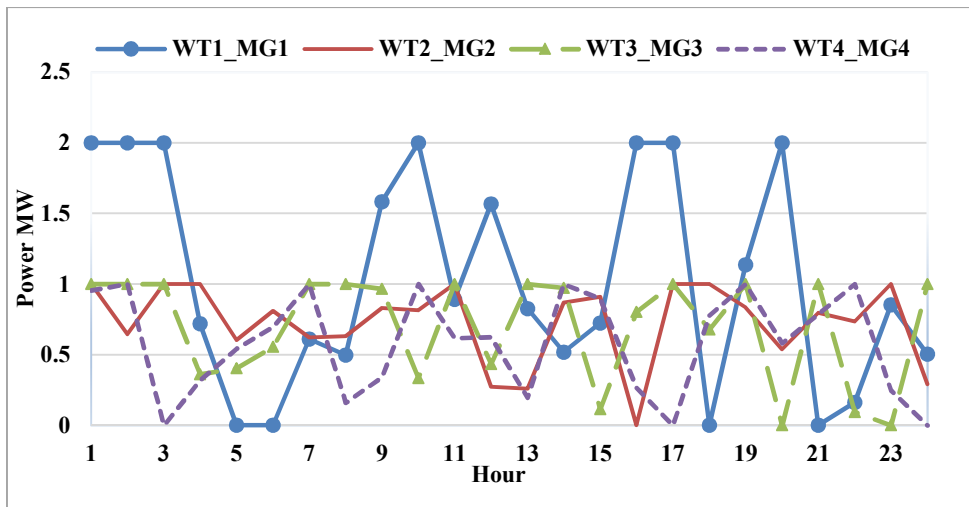


Figure 5. Available wind power in MMG

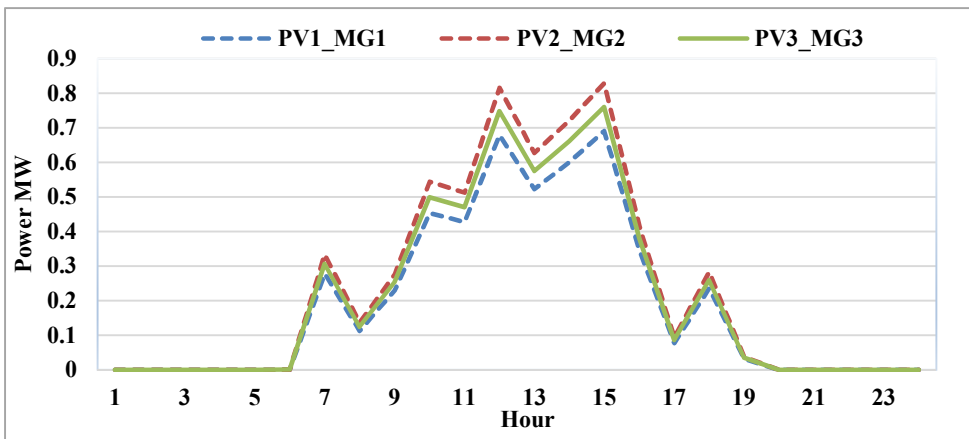
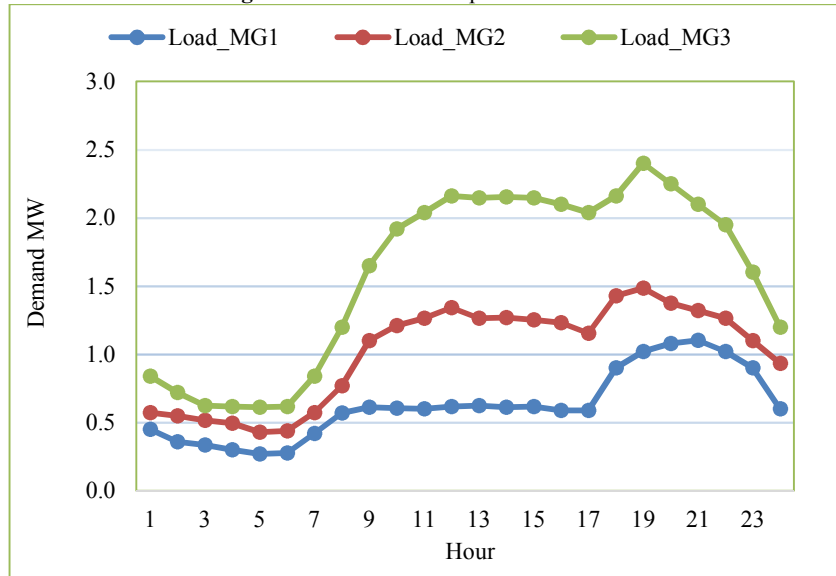
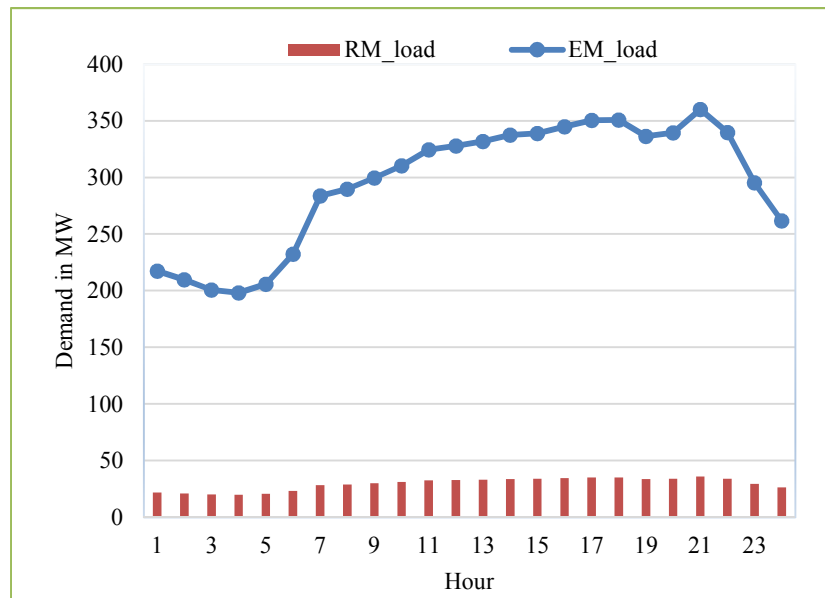


Figure 6. Available solar power in MMG**Figure 7.** Load data of MMG**Figure 8.** Load demand in EM and RM

The study is divided into three cases. The contingency analysis is also performed for all three cases. The considered contingencies are as follows: conventional generator No. 5 (G5) is out of service, line 3 outage, line 6 outage, and line 8 outage of the main grid (IEEE 30 bus system).

Case 1: When CGs in the main grid participate in EM and ASM.

Case 2: CGs will engage in EM and RM, whereas MMG will participate in EM.

Case 3: When MMG and the main grid both will engage in EM and ASM.

Case 1: When CGs in the main grid participate in EM and ASM

In this case, only CGs will engage in EM and RM. The ramp rate of CGs is taken as almost 10 % of the maximum power of the generator. The maximum reserve of each generator is taken as the maximum capacity minus the power generated at

peak load. The CGs will bid energy at a higher price in RM than EM to gain maximum profit in the reserve market. They send their bid of energy and price for both of the markets to the ISO. The ISO will perform simultaneous optimization for both markets according to the bids received from the CGs. The reserve capacity available by each CG is equal to the minimum of maximum reserve bid by the generator and its 10 mins ramp rate. The power generated by generators in EM and RM should always be less than or equal to the maximum power available. The energy dispatched by CGs in the energy and reserve market is shown in Figure 9 and Figure 10, respectively. The hourly generation cost is EM and RM in Case 1 (no outage) is shown in Figure 11. The total cost including energy and reserve for a day is 22118.92 \$ day⁻¹. The total reserve cost and power loss are 1540.299 \$ day⁻¹ and 233.3481 MW, respectively. The payment total load is 27534.04 \$ day⁻¹. The Table 3 shows the comparative analysis between Case 1 (no outage case) and different contingency conditions. When compared with Case 1 (no outage), the % increment rates in the generation cost, reserve cost, and power

loss in Case 1 with gen outage are 1.43 %, 0.47 %, and 5.04 %, respectively. Similarly, due to the outage of Line 3 of the main grid (the line connecting Buses 2 and 4), The % increment rates in the generation cost and power loss are 0.26 % and 6.01 %. The outage of Line 6 of the main grid (connecting bus 2 and 6) increases the generation cost and power loss by 0.46 % and 10.79 %, respectively. The outage of Line 8 (connecting buses 5 and 7) will increase the generation cost and power loss by 0.019 % and 0.44 %, respectively. From the results, it can be concluded that the outage of the generator has a significant effect on the total generation cost, reserve cost, and active power loss of the system. However, the line outage is not affecting the reserve cost, but has a significant effect on the generation cost and power loss. The reserve cost is the same in all the cases because only three CGs (G1, G2, and G3) are participating in supplying the demand in the reserve market and these line outages are not affecting their generation in each hour.

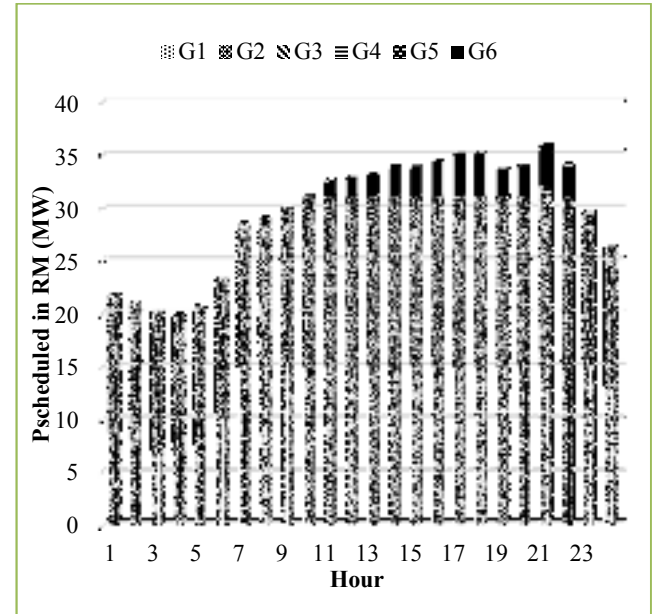


Figure 9. Power scheduled in the energy market in day-ahead market in Case 1 (no outage)

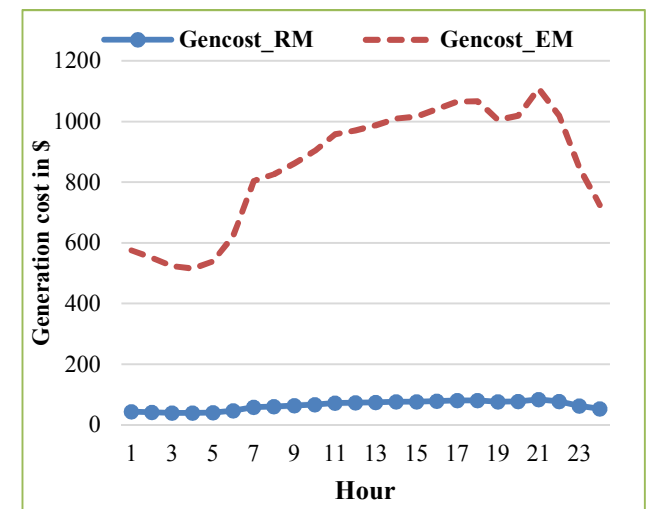


Figure 10. Power scheduled in reserve market in day-ahead market in Case 1 (no outage)

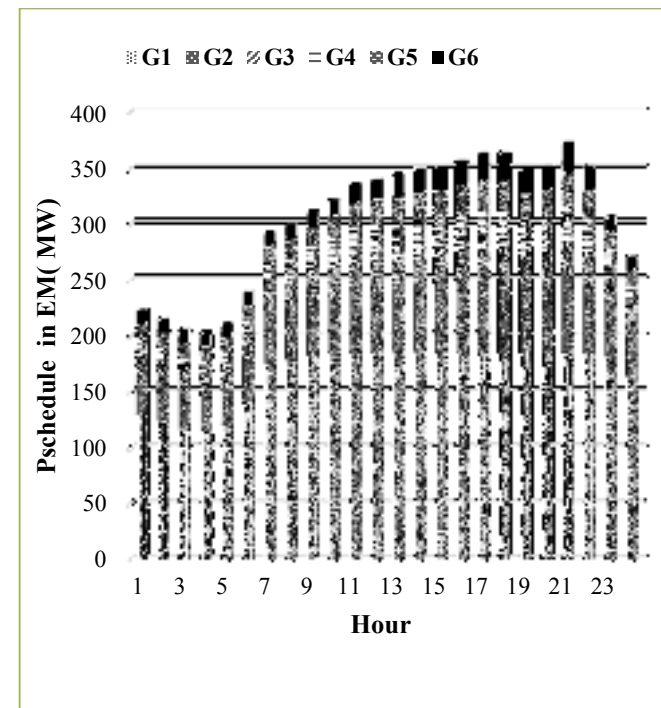


Figure 11. Hourly generation cost in EM and RM market in Case 1 (no outage)

Table 3. Comparative analysis between Case 1 (no outage) and different contingency conditions

Case 1	Generation cost (\$ day ⁻¹)	Reserve cost (\$ day ⁻¹)	Power loss (MW day ⁻¹)	% increment in gen cost	% increment in reserve cost	% increment in power loss
No outage	22118.92	1540.29	233.35	-	-	-
Gen5 out	22435.68	1547.55	245.11	1.43	0.47	5.04
Line 3 out	22176.43	1540.29	247.37	0.26	0	6.01
Line 6 out	22222.54	1540.3	258.54	0.46	0	10.79
Line 8 out	22123.23	1540.29	234.39	0.019	0	0.44

Case 2: When CGs will engage in EM and RM, MMG will participate in EM

In this case, the MMG will participate in the energy market, but the CGs will engage in both markets. The presence of MMG in EM will affect the dispatch of CGs in EM, whereas the reserve market will be the same as in Case 1. In this case, the RES available in MMG will dispatch to its full limit in energy market. This will reduce the energy cost in EM,

because the RES is the cheaper source than the CGs. Maximum energy transferred from MMG to the main grid is 6 MW. The power schedule by MMG in EM, load, and power transfer from MMG to the main grid is shown in Figure 12. From the Figure 12, it is observed that the MMG will first satisfy its load and then, transfer the surplus power to the main grid. The comparative analysis between Case 2 (no outage) and its contingency cases is shown in Table 4. When compared with Case 2 (no outage), the % increments in the

generation cost, reserve cost, and power loss in Case 2 with generator outage are 1.36 %, 0.40 %, and 5.16 %, respectively. Similarly, due to the outage of Line 3 of the main grid (a line connecting Buses 2 and 4), the % increment rate in the generation cost and power loss are 0.25 % and 5.88 %. The outage of Line 6 of the main grid (connecting Buses 2 and 6) increases the generation cost and power loss by 0.45 % and 10.47 %, respectively. The outage of Line 8 (connecting Buses 5 and 7) will increase the generation cost and power loss by 0.023 % and 0.55 %, respectively. The outage of Line 8 is having the least impact on the generation cost and the power loss. The Table 5 shows the power dispatch from various sources in MMG in the energy market. In this case, it is also observed that the RES is fully utilized in EM. The power scheduled by CGs in EM is reduced mainly in the valley period, i.e., from hour 1 to hour 10 and shown in Figure 13. In Case 2 (no outage), the total energy cost is 22096.71 \$ day⁻¹ and the reserve cost will be the same as in

Case 1. The power loss and load payments are 230.593 MW day⁻¹ and 27522.61 \$ day⁻¹, respectively.

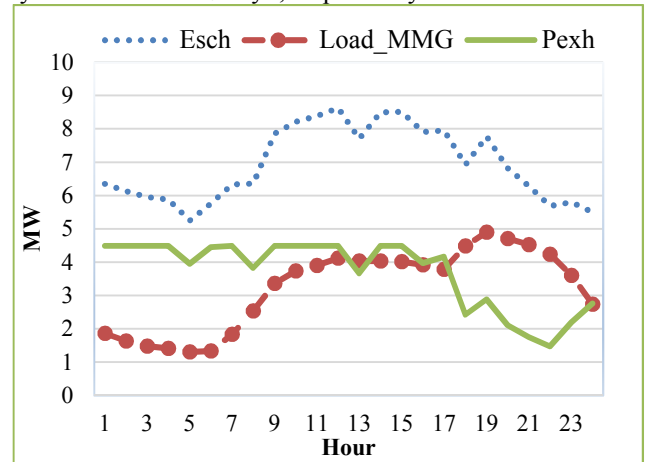


Figure 12. Energy scheduled, load, and Pexh in MMG

Table 4. Comparative analysis between Case 2 (no outage) and different contingency conditions

Case 2	Generation cost (\$ day ⁻¹)	Reserve cost (\$ day ⁻¹)	Power loss (MW day ⁻¹)	% increment in gen cost	% increment in reserve cost	% increment in power loss
No outage	22096.71	1540.29	230.59	-	-	-
Gen5 out	22396.13	1546.49	242.48	1.36	0.40	5.16
Line 3 out	22151.79	1540.29	244.16	0.25	0	5.88
Line 6 out	22195.44	1540.29	254.74	0.45	0	10.47
Line 8 out	22101.81	1540.30	231.85	0.023	0	0.55

Table 5. Power dispatch (MW) in MMG

No.	WT1 MG1	PV1 MG1	FC MG1	MT MG1	PV2 MG2	DG MG2	WT MG2	WT1 MG3	PV3 MG3	CHP MG3	WT2 MG3
1	2.00	0.00	1.00	0.00	0.00	0.00	1.00	1.00	0.00	0.40	0.95
2	2.00	0.00	1.00	0.08	0.00	0.00	0.64	1.00	0.00	0.40	1.00
3	2.00	0.00	1.00	0.55	0.00	0.00	1.00	1.00	0.00	0.40	0.00
4	0.72	0.00	1.00	1.50	0.00	0.58	1.00	0.36	0.00	0.40	0.32
5	0.00	0.00	1.00	1.50	0.00	0.80	0.60	0.40	0.00	0.40	0.54
6	0.00	0.00	1.00	1.50	0.00	0.80	0.81	0.56	0.00	0.40	0.70
7	0.61	0.28	1.00	0.78	0.33	0.00	0.62	1.00	0.31	0.40	1.00
8	0.50	0.11	1.00	1.50	0.14	0.80	0.63	1.00	0.12	0.40	0.16
9	1.58	0.23	1.00	1.50	0.28	0.48	0.83	0.97	0.25	0.40	0.34
10	2.00	0.45	1.00	1.17	0.54	0.00	0.82	0.33	0.50	0.40	1.00
11	0.89	0.43	1.00	1.50	0.51	0.57	1.00	1.00	0.47	0.40	0.62
12	1.57	0.68	1.00	1.50	0.82	0.59	0.27	0.43	0.75	0.40	0.62
13	0.82	0.52	1.00	1.50	0.63	0.80	0.26	1.00	0.57	0.40	0.20
14	0.52	0.60	1.00	1.50	0.72	0.27	0.87	0.97	0.66	0.40	1.00
15	0.72	0.69	1.00	1.50	0.83	0.69	0.91	0.12	0.76	0.40	0.90
16	2.00	0.35	1.00	1.50	0.41	0.80	0.00	0.80	0.38	0.40	0.27
17	2.00	0.08	1.00	1.50	0.09	0.80	1.00	1.00	0.09	0.40	0.00
18	0.00	0.24	1.00	1.50	0.28	0.80	1.00	0.68	0.26	0.40	0.78
19	1.14	0.03	1.00	1.50	0.04	0.80	0.83	1.00	0.04	0.40	1.00
20	2.00	0.00	1.00	1.50	0.00	0.80	0.54	0.00	0.00	0.40	0.58
21	0.00	0.00	1.00	1.50	0.00	0.80	0.80	1.00	0.00	0.40	0.79
22	0.16	0.00	1.00	1.50	0.00	0.80	0.74	0.09	0.00	0.40	1.00
23	0.85	0.00	1.00	1.50	0.00	0.80	1.00	0.00	0.00	0.40	0.25

24	0.50	0.00	1.00	1.50	0.00	0.80	0.29	1.00	0.00	0.40	0.00
----	------	------	------	------	------	------	------	------	------	------	------

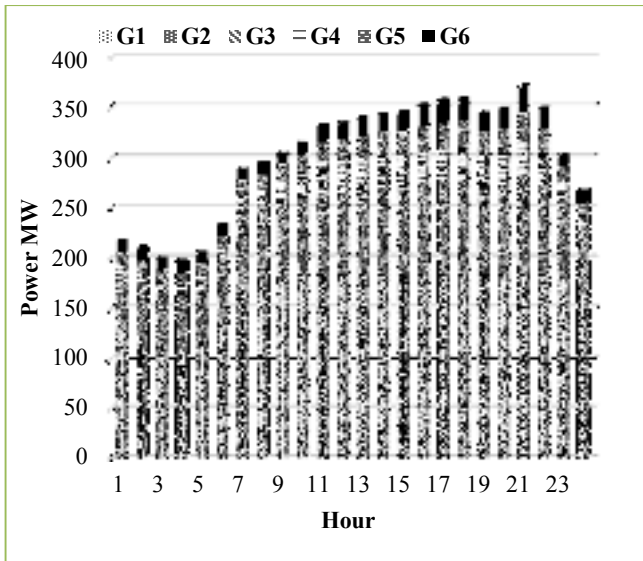


Figure 13. Power schedule by CGs in EM in Case 2 (no outage)

(which connects Buses 5 and 7) will raise the cost of generation by 0.023 % and the power loss by 0.54 %. The summary of all the cases with no contingency is shown in Table 7. It is observed that in case of the generator outage (G5 out) in the main grid, the total generation cost increased significantly from 22118.92 \$ day⁻¹ to 22435.68 \$ day⁻¹ and the real power loss increased from 233.35 MW day⁻¹ to 245.11 MW day⁻¹. However, due to the participation of MMG, generation cost and power loss are reduced to 22375.60 \$ day⁻¹ and 243.35 MW day⁻¹, respectively. Similarly, if we consider the case of Line 3 outage, when only CGs of the main grid are contributing to EM and RM in Case 1, the generation cost and power losses are 22176.43 \$ day⁻¹ and 247.377 MW day⁻¹, respectively. However, in case of the same contingency of Line 3 outage, if we take Case 3 when MMG is contributing to the EM and RM, generation cost and power loss are reduced to 22149.38 \$ day⁻¹ and 244.165 MW day⁻¹, respectively. From the results, it can be concluded that the participation of MMG in EM and RM will not only bring about economic and technical benefits to the power system during normal conditions but also support the main grid during contingency conditions.

Case 3: When MMG and the main grid both will engage in EM and ASM

In this case, the conventional as well as the DGs in MMG will participate in both markets. This will affect the dispatch of CGs in the reserve market. As in the previous case, they are dispatched in RM though they have a higher cost. The maximum reserve of DGs in MMG is taken as 50 % of the installed capacity. The dispatch of DGs in RM is shown in Figure 14. From Figure 14, it is observed that all dispatchable DGs are either dispatched in EM or result from their high cost not dispatched in RM. The total energy cost and reserve cost in this case are 22094.30 \$ MW⁻¹ and 1534.86 \$ MW⁻¹, respectively. The power loss and total load payment are 230.58 \$ MW⁻¹ and 27542.5 \$ day⁻¹. The comparative analysis between Case 3 (no outage) and contingency cases is shown in Table 6. Compared to Case 3 (no outage), the percentage of increase in generating cost, reserve cost, and power loss is 1.27 %, 0.49 %, and 5.53 %, respectively, in Case 3 with generator outage. Similarly, owing to the outage of Line 3 of the main grid (the line linking Buses 2 and 4), the generation cost and power loss increased by 0.25 % and 5.89 %, respectively. The failure of Line 6 of the main grid (which connects Buses 2 and 6) increases the generating cost by 0.46 % and the power loss by 10.47 %. The loss of Line 8

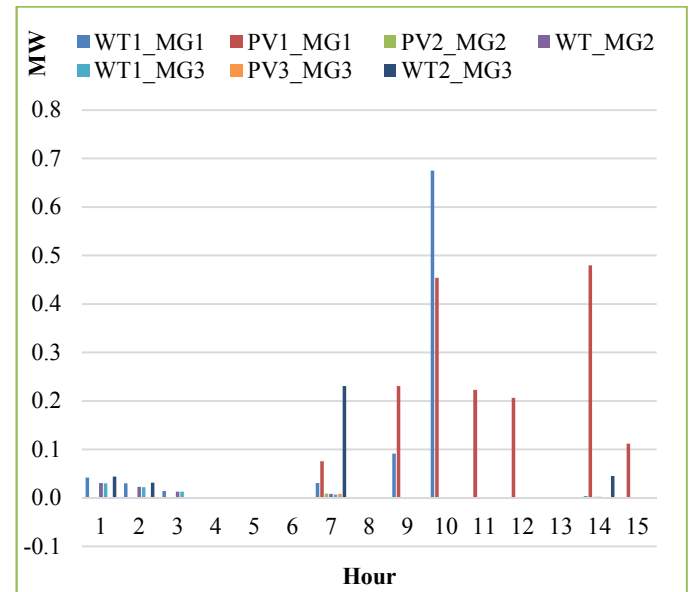


Figure 14. Dispatch of RES-based DG in MMG in the RM

Table 6. Comparative analysis between Case 3 (no outage) and different contingency conditions

Case3	Generation cost (\$ day ⁻¹)	Reserve cost (\$ day ⁻¹)	Power loss (MW day ⁻¹)	% increment in gen cost	% increment in reserve cost	% increment in power loss
No outage	22094.3	1534.86	230.58	-	-	-
Gen5 out	22375.61	1542.52	243.35	1.27	0.49	5.53
Line 3 out	22149.38	1534.86	244.17	0.25	0	5.89
Line 6 out	22193.02	1534.86	254.73	0.46	0	10.47
Line 8 out	22099.39	1534.86	231.83	0.023	0	0.54

Table 7. Comparison between base cases in case of no outage

No. outage cases	Total Gencost (\$ day ⁻¹)	Total reserve cost (\$ day ⁻¹)	Power loss MW day ⁻¹	% reduction in Gencost	% reduction in Rcost	% reduction in Ploss
Case1	22118.92	1540.29	233.35	-	-	-
Case2	22096.71	1540.29	230.593	0.104	-	1.181

Case3	22094.3	1534.86	230.58	0.111	0.352	1.201
-------	---------	---------	--------	-------	-------	-------

4. CONCLUSIONS

In this study, the energy management of multi-microgrids was performed in the joint energy and ancillary service market. The MMG was composed of dispatchable and non-dispatchable DGs and loads. The RES was considered as the consumers of ramping services due to its volatile nature. However, when they are strategically placed in integration with other sources, they can provide energy in both the energy market and ancillary services market. In this study, the MMG strategically contributed to both the energy and ancillary services market by effectively utilizing all its resources. In Case 1, when there were only CGs, the energy and reserve cost was high and power loss was also high. However, through the participation of MMG in the energy and reserve market, the total generation cost, reserve cost, and power loss were reduced to 0.11 %, 0.325 %, and 1.201 %, respectively. In this study, the system was subjected to N-1 contingency and it was observed that MMG would support the grid in not only normal operation but also contingency conditions. During contingency, the contribution of MMG to EM and RM would reduce the generation cost, reserve cost, and power loss as compared to the case when only CGs would be present in the system. This study can be further extended by the placement of energy storage for effectively utilizing the surplus RES available.

5. ACKNOWLEDGEMENT

The authors are thankful to Sardar Vallabhbhai National Institute of Technology for providing good research environment.

NOMENCLATURE

TC	Total cost (\$/MW)
$CE_i(P_i)$	Energy cost of i^{th} CG of main grid (\$/MW)
$CR_i(R_i)$	Reserve cost of i^{th} generator of main grid (\$/MW)
P_i	Active power dispatch by i^{th} CG of main grid (MW)
R_i	Reserve power available with i^{th} CG (MW)
$CE_j(P_j)$	Energy cost of j^{th} generator of MMG (\$/MW)
$CR_j(R_j)$	Reserve cost of j^{th} generator of MMG (\$/MW)
P_j	Active power dispatch by j^{th} generator of MMG (MW)
R_j	Reserve power available j^{th} generator of MMG (MW)
i	Generator number in main grid
j	Generator number in MMG
N_G	Total number of CGs in main grid
N_{MMG}	Total number of generators in MMG
h	Hour (1 to 24)
RR_i	Ramp rate of i^{th} CG in main grid (MW/min)
$V(h)$	Voltage of PV cell at h hour (volts)
V_{OC}	Open circuit voltage
I_{SC}	Short circuit current
V_{MPP}	Voltage at maximum power point
P_{pv}	Power generated by PV module
α	Cost coefficient (\$/MW ² h)
γ	Cost coefficient (\$/MW)
$P_{i,\text{max}}$	Maximum power available with i^{th} generator
V_{min}	Minimum voltage
V_{max}	Maximum voltage
P_{WT}	Power generated by WTG (MW)
P_r	Rated wind power (MW)
v_i	Actual wind speed (m/sec)
S_a	Solar irradiation (kW/m ²)
v_{in}	Cut-in wind speed (m/sec)

v_{out}	Cut-out velocity (m/sec)
k	Shape factor
c	Scale factor
σ	Standard deviation
μ	mean
N	Number of PV modules
FF	Fill factor
$I(h)$	Current of PV cell at h hour (amps)
I_{MPP}	Current at maximum power point
N_{OT}	Nominal operating temperature (°C)
T_a	Ambient temperature (°C)
T_c	Cell temperature (°C)
β	Cost coefficient (\$/MWh)

Abbreviation

ASM	Ancillary Services Market
CHP	Combined Heat Power
DER	Distributed Energy Sources
DG	Distributed Generation
Disco	Distribution Company
Ecost	Energy Cost
EM	Energy Market
FC	Fuel Cell
Genco	Generating Company
Gencost	Generation Cost
GHG	Green House Gas
ISO	Independent System Operator
LC	Local Controller
LMP	Locational Marginal Price
MCP	Market Clearing Price
MGCC	Microgrid Central Controller
MMG	Multi-Microgrid
MMGEMS	Multi-Microgrid Energy Management System
MT	Micro-Turbine
PDF	Probability Distribution Function
Ploss	Power Loss
PV	Photo Voltaic
Rcost	Reserve Cost
RES	Renewable Energy Sources
RM	Reserve Market
WTG	Wind Turbine Generator

REFERENCES

- Wang, J., Zhong, H., Tang, W., Rajagopal, R., Xia, Q., Kang, C. and Wang, Y., "Optimal bidding strategy for microgrids in joint energy and ancillary service markets considering flexible ramping products", *Applied Energy*, Vol. 205, (2017), 294-303. (<https://doi.org/10.1016/j.apenergy.2017.07.047>).
- Sardou, I.G., Khodayar, M.E., Khaledian, K., Soleimani-Damaneh, M. and Ameli, M.T., "Energy and reserve market clearing with microgrid aggregators", *IEEE Transactions on Smart Grid*, Vol. 7, (2015), 2703-2712. (<https://doi.org/10.1109/TSG.2015.2408114>).
- Guo, Z., Pinson, P., Chen, S., Yang, Q. and Yang, Z., "Chance-constrained peer-to-peer joint energy and reserve market considering renewable generation uncertainty", *IEEE Transactions on Smart Grid*, Vol. 12, (2020), 798-809. (<https://doi.org/10.1109/TSG.2020.3019603>).
- Jain, R. and Mahajan, V., "Technical and fiscal benefits of committing DG in energy market during contingency", *Proceedings of IEEE International Conference on Power Electronics, Drives and Energy Systems (PEDES)*, Chennai, India, (2018), 1-5. (<https://doi.org/10.1109/PEDES.2018.8707584>).
- Cheung, K.W., Shamsollahi, P., Sun, D., Milligan, J. and Potishnak, M., "Energy and ancillary service dispatch for the interim ISO New England electricity market", *Proceedings of the 21st International Conference on Power Industry Computer Applications. Connecting Utilities. PICA 99. To the Millennium and Beyond (Cat. No. 99CH36351)*, Santa Clara, CA, USA, (1999), 47-53. (<https://doi.org/10.1109/PICA.1999.779384>).

6. Hu, Q., Zhu, Z., Bu, S., Chan, K.W. and Li, F., "A multi-market nanogrid P2P energy and ancillary service trading paradigm: Mechanisms and implementations", *Applied Energy*, Vol. 293, (2021), 116938. (<https://doi.org/10.1016/j.apenergy.2021.116938>).
7. Zhang, K., Troitzsch, S., Hanif, S. and Hamacher, T., "Coordinated market design for peer-to-peer energy trade and ancillary services in distribution grids", *IEEE Transactions on Smart Grid*, Vol. 11, No. 4, (2020), 2929-2941. (<https://doi.org/10.1109/TSG.2020.2966216>).
8. Gazijahani, F.S., Ajoulabadi, A., Ravadanegh, S.N. and Salehi, J., "Joint energy and reserve scheduling of renewable powered microgrids accommodating price responsive demand by scenario: A risk-based augmented epsilon-constraint approach", *Journal of Cleaner Production*, Vol. 262, (2020), 121365. (<https://doi.org/10.1016/j.jclepro.2020.121365>).
9. Tang, Z., Liu, Y., Wu, L., Liu, J. and Gao, H., "Reserve model of energy storage in day-ahead joint energy and reserve markets: A stochastic uc solution", *IEEE Transactions on Smart Grid*, Vol. 12, No. 1, (2020), 372-382. (<https://doi.org/10.1109/TSG.2020.3009114>).
10. Roy, S., Banshwar, A., Sharma, N. K. and Sood, Y.R., "Simultaneous optimization of renewable energy based pumped storage scheme in energy and ancillary services market under deregulated power sector", *Journal of Intelligent & Fuzzy Systems*, Vol. 35, 5033-5043. (<https://doi.org/10.3233/JIFS-169787>).
11. Lasseter, B., "Microgrids [distributed power generation]", *Proceedings of IEEE Power Engineering Society Winter Meeting (Cat. No. 01CH37194)*, Columbus, OH, USA, (2001), 146-149. (<https://doi.org/10.1109/PESW.2001.917020>).
12. Rahmani, M., Faghihi, F., Moradi CheshmehBeigi, H. and Hosseini, S.M., "Frequency control of islanded microgrids based on fuzzy cooperative and influence of STATCOM on frequency of microgrids", *Journal of Renewable Energy and Environment (JREE)*, Vol. 5, No. 4, (2018), 27-33. (<https://dx.doi.org/10.30501/jree.2018.94119>).
13. Mahajan, V. and Jain, R., "Energy management in deregulated power market with integration of microgrid", *Deregulated electricity structures and smart grids*, CRC Press, (2022), 47-62. (<https://www.taylorfrancis.com/chapters/edit/10.1201/9781003278030-3/energy-management-deregulated-power-market-integration-microgrid-vasundhara-mahajan-ritu-jain>).
14. Teo, T.T., Logenthiran, T., Woo, W.L., Abidi, K., John, T., Wade, N.S., Greenwood, D.M., Patsios, C. and Taylor, P.C., "Optimization of fuzzy energy-management system for grid-connected microgrid using NSGA-II", *IEEE Transactions on Cybernetics*, Vol. 51, No. 11, (2020), 5375-5386. (<https://doi.org/10.1109/TCYB.2020.3031109>).
15. Kumar, S., Saket, R., Dheer, D.K., Sanjeevikumar, P., Holm-Nielsen, J.B. and Blaabjerg, F., "Layout optimisation algorithms and reliability assessment of wind farm for microgrid integration: A comprehensive review", *IET Renewable Power Generation*, Vol. 15, No. 10, (2021), 2063-2084. (<https://doi.org/10.1049/rpg2.12060>).
16. Sabzehgar, R., Kazemi, M., Rasouli, M. and Fajri, P., "Cost optimization and reliability assessment of a microgrid with large-scale plug-in electric vehicles participating in demand response programs", *International Journal of Green Energy*, Vol. 17, No. 2, (2020), 127-136. (<https://doi.org/10.1080/15435075.2019.1700125>).
17. Chen, Y., Li, J. and He, L., "Tradeoffs in cost competitiveness and emission reduction within microgrid sustainable development considering price-based demand response", *Science of The Total Environment*, Vol. 703, (2019), 135545. (<https://doi.org/10.1016/j.scitotenv.2019.135545>).
18. Hannan, M., Faisal, M., Ker, P.J., Begum, R., Dong, Z. and Zhang, C., "Review of optimal methods and algorithms for sizing energy storage systems to achieve decarbonization in microgrid applications", *Renewable and Sustainable Energy Reviews*, Vol. 131, 110022. (<https://doi.org/10.1016/j.rser.2020.110022>).
19. Habibi, F., Khosravi, F., Kharrati, S. and Karimi, S., "Utilizing RDPSO algorithm for economic-environmental load dispatch modeling considering distributed energy resources", *Electrica Journal*, Vol. 21, No. 3, 444-457. (<https://doi.org/10.5152/electr.2021.21025>).
20. Shahidehpour, M., "Role of smart microgrid in a perfect power system", *Proceedings of IEEE PES General Meeting*, Minneapolis, MN, USA, (2010). (<https://doi.org/10.1109/PES.2010.5590068>).
21. Makkiabadi, M., Hoseinzadeh, S., Mohammadi, M., Nowdeh, S.A., Bayati, S., Jafaraghaei, U., Mirkiaei, S.M. and Assad, M.E.H., "Energy feasibility of hybrid PV/wind systems with electricity generation assessment under Iran environment", *Applied Solar Energy*, Vol. 56, (2021), 517-525. (<https://doi.org/10.3103/S0003701X20060079>).
22. Nazari, M.A., El Haj Assad, M., Haghghat, S. and Maleki, A., "Applying TOPSIS method for wind farm site selection in Iran", *Proceedings of 2020 Advances in Science and Engineering Technology International Conferences (ASET)*, Dubai, United Arab Emirates, (2020), 1-4. (<https://doi.org/10.1109/ASET48392.2020.9118223>).
23. Abido, L.K., Bani-Hani, E., El Haj Assad, M., AlShabi, M., Soudan, B. and Oriaje, A.T., "Effects of environmental and turbine parameters on energy gains from wind farm system: Artificial neural network simulations", *Wind Engineering*, Vol. 44, (2020), 181-195. (<https://doi.org/10.1177%2F0309524X19849834>).
24. AlShabi, M., Ghenai, C., Bettayeb, M., Ahmad, F.F. and A El Haj Assad, M., "Multi-group grey wolf optimizer (MG-GWO) for estimating photovoltaic solar cell model", *Journal of Thermal Analysis and Calorimetry*, Vol. 144, (2021), 1655-1670. (<https://doi.org/10.1007/s10973-020-09895-2>).
25. Solanki, C.S., *Solar photovoltaics: Fundamentals, technologies and applications*, Phi learning pvt. Ltd., (2015). (https://www.google.com/books/edition/Solar_Photovoltaics/y1W2CAA_AQBAJ?hl=en&gbpv=1&printsec=frontcover).
26. Gheyraati, M., Akram, A. and Ghasemi-Mobtaker, H., "Optimum orientation of the multi-span greenhouse for maximum capture of solar energy in central region of Iran", *Journal of Renewable Energy and Environment (JREE)*, Vol. 9, No. 3, (2022), 65-74. (<https://dx.doi.org/10.30501/jree.2022.305780.1259>).
27. Hachicha, A.A., Al-Sawafta, I. and Said, Z., "Impact of dust on the performance of solar photovoltaic (PV) systems under United Arab Emirates weather conditions", *Renewable Energy*, Vol. 141, (2019), 287-297. (<https://doi.org/10.1016/j.renene.2019.04.004>).
28. Malik, P., Chandel, R. and Chandel, S.S., "A power prediction model and its validation for a roof top photovoltaic power plant considering module degradation", *Solar Energy*, Vol. 224, (2021), 184-194. (<https://doi.org/10.1016/j.solener.2021.06.015>).
29. Ghadikolaei, S.S.C., "Solar photovoltaic cells performance improvement by cooling technology: An overall review", *International Journal of Hydrogen Energy*, Vol. 46, (2021), 10939-10972. (<https://doi.org/10.1016/j.ijhydene.2020.12.164>).
30. Pachauri, R.K., Bai, J., Kansal, I., Mahela, O.P. and Khan, B., "Shade dispersion methodologies for performance improvement of classical total cross-tied photovoltaic array configuration under partial shading conditions", *IET Renewable Power Generation*, Vol. 15, (2021), 1796-1811. (<https://doi.org/10.1049/rpg2.12147>).
31. Hou, C., Hu, X. and Hui, D., "Hierarchical control techniques applied in micro-grid", *Proceedings of International Conference on Power System Technology*, Zhejiang, China, (2010), 1-5. (<https://doi.org/10.1109/POWERCON.2010.5666418>).
32. Gupta, S., Maulik, A., Das, D. and Singh, A., "Coordinated stochastic optimal energy management of grid-connected microgrids considering demand response, plug-in hybrid electric vehicles, and smart transformers", *Renewable and Sustainable Energy Reviews*, Vol. 155, (2021), 111861. (<https://doi.org/10.1016/j.rser.2021.111861>).
33. Sharma, S., Sood, Y.R., Sharma, N.K., Bajaj, M., Zawbaa, H.M., Turkey, R.A. and Kamel, S., "Modeling and sensitivity analysis of grid-connected hybrid green microgrid system", *Ain Shams Engineering Journal*, Vol. 13, No. 4, (2022), 101679. (<https://doi.org/10.1016/j.asej.2021.101679>).
34. Zeinal-Kheiri, S., Shotorbani, A.M. and Mohammadi-Ivatloo, B., "Real-time energy management of grid-connected microgrid with flexible and delay-tolerant loads", *Journal of Modern Power Systems and Clean Energy*, Vol. 8, (2020), 1196-1207. (<https://doi.org/10.35833/MPCE.2018.000615>).
35. Arumugam, P. and Kuppan, V., "A GBDT-SOA approach for the system modelling of optimal energy management in grid-connected micro-grid system", *International Journal of Energy Research*, Vol. 45, No. 5, (2021), 6765-6783. (<https://doi.org/10.1002/er.6270>).
36. Hatzigiorgiou, N., Contaxis, G., Matos, M., Lopes, J.P., Kariniotakis, G., Mayer, D., Halliday, J., Dutton, G., Dokopoulos, P., Bakirtzis, A. and Stefanakis, J., "Energy management and control of island power systems with increased penetration from renewable sources", *Proceedings of IEEE Power Engineering Society Winter Meeting (Cat. No. 02CH37309)*, New York, NY, USA, (2002), 335-339. (<https://doi.org/10.1109/PESW.2002.985008>).
37. Oyarzabal, J., Jimeno, J., Ruela, J., Engler, A. and Hardt, C., "Agent based micro grid management system", *Proceedings of International*

- Conference on Future Power Systems*, Amsterdam, Netherlands, (2005), 6. (<https://doi.org/10.1109/FPS.2005.204230>).
38. Zhou, B., Zou, J., Chung, C.Y., Wang, H., Liu, N., Voropai, N. and Xu, D., "Multi-Microgrid energy management systems: Architecture, communication, and scheduling strategies", *Journal of Modern Power Systems and Clean Energy*, Vol. 9, No. 3, (2021), 463-476. (<https://doi.org/10.35833/MPCE.2019.000237>).
 39. Logenthiran, T., Srinivasan, D., Khambadkone, A.M. and Aung, H.N., "Multiagent system for real-time operation of a microgrid in real-time digital simulator", *IEEE Transactions on Smart Grids*, Vol. 3, No. 2, (2012), 925-933. (<https://doi.org/10.1109/TSG.2012.2189028>).
 40. Kaur, J., Sood, Y.R. and Shrivastava, R., "A two-layer optimization approach for renewable energy management of green microgrid in deregulated power sector", *Journal of Renewable and Sustainable Energy*, Vol. 9, No. 6, (2017), 065905. (<https://doi.org/10.1063/1.4986342>).
 41. Gupta, N., "A review on the inclusion of wind generation in power system studies", *Renewable and Sustainable Energy Reviews*, Vol. 59, (2016), 530-543. (<https://doi.org/10.1016/j.rser.2016.01.009>).
 42. Li, J. and Wei, W., "Probabilistic evaluation of available power of a renewable generation system consisting of wind turbines and storage batteries: A Markov chain method", *Journal of Renewable and Sustainable Energy*, Vol. 6, (2014), 013139. (<https://doi.org/10.1063/1.4866259>).
 43. Gupta, N., "Gauss-quadrature-based probabilistic load flow method with voltage-dependent loads including WTGS, PV, and EV charging uncertainties", *IEEE Transactions on Industry Applications*, Vol. 54, No. 6, (2018), 6485-6497. (<https://doi.org/10.1109/TIA.2018.2855164>).
 44. Alsac, O. and Stott, B., "Optimal load flow with steady-state security", *IEEE Transactions on Power Apparatus and Systems*, Vol. PAS-93, No. 3, (1974), 745-751. (<https://doi.org/10.1109/TPAS.1974.293972>).
 45. Zimmerman, R.D., Murillo-Sánchez, C.E. and Gan, D., "MATPOWER: A MATLAB power system simulation package", Manual, Power Systems Engineering Research Center, Ithaca NY, Vol. 1, (1997). (<https://matpower.org/>).
 46. Tsikalakis, A.G. and Hatziargyriou, N.D., "Centralized control for optimizing microgrids operation", *Proceedings of IEEE Power and Energy Society General Meeting*, Detroit, MI, USA, (2011), 1-8. (<https://doi.org/10.1109/PES.2011.6039737>).
 47. N. D. Catalog, Available: (<https://data.nrel.gov/>).
 48. Prajapati, V.K. and Mahajan, V., "Demand response based congestion management of power system with uncertain renewable resources", *International Journal of Ambient Energy*, Vol. 43, (2019), 1-14. (<https://doi.org/10.1080/01430750.2019.1630307>).
 49. Papathanassiou, S., Hatziargyriou, N. and Strunz, K., "A benchmark low voltage microgrid network", *Proceedings of the CIGRE Symposium: Power Systems with Dispersed Generation*, Vol. 1, Paris, CIGRE, (2005), 1-8. (https://www.academia.edu/download/39917771/A_Benchmark_Low_Voltage_Microgrid_Networ20151111-16466-zv17xp.pdf).
 50. P. ISO, Available: (<https://www.pjm.com/markets-and-operations/energy.aspx>).



Research Article

Development of the Low-Economic-Risk Microgrids to Establish Environmental-Friendly Industries

Mohammad Hossein Jahangir*, Arash Kargarzadeh, Mohammad Montazeri

Department of Renewable Energies and Environment, Faculty of New Science and Technologies, University of Tehran, P. O. Box: 1439957131, Tehran, Iran.

PAPER INFO

Paper History:

Received: 26 February 2022

Revised: 18 June 2022

Accepted: 29 June 2022

Keywords:

Micro Grid,
Green Factory,
Carbon Emission,
Deferrable Load,
Economic Analysis

ABSTRACT

As one of the main consumers of electricity, industries account for in releasing a large amount of emission. Using renewable energies to feed factories is not an easy task and they should be economically viable to compete with fossil fuels. The goal of this study is to analyze the possibilities of using energy local area networks in off-grid and on-grid modes in an industrial project by considering and calculating all primary and deferrable loads in detail for the first time. The industrial project is sensitive and all possibilities should be considered closely to avoid economic losses. In this case, changes in electrical loads during the project, degradation of components, environmental risks, and economic risks of the investment (for each scenario) are considered and determined too. The results indicate that component degradation can cause 24,000 kWh drop in total electricity production at the end of the project and the total biogas consumption increases from 742 kg/yr to 9330 kg/yr. The results also show that the on-grid scenario (solar/battery) with the Net Present Cost of 200,000\$ will be an easy and low-risk choice for investment, but has high environmental risks. On the other hand, the stand-alone scenario (solar/wind/bio/battery) with Net Present Cost of 598,000\$ minimizes the environmental risks at the expense of high investment risk. A proper comparison between the multi-year and single-year modes at the end of the project ensures the high accuracy of techno-economic analysis in terms of optimum system types, emissions, and economics.

<https://doi.org/10.30501/jree.2022.330754.1338>

1. INTRODUCTION

Renewable energies and hybrid systems have been developing in recent years and research on their possibilities is growing in scope. Most studies addressing these systems are validated by HOMER (Hybrid Optimization of Model with Multiple Energy Resources) pro software enjoying the ability to simulate multiple systems together and to optimize them [1]. Microgrids are more reliable and cheaper than single energy systems and can be installed in regions without access to grid power like rural regions [2]. Table 1 shows detailed information and results of recent techno-economic studies over hybrid renewable energy systems.

The use of hybrid energy systems for factories and industrial projects is on the rise recently as industries are one the largest producers of emissions [10]. Table 2 shows economic, technical, and environmental information of recent researches over establishing green factories.

However, failing to consider the effects of inflation rate and discount rate fluctuations, almost all studies on establishing green factories did not predict the effects of development of the factory that may change the electrical load and none of

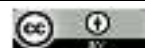
them considered the degradation of installed components during the project lifetime. The goal of this paper is to introduce an accurate plan for establishing green industries. This study attempts to consider and determine the effects of fluctuations in inflation and discount rates on the most important economic and environmental parameters of an industrial project using sensitivity analysis of HOMER pro software. This will show the amount of both economic and environmental risks of establishing green factories for different scenarios. Moreover, for the first time, the deferrable load of an industrial factory will be considered and determined in detail along with the effects of photovoltaic panel degradation and changes in electrical loads during the project using multi-year module of HOMER pro software. This will encourage factory managers around the world to use hybrid renewable energy systems and save the environment while investing their money in a safe project.

2. CASE STUDY

2.1. Factory information

The adopted case study is a factory that manufactures the needed machinery for petrochemical industries. The factory is located in Shamsabad Industrial town in Tehran, Iran. The area where factory is located is 2450 m² and its main structure

*Corresponding Author's Email: mh.jahangir@ut.ac.ir (M.H. Jahangir)
URL: https://www.jree.ir/article_155103.html



is 1000 m². There is also a technical department featuring the area of 120 m² and a parking area with 45m². Figure 1 shows details of the factory area in a map.

2.2. Electrical load

The factory has a primary electrical load mainly derived from industrial machines. There is also a deferrable load which is available due to use of water pumps and air compressors.

2.2.1. Primary load

Table 3 shows the consumption values for the past three years and explains how much they increase after each year. The primary electrical load profile is also shown in Figure 2 in detail.

According to Figure 2, the maximum monthly peak load is 165 kW and the daily peak load is 90 kW.

Table 1. Detailed information and results of recent findings over hybrid renewable energy systems

Location	Load type	Year	Grid	System	Results	Ref.
Tripoli	Electrical	2020	Off	PV ² /FC ³ /Bat ⁴	It was found that hybridizing photovoltaic panels with fuel cells ensured a better minimum threshold power of 5 kW than solar thermal energy and fuel cells.	[3]
China	Electrical	2020	Off	PV/WT ⁵ //HSPSI ⁶	A real hybrid renewable energy system that is using pumped-storage system instead of batteries was studied, which indicated that such systems could considerably reduce the capital cost and PV/WT/HSPSI was the most cost-effective combination.	[4]
Honduras	Electrical	2021	On	PV/bio/Bat	A Gasifier was designed and coupled with PV panels. For the first time, a gasifier was used in HOMER software to simulate a microgrid for rural areas.	[5]
Turkey	Electrical	2021	Both	PV/WT/FC/HE ⁷	HOMER Software was utilized to analyze the penetration levels of resources in both on-grid and off-grid systems in rural regions.	[6]
Mexico	Electrical	2022	Both	PV/WT/FC/Bat	A techno-economic study was done to implement a Hydrogen based Power to Gas to Power (P2G2P) in a microgrid, located in Mexico. This study explains that by using hydrogen and fuel cells to substitute diesel generators, it is possible to reduce CO ₂ emission by 27 %.	[7]
Iran	Electrical	2022	Both	PV/WT/bio/Bat	The paper goal is to reduce the emissions of industrial livestock farms using several microgrids. This study also created a scenario that could help all livestock farms of a country to use their biomass to produce green energy.	[8]
Nepal	Electrical	2022	Off	PV/Diesel	An off-grid microgrid for both Diesel Generators (DG) and solar PV based systems was designed using HOMER. The final DG-based microgrid system reduced fuel consumption by 19 % and costs of the system by 5 %.	[9]

Table 2. Detailed techno-economic-environmental results of recent studies on environmental-friendly industries

Industry	System	NPC (\$)	COE (\$/kWh)	CO ₂ (kg/yr)	Emission desc.	Ref.
Telecom	PV/DG/Bat	401,000	1.28	-60,595	-	[11]
Generic	PV/WT/DG/Bat	1,684,118	0.19	-278,191	Compared with diesel only	[12]
Cement	PV/WT/Bat/Grid	-	0.20	-71,373 Tons	In total	[13]
Cement	PV/BG/Bat	□ 22 M	0.14	35,731	-	[14]
Dairy	PV/WT/DG/Grid	□ 14.3 M	0.02	-205,334	Compared with grid only	[15]

² Photovoltaic

³ Fuel Cell

⁴ Battery

⁵ Wind Turbine

⁶ Pumped Storage

⁷ Hydro Electric



Figure 1. Area details of the case study (KSJ factory)

Table 3. Average power consumption of the factory

Year	Ave. monthly consumption (kWh/month)	Ave. daily consumption (kWh/day)	Increase (%)
2019	5201.5	173.4	9 %
2018	4771.5	159.1	14 %
2017	4170	139.0	-

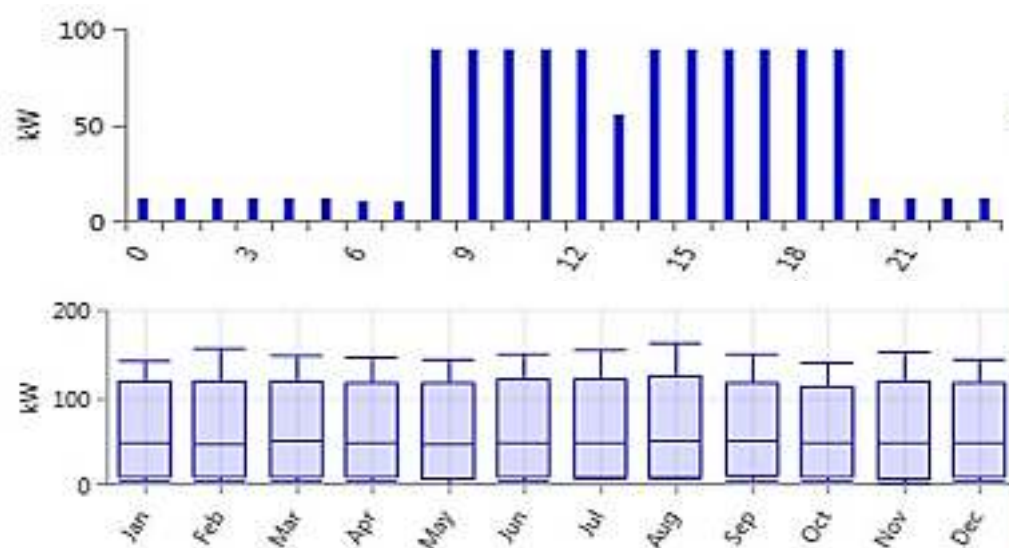


Figure 2. Primary electrical load of the selected factory. (Up: daily load profile, down: seasonal load profile)

2.2.2. Deferrable load

The deferrable load consists of two water pumps and two air compressors. Calculating the deferrable load and its parameters is the next step of the work. The peak load of the deferrable load is equal to load of pumps and compressors and can be easily determined using Eq. 1 in Table 4 [16].

Scaled annual average (kWh/day) is the next needed parameter in this part. HOMER Pro software can automatically determine this number if the user adds the average load of each month [16]. The average time that each of these devices remained operational during all months of one year is measured. Table 5 is available and the scaled

annual average value will therefore be determined automatically.

By setting up the deferrable load chart in HOMER pro software using data available in Table 5, the scaled annual average is determined and reported as 4.34 kWh/day.

Storage capacity calculation represents the last step in completing the data of deferrable load. Storage capacity is

equal to the time when pumps or air compressors need to fill their tanks and it should be reported in kWh [16]. The storage capacity of water pumps is equal to 2.22 kWh. The storage capacity of each compressor is also 0.37 kWh. In this case, the total storage capacity for the deferrable load is equal to 2.96 kWh. Table 6 shows a summary of assumptions and results of storage capacity calculations.

Table 4. Deferrable load equation

Equation	Eq. No.	Ref.
$\Sigma P_{\text{Components}} = \text{Peak Load}$ $P_{\text{pump no.1}} + P_{\text{pump no.2}} + P_{\text{comp. no.1}} + P_{\text{comp. no.2}} = \text{Peak Load}$	1	[16]

Table 5. Information of each available deferrable load in the factory during one year

Month	Ave. operation time (hour)		Ave. consumption (kWh/d)		Total consumption (kWh/d)
	Pumps	Compressors	Pumps	Compressors	
January	2	1.34	0.74	2.95	3.7
February	2	1.34	0.74	2.95	3.7
March	2	1.34	0.74	2.95	3.7
April	1	1	0.37	2.2	2.57
May	2	1.34	0.74	2.95	3.7
June	4	1.67	1.5	3.67	5.17
July	6	1.34	2.2	2.95	5.15
August	7	1.67	2.6	3.67	6.27
September	4	2.5	1.5	5.5	7
October	2	1.34	0.74	2.95	3.7
November	2	1.34	0.74	2.95	3.7
December	2	1.34	0.74	2.95	3.7

Table 6. Assumptions and results of storage capacity calculations

Device	Power (kW)	Quantity	Storage capacity (m ³)	Filling time (hour)	Total storage capacity (kWh)
Water pump	0.37	2	10	3	2.22
Air compressor	2.2	2	0.3	0.17	0.74

3. ENERGY RESOURCES

3.1. Solar energy

Photovoltaic panels can be installed at the roof top of the main structure, technical department, and parking (Figure 1). By considering half of the rooftop of the main structure that faces the sun, the roof of technical department, and parking, 665 m² available space for installing panels is available.

Figure 3 shows the solar GHI and clearness index information of the area where the case study is located. This information is available from NASA website [17].

HOMER software uses Eq. 2 to calculate the output power of photovoltaic panels (Table 7) [18]. where Y_{PV} is the rated capacity of photovoltaic panels, f_{PV} the derating factor, G_T the solar radiation incident, $G_{T,STC}$ solar radiation incident under Standard Test Condition (STC) of photovoltaic panels, α_P the temperature coefficient of PVs available in the data sheet of solar panels, T_C the temperature at which PVs are working,

and $T_{C,STC}$ equal to the temperature of the standard test condition of the photovoltaic panels.

Table 7. Out power of PVs equation

Equation	Eq. No.	Ref.
$P_{PV} = Y_{PV} f_{PV} \left(\frac{G_T}{G_{T,STC}} \right) \left(1 + \alpha_P (T_C - T_{C,STC}) \right)$	2	[18]

As shown in Eq. 2, the temperature also affects the efficiency of solar panels and the average daily temperature of the selected environment where the factory is established is gathered using the same method that solar GHI and clearness index were achieved, as shown in Figure 4.

The data of ambient temperature in Figure 4 is employed to calculate the temperature of PVs using Eq. 3 (Table 8) [19].

Table 8. Impact of temperature on PVs equation

Equation	Eq. No.	Ref.
$\alpha\tau G_T = U_L(T_C - T_a) + \eta_c G_T$	3	[19]

belong to the cover that is over them, U_L the coefficient of heat transfer, T_a the ambient temperature which is available from the data in Figure 4, and η_c belongs to the electrical efficiency of the solar panels.

where α is equal to the solar absorption of the photovoltaic panels, τ is related to the solar transmittance of PVs that

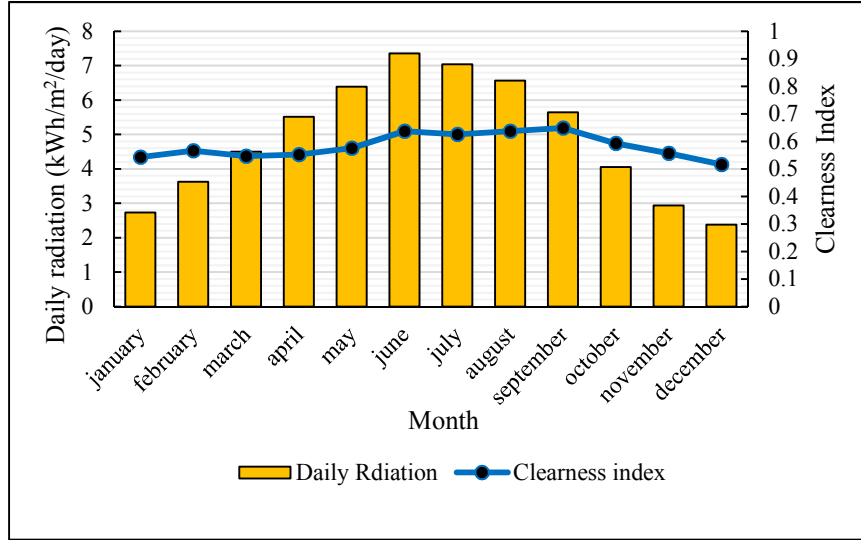


Figure 3. Solar GHI and clearness index of the selected factory’s environment [17]

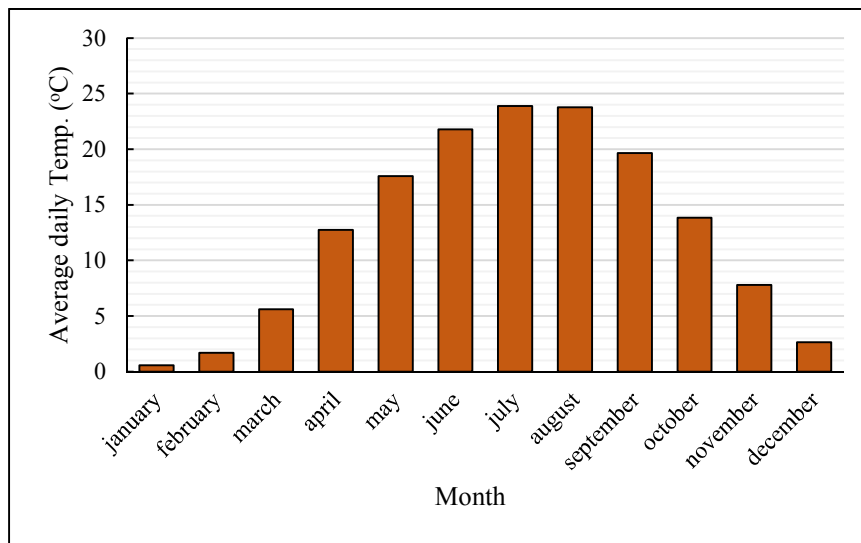


Figure 4. Average daily temperature of the selected factory’s environment

3.2. Wind energy

Given that wind turbines can be operational for 24 hour of the day and produce power, they are necessary components for stand-alone energy hub systems [20]. HOMER pro software uses the power curve of wind turbines to calculate their output power in every time step using the ambient wind data in Figure 5 [21].

In order to determine and achieve the power curve of the wind turbine, Eq. 4 in Table 9 is used for calculating output power of the wind turbine [22].

Table 9. Wind turbine output power equation

Equation	Eq. No.	Ref.

$P_{WT}(t) = \begin{cases} \alpha V^3(t) - \beta P_R & V_{Ci} < V < V_r \\ P_R & V_r < V < V_{Co} \\ 0 & \text{else} \end{cases}$	4	[22]
---	---	------

where V_r belongs to the rated speed, V_{Ci} is equal to the cut-in speed, V_{Co} is related to the cut-off speed, P_R is the rated power of the wind turbine, $\alpha = \frac{P_r}{V_r^3 - V_{Ci}^3}$, and $\beta = \frac{V_{Ci}^3}{V_r^3 - V_{Ci}^3}$.

The wind speed data shown in Figure 5 belong to the 50 m above the surface of the earth. In order to determine the speed of the wind that reaches the blades of wind turbines and calculate the power of the wind turbine (Eq. 4), Eq. 5 is employed (Table 10) [22].

Table 10. Equation of the wind speed which reaches the blades

Equation	Eq. No.	Ref.

$V = V_h \left(\frac{h}{h_r} \right)^Y$	5	[22]
--	---	------

where V is equal to the wind speed at the height of the hub, V_h is the wind speed that is available in Figure 5, h_r is equal to 50 m, h is the hub height, and Y ranges between 0.14 and 0.25.

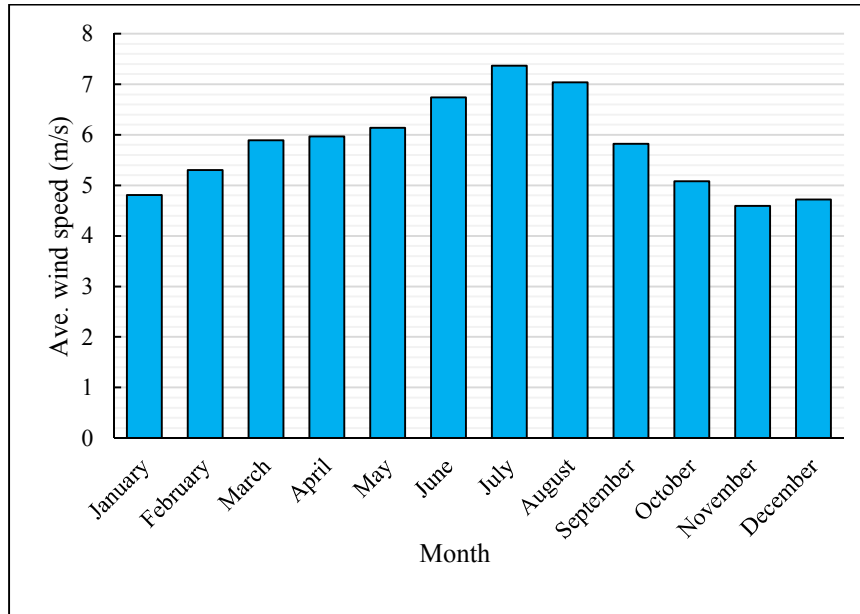


Figure 5. Average wind speed of the selected factory's environment

3.3. Grid network

Being connected to the grid network gives the system a chance to sell the surplus green energy and provides both economic and environmental profits. There are some hours during the working hours of factory when renewable energies may not be available. In this case, the factory can use grid power to avoid the capacity shortages in grid-connected scenarios. The system will do so at the cost of producing emissions and paying carbon taxes. Emission content values of grid network and carbon taxes are shown in Table 11.

Table 11. Emission penalties and emission contents [23, 24]

Emission	Emission penalties (\$/t)	Emission contents (gr/kWh)
CO ₂	2.86	660.65
CO	54	0.62
SO ₂	521.5	1.66
NO _x	171.5	2.38
Unburnt hydrocarbons	60	180.18
Particulate matter	1228.6	0.12

There is an average of 30 times grid power outage in this industrial town over the course of a year with the average of 2-hour shortage for each one that considerably affects the operations of the factory. Figure 6 shows the grid power outage times in a year.

Grid prices in Iran and the corresponding schedule in different months and hours are also shown in Figure 7 and explained further in Table 12 [24]. Note that charging battery from grid power and also grid sales from battery are not allowed at all.

3.4. Fuel resources

Using generators that consume fuels to produce power is common among factories and they act as backup systems [25]. Fuel resources are always available and can provide enough electricity for energy-local area networks when the renewable energies are not available, but they mostly do so at the expense of producing emissions. The case study of the paper uses a diesel generator to provide electricity during grid outages. Although it is possible to hybrid the diesel power with wind energy, solar energy, and grid power, it should be considered that diesel fuel causes emission and the goal of the paper is to minimize the use of fossil fuels and establish a green factory. In this case, using biofuels instead of diesel is recommended and Biogas (bio-methane) is going to be used instead of diesel fuel in the simulations at a price of 1.1 \$/kg [26]. Biogas produces 60-80 % less greenhouse gas and can provide power for the hybrid energy systems while reducing the emissions [27]. Buying biogas instead of diesel and using it as a backup energy source can also encourage industrial livestock farms to produce green fuels from their produced biomass and help the environment while investing in green energies.

4. COMPONENTS AND SCENARIO

In this part, all technical and economic information of used components is gathered and discussed over. The hybrid renewable energy system that is going to supply the energy demands of this factory was also studied in both off-grid and on-grid modes. Figure 8 shows the schematic of the system and all the components used.

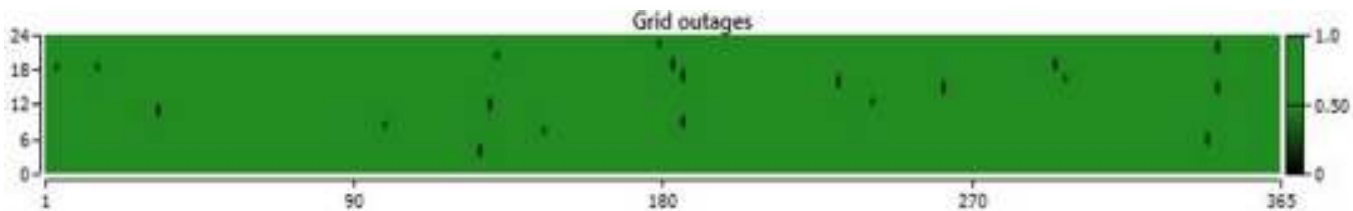


Figure 6. Grid outage times of the industrial town during one year



Figure 7. Grid rate schedule of Iran during different hours and months [24]

Table 12. Grid rates and electricity prices of Iran [24]

Rate	Price (\$/kWh)	Color
Low-power-consumption hours in non-summer season	0.05	Yellow
Medium-power-consumption hours in non-summer season	0.07	Purple
High-power-consumption hours in non-summer season	0.10	Red
Low-power-consumption hours in summer season	0.06	Orange
Medium-power-consumption hours in summer season	0.08	Light Purple
High-power-consumption hours in summer season	0.12	Light Green

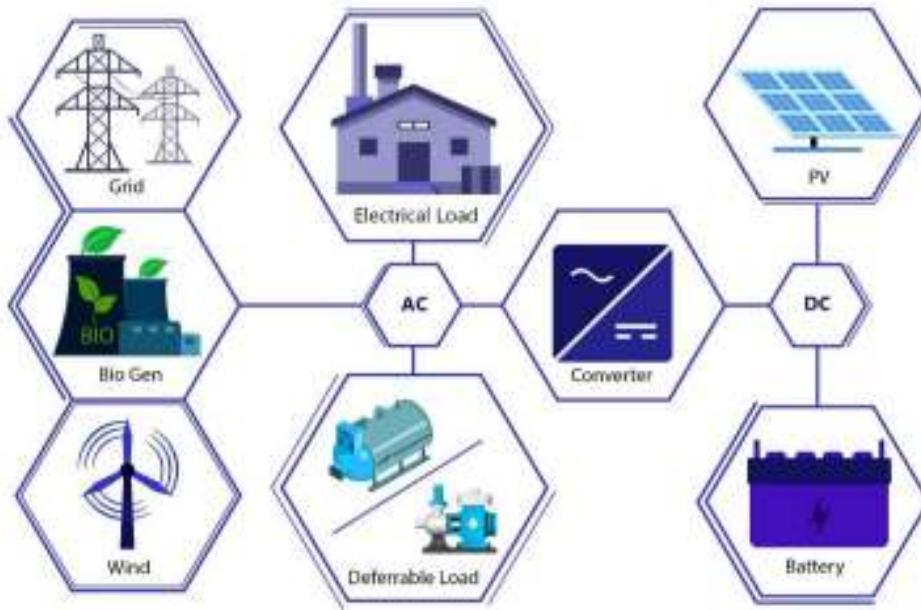


Figure 8. Schematic of the system which is going to supply energy demands of the factory

4.1. Photovoltaic panel

There is a limited space of 665 m² for installing the solar panels at the rooftop of the factor. Table 13 shows the characteristics and information of selected solar panels.

The solar panel data sheet also provides a chart that shows the warranted output during the operational years of the solar panel (Figure 9) [29].

Figure 9 indicates that installed solar panels will degrade 0.68 percent each year and will not have constant output during the lifetime of the project.

Table 13. Technical and economic information of selected photovoltaic panels

Name	Value	Unit	Ref.
Module type	TBM72-370M	-	[28]
Module dimension	1956 × 992 × 40	mm	
Maximum power (P _{max})	370	W	
Maximum voltage	39.59	V	
Maximum current	9.35	A	
Open-circuit voltage	48.04	V	
Short-circuit current	9.83	A	
Module efficiency	19.06	%	
Operating temp.	-40 ~ +85	°C	
Nominal module operating temperature	40.2 ± 2	°C	
Temp. coefficient of P _{max}	-0.39	-	[29]
Capital and replacement cost per kW	1300	\$	
O & M Cost	20	\$/yr	

4.2. Converter and electrical storage

In order to consume the DC output of solar panels and electrical storages (batteries) and store the AC output of biogas generator and wind turbines, the system uses converters to transform DC to AC, and vice versa. The output of the converter also affects the output power of PVs as shown in Eq. 6 in Table 14 [24].

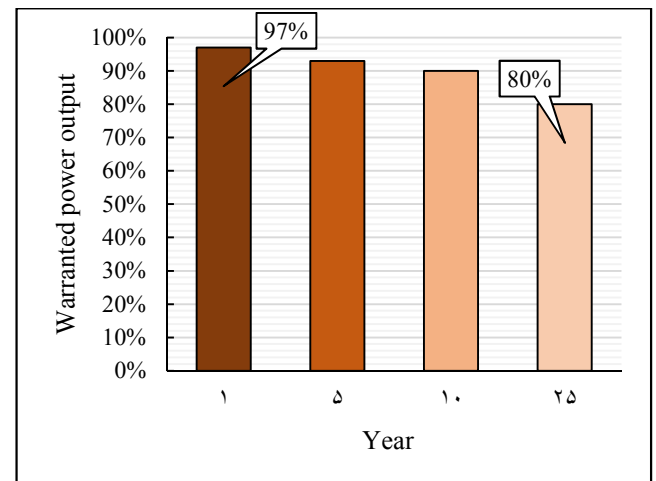


Figure 9. PV warranted output during 25 operational years [28]

Table 14. Converter output power equations

Equation	Eq. No.	Ref.
$P_{cnv.out} = \eta_{cnv} P_{PV}$	6	[24]

where η_{cnv} is equal to the efficiency of the converter and is assumed to be 90 %.

The optimization ability of HOMER pro software is used here and the values of 0, 50, 100, and 200 kW are chosen for converter to determine the best result for use in this project. Table 15 shows the summarized information of the converter.

Table 15. Summarized information of the installed converters

Component	Type	Simulation rates (kW)	Life time (yr)	Capital cost (\$)	Replacement cost (\$)	O & M (\$/yr)	Ref.
-----------	------	-----------------------	----------------	-------------------	-----------------------	---------------	------

Converter	Generic	0, 50, 100, 200	15	600	600	10	[30]
------------------	---------	-----------------	----	-----	-----	----	------

Surrette 4 KS 25P flooded deep cycle battery is chosen in this study. Each of these batteries has a nominal capacity of 7.55 kWh and the corresponding values of 0, 20, and 50 are chosen for optimization. Data sheet of the selected batteries is shown in Table 16 [24].

Table 16. Technical data and information of Surrette 4 KS 25P battery

Name	Value	Unit	Ref.
Nominal voltage	4	V	[24]
Nominal capacity	1350	Ah	
Nominal capacity	7.55	kWh	
Life time	20	yr	[31]
Capital cost	1259	\$	
Replacement cost	1100	\$	
O & M cost	10	\$/yr	

4.3. Wind turbine

Due to the average wind speed during past 22 years ranging between 5 and 8 m/s, generic wind turbines with the nominal capacity of 10 kW are used and the numbers of 0, 1, and 2 are chosen for optimizations in HOMER pro software. Table 17 shows the summarized technical and economic information of the selected wind turbines.

Table 17. Data sheet and economic information of wind turbines

Name	Value	Unit	Ref.
Rated power	10	kW	[11]
Life time	20	yr	
Capital cost	45000	\$	
Replacement cost	30000	\$	
O & M cost	500	\$/year	

Figure 10 shows the power curve of the chosen 10 kW wind turbine used in HOMER pro software for wind power simulations [32, 33].

4.4. Biogas generator

In order to use the potentials of biofuel resources, a biogas generator is used in the simulation. The capital cost for a biogas generator is 1500 \$/kW with the same value for its replacement, O & M cost of it is 60 \$/yr hour, and its life time is assumed to be 20,000 hours [29]. The main use of this biogas generator is for backup during the times that other renewable energies are not available to prevent the capacity shortages. Using a backup system will also reduce the use of batteries, too. The values of 0, 10, 25, and 50 kW for biogas generator are used for optimization in HOMER pro software.

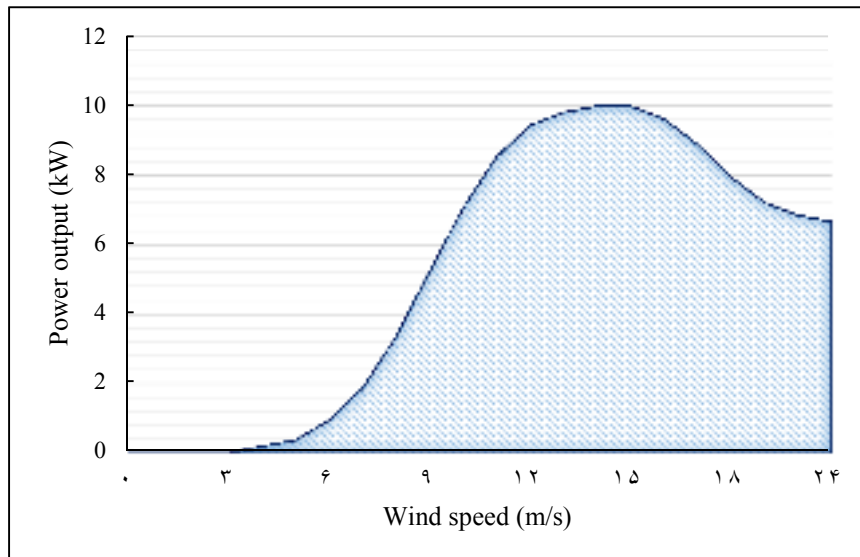


Figure 10. Power curve of generic 10 kW wind turbine [32]

5. PROJECT MANAGMENT

In this part, the paper will explain economics of the simulation and the effects of variable changes during the project life time.

5.1. Multi-year module

This module will help simulate the variable changes in the project during its life time and discuss its effects. Multi-year module is capable of simulating photovoltaic panel degradation and continuous changes in electrical loads (both primary and deferrable loads).

5.1.1. PV degradation

The photovoltaic panels will degrade 0.68 percent after each year and this will affect the investment of solar energy. In this case, the factory may need greater backup energy. To ensure that the simulation has enough insurance to be used in the real world, given that it is an industrial project and economic losses should be minimized, this degradation is considered in multi-year module of HOMER pro software.

5.1.2. Increase of electrical load

The increase in the electrical load of the factory is shown in the electrical consumption of the past three years in Table 3. This means that the project reaches the fifth year by the time, the electrical loads will be 1.5 times larger than their first value. By considering this increased amount of power consumption, the investors of hybrid renewable energies can make sure that their factories will no longer have the problem of future capacity shortages.

5.2. Economics and sensitivity module

The life time of this industrial project is assumed to be 25 years. At the time of writing this paper, the nominal discount rate is 18 % and the inflation rate is 15 % [24]. However, it is possible that these values of discount rate and inflation rate change during the project life time [34]. In this case, the sensitivity module of HOMER pro software is employed to analyze the future possibilities and plan for them. The average 5 % of changes for each of these economic parameters is assumed [35]. Table 18 shows the summarized information of the assumptions of project management part in the simulations.

Table 18. Assumptions of the project management part in the simulations

Name	Project life time (year)	Nominal discount rate (%)	Expected inflation rate (%)	PV degradation (%/yr)	Increase of loads until year 5 (%/yr)
Value	25	13, 18, 23	10, 15, 20	0.68	10

6. RESULTS AND DISCUSSION

Summarized results of both off-grid and on-grid scenarios are shown in Table 19.

6.1. Grid-connected system

The advantage of using grid-connected systems is that there is a possibility to sell the surplus energy to the grid at non-peak hours and at times when the factory is not operational and yet, the components and the system are producing electricity using renewable energy resources. Selling the surplus green energy will provide both economic and environmental profits.

Among the optimal on-grid systems that are shown in Table 19, the application of photovoltaic panels without the use of wind turbines and biogas generator in Scenario 1 has the lowest NPC, COE, and initial capital cost and can be chosen as the most economic system. In order to show the costs of the system in Scenario 1 in detail, a chart is established and shown Figure 11.

Operation of the solar panels is important, especially due to the changes that are programmed in the multi-year module. Figure 12 shows the PV output during a day in its initial state in the 1st year and Table 20 compares this initial state with 5th, 10th, and 25th years of the project.

Table 19. Best results of off-grid and on-grid scenarios (present inflation and discount rates)

Scenario	Components					Grid		Costs			
	PV (kW)	Wind turbine (Qty.)	Bio Gen. (kW)	Battery (Qty.)	Converter (kW)	Purchased (kWh)	Sold (kWh)	NPC (\$)	COE (\$)	Initial capital (\$)	
On-grid	1	100	-	-	20	50	31,693	63,489	200,415	0.070	195,180
	2	100	-	10	20	50	31,693	63,493	207,729	0.072	210,180
	3	100	1	-	50	50	26,995	72,154	231,476	0.076	240,780
Off-grid	1	100	2	25	50	50	-	-	597,970	0.35	360,450
	2	100	-	25	50	50	-	-	651,058	0.38	270,450
	3	100	2	50	-	50	-	-	9.25 M	5.42	335,000

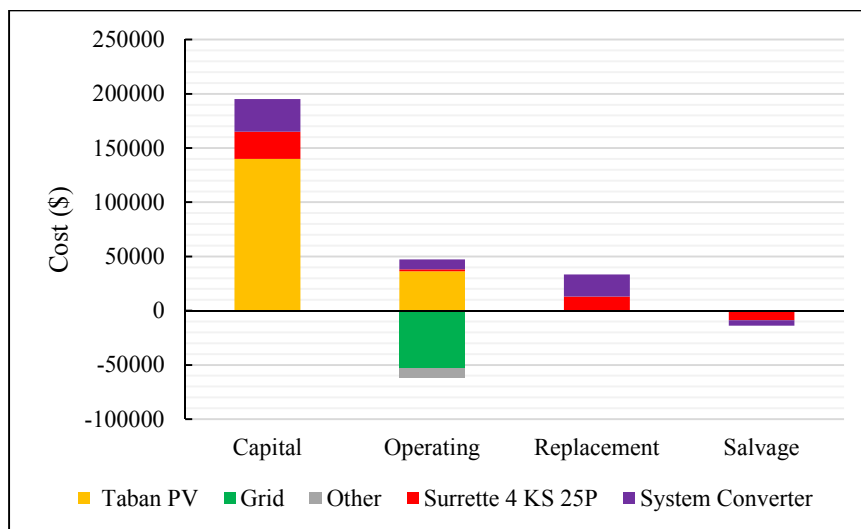


Figure 11. Cost summary of the optimum on-grid system (PV/battery/grid)

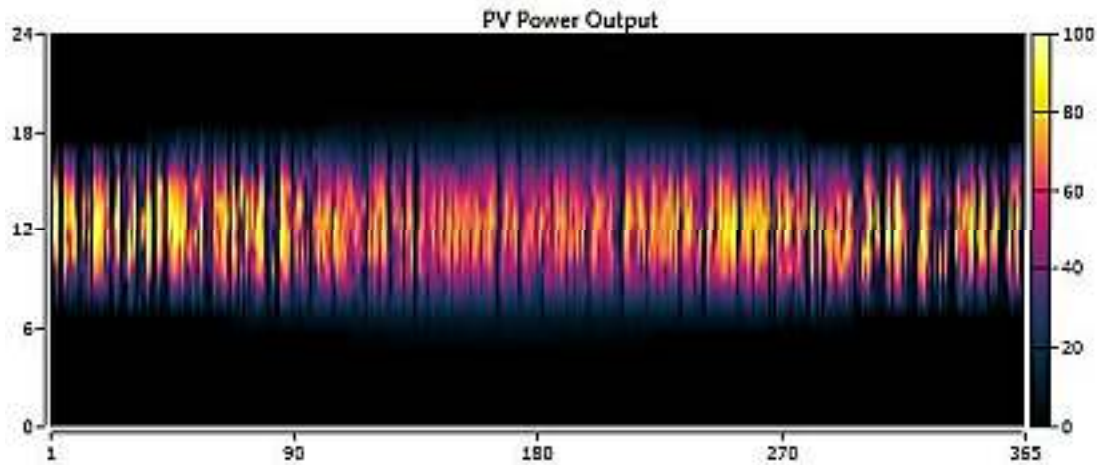


Figure 12. PV power output in its initial state in year 1

Table 20. Compression between the states of PVs during the project life time

Year	Maximum output (kW)	PV penetration (%)	Levelized cost (\$/kWh)	Total production (kWh/yr)
1	98.2	250	0.061	158,254
5	95.6	162	0.063	153,994
10	92.4	157	0.065	148,829
25	83.4	142	0.072	134,350

According to Table 20, PV penetration experienced a significant reduction after 5 years and reached the amount of 162 % from its initial value (250 %) due to increase in primary and deferrable loads of the factory. However, even after this time, degradation of PV panels during the project life time has a considerable effect on its penetration and electricity production. The total reduction in the production of PVs is near 24,000 kWh/yr. The amount power that the factory consumes from grid during the day when the factory is operational is also affected by PV degradation, as shown in Figure 13.

Figure 13 shows the effects of PV degradation on grid status and explains how it influences needed power and the way that the system works. Comparison of the 1st year and last year of the project indicates that the amount of excess energy that can be sold to the grid is reduced at the 25th year and also, greater energy is purchased from the grid during the final hours of the day.

The optimal system can be different for each economic condition and the sensitivity analysis has the ability to indicate each one clearly. Figure 14 shows the optimal system type for each economic condition and the effect of both inflation and discount rates on the operating hybrid renewable energy system type.

On-grid results shown in Table 19 are at the center of Figure 14; however, higher discount rate (more than 20 %) and lower inflation rate (lower than 13 %) will prompt the system to use biogas generators instead of using PVs. Reduction of discount rate will also make the system use PVs and biogas energy together. There is also a small chance that the system uses biogas generator, PV, and wind turbine together if the inflation rate reaches the value of 20 % while the discount rate is 13 %. Fluctuations of inflation and discount rates also affect the NPC of the project and these effects are shown in a surface plot in Figure 15.

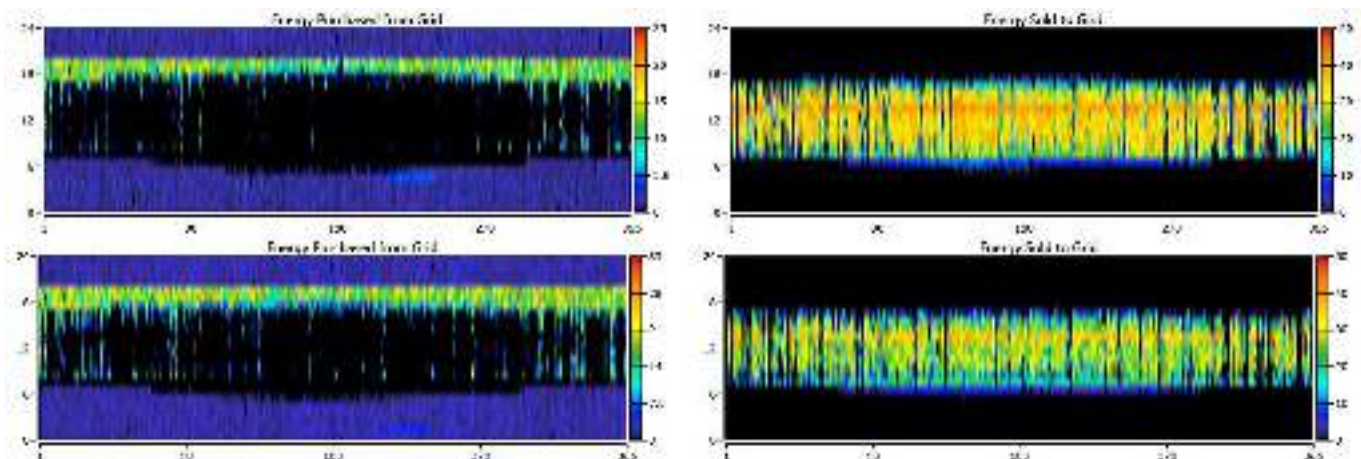


Figure 13. Grid status during the project life time (up: 1st year, down: 25th year)

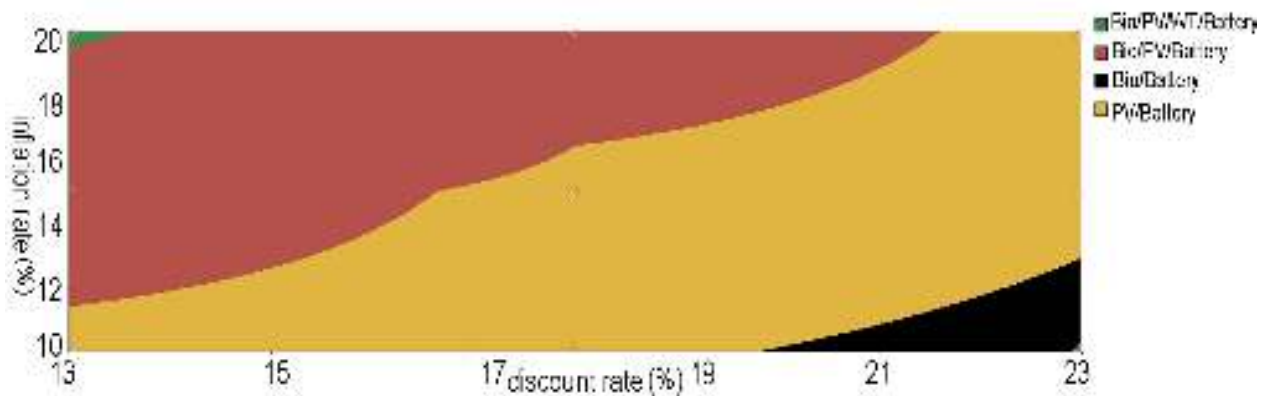


Figure 14. Optimal system type for each economic condition (on-grid system)

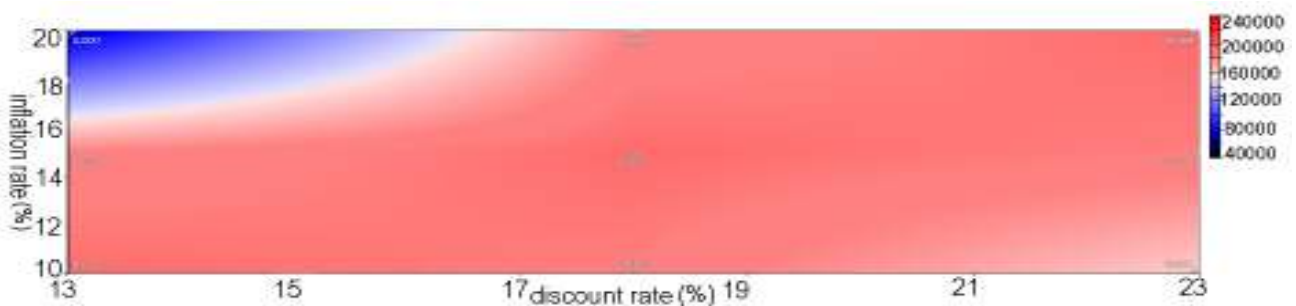


Figure 15. Surface plot of Net Present Cost in the grid-connected scenario

The surface plot of NPC indicates that lower discount and higher inflation will lead to reduced NPC and COE and the inflation rate of 20 % and discount rate of 13 % have the lowest NPC and COE, which belong to the PV/bio/WT/battery system. The inflation rate of 10 % and the discount rate of 23 % also reduce the NPC while creating the highest COE.

In addition to optimum system type, NPC, and COE, economic fluctuations can also affect the emissions. Figure 16

shows the effects of inflation rate and discount rate on CO₂ emissions and the environmental effects of this project.

Figure 16 indicates that when the inflation rate increases and discount rate decreases, the bio/battery system will produce carbon emissions while other optimum systems of the factory are all negative-carbon producers. CO₂ emissions of the on-grid system vary between -60,000 kg/yr and 90,000 kg/yr.

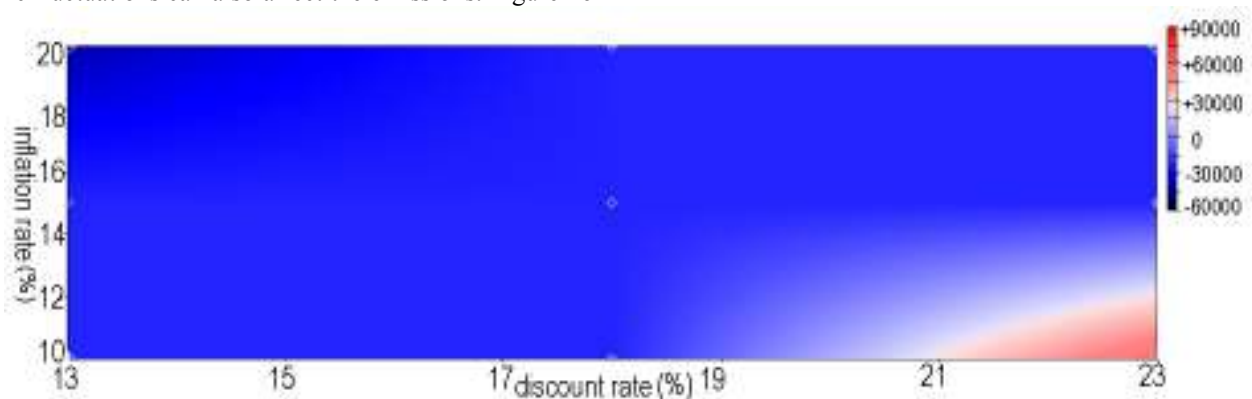


Figure 16. Surface plot of average CO₂ emissions per year in the grid-connected scenario

6.2. Stand-alone system

In this part, this paper attempts to analyze the stand-alone system to determine what it will take to make an industrial factory off-grid and use total renewable energies to make it become a green factory. Cost summary for the optimum off-grid scenario involving the present inflation rate and discount rate is shown in Figure 17.

As is given in Figure 17, the largest capital cost in this scenario belongs to PVs followed by wind turbines, given that the lifetime of the project is 25 years.

In this scenario, wind turbines and biogas generator should be analyzed as new components of the system in the off-grid mode. Figure 18 shows the status and production of wind turbines in the off-grid system.

Degradation of PV panels (24,000 kWh drop in total production) and increase of electrical loads have greater

effects on this scenario as the factory does not have the support of the grid power. In this case, wind turbines and biogas generator should produce enough electricity to keep the factory operational. Table 21 shows the status of biogas generator and biofuel consumption during the project lifetime. According to Table 21, the operational hours of biogas generator and its production increase after 5 years due to a 10 % increase in electrical loads of the factory. Comparison of the scenarios indicates that the degradation of the PVs leads the system to use more biogas after each year in the off-grid scenario. PV degradation itself leads the system to increase the use of biogas generator. The amount of biogas consumption reaches 9330 kg/yr in the 25th year from 7260 kg/yr in the 5th year of the project.

Lack of grid power forces the system to use more batteries, and 30 batteries are added to the stand-alone system to make sure that it is going to meet capacity shortages. Figure 19 shows the status of batteries in the stand-alone system in the 1st, 10th, and 25th years from top to down, respectively.

Figure 19 indicates that effects of the continuous changes that are simulated in the multi-year module on the storage system. As the project progresses, the system uses more stored energy to supply the factory.

Figure 20 shows the results of sensitivity analysis in off-grid system types, and Figure 21 shows the effects of inflation rate and discount rate on the economic parameters of the project.

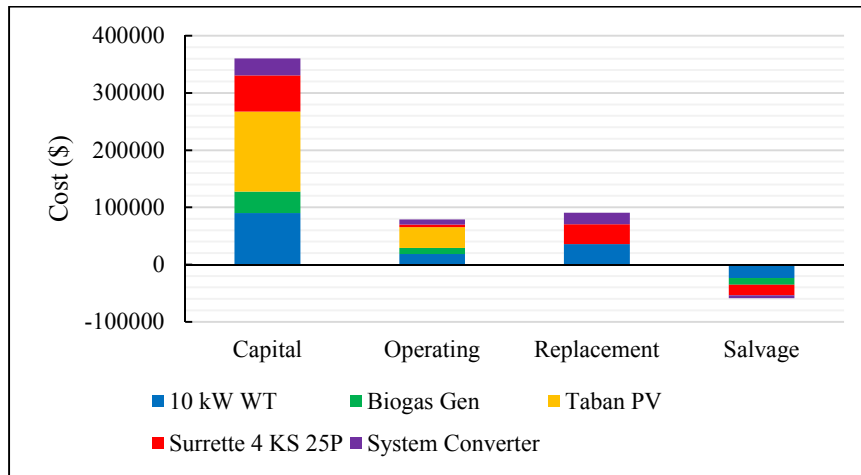


Figure 17. Cost summary for the optimum off-grid system (PV/WT/bio/battery)

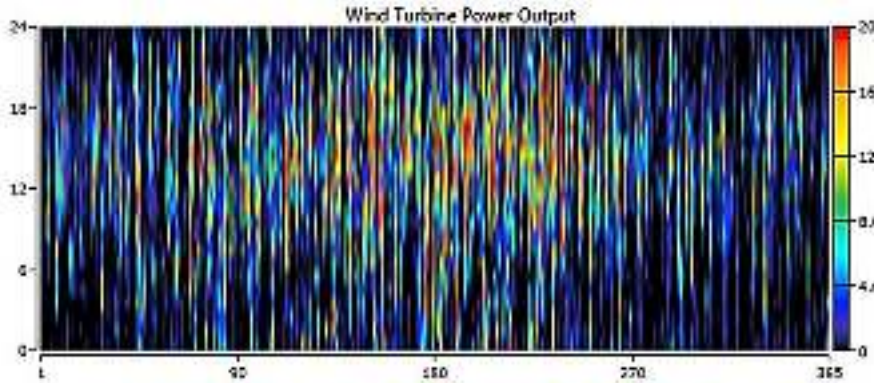


Figure 18. Wind turbine output during one year (off-grid scenario)

Table 21. Status of biogas generator during the project lifetime (off-grid scenario)

Year	Hours of operation (hrs/yr)	Number of starts (Qnt/yr)	Electrical production (kWh/yr)	Biogas consumption (kg/yr)
1	27	17	338	742
5	248	127	3320	7260
10	267	130	3561	7789
25	315	154	4271	9330

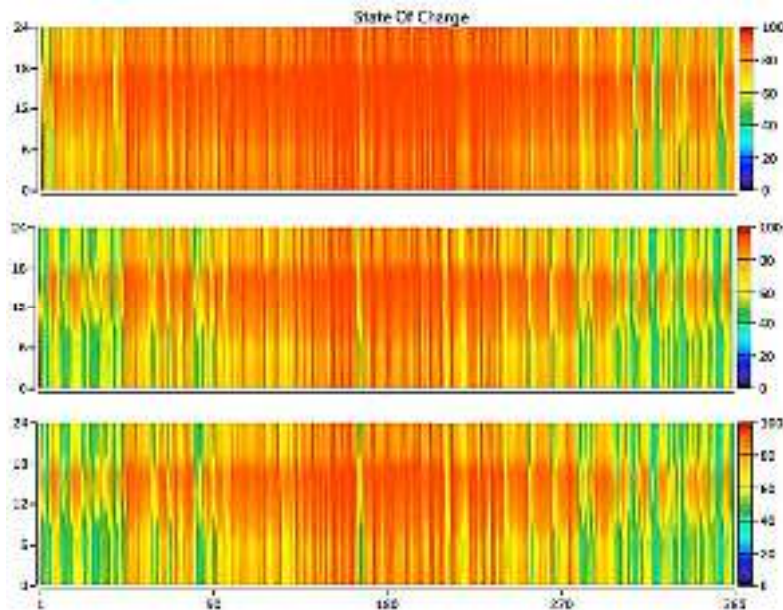


Figure 19. Status of batteries during 1st, 10th, and last years (from top to down, respectively)

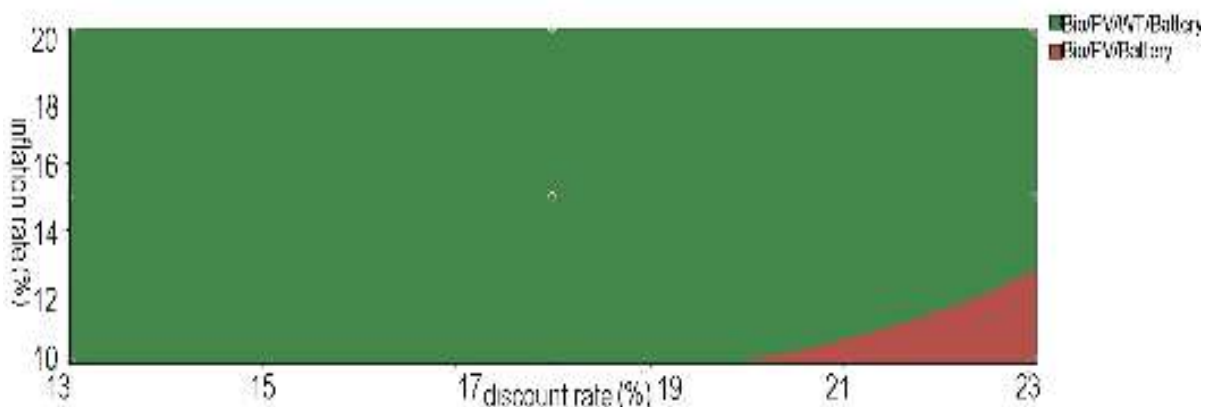


Figure 20. Surface plot of optimal system type in the off-grid scenario

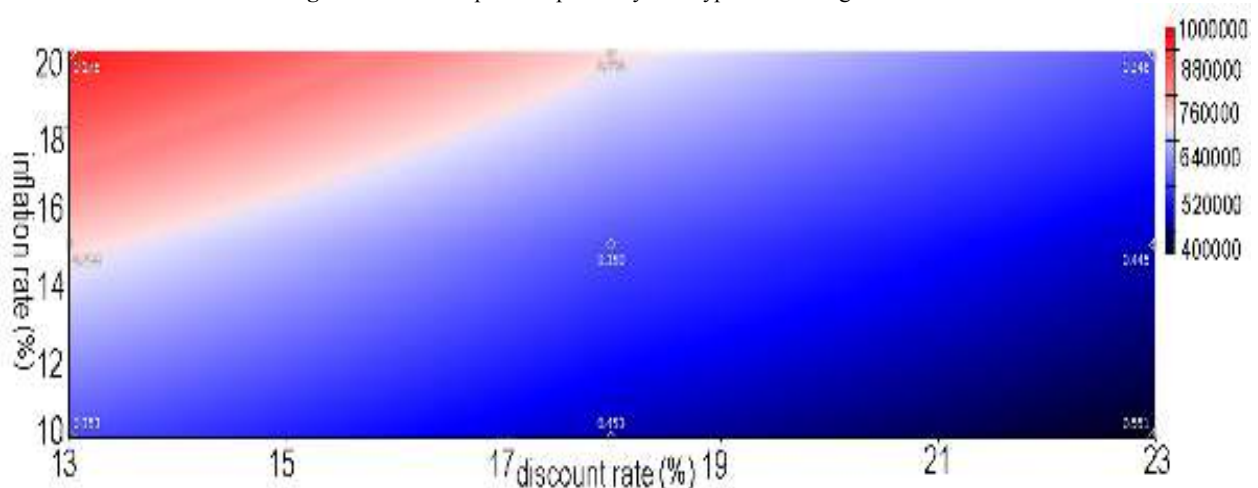


Figure 21. Surface plot of NPC in the off-grid scenario

The center of Figure 20 shows the current status of the stand-alone system; however, when the discount rate increases and the inflation rate decreases, the system will delete wind turbines and avoid using them. The center of the NPC surface plot (Figure 21) also shows the status of the present investment and changes in NPC and COE are predicted to help the factory to decide whether this is affordable to use this

project or not. Comparison of the scenarios explains that inflation rate and discount rate fluctuations have significant effects on the stand-alone scenario, compared to the grid-connected scenario. Environmental effects of economic fluctuations are also shown in a surface plot in Figure 22.

Unlike the on-grid scenario, the off-grid system cannot become a negative-carbon producer as it is not connected to

the grid and cannot sell the surplus green energy. Carbon emission of the stand-alone system only varies between 500 kg/yr and 1100 kg/yr. However, the amount of carbon

emissions produced by the on-grid system will significantly change and increase when inflation rate decreases and discount rate decreases.

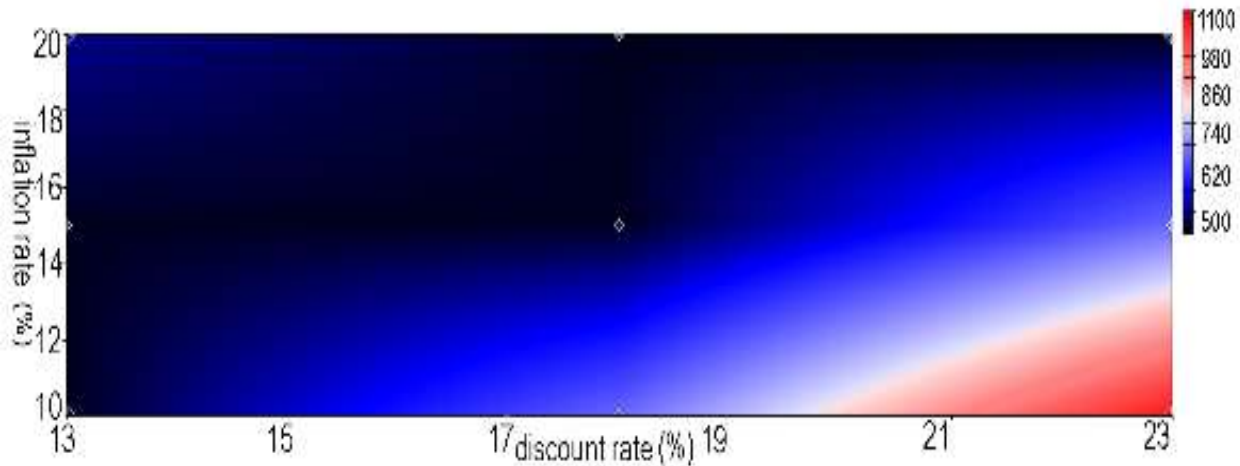


Figure 22. Surface plot of average CO₂ emissions per year in the stand-alone scenario

6.3. Multi-year/single-year compression

The results and effects of using the multi-year module on the whole project consisting of the changes of the optimum system type, NPC, COE, and carbon emissions are analyzed and reported in this part. Effect of economic fluctuations without enabling multi-year module in the simulations on the optimum system type of the grid-connected system is shown in a surface plot in Figure 23.

According to Figure 23, effects of fluctuations of inflation and discount rates while multi-year module is disabled creates four different optimum systems. The optimum systems shown in Figure 23 totally differ from those that are obtained in Figure 14. Although the present system at the center of Figure 23 is the same as the one in Figure 14 (PV/battery), using multi-year module of HOMER pro software significantly affects the installed systems in other economic conditions.

Increasing the inflation rate deletes the battery component in the single-year model and adds the biogas generator. If the inflation rate reaches 16 % and discount rate decrease to 15 %, batteries will be added to the PV/bio system again. Stand-alone system is no exception and disabling the multi-year module will affect the optimum system type of it, too. Effect of economic fluctuations while the multi-year module is not enabled on the off-grid system is shows in Figure 24.

Figure 24 indicates that disabling the multi-year module will delete the wind turbine component in the present condition. The wind turbine can only be added to the bio/PV/battery system if the inflation rate reaches 19 % and discount rate goes under 14 %. Table 22 compares the amount of NPC and COE of the multi-year mode with those in the single-year mode. Note that this compression belongs to the present inflation rate and discount rate.

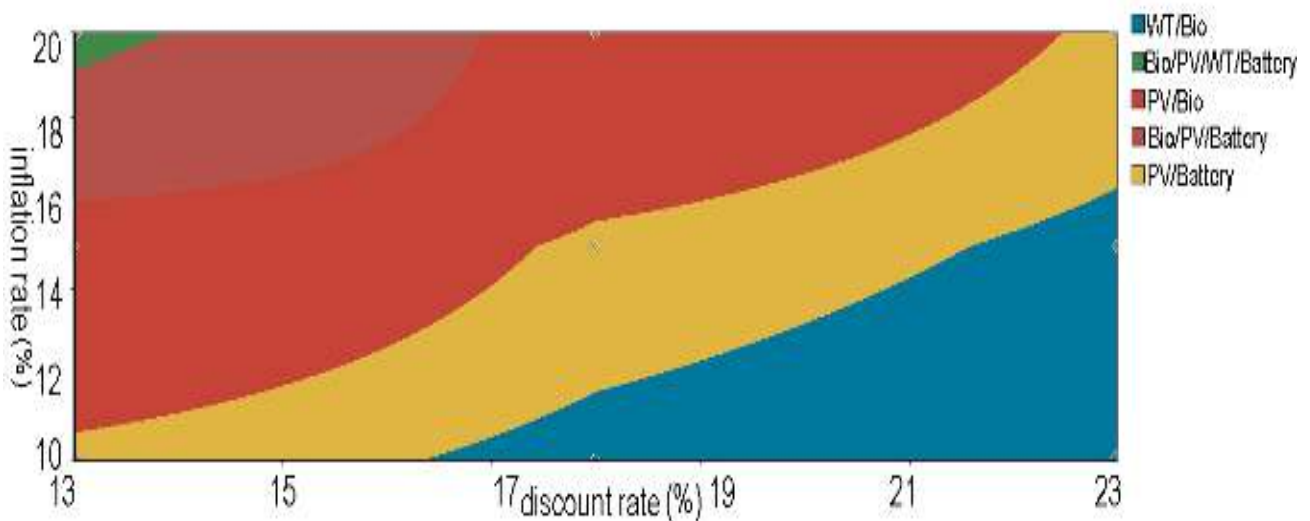


Figure 23. Surface plot of the optimum system type while the multi-year module is disabled (on-grid mode)

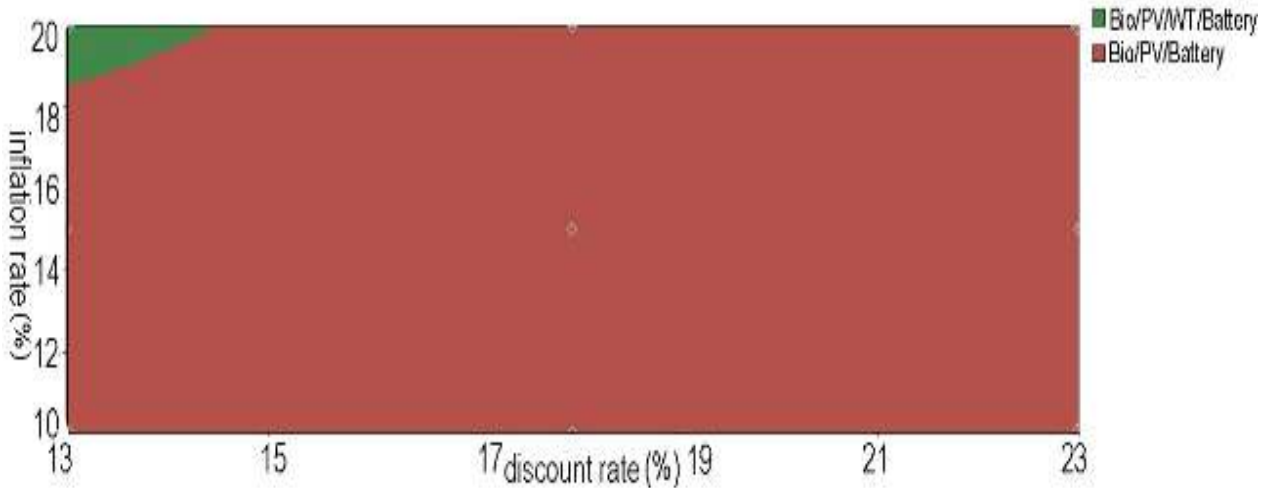


Figure 24. Surface plot of the optimum system type while the multi-year module is disabled (off-grid mode)

Table 22. Multi-year module effects on NPC and COE

Parameter	Multi-year	Grid-connected	Stand-alone	Unit
NPC	■	200,415	597,970	\$
NPC	□	144,620	371,074	\$
COE	■	0.07	0.35	\$/kWh
COE	□	0.0528	0.314	\$/kWh

The difference between the NPCs of the grid-connected system between the multi-year mode and the single-year mode, which is shown in Table 22, is 55,795 \$. For the stand-alone system, the amount of difference is equal to 226,896 \$. From this difference between the NPC values, it can be obtained that using the multi-year module of the HOMER pro software improved the simulations by adding greater accuracy to them. In addition to economic parameters, emissions can also be analyzed more accurately. Carbon emission trend of designed energy hubs for both single-year and multi-year modes is shown in Figure 25 (Present inflation rate and discount rate).

Changing the CO₂ emission during the project life time due to PV degradation and changes of electrical loads is clear in Figure 25. Further, by disabling the multi-year module, CO₂ emission of both on-grid and off-grid systems remains a constant value. The grid-connected system saves 43,819 kg of CO₂ per year. By enabling the multi-year module, this value will change as the project progresses and will reach 14,673 kg/yr in the last year. The stand-alone system only emits 149 kg/yr in the single-year mode. However, by employing the multi-year module of HOMER pro software, the amount of emitted CO₂ in the off-grid system will increase and reach 655 kg/yr in the 25th year of the project.

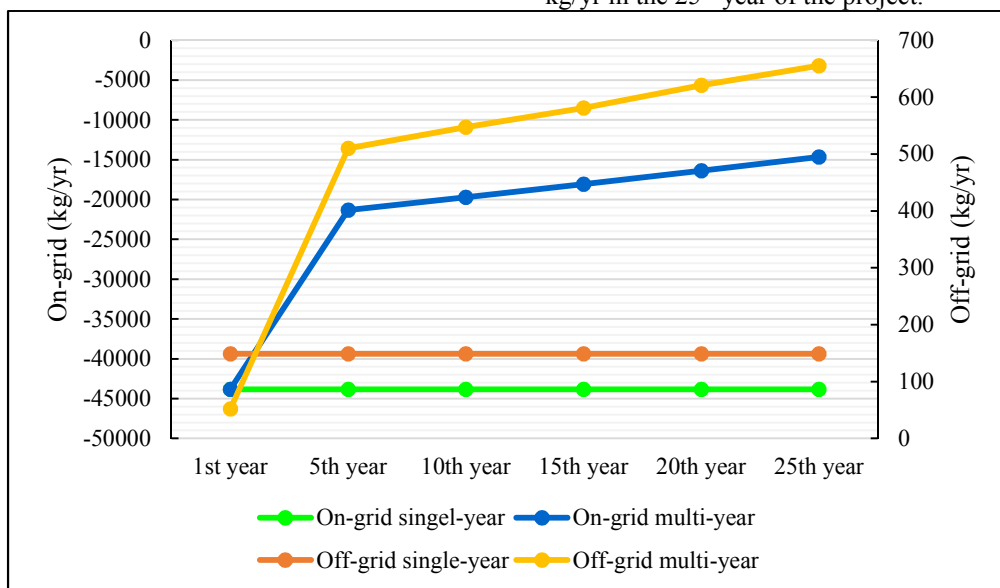


Figure 25. Effects of the multi-year module on the carbon emission trend of the system

7. CONCLUSIONS

This paper, for the first time, aimed to investigate the use of green energies in factories and industrial projects by considering the industrial deferrable load, changes in electrical load, degradation of components, and economic fluctuations. Most factories use air compressors and pumps in their production lines. The most important results of this research are given as follows:

- Increasing the electrical consumption of the factory and degradation of PVs together reduces the solar energy penetration from 250 % in the 1st year to 142 % in the last year and also, increases the leveled cost of solar energy from 0.061 \$/kWh in the beginning of the project to 0.072 \$/kWh in the 25th year (optimum grid-connected scenario).
- Increasing the electrical loads of the factory and reducing solar panels production can increase the use of biogas from 742 kg/yr at the beginning of the project to 9330 kg/yr at the end of the project. The electrical production of the biogas generator also reaches 4271 kWh/yr in the 25th year from 338 kWh/yr in the 1st year.
- Economic fluctuations lead the simulation to choose two off-grid systems: PV/bio/WT/battery and PV/bio/battery.
- Fluctuations of economics do not have considerable effects on carbon emissions of stand-alone systems, but may significantly increase the carbon emissions of on-grid systems.
- Comparison of the single-year mode and multi-year mode indicates that disabling the multi-year module will totally change optimum system types of both on-grid and off-grid systems. However, the present grid-connected system will remain a PV/battery system, while the optimum stand-alone system will be changed into PV/bio/battery.

8. ACKNOWLEDGEMENT

The authors like to thank the managers of the KSJ factory for their cooperation and providing data for the research. This research did not receive any specific grant from funding agencies in the public, commercial, or not-for-profit sectors.

NOMENCLATURE

Bat	Battery
BG	Biogas generator
COE	Cost of Energy (\$/kWh)
DG	Diesel generator
eLAN	Energy local area network
FC	Fuel cell
HE	Hydro Electric
HSPSI	Pumped Storage
KSJ	Name of the Case Study Factory
NOCT	Nominal Operating Cell Temperature (°C)
NPC	Net Present Cost (\$)
O & M	Operating and Maintenance
OC	Operating Cost (\$)
PV	Photovoltaic
STC	Standard Test Condition
WT	Wind Turbine

Greek letters

τ	Solar transmittance of the cover over PV array (%)
μ	temperature coefficient (-)

REFERENCES

1. Bukar, A.L. and Tan, C.W., "A review on stand-alone photovoltaic-wind energy system with fuel cell: System optimization and energy management strategy", *Journal of Cleaner Production*, Vol. 221, (2019), 73-88. (<https://doi.org/10.1016/j.jclepro.2019.02.228>).
2. Akikur, R.K., Saidur, R., Ping, H.W. and Ullah, K.R., "Comparative study of stand-alone and hybrid solar energy systems suitable for off-grid rural electrification: A review", *Renewable and Sustainable Energy Reviews*, Vol. 27, (2013), 738-752. (<https://doi.org/10.1016/j.rser.2013.06.043>).
3. Haddad, A., Ramadan, M., Khaled, M., Ramadan, H. and Becherif, M., "Study of hybrid energy system coupling fuel cell, solar thermal system and photovoltaic cell", *International Journal of Hydrogen*, Vol. 45, No. 25, (2020), 13564-13574. (<https://doi.org/10.1016/j.ijhydene.2018.06.019>).
4. Xu, X., Hu, W., Cao, D., Huang, Q., Chen, C. and Chen, Z., "Optimized sizing of a standalone PV-wind-hydropower station with pumped-storage installation hybrid energy system", *Renewable Energy*, Vol. 147, Part 1, (2020), 1418-1431. (<https://doi.org/10.1016/j.renene.2019.09.099>).
5. Ribó-Pérez, D., Herraiz-Cañete, Á., Alfonso-Solar, D., Vargas-Salgado, C. and Gómez-Navarro, T., "Modelling biomass gasifiers in hybrid renewable energy microgrids: A complete procedure for enabling gasifiers simulation in HOMER", *Renewable Energy*, Vol. 174, (2021), 501-512. (<https://doi.org/10.1016/j.renene.2021.04.083>).
6. Purlu, M., Beyarslan, S. and Turkay, B.E., "Optimal design of hybrid grid-connected microgrid with renewable energy and storage in a rural area in Turkey by using HOMER", *Proceedings of 13th International Conference on Electrical and Electronics Engineering (ELECO)*, IEEE, (2021), 263-267. (<https://doi.org/10.23919/ELECO54474.2021.9677788>).
7. De la Cruz-Soto, J., Azkona-Bedia, I., Velazquez-Limon, N. and Romero-Castanon, T., "A techno-economic study for a hydrogen storage system in a microgrid located in baja California, Mexico. Levelized cost of energy for power to gas to power scenarios", *International Journal of Hydrogen Energy*, Vol. 47, No. 20, (2022), 30050-30061. (<https://doi.org/10.1016/j.ijhydene.2022.03.026>).
8. Jahangir, M.H., Montazeri, M., Mousavi, S.A. and Kargarzadeh, A., "Reducing carbon emissions of industrial large livestock farms using hybrid renewable energy systems", *Renewable Energy*, Vol. 189, (2022), 52-65. (<https://doi.org/10.1016/j.renene.2022.02.022>).
9. Shakya, S.R., Bajracharya, I., Vaidya, R.A., Bhawe, P., Sharma, A., Rupakheti, M. and Bajracharya, T.R., "Estimation of air pollutant emissions from captive diesel generators and its mitigation potential through microgrid and solar energy", *Energy reports*, Vol. 8, (2022), 3251-3262. (<https://doi.org/10.1016/j.egy.2022.02.084>).
10. Roth, A., Boix, M., Gerbaud, V., Montastruc, L. and Etur, P., "A flexible metamodel architecture for optimal design of Hybrid Renewable Energy Systems (HRES)–Case study of a stand-alone HRES for a factory in Tropical Island", *Journal of Cleaner Production*, Vol. 223, (2019), 214-225. (<https://doi.org/10.1016/j.jclepro.2019.03.095>).
11. Ogunjuigbe, A. and Ayodele, T., "Techno-economic analysis of stand-alone hybrid energy system for Nigerian telecom industry", *International Journal of Renewable Energy Technology*, Vol. 7, No. 2, (2016), 148-162. (<https://www.inderscienceonline.com/doi/abs/10.1504/IJRET.2016.076089>).
12. Diab, F., Lan, H., Zhang, L. and Ali, S., "An environmentally friendly factory in Egypt based on hybrid photovoltaic/wind/diesel/battery system", *Journal of Cleaner Production*, Vol. 112, Part 5, 3884-3894. (<https://doi.org/10.1016/j.jclepro.2015.07.008>).
13. Al-Ghussain, L., Ahmed, H. and Haneef, F., "Optimization of hybrid PV-wind system: Case study Al-Tafilah cement factory, Jordan", *Sustainable Energy Technologies and Assessments*, Vol. 30, (2018), 24-36. (<https://doi.org/10.1016/j.seta.2018.08.008>).
14. Makhija, S.P. and Dubey, S., "Feasibility analysis of biomass-based grid-integrated and stand-alone hybrid energy systems for a cement plant in India", *Environment, Development and Sustainability*, Vol. 21, No. 2, (2019), 861-878. (<https://doi.org/10.1007/s10668-017-0064-0>).
15. Mirzaei, M. and Vahidi, B., "Feasibility analysis and optimal planning of renewable energy systems for industrial loads of a dairy factory in Tehran, Iran", *Journal of Renewable and Sustainable Energy*, Vol. 7, No. 6, (2015), 063114. (<https://doi.org/10.1063/1.4936591>).

16. Shezan, S.A., Julai, S., Kibria, M., Ullah, K., Saidur, R., Chong, W. and Akikur, R., "Performance analysis of an off-grid wind-PV (photovoltaic)-diesel-battery hybrid energy system feasible for remote areas", *Journal of Cleaner Production*, Vol. 125, 121-132. (<https://doi.org/10.1016/j.jclepro.2016.03.014>).
17. HOMER, Designing of the deferrable load, (2020). (https://www.homerenergy.com/products/pro/docs/latest/deferrable_load.html), (Accessed 29 March 2020).
18. Izadyar, N., Ong, H.C., Chong, W.T., Mojumder, J.C. and Leong, K., "Investigation of potential hybrid renewable energy at various rural areas in Malaysia", *Journal of Cleaner Production*, Vol. 139, (2016), 61-73. (<https://doi.org/10.1016/j.jclepro.2016.07.167>).
19. Singh, A., Baredar, P. and Gupta, B., "Techno-economic feasibility analysis of hydrogen fuel cell and solar photovoltaic hybrid renewable energy system for academic research building", *Energy Conversion and Management*, Vol. 145, (2017), 398-414. (<https://doi.org/10.1016/j.enconman.2017.05.014>).
20. Mandal, S., Das, B.K. and Hoque, N., "Optimum sizing of a stand-alone hybrid energy system for rural electrification in Bangladesh", *Journal of Cleaner Production*, Vol. 200, (2018), 12-27. (<https://doi.org/10.1016/j.jclepro.2018.07.257>).
21. Zahboune, H., Zouggar, S., Krajacic, G., Varbanov, P.S., Elhafyani, M. and Ziani, E., "Optimal hybrid renewable energy design in autonomous system using Modified Electric System Cascade Analysis and Homer software", *Energy Conversion and Management*, Vol. 126, 909-922. (<https://doi.org/10.1016/j.enconman.2016.08.061>).
22. Sarkar, T., Bhattacharjee, A., Samanta, H., Bhattacharya, K. and Saha, H., "Optimal design and implementation of solar PV-wind-biogas-VRFB storage integrated smart hybrid microgrid for ensuring zero loss of power supply probability", *Energy Conversion and Management*, Vol. 191, (2019), 102-118. (<https://doi.org/10.1016/j.enconman.2019.04.025>).
23. Belfkira, R., Zhang, L. and Barakat, G., "Optimal sizing study of hybrid wind/PV/diesel power generation unit", *Solar Energy*, Vol. 85, No. 1, (2011), 100-110. (<https://doi.org/10.1016/j.solener.2010.10.018>).
24. Hanafizadeh, P., Eshraghi, J., Ahmadi, P. and Sattari, A., "Evaluation and sizing of a CCHP system for a commercial and office buildings", *Journal of Building Engineering*, Vol. 5, (2016), 67-78. (<https://doi.org/10.1016/j.jobbe.2015.11.003>).
25. Jahangir, M.H., Javanshir, F. and Kargarzadeh, A., "Economic analysis and optimal design of hydrogen/diesel backup system to improve energy hubs providing the demands of sport complexes", *International Journal of Hydrogen Energy*, Vol. 46, No. 27, (2021), 14109-14129. (<https://doi.org/10.1016/j.ijhydene.2021.01.187>).
26. Halabi, L.M., Mekhilef, S., Olatomiwa, L. and Hazelton, J., "Performance analysis of hybrid PV/diesel/battery system using HOMER: A case study Sabah, Malaysia", *Energy Conversion and Management*, Vol. 144, (2017), 322-339. (<https://doi.org/10.1016/j.enconman.2017.04.070>).
27. Poeschl, M., Ward, S. and Owende, P., "Prospects for expanded utilization of biogas in Germany", *Renewable and Sustainable Energy Reviews*, Vol. 14, No. 7, (2010), 1782-1797. (<https://doi.org/10.1016/j.rser.2010.04.010>).
28. IRENA, Biogas Cost Reductions to Boost Sustainable Transport, (2017). (<https://www.irena.org/newsroom/articles/2017/Mar/Biogas-Cost-Reductions-to-Boost-Sustainable-Transport>), (Accessed 7 April 2020).
29. Taban, e.d.c., PERC Mono Crystalline 72 Cell Module, (2019). (<https://tabanenergy.ir/wp-content/pdf/catalogue5BB-Mono-Feb2019.pdf>), (Accessed 16 April 2020).
30. Mohammadi, M., Ghasempour, R., Astarai, F.R., Ahmadi, E., Aligholian, A. and Toopshekan, A., "Optimal planning of renewable energy resource for a residential house considering economic and reliability criteria", *International Journal of Electrical Power & Energy Systems*, Vol. 96, 261-273. (<https://doi.org/10.1016/j.ijepes.2017.10.017>).
31. Rad, M.A.V., Ghasempour, R., Rahdan, P., Mousavi, S. and Arastounia, M., "Techno-economic analysis of a hybrid power system based on the cost-effective hydrogen production method for rural electrification, a case study in Iran", *Energy*, Vol. 190, (2020), 116421. (<https://doi.org/10.1016/j.energy.2019.116421>).
32. Li, C., Zhou, D. and Zheng, Y., "Techno-economic comparative study of grid-connected PV power systems in five climate zones, China", *Energy*, Vol. 165, Part B, (2018), 1352-1369. (<https://doi.org/10.1016/j.energy.2018.10.062>).
33. Gökçek, M., "Integration of hybrid power (wind-photovoltaic-diesel-battery) and seawater reverse osmosis systems for small-scale desalination applications", *Desalination*, Vol. 435, (2018), 210-220. (<https://doi.org/10.1016/j.desal.2017.07.006>).
34. Aziz, A.S., Tajuddin, M.F.N., Adzman, M.R., Azmi, A. and Ramli, M.A., "Optimization and sensitivity analysis of standalone hybrid energy systems for rural electrification: A case study of Iraq", *Renewable Energy*, Vol. 138, 775-792. (<https://doi.org/10.1016/j.renene.2019.02.004>).
35. Shahzad, M.K., Zahid, A., ur Rashid, T., Rehan, M.A., Ali, M. and Ahmad, M., "Techno-economic feasibility analysis of a solar-biomass off grid system for the electrification of remote rural areas in Pakistan using HOMER software", *Renewable Energy*, Vol. 106, 264-273. (<https://doi.org/10.1016/j.renene.2017.01.033>).



Technical Note

Analysis of Biogas Recovery from Liquid Dairy Manure Waste by Anaerobic Digestion

Fatemeh Norouzi^a, Morteza Hosseinpour^{b*}, Saeed Talebi^a

^a Department of Energy Engineering and Physics, Amirkabir University of Technology (Tehran Polytechnic), P. O. Box: 15875-4413, Tehran, Iran.

^b Department of Renewable Energy Research, Niroo Research Institute (NRI), Tehran, Iran.

PAPER INFO

Paper History:

Received: 12 April 2022

Revised: 03 August 2022

Accepted: 12 August 2022

Keywords:

Anaerobic Digestion,

Biogas,

Process Simulation,

Liquid Dairy Manure

ABSTRACT

In this paper, an industrial dairy farm unit was taken as a case study to carry out the applicable technical assessment for the construction of a biogas plant using a combined heat and power (CHP) unit. A comprehensive sensitivity analysis was applied to examine the effectiveness of the operational parameters and feed composition in the purity and production rate of biogas. Aspen Plus was used to implement the anaerobic digestion process. The results showed that any increase in the digester's operational performance and mass rate of feedstock water led to the modification of biomethane content, but dropped in biogas mass flow rate. Moreover, an increase in the mass rate of carbohydrates, protein, and organic load rate (OLR) of feedstock reduces methane composition. Besides, increasing the rate of lipids has raised the rate of methane production and its composition.

<https://doi.org/10.30501/jree.2022.336371.1354>

1. INTRODUCTION

Nowadays, dairy products include more than 30 % of the gross volume of agricultural wastes in developing countries [1]. This value has an ever-increasing growth due to income and population growth and changes in lifestyle and diet. Dairy products create around 60 million tons of waste annually, about 20 % of the total globally produced wastes [2]. Such an enormous quantity of wastes accumulated without suitable management is quite hazardous to the environment. They would cause a series of irreversible damages to water and soil, environmental contaminations like pollution of aquifers, groundwater eutrophication, accumulation of nutrients in soil, dispersion pathogens, accumulation of toxic ingredients, and greenhouse gas emissions (methane, oxide nitrogen, and ammonia) [3, 4]. Farm-based management approaches could reduce these issues in dairies. Anaerobic digestion is one of the most attractive and economical ways based on environmental regulations [5, 6]. By producing heat and power and remaining digestate as organic compost, this method can decrease the organic waste volume and increase the total efficiency of resources [7]. Anaerobic digestion has four stages where in each stage, a group of microorganisms degrades primary substrates and leaves them to the next stage [8]:

- Hydrolysis: In this stage, complex organic molecules are converted into monomeric compounds by hydrolyzing bacteria, and all non-dissolved particles change into

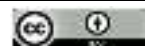
aqueous solutions that would become usable for microorganisms [9]. During this stage, carbohydrate, lipid, protein, lignin, and nonorganic materials break down into simple molecules such as sugar, alcohol, short-chain fatty acids, amino acid, aromatic compounds, non-degradable organic materials, and nonorganic materials. It should be noted that lignin degradation is complicated due to its weak solvability, molecular largeness, and complicated structure.

- Acidogenesis (fermentation): After the fermentation of primary molecules and their transformation into monomeric compounds, all monomers are converted into short-chain organic acids, acetic acids, propionic acids, butyric acids, pentanoic acids, hydrogen, CO₂, and other compounds by acidogenic bacteria. Also, alcohols like ethanol and methanol can be extracted from the remaining substrates. Also, aldehydes and oxygen are produced in this stage. Finally, all produced products are left to the methanogenic bacteria [10-13].
- Acetogenic phase: In the third stage, the decomposed substrates are converted into CO₂, H₂, and acetate by acetogenic bacteria. The hydrogen released during this stage has toxic effects on the process [13].
- Methanogenic phase: The last step of the anaerobic digestion process is the methanogenic phase. In this stage, methanogens produce methane by utilizing the previously produced products (CO₂, hydrogen, and acetate). This phase is carried out by two groups of microorganisms. The first one converts acetate into methane and CO₂ and the second group uses hydrogen as a donor and CO₂ as an

*Corresponding Author's Email: mhosseinpour@nri.ac.ir (M. Hosseinpour)

URL: https://www.jree.ir/article_156474.html

Please cite this article as: Norouzi, F., Hosseinpour, M. and Talebi, S., "Analysis of biogas recovery from liquid dairy manure waste by anaerobic digestion", *Journal of Renewable Energy and Environment (JREE)*, Vol. 10, No. 2, (2023), 125-132. (<https://doi.org/10.30501/jree.2022.336371.1354>).



acceptor to produce methane. The methane production process takes a long time via methanogenic bacteria in the range of 3-50 days [14, 15].

Any degradable and organic material can be used as the feedstock of anaerobic digestion that can be transformed into methane (CH_4), carbon dioxide (CO_2), and other gases through biological processes [16-18]. CH_4 usually comprises about 45-75 % of the total biogas volume. Based on the CH_4 volume percentage, the lower heating value (LHV) of biogas varies between 16-28 MJ/m^3 [7]. The composition and ingredients of feedstocks significantly affect the efficiency of producing biogas [7, 19]. Due to the physical properties, organic content, and abundance, dairy manures are known as the best biomass and feed for biogas units, especially in developing countries [20]. Carbohydrates, proteins, and lipids are the main compositions of dairy manures that would be very attractive due to their anaerobic bacteria, high water contents (acting as a solvent), and low price [6, 7]. Dairy manure is one of the richest sources of carbohydrates (cellulose, hemicellulose, lignin, sugar, and starch), accounting for over 80 % of organic materials. According to a report published by International Energy Agency (IEA), the agriculture sector will be the biggest biogas producer in the world up to 2040, and animal and agricultural wastes will account for 40 % and 35 % of the total globally produced biogas, respectively [7]. Also, this agency predicts a 2.5 % annual growth in animal waste. The European Union and China are the biggest producers of biogas in this sector [7].

Operational condition including temperature, pressure, pH, retention time, carbon-to-nitrogen ratio, ammonia

concentration, and long-chain fatty acid concentration affect the digestion process in terms of its performance and stability. Hence, optimal conditions can bring about the health and growth of microorganisms which would be necessary for continuous digestion process [17, 21, 22]. Accordingly, implementation and simulation of anaerobic digestion is a scientific and complicated process. Many studies have been carried out on modeling. Among them, Anaerobic Digestion Model NO. 1 (ADM1), a mathematical model developed by the International Water Association (IWA) task group [23], is a precise and complete one over its information, reactions, and kinetic calculations. Angelidaki et al. introduced a model covering most of inhibiting factors like free ammonia, volatile fatty acids (VFAs), and long-chain fatty acids [24]. However, this model is characterized by some defects including not considering hydrogen and temperature parameters. Al-Rabiei et al. [25] developed a process simulation model (PSM) and implemented sensitivity analyses considering the effect of hydrogen injection, substrate concentration, and operational parameters on raising the production efficiency of biogas, quantitatively and qualitatively. However, only limited attention has been dedicated to the simulation of anaerobic digestion via physical-chemical processes and parameters affecting biogas production efficiency [13, 25-27]. Hence, this paper aims to conduct a process study of dairy waste produced in livestock farms and production of value-added streams, including biogas and digestate. Moreover, the effect of operational parameters and some inhibitors on CH_4 production was studied.

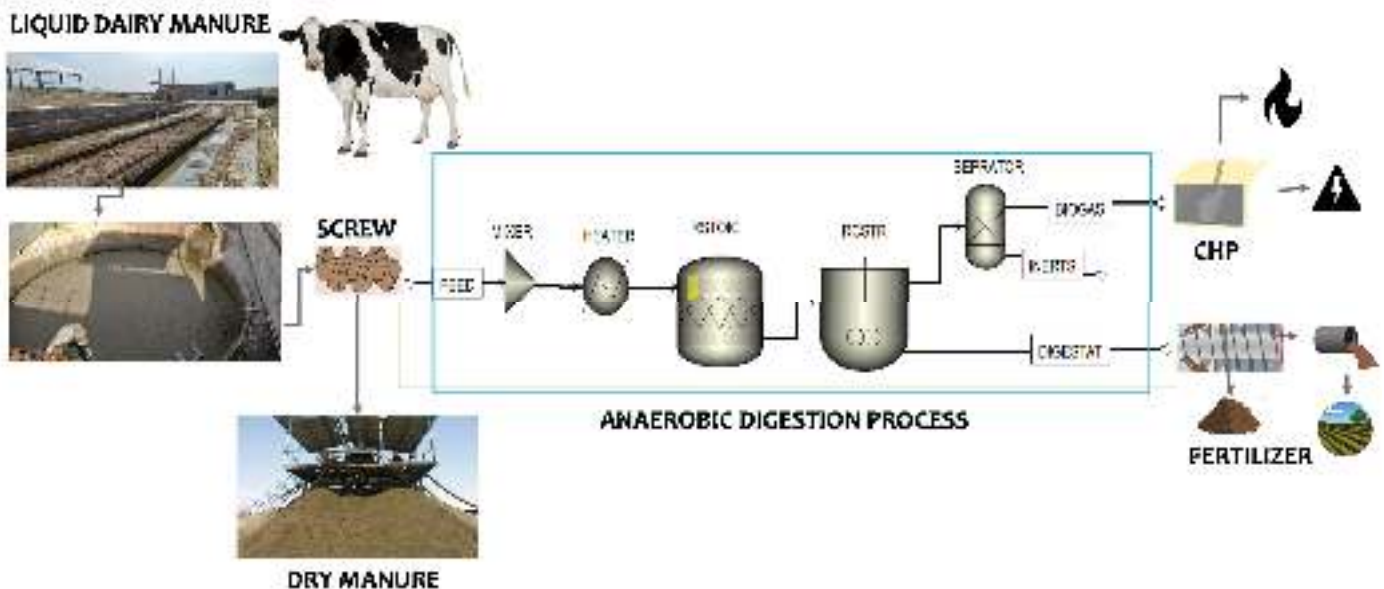


Figure 1. Schematic of anaerobic digestion process from raw material to end products

2. EXPERIMENTAL

2.1. Case study description

An industrial dairy farm is a case study for the integrated management of livestock-made dairy manures. This unit is located in the southeastern province of Khorasan Razavi and has 1620 head of livestock, including cattle and dairy cows. The average weight of cows is around 670 kg, and each one produces approximately 0.048 m^3 manure daily. The keeping system is based on freestalls, and the flushed-water system is

used for waste collection, washing, and sand scratching. It should be noted that before storing the wastes, solid-liquid separation is needed because the solid particles derived from livestock beds can cause many problems during the pumping of waste and dislocation, and their concentration over time decreases the capacity of the waste storage system (see Fig. 1). Moreover, mechanical separators can facilitate recycling wastes and land applications. More information about this case is shown in Table 1.

Table 1. Animal husbandry, liquid dairy manure, and biogas components information [28]

Animal husbandry	
Total number of mature animals (head)	1620
Type of keeping and washing system	Free stall-flushed water system
Bed type	Sand
The volume of manure produced per animal (m ³ /day)	0.048
The volume of consumed water by each animal (m ³ /day)	0.01
Yearly produced waste (m ³ /day)	34295
Total solid (%) [5]	9.5
Volatile solid (%) [29]	4.355
Liquid dairy manure	
Main components of liquid dairy manure [26]	(% TS)
Carbohydrates (cellulose, hemicellulose, lignin, and starch)	90.2
Fat	1.5
Protein	8.3
Elemental composition of manure (typically dry)	See [30]
Biogas	
Biogas yield (m ³ /t ODM) [5]	300
Main components of biogas:	Composition (%)
CH ₄	50-75
CO ₂	25-50
N ₂	0-10
H ₂	0-1
H ₂ S	0-3

2.2. Process design

In this process, the degradable materials were decomposed in the absence of oxygen and converted into CH₄, CO₂, and other gases [5, 13, 31]. Table 1 shows the biogas compounds from the anaerobic digestion process. The PSM was chosen to model the anaerobic digestion process. The model, developed by Karthik Rajendran [26], is a library model estimating the productions of the anaerobic digestion process from any organic feedstock in different process conditions. This model includes 46 reactions (13 reactions of hydrolysis and 33 reactions related to acidogenic, acetogenic, and methanogenic stages) and inhibitions such as pH, ammonia concentration, load rate, retention time, and ten calculator blocks. The model has investigated biogas reactors working in 55 °C thermophilic conditions. Due to the comprehensiveness of the model (in terms of reactions, kinetic, stoichiometry, and inhibition factors), it was selected as the implemented model. Aspen Plus software was used to simulate the process. Making the right choice of the thermodynamic model is crucial since

its inappropriate selection affects the calculations and can yield results ranging from non-optimal to catastrophic. The thermodynamic model NRTL is chosen as the property package. The reason for this selection is its ability to compute the activity coefficient and the molar fraction [13]. The heater was also used to increase the feed temperature up to 55 °C. All the kinetic reactions are followed by the power-law model and are represented by first-order kinetics. Acid-base reactions are carried out as equilibrium reactions.

The Aspen Process model is shown in Figure 1. Apparently, the digestion process takes place within two phases: the first phase is hydrolysis in which all of the reactions were carried out by stoichiometric and based on the extent of the reaction inside a stoichiometric reactor. The second stage comprised acidogenic, acetogenic, and methanogenic steps. The output of the first reactor is carbohydrate, lipid, and protein monomers added to the continuous stirred tank reactor (CSTR). At real biogas power plants, the same reactor model is used. In this reactor, the feedstock is continuously mixed, entered, and exited. Acidogenic, acetogenic, and methanogenic reactions were operated based on kinetic reactions. Residence time was chosen as the design and reactor simulation parameter. The CSTR reactor has one source stream and two product streams: biogas and digestate. The flow of biogas contains inert gases which must be separated by the splitter component during the separation process. Feedstock characteristics and process parameters such as temperature, pressure, load rate, and retention time are shown in Tables 2 [13, 20, 32]. Since the degradation of lignin is highly complicated and time-consuming, it is considered an inert component.

Table 2. Liquid dairy manure composition used as feedstock and presumed operational parameters in the Aspen Plus model

Component (dry composition)	
Cellulose	0.204
Hemicellulose	0.086
Glucose	0.257
Protein (glycine)	0.083
Triolein	0.015
Lignin	0.20
Inert	0.155
Assumed operational parameters of the process	
Reactor temperature (°C)	55
Reactor pressure (atm)	1
Hydraulic retention time (day)	15
Volumetric flow rate* (m ³ /day)	93.96
* volume of manure and consumed water	

3. RESULTS AND DISCUSSION

3.1. Biogas production and compounds

Table 3 shows the biogas composition from the simulation. CH₄ and CO₂ make up 54 % and 37 % of biogas, respectively. The left 9 % includes other gasses: water vapor, hydrogen sulfide (H₂S), nitrogen, ethanol, and ammonia. About 95 % of feed is converted into digestate, and its compound is shown in Table 3. To investigate the effect of operational parameters and the composition of the liquid dairy manure on the composition of CH₄, sensitivity analysis is performed.

Table 3. Biogas compounds and characteristics resulting from the anaerobic digestion process

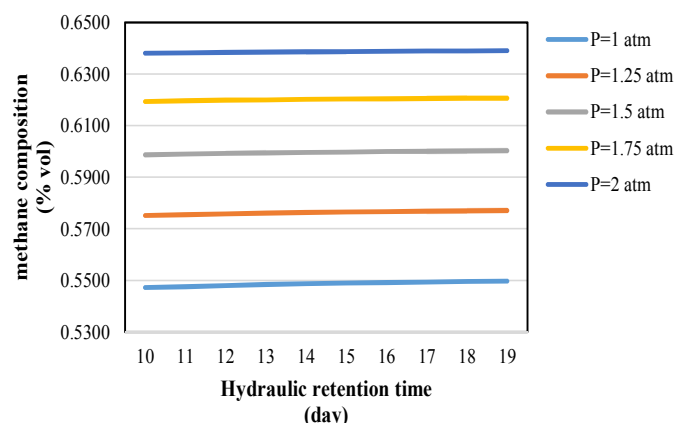
Biogas	
Biogas flow (m ³ /day)	1306
Enthalpy flow (kW)	300
Density (kg/m ³)	1.12
Component	Composition (%)
CH ₄	0.54
CO ₂	0.37
H ₂ O	0.02
H ₂ S	0.009
NH ₃	0.003
C ₂ H ₅ OH	0.004
H ₂	0.002
Digestate	
Biogas flow (m ³ /day)	105.3
Enthalpy flow (KW)	-16710
Density (kg/m ³)	1.003
Component	Composition (%)
Water	0.84
CO ₂	0.01
Glucose	0.04
Cellulose	0.01
Hemicellulose	0.006
Ethanol	0.008
Protein	0.001
Ammonia	0.001
Inert	0.06

3.1.1. Effect of the hydraulic retention time and operational pressure

The Hydraulic Retention Time (HRT) indicates the time it takes to exchange the entire feedstock volume in the reactor and this is dependent on feed composition, reactor temperature and volume, and reaction kinetic rates. Due to longer HRT, the volume of the reactor and investment cost will also increase. On the other hand, lower HRT inhibits the growth and activity of microorganisms and increases the accumulation of VFAs [33]. HRT must be long enough so that the number of microorganisms removed with digestate would not exceed the number of regenerated microorganisms [34]. The residence time required for duplicating anaerobic bacteria is at least 10 days [6]. Besides, the operating pressure is one of the most critical process parameters affecting anaerobic digestion. The solubility of some components in the liquid phase depends on the pressure of the digester [25]. For example, since compounds such as CO₂ and triglycerides have acid-based reactions, they affect the pH level and inhibit the toxic effect of ammonia and non-ionized hydrogen sulfide [21, 35, 36].

As shown in Figure 2, the volume percentage of CH₄ increased by increasing digester pressure, but a higher HTR

did not significantly affect the composition of CH₄ product. The reason for this trend is the availability of the substrates that have been reduced and decomposed. In addition, the increase in retention time increases the risk of VFA accumulation. This increase leads to a decrease in the pH level and inhibits the activity of microorganisms, especially methanogenic microorganisms. However, accumulation of VFAs does not always reduce pH levels, and it depends on the capacity of the digester and alkalinity of feedstock. It can be concluded that increasing the operating pressure will reduce the content of CH₄ product and cause the formation of the inhibitor effects on the process.

**Figure 2.** Effect of retention time on composition of biogas at different digestion pressures

3.1.2. Effect of carbon-to-nitrogen ratio

The C/N ratio shows the nutrient content of substrates [37]. Too low or high C/N ratios can inhibit or even stop the digestion process. At high C/N ratios, methanogenic microorganisms rapidly consume nitrogen in the substrates, and the lack of nitrogen disrupts the growth and duplication of microorganisms and reduces biogas efficiency [38, 39]. On the other hand, at a low C/N ratio, ammonia is produced from the decomposition of excess ammonia nitrogen, which is toxic to the health and growth of microbes and increases the risk of ammonia inhibition [13]. Since carbon is the main element of carbohydrates to study the effect of carbon-to-nitrogen ratio on the anaerobic digestion process, carbohydrate is considered a representative of carbon [27]. Carbohydrates are substances resisting decomposition; therefore, pretreatment is needed to hydrolyze them [40]. The addition of enzymes is one of the best ways to increase the efficiency of biogas production from carbohydrate-rich organic substrates [19]. Because of their smaller size, higher solubility, and greater dynamism of enzymes, they have more access to substrates and the digestion process occurs faster [41]. According to Figure 3, increasing the mass rate of carbohydrates and digestion retention time decreases the biomethane content. This declining trend results from the resistance of carbohydrates to degradation and decomposition by hydrolyzing microorganisms, reducing the rate of hydrolysis, and process efficiency. Also, increasing the mass rate of carbohydrates leads to the reduction and deficiency of nutrients required for the activity of microorganisms and also, it increases the production rate of VFAs and long-chain fatty acids resulting from the acidification process [42].

3.1.3. Effect of fatty acids

The concentration of fatty acids has a direct effect on digester stability [37]. Fatty acids and glycerol are intermediate components produced by fat (lipids) hydrolysis. First, Glycerol is decomposed into propionic acid during the acidification process and then, decomposed into hydrogen, CO₂, and acetic acid during the acetogenic process along with long-chain fatty acids [19]. Finally, hydrogen and CO₂ are converted into CH₄ during the hydrogen utilizing step reactions and acetic acid during acetoacetic reaction [12]. Due to the high degradability of fat-rich substrates, the yield of biogas production from them is high [42]. The potential for CH₄ production from this biomass is 170 % and 111 % higher than feedstocks, which are rich in carbohydrates and proteins, respectively [43]. However, excessive concentrations of fatty acids reduce the pH level [6, 42]. Figure 4 shows the effect of fat mass flow rate on CH₄ composition and volume flow at different HRTs. As can be seen, by increasing the amount of lipid, the CH₄ composition would be modified. The upward trend is due to more volatile organic substrates, which are available to microorganisms, and the high alkalinity of dairy manure preventing excessive accumulation of VFAs.

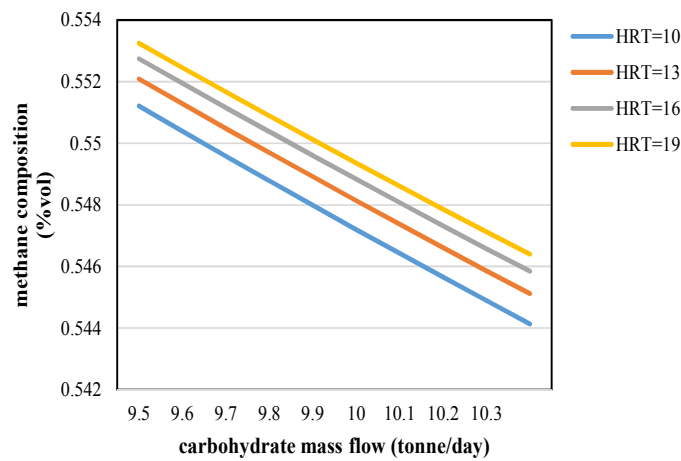


Figure 3. Effect of carbohydrate rate on the composition of biogas at different retention times

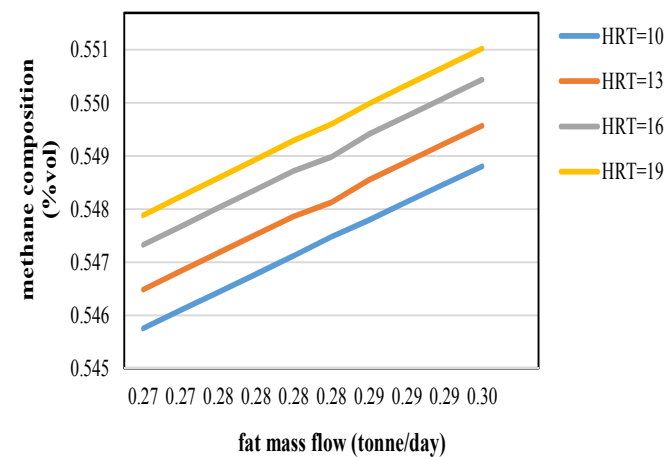


Figure 4. Effect of lipid on biogas composition of at different retention times

3.1.4. Effect of ammonia

The amino acids produced during the process of protein hydrolysis are converted into ammonia by Stickland reactions. Ammonia is essential for the growth and nutrition of bacteria,

but its excessive concentration interferes with the activity of methanogenic bacteria and can be perceived as an inhibitory parameter for the process [6, 44]. According to findings, protein-rich biomass is not a viable resource for biogas production, and even it can stop the anaerobic digestion process [45]. According to Figure 5, the addition of protein increases the biomethane content. Due to the high concentration of dairy manure ammonia (derived from livestock urine), the ammonia obtained from protein breakdown intensifies the ammonia inhibition effect and reduces the biomethane purity. One way to reduce the concentration of ammonia is the addition of calcium hydroxide (Ca(OH)₂), magnesium hydroxide (Mg(OH)₂), and sodium hydroxide (NaOH) [46-48]. The concentration of free ammonia is directly related to temperature, and temperature control affects the dissolution rate of the ammonia component. Increasing the temperature increases the solubility of the ammonia and increases the risk of ammonia inhibition [46].

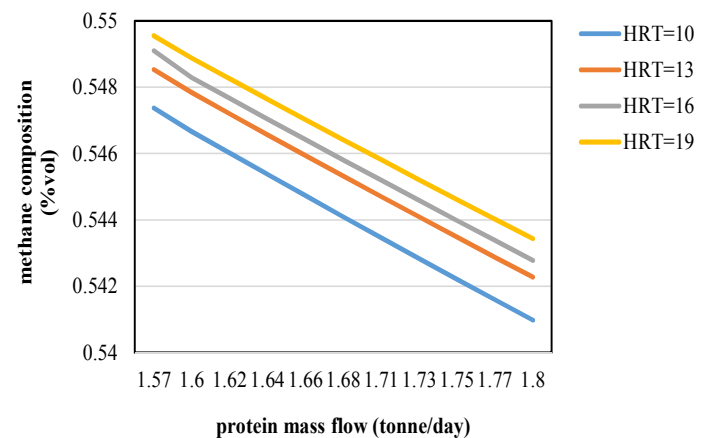


Figure 5. Methane composition as a function of mass protein rate at different retention times

3.1.5. Effect of water

The balanced amount of dry matter and water in the feedstock are vital factors in the design of the anaerobic digestion process. The water content of feedstock affects the growth rate of cells. If the water content is too high, less dry matter will be available to microorganisms, and the process will not be economical. Also, if the amount of water is too low, cell growth will be delayed and the material conversion becomes a limiting factor [49]. Figure 6 show the decline in biomethane content as the water rate increases.

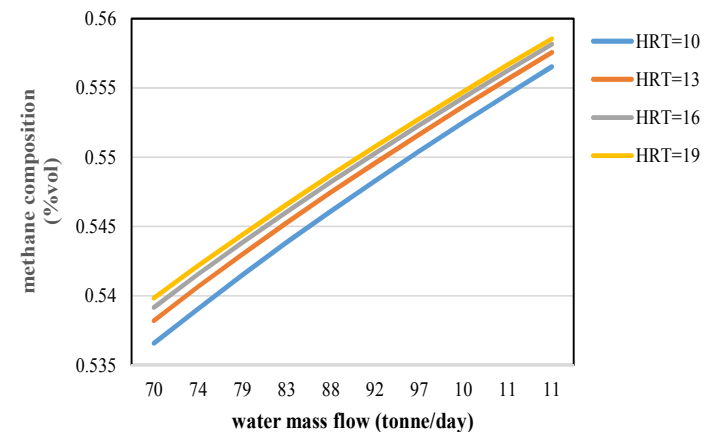


Figure 6. Effect of protein on composition of biogas at different retention times

3.1.6. The effect of organic load rate on CH₄ gas production

The OLR represents the amount of volatile solid mass entered into the digester per unit of time. This parameter is often defined as the mass flow rate of volatile solids (e.g., kg VS per day). According to Fig.7, the addition of the OLR led to a decrease in CH₄ composition. This declining trend is due to the composition of liquid dairy manure and the operating conditions of the process. The major composition of liquid dairy manure is fiber (carbohydrates) and will have a more significant impact on the digestion process than other dairy manure compounds.

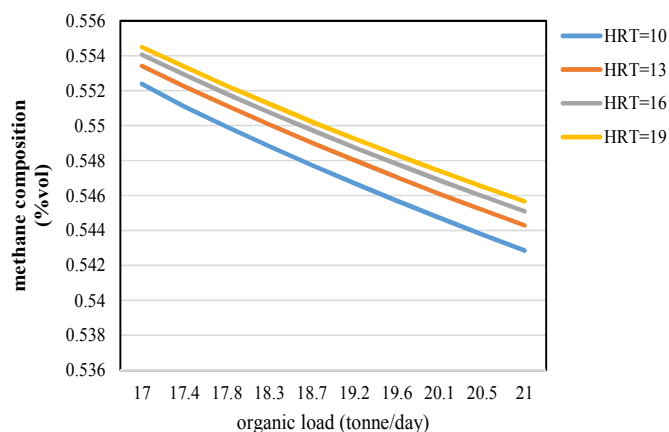


Figure 7. Effect of OLR on composition of biogas at different retention times

As discussed in previous sections, with increasing the mass flow of carbohydrates and proteins, the CH₄ composition decreased. Further, increasing the OLR has increased the methane production rate. The effect of increasing retention time is not significant and even negligible. It is due to the percentage of volatile organic matter in liquid dairy manure, which is lower than other degradable organic matter. As a result, the degradable substrates are consumed quickly, and the increase in retention time does not have a significant impact on the increment of CH₄ production efficiency.

4. CONCLUSIONS

Anaerobic digestion is one of the most appealing waste management systems in developing countries which, in addition to producing value-added materials (biogas and digestate), has significant impacts on reducing adverse environmental problems. The technical performance of this industrial unit was evaluated by selecting a typical industrial livestock farm using the anaerobic digestion system to manage the liquid dairy manure produced on dairy farms. The PSM model is one of the most comprehensive models; thus, it was implemented for anaerobic digestion at a thermophilic temperature of 55 °C and pressure of 1 atm. According to the results, biogas compounds include 54 % biomethane, 36 % CO₂, and around 5 % of trace elements, hence being in good agreement with the results of previous studies. Besides, 1306m³ of biogas and 105 tons of digestate were produced daily under specified operating conditions. To examine the effect of process operating conditions and liquid dairy manure compounds on the efficiency of biomethane production, sensitivity analysis was performed. According to the results, since the solubility of some compounds at the liquid phase depends on digestion pressure, increasing this parameter

reduces the ammonia inhibition and increases the biomethane composition. The increase in carbohydrates mass rate and OLR increased the inhibition of the fatty acids, and increasing the mass rate of protein increased the ammonia inhibition effect and reduced CH₄ composition. As demonstrated by the results, an increase in lipid mass rate increases biomethane composition. The increase in process water led to an increase in the composition of produced biomethane.

5. ACKNOWLEDGEMENT

The authors wish to acknowledge Niroo Research Institute (NRI) as the scientific supporter of this publication.

NOMENCLATURE

LHV	Lower Heating Value
PSM	Process Simulation Model
CSTR	Continuous Stirred Tank Reactor
HRT	Hydraulic Retention Time
VFA	Volatile Fatty Acids
OLR	Organic Load Rate
CHP	Combined Heat and Power

REFERENCES

- George, M., Harper, J., Davy, J., Becchetti, T. and Maier, G., "Ecology and management of annual rangelands series: Livestock production", *University of California Agriculture & Natural Resources: Rangelands and Grazing Livestock*, (2020), 1-24. (<https://doi.org/10.3733/ucanr.8546>).
- Muller, Z. O., "Feed from animal wastes: State of knowledge", *FAO Animal Production and Health Paper*, (1980). (<https://www.fao.org/3/x6518e/x6518e00.htm>).
- Zeb, I., Ma, J., Frear, C., Zhao, Q., Ndegwa, P., Yao, Y. and Kafle, G.K., "Recycling separated liquid-effluent to dilute feedstock in anaerobic digestion of dairy manure", *Energy*, Vol. 119, (2017), 1144-1151. (<https://doi.org/10.1016/j.energy.2016.11.075>).
- Kozłowski, K., Pietrzykowski, M., Czekala, W., Dach, J., Kowalczyk-Juško, A., Józwiakowski, K. and Brzoski, M., "Energetic and economic analysis of biogas plant with using the dairy industry waste", *Energy*, 183, (2019), 1023-1031. (<https://doi.org/10.1016/j.energy.2019.06.179>).
- Akbulut, A., "Techno-economic analysis of electricity and heat generation from farm-scale biogas plant: Çiçekdağı case study", *Energy*, Vol. 44, No. 1, (2012), 381-390. (<https://doi.org/10.1016/j.energy.2012.06.017>).
- Teodorita, A.S., Dominik, R., Heinz, P., Michael, K., Tobias, F., Silke, V. and Rainer, J., *Biogas handbook*, University of Southern Denmark, Denmark, (2008). (<https://www.lemvigbiogas.com/BiogasHandbook.pdf>).
- International Energy Agency, "Outlook for biogas and biomethane: Prospects for organic growth", (2020). (<https://doi.org/10.1787/040c8cd2-en>).
- Uddin, M.M. and Wright M.M., "Anaerobic digestion fundamentals, challenges, and technological advances", *Physical Sciences Reviews*, (2022), 1-19 (<https://doi.org/10.1515/psr-2021-0068>).
- Angelidaki, I., Chen, X., Cui, J., Kaparaju, P. and Ellegaard, L., "Thermophilic anaerobic digestion of source-sorted organic fraction of household municipal solid waste: Start-up procedure for continuously stirred tank reactor", *Water Research*, Vol. 40, (2006), 2621-2628. (<https://doi.org/10.1016/j.watres.2006.05.015>).
- Reith, J.H., Wijffels, R.H. and Barten, H., *Bio-methane and bio-hydrogen: Status and perspectives of biological methane and hydrogen production*, Dutch Biological Hydrogen Foundation, (2003), 166. (<https://www.irwash.org/sites/default/files/Reith-2003-Bio.pdf>).
- Moestedt, J., Pålledal, S.N., Schnürer, A. and Nordell, E., "Biogas production from thin stillage on an industrial scale-experience and optimisation", *Energies*, Vol. 6, No. 11, (2013), 5642-5655. (<https://doi.org/10.3390/en6115642>).
- Ziemiński, K. and Frąc, M., "Methane fermentation process as anaerobic digestion of biomass: Transformations, stages and microorganisms",

- African Journal of Biotechnology*, Vol. 11, No. 18, (2012). (<https://www.ajol.info/index.php/ajb/article/view/101067>).
13. Al-Rubaye, H., Karambelkar, S., Shivashankaraiah, M.M. and Smith, J.D., "Process simulation of two-stage anaerobic digestion for methane production", *Biofuels*, Vol. 10, (2019), 181-191. (<https://doi.org/10.1080/17597269.2017.1309854>).
 14. Appels, L., Baeyens, J., Degreé, J. and Dewil, R., "Principles and potential of the anaerobic digestion of waste-activated sludge", *Progress in Energy and Combustion Science*, Vol. 34, No. 6, (2008), 755-781. (<https://doi.org/10.1016/j.peccs.2008.06.002>).
 15. Gerardi, M.H., *The microbiology of anaerobic digesters*, John Wiley & Sons, (2003). (<https://onlinelibrary.wiley.com/doi/book/10.1002/0471468967>).
 16. Marinescu, M., Dumitru, M. and Lăcătușu, A.R., "Biodegradation of petroleum hydrocarbons in an artificial polluted soil", *Journal of Agricultural Science*, Vol. 41, No. 2, (2009), 157-162. (<https://agricultura.usab-tm.ro/Simpo2009pdf/Simpo%202009%20vol%202/Sectiunea%205/05%20Mariana%20Marinescu.pdf>).
 17. Lorenzo-Llanes, J., Pagés-Díaz, J., Kalogirou, E. and Contino, F., "Development and application in Aspen Plus of a process simulation model for the anaerobic digestion of vinasses in UASB reactors: Hydrodynamics and biochemical reactions", *Journal of Environmental Chemical Engineering*, Vol. 8, No. 2, (2020), 103540. (<https://doi.org/10.1016/j.jece.2019.103540>).
 18. Mabalane, P.N., Oboirien, B.O., Sadiku, E.R. and Masukume, M.A., "Techno-economic analysis of anaerobic digestion and gasification hybrid system: Energy recovery from municipal solid waste in South Africa", *Waste and Biomass Valorization*, Vol. 12, (2021), 1167-1184. (<https://doi.org/10.1007/s12649-020-01043-z>).
 19. Rasapoor, M., Young, B., Brar, R., Sarmah, A., Zhuang, W.Q. and Baroutian, S., "Recognizing the challenges of anaerobic digestion: Critical steps toward improving biogas generation", *Fuel*, Vol. 261, (2020), 116497. (<https://doi.org/10.1016/j.fuel.2019.116497>).
 20. Achinas, S., Martherus, D., Krooneman, J. and Euverink, G.J.W., "Preliminary assessment of a biogas-based power plant from organic waste in the North Netherlands", *Energies*, Vol. 12, No. 2, (2019), 4034. (<https://doi.org/10.3390/en12214034>).
 21. Ravendran, R.R., Abdulrazik, A. and Zailan, R., "Aspen Plus simulation of optimal biogas production in anaerobic digestion process", *Proceedings of IOP Conference Series: Materials Science and Engineering, Volume 702, 1st ProSES Symposium 2019*, Kuantan, Pahang, Malaysia, (2019), 012001. (<https://iopscience.iop.org/article/10.1088/1757-899X/702/1/012001>).
 22. Anukam, A., Mohammadi, A., Naqvi, M. and Granström, K., "A review of the chemistry of anaerobic digestion: Methods of accelerating and optimizing process efficiency", *Processes*, Vol. 7, No. 8, (2019), 1-19. (<https://doi.org/10.3390/pr7080504>).
 23. Batstone, D.J. and Keller, J., "Industrial applications of the IWA anaerobic digestion model No. 1 (ADM1)", *Water Science and Technology*, Vol. 47, (2003), 199-206. (<https://doi.org/10.2166/wst.2003.0647>).
 24. Angelidaki, I., Ellegaard, L. and Ahring, B.K., "A comprehensive model of anaerobic bioconversion of complex substrates to biogas", *Biotechnology and Bioengineering*, Vol. 63, (1999), 363-372. ([https://doi.org/10.1002/\(SICI\)1097-0290\(19990505\)63:3%3C363::AID-BIT13%3E3.0.CO;2-Z](https://doi.org/10.1002/(SICI)1097-0290(19990505)63:3%3C363::AID-BIT13%3E3.0.CO;2-Z)).
 25. Al-rubaye, H., Karambelkar, S., Shivashankaraiah, M.M. and Smith, J.D., "Process simulation of two-stage anaerobic digestion for methane production", *Biofuels*, Vol. 10, No. 2, (2017), 1-11. (<https://doi.org/10.1080/17597269.2017.1309854>).
 26. Rajendran, K., Kankanala, H.R., Lundin, M. and Taherzadeh, M.J., "A novel Process Simulation Model (PSM) for anaerobic digestion using Aspen Plus", *Bioresour. Technol.*, Vol. 168, (2014), 7-13. (<https://doi.org/10.1016/j.biortech.2014.01.051>).
 27. Harun, N., Hassan, Z., Zainol, N., Ibrahim, W.H.W. and Hashim, H., "Anaerobic digestion process of food waste for biogas production: A simulation approach", *Chemical Engineering and Technology*, Vol. 42, No. 4, (2019), 1834-1839. (<https://doi.org/10.1002/ceat.201800637>).
 28. Rouse, S., *Precise biogas flow measurement: Overcoming the challenges of changing gas composition*, (2013). (<https://www.sierrainstruments.com/userfiles/file/wpsirriabiogas.pdf>).
 29. Rico, C., Rico, J.L., Tejero, I., Muñoz, N. and Gómez, B., "Anaerobic digestion of the liquid fraction of dairy manure in pilot plant for biogas production: Residual methane yield of digestate", *Waste Management*, Vol. 31, No. 9-10, (2011), 2167-2173. (<https://doi.org/10.1016/j.wasman.2011.04.018>).
 30. Morvan, T., Gogé, F., Oboyet, T., Carel, O. and Fouad, Y.A., "Dataset of the chemical composition and near-infrared spectroscopy measurements of raw cattle, poultry and pig manure", *Data in Brief*, Vol. 39, (2021). (<https://doi.org/10.1016/j.dib.2021.107475>).
 31. Picardo, A., Soltero, V.M., Peralta, M.E. and Chacartegui, R., "District heating based on biogas from wastewater treatment plant", *Energy*, Vol. 180, 649-664 (2019). (<https://doi.org/10.1016/j.energy.2019.05.123>).
 32. Labatut, R.A., Angenent, L.T. and Scott, N.R., "Conventional mesophilic vs. thermophilic anaerobic digestion: A trade-off between performance and stability?", *Water Research*, Vol. 53, (2014), 249-258. (<https://doi.org/10.1016/j.watres.2014.01.035>).
 33. Nges, I.A. and Liu, J., "Effects of solid retention time on anaerobic digestion of dewatered-sewage sludge in mesophilic and thermophilic conditions", *Renewable Energy*, Vol. 35, (2010), 2200-2206. (<https://doi.org/10.1016/j.biortech.2014.10.102>).
 34. Dareioti, M.A. and Kornaros, M., "Anaerobic mesophilic co-digestion of ensiled sorghum, cheese whey and liquid cow manure in a two-stage CSTR system: Effect of hydraulic retention time", *Bioresour. Technol.*, Vol. 175, (2015), 553-562. (<https://doi.org/10.1016/j.biortech.2014.10.102>).
 35. Kumar, A. and Samadder, S.R., "Performance evaluation of anaerobic digestion technology for energy recovery from organic fraction of municipal solid waste: A review", *Energy*, Vol. 197, (2020). (<https://doi.org/10.1016/j.energy.2020.117253>).
 36. Vavilin, V.A., Vasiliev, V.B. and Rytov, S.V., "Modelling of gas pressure effects on anaerobic digestion", *Bioresour. Technol.*, Vol. 52, No. 1, (1995), 25-32. ([https://doi.org/10.1016/0960-8524\(94\)00148-T](https://doi.org/10.1016/0960-8524(94)00148-T)).
 37. Mao, C., Feng, Y., Wang, X. and Ren, G., "Review on research achievements of biogas from anaerobic digestion", *Renewable and Sustainable Energy Reviews*, Vol. 45, (2015), 540-555. (<https://doi.org/10.1016/j.rser.2015.02.032>).
 38. Rodriguez, C., Alaswad, A., El-Hassan, Z. and Olabi, A.G., "Waste paper and macroalgae co-digestion effect on methane production", *Energy*, Vol. 154, (2018), 119-125. (<https://doi.org/10.1016/j.energy.2018.04.115>).
 39. Kothari, R., Pandey, A.K., Kumar, S., Tyagi, V.V. and Tyagi, S.K., "Different aspects of dry anaerobic digestion for bio-energy: An overview", *Renewable and Sustainable Energy Reviews*, Vol. 39, (2014), 174-195. (<https://doi.org/10.1016/j.rser.2014.07.011>).
 40. Palatsi, J., Viñas, M., Guivernau, M., Fernandez, B. and Flotats, X., "Anaerobic digestion of slaughterhouse waste: Main process limitations and microbial community interactions", *Bioresour. Technol.*, Vol. 102, (2011), 2219-2227. (<https://doi.org/10.1016/j.biortech.2010.09.121>).
 41. Romero-Güiza, M.S., Vila, J., Mata-Alvarez, J., Chimenos, J.M. and Astals, S., "The role of additives on anaerobic digestion: A review", *Renewable and Sustainable Energy Reviews*, Vol. 58, (2016), 1486-1499. (<https://doi.org/10.1016/j.rser.2015.12.094>).
 42. Siddique, M.N.I. and Wahid, Z.A., "Achievements and perspectives of anaerobic co-digestion: A review", *Journal of Cleaner Production*, Vol. 194, (2018), 359-371. (<https://doi.org/10.1016/j.jclepro.2018.05.155>).
 43. Harris, P.W., Schmidt, T. and McCabe, B.K., "Impact of thermobaric pre-treatment on the continuous anaerobic digestion of high-fat cattle slaughterhouse waste", *Biochemical Engineering Journal*, Vol. 134, (2018), 108-113. (<https://doi.org/10.1016/j.bej.2018.03.007>).
 44. Kovács, E., Wirth, R., Maróti, G., Bagi, Z., Rákhely, G. and Kovács, K.L., "Biogas production from protein-rich biomass: Fed-batch anaerobic fermentation of casein and of pig blood and associated changes in microbial community composition", *PLoS ONE*, Vol. 8, No. 10, (2013), e77265. (<https://doi.org/10.1371/journal.pone.0077265>).
 45. Perle, M., Kimchie, S. and Shelef, G., "Some biochemical aspects of the anaerobic degradation of dairy wastewater", *Water Research*, Vol. 29, No. 6, (1995), 1549-1554. ([https://doi.org/10.1016/0043-1354\(94\)00248-6](https://doi.org/10.1016/0043-1354(94)00248-6)).
 46. Schnürer, A. and Jarvis, Å., *Mikrobiologisk handbok för biogas anläggningar*, Svenskt Gastekniskt Center, (2009). (<https://www.avfallsverige.se/>).
 47. Elsayed, M., Andres, Y., Blel, W., Gad, A. and Ahmed, A., "Effect of VS organic loads and buckwheat husk on methane production by

- anaerobic co-digestion of primary sludge and wheat straw", *Energy Conversion and Management*, Vol. 117, (2016), 538-547. (<https://doi.org/10.1016/j.enconman.2016.03.064>).
48. Daneshgar, S., Buttafava, A., Capsoni, D., Callegari, A. and Capodaglio, A.G., "Impact of pH and ionic molar ratios on phosphorous forms precipitation and recovery from different wastewater sludges", *Resources*, Vol. 7, No. 4, (2018). (<https://doi.org/10.3390/resources7040071>).
49. Deublein, D., Editors, A.S., Gmbh, W.V. and Kгаа, C., "Book review biogas from waste and renewable resources: An introduction", *Environmental Engineering and Management Journal*, Vol. 7, No. 4, (2008), 483-485. (http://www.eemj.icpm.tuiasi.ro/pdfs/vol7/no4/32_Book%20Rev_Biogas.pdf).

ABSTRACTS

Experimental Investigation into the Combustion, Performance, and Emission Characteristics of Oxygenated DEE and Ethanol Blending with KOME Biodiesel Fuelled CI Engine

Krishnarao Rajaram Patil*

Department of Mechanical Engineering, Marathwada Mitramandal's College of Engineering, Pune Affiliated to Savitribai Phule Pune University, P. O. Box: 411052, Pune, Maharashtra, India.

PAPER INFO

Paper History:

Received: 15 February 2022

Revised: 19 April 2022

Accepted: 26 April 2022

Keywords:

DEE-Ethanol-KOME Biodiesel Blend,
CI Engine,
Combustion Behaviour,
Engine Performance,
Emission Characteristics

ABSTRACT

The present study aims to develop different strategies for better utilization of oxygenated Diethyl ether and ethanol as supplementary fuels by blending them with biodiesel as the base fuel in CI engines. The used biodiesel used was readily available Karanja Oil Methyl Ester (KOME), its scientific name being *Pongamia Pinnata*. Initially, 5 %, 10 %, 15 %, and 20 % amounts of ethanol (volume) were mixed with biodiesel. Further, the optimum selected blend BE15 was mixed with 5 %, 10 %, 15 %, and 20 % DEE by volume to make the ternary blend. This DEE-ethanol-biodiesel blend was tested on the same engine under the same conditions. The experimental results exhibited that the DEE-ethanol-biodiesel ternary blend, BE15DE10, mitigated BTE by 8.89 % and the smoke, NO_x, and CO emissions by 15.66 %, 50.7 %, and 18.5 %, respectively, compared with neat biodiesel. The HC emission exhibited a slightly increasing trend. The results summarize the trade-off between smoke and NO_x reduction using DEE and ethanol oxygenated fuels. The addition of ethanol by 15 % and DEE up to 10 % by volume to biodiesel could be considered the most favorable blend without any significant modifications in the CI engine.

<https://doi.org/10.30501/jree.2022.328607.1330>

2423-7469/© 2023 The Author(s). Published by MERC. This is an open access article under the CC BY license (<https://creativecommons.org/licenses/by/4.0/>).



چکیده

هدف از مطالعه حاضر، توسعه استراتژی‌های مختلف برای استفاده بهتر از دی‌اتیل اتر اکسیژن دار و اتانول به عنوان سوخت‌های مکمل با ترکیب آنها با بیودیزل به عنوان سوخت پایه در موتورهای احتراق تراکمی (CI) است. بیودیزل مورد استفاده، متیل استر روغن کارانجا (KOME) بود که نام علمی آن *Pongamia Pinnata* است. در ابتدا مقادیر ۵٪، ۱۰٪، ۱۵٪ و ۲۰٪ اتانول (حجمی) با بیودیزل مخلوط شد. علاوه بر این، مخلوط انتخابی بهینه BE15 با ۵٪، ۱۰٪، ۱۵٪ و ۲۰٪ DEE حجمی برای ساخت ترکیب سه تایی مخلوط شد. این ترکیب DEE-اتانول-بیودیزل بر روی همان موتور تحت شرایط یکسان آزمایش شد. نتایج تجربی نشان داد که ترکیب سه تایی DEE-اتانول-بیودیزل، BE15DE10، BTE را به میزان ۸/۸۹ درصد و انتشار دود، NO_x و CO را به ترتیب ۱۵/۶۶ درصد، ۵۰/۷ درصد و ۱۸/۵ درصد در مقایسه با بیودیزل تمیز کاهش داد. انتشار HC روند ملایم افزایشی را نشان داد. نتایج، تبادل بین دود و کاهش NO_x با استفاده از سوخت‌های DEE و اکسیژن دار اتانول را خلاصه می‌کنند. افزودن اتانول ۱۵ درصد و DEE تا ۱۰ درصد حجمی به بیودیزل، می‌تواند مطلوب‌ترین ترکیب بدون هیچ گونه تغییر قابل توجهی در موتور CI در نظر گرفته شود.

Optimal Location and Sizing of Wind Turbines and Photovoltaic Cells in the Grid for Load Supply Using Improved Genetic Algorithm

Ming Hung Lin ^a, Jiun Hung Lin ^b, Mamdouh El Haj Assad ^{c*}, Reza Alayi ^{d,e*}, Seyed Reza Seyednouri ^f

^a Department of Electrical Engineering, Cheng Shiu University, 83347, Kaohsiung City, Taiwan, China.

^b College of Electrical Engineering and Computer Science, National Kaohsiung University of Science and Technology, 811, Kaohsiung City, Taiwan, China.

^c Department of Sustainable and Renewable Energy Engineering, University of Sharjah, P. O. Box: 27272, Sharjah, United Arab Emirates.

^d Department of Mechanics, Germe Branch, Islamic Azad University, P. O. Box: 5651763764, Germe, Ardabil, Iran.

^e Energy Research Center, Shahrekord Branch, Islamic Azad University, Shahrekord, Chaharmahal and Bakhtiari, Iran.

^f Young Researchers and Elite Club, Germe Branch, Islamic Azad University, P. O. Box: 5651763764, Germe, Ardabil, Iran.

PAPER INFO

Paper History:

Received: 30 January 2022

Revised: 19 June 2022

Accepted: 23 June 2022

Keywords:

Optimal Placement,
Improved Genetic Algorithm,
Distributed Production,
Loss Reduction,
Combined System

ABSTRACT

The optimal combination of distributed generation units in recent years has been designed to improve the reliability of distributed generation systems as well as to reduce losses in electrical distribution systems. In this research, the improved Genetic Algorithm has been proposed as a powerful optimization algorithm for optimizing problem variables. The objective function of this paper includes power loss reduction, hybrid system reliability, voltage profile, optimal size of distributed generation unit, and finally improvement of the construction cost of combined wind and solar power plants. Therefore, the problem variables are subject to reliable load supply and the lowest possible cost during the optimization process. In order to achieve this goal in this study, the IEEE standard 30-bus network is examined. The results of the system simulation show the reduction of total system losses after DG installation compared to the state without DG and the improvement of other variable values in this network. This loss index after installing DG in the desired bus has a reduction of about 200 kWh during the year and has a value equal to 126.42 kWh per year.

<https://doi.org/10.30501/jree.2022.327250.1321>

2423-7469/© 2023 The Author(s). Published by MERC. This is an open access article under the CC BY license (<https://creativecommons.org/licenses/by/4.0/>).



چکیده

ترکیب بهینه واحدهای تولید پراکنده در سال‌های اخیر برای بهبود قابلیت اطمینان سیستم‌های تولید پراکنده و همچنین کاهش تلفات در سیستم‌های توزیع برق طراحی شده است. در این تحقیق، الگوریتم ژنتیک بهبودیافته به عنوان یک الگوریتم بهینه‌سازی قدرتمند برای بهینه‌سازی متغیرهای مسئله پیشنهاد شده است. تابع هدف این مقاله شامل کاهش تلفات توان، قابلیت اطمینان سیستم هیبریدی، پروفایل ولتاژ، اندازه بهینه واحد تولید پراکنده و در نهایت بهبود هزینه ساخت نیروگاه‌های ترکیبی بادی و خورشیدی است. بنابراین، متغیرهای مشکل در طول فرآیند بهینه‌سازی مشمول تأمین بار مطمئن و کمترین هزینه ممکن می‌شوند. به منظور دستیابی به این هدف در این تحقیق، شبکه ۳۰ باس استاندارد IEEE مورد بررسی قرار گرفته است. نتایج شبیه‌سازی سیستم نشان‌دهنده کاهش تلفات کل سیستم پس از نصب DG نسبت به حالت بدون DG و بهبود سایر مقادیر متغیر در این شبکه است. این شاخص تلفات پس از نصب DG در باس مورد نظر در طول سال حدود ۲۰۰ کیلووات ساعت کاهش داشته و مقداری معادل ۱۲۶/۴۲ کیلووات ساعت در سال دارد.

Evaluation of the Experimental Performance of an Asphalt Solar Air Collector

Armin Motamed Sadr, Mehran Ameri*, Ebrahim Jahanshahi Javaran

Department of Mechanical Engineering, School of Engineering, Shahid Bahonar University of Kerman, P. O. Box: 76169-14111, Kerman, Iran.

PAPER INFO

Paper History:

Received: 17 March 2022

Revised: 26 June 2022

Accepted: 06 July 2022

Keywords:

Asphalt Collector,
Air,
Solar Energy,
Efficiency

ABSTRACT

In this research, the performance of an asphalt solar air collector was experimentally tested and the daily thermal and exergy efficiencies of the collector were analyzed. The sun's radiant energy is absorbed by asphalt and converted into thermal energy. Then, it is transmitted to aluminum pipes buried under the asphalt and, finally, to the air passing through the pipes. A suction fan induces the ambient air to the collector. The experimental results show that the daily thermal efficiencies at mass flow rates of 0.007 (kg/s) and 0.014 (kg/s) are 11.98 % and 24.10 % and daily exergy efficiencies are 0.34 % and 0.66 %, respectively, showing the increase in daily energy and exergy efficiencies with increasing the air mass flow rate. In addition, results show that as the flow rate increases, the outlet air temperature decreases. The presence of temperature difference between the inlet and outlet of the collector in the last hours of the day, when the sun's radiation is low, indicates that asphalt acts as a thermal energy storage medium.

<https://doi.org/10.30501/jree.2022.334587.1347>

2423-7469/© 2023 The Author(s). Published by MERC. This is an open access article under the CC BY license (<https://creativecommons.org/licenses/by/4.0/>).



چکیده

در این تحقیق، عملکرد یک کلکتور هوایی خورشیدی آسفالت مورد آزمایش قرار گرفت و بازده حرارتی و انرژی کلکتور بصورت روزانه بررسی شدند. انرژی تابشی خورشید توسط آسفالت جذب و به انرژی حرارتی تبدیل و سپس به لوله های آلومینیومی دفن شده در زیر آسفالت و در نهایت به هوای داخل لوله ها منتقل می شود. یک فن مکند، هوای محیط را به کلکتور مکش می کند. نتایج بدست آمده از آزمایش نشان می دهند که بازده روزانه حرارتی در دبی های جرمی 0/007 (kg/s) و 0/014 (kg/s) به ترتیب 11/98 % و 24/10 % و بازده روزانه انرژی نیز به ترتیب برابر با 0/34 % و 0/66 % می باشند که نشان دهنده افزایش بازده روزانه انرژی و انرژی کلکتور با افزایش دبی جریان می باشد. همچنین، با افزایش دبی جریان، دمای هوای خروجی نیز کاهش پیدا می کند. وجود اختلاف دما در ورودی و خروجی کلکتور در ساعات پایانی روز که تشعشع خورشید ناچیز است، حاکی از این است که آسفالت به عنوان یک محیط ذخیره ساز انرژی حرارتی عمل می کند.

An Optimal Master-Slave Model for Stochastic Planning of AC-DC Hybrid Distribution Systems

Zeinab Sabzian-Molaei^a, Esmaeel Rokrok^{b*}, Meysam Doostizadeh^b

^a Department of Electrical Engineering, Khorramabad Branch, Islamic Azad University, Khorramabad, Lorestan, Iran.

^b Department of Electrical Engineering, Lorestan University, Khorramabad, Lorestan, Iran.

PAPER INFO

Paper History:

Received: 05 January 2022

Revised: 02 June 2022

Accepted: 14 June 2022

Keywords:

AC-DC Distribution Systems,
Stochastic Planning,
Graph Theory,
Converter Efficiency Curve,
Distributed Energy Resources,
Electric Vehicle Charging Stations

ABSTRACT

In this study, a novel stochastic planning method is proposed for AC-DC hybrid distribution networks. The proposed approach is based on the graph theory, and the optimal AC-DC structure of the network is selected among the system spanning trees. The presented method is a Mixed Integer Nonlinear Programming (MINLP) problem, which is solved using genetic algorithm. The buses and lines of the network can be either AC or DC to minimize the system investment costs in the master optimization problem. The location and capacity of the Distributed Energy Resources (DERs) as well as the site and size of the Electric Vehicle (EV) charging stations are optimized in the slave problem to minimize the network losses and system costs. The proposed model utilizes Monte Carlo simulation to deal with the stochastic variations of the renewable energy resources power and load demands. Besides, the converter efficiency curve in the proposed planning problem is modeled based on a function of its input current using PLECS software. The proposed approach for network design can be applied to different DG resources and AC-DC loads. The comparison between the simulation results of the proposed approach and the conventional AC planning method demonstrates the efficiency of the proposed model in reducing network losses and system costs.

<https://doi.org/10.30501/jree.2022.323167.1309>

2423-7469/© 2023 The Author(s). Published by MERC. This is an open access article under the CC BY license (<https://creativecommons.org/licenses/by/4.0/>).



چکیده

این مقاله یک روش جدید برنامه‌ریزی تصادفی برای شبکه‌های توزیع ترکیبی معرفی می‌کند. مدل ارائه شده بر مبنای تئوری گراف می‌باشد و ساختار بهینه‌ی AC-DC شبکه از میان مجموعه درخت‌های پوشای سیستم انتخاب می‌شود. روش ارائه شده یک مسئله برنامه نویسی مختلط عدد صحیح غیرخطی است که توسط الگوریتم ژنتیک حل می‌شود. به منظور کمینه کردن هزینه‌های سرمایه‌گذاری سیستم، در مسئله اصلی بهینه‌سازی، باس‌ها و خطوط شبکه می‌توانند AC یا DC باشند. همچنین، با هدف کمینه کردن تلفات و هزینه عملکرد سیستم، مکان و ظرفیت منابع تولید تجدیدپذیر و نیز ایستگاه‌های شارژ خودرو برقی، در مسئله فرعی بهینه می‌شوند. مدل پیشنهادی از روش شبیه سازی مونت کارلو جهت رسیدگی به تغییرات تصادفی توان منابع تجدیدپذیر و همچنین تقاضای بارها استفاده می‌کند. به علاوه، در مسئله برنامه‌ریزی پیشنهادی، منحنی بازدهی کانورتر بر اساس تابعی از جریان ورودی آن توسط نرم‌افزار PLECS مدل شده است. در نهایت، روش ارائه شده برای طراحی یک شبکه، شامل انواع منابع تولیدی و بارهای AC-DC به کار برده می‌شود. مقایسه نتایج شبیه‌سازی به روش پیشنهادی با روش برنامه‌ریزی سنتی AC، کارایی مدل پیشنهادی را در کاهش تلفات و هزینه‌های سیستم، نشان می‌دهد.

Biogas Production by Co-Digestion of Food Waste with Sewage Sludge and Poultry Litter: A Way Towards Sustainable Waste-to-Energy Conversion

Uttam Bista, Bhawana Rayamajhi, Bipasyana Dhungana, Sunil Prasad Lohani*

Renewable and Sustainable Energy Laboratory, Department of Mechanical Engineering, School of Engineering, Kathmandu University, P. O. Box: 6250, Dhulikhel, Nepal.

PAPER INFO

Paper History:

Received: 10 March 2022

Revised: 01 May 2022

Accepted: 21 May 2022

Keywords:

Co-Digestion,
Biogas,
Waste,
Temperature,
Sustainability

ABSTRACT

Anaerobic digestion is one of the most effective technologies for managing degradable waste, which produces renewable energy and digestate as the byproduct. In this study, sewage sludge (SS), poultry litter (PL), and food waste (FW) were co-digested at ratios (SS:PL:FW 2:1:1) with 8 % total solid content at ambient temperature (average 22 °C) and controlled temperature (35 °C) in summer. The synergistic effects of co-digesting substrates enhance the biogas production potential when digested at an optimized ratio. The maximum biogas yield was 688.7 L/kgV_{Sa} at the controlled temperature and 462.3 L/kgV_{Sa} at ambient temperature. The ambient reactor had a methane composition of 55 %, while the controlled temperature reactor had about 60 %. The results provide approaches to increase biogas production in the anaerobic digestion process through co-digestion and controlled mesophilic temperature. Biogas production from anaerobic co-digestion could significantly transform waste into energy in low-income countries to achieve the objective of clean energy production and environmental sustainability.

<https://doi.org/10.30501/jree.2022.333462.1342>

2423-7469/© 2023 The Author(s). Published by MERC. This is an open access article under the CC BY license (<https://creativecommons.org/licenses/by/4.0/>).



چکیده

هضم بی‌هوازی یکی از مؤثرترین فناوری‌ها برای مدیریت زباله‌های تجزیه‌پذیر است که انرژی‌های تجدیدپذیر و محصول هضم را به عنوان محصول جانبی تولید می‌کند. در این مطالعه، لجن فاضلاب (SS)، کودهای حیوانی (PL) و ضایعات غذایی (FW) در نسبت‌های (SS:PL:FW 2:1:1) با ۸ درصد محتوای جامد کل با میانگین دمای ۲۲ درجه سانتیگراد و دمای کنترل شده (۳۵ درجه سانتیگراد) در فصل تابستان در دمای محیط هضم شدند. اثرات هم‌افزایی بسترهای هضم هم‌زمان، پتانسیل تولید بیوگاز را در صورت هضم با نسبت بهینه افزایش می‌دهد. حداکثر بازده تولید بیوگاز ۶۸۸/۷ L/kgV_{Sa} در دمای کنترل شده و ۴۶۲/۳ L/kgV_{Sa} در دمای محیط بدست آمد. راکتور محیط دارای ترکیب متان ۵۵٪ و راکتور دمای کنترل شده حدود ۶۰٪ بود. نتایج، رویکردهایی را برای افزایش تولید بیوگاز در فرآیند هضم بی‌هوازی از طریق هضم هم‌زمان و دمای مزوفیل کنترل شده ارائه می‌کنند. در کشورهای کم‌درآمد تولید بیوگاز از هضم هم‌زمان بی‌هوازی می‌تواند به طور قابل توجهی زباله‌ها را به انرژی تبدیل کند تا به هدف تولید انرژی پاک و پایداری زیست‌محیطی دست یابد.

Investigation of the Enhancement of Thermophysical Properties of New Combinations of MWCNTs with Several PCMs Consisting of a Type of Paraffin in Comparison with Some Mineral Compounds (AN-MN-6H₂O)

Seyed Amir Hassan Bathaei ^a, Masoud Iranmanesh ^{a*}, Hossein Amiri ^a, Hajir Kourki ^b

^a Department of Energy, Institute of Science and High Technology and Environmental Sciences, Graduate University of Advanced Technology, Kerman, Iran.

^b Department of Chemical Engineering, Polymer Engineering Group, Institute of Science and High Technology and Environmental Sciences, Graduate University of Advanced Technology, Kerman, Iran.

PAPER INFO

Paper History:

Received: 08 May 2022

Revised: 12 June 2022

Accepted: 28 June 2022

Keywords:

Solar Thermal Energy Storage,
Phase Change Materials,
Paraffin,
MWCNTs,
Thermophysical Properties

ABSTRACT

Thermal Energy Storage (TES) for solar thermal systems has attracted great attention because of the intermittent availability of solar energy. In the current paper, new combinations of several Phase Change Materials (PCMs) including a type of paraffin and some mineral compounds like ammonium nitrate and magnesium nitrate hexahydrate were examined and their thermophysical properties were compared. This study targets solar heating systems at different temperature intervals for the TES. Another new approach of this study is to determine the effect of Multi-Wall Carbon Nanotubes (MWCNTs) with two diameters (D) of 8 and 10-20 nm on paraffin's thermophysical property to improve these properties. An innovative method was used to measure Electrical Conductivity (EC) as it is easier to measure than thermal conductivity (K) to study the effect of nanoparticles on PCM behavior. The results showed that the highest values of improvement over paraffin properties were related to 5 % nanoparticle additive for both nanoparticle diameters among the percentages studied. The addition of 5 % nanoparticles with 10-20 nm and 8 nm to paraffin at 25 °C increased heat conductivity by 142 % and 156 %, respectively. The addition of nanoparticles to paraffin improved EC several times such that a diameter of 8 nm made a 300 % increase in EC compared to 10-20 nm.

<https://doi.org/10.30501/jree.2022.339549.1363>

2423-7469/© 2023 The Author(s). Published by MERC. This is an open access article under the CC BY license (<https://creativecommons.org/licenses/by/4.0/>).



چکیده

ذخیره‌سازی انرژی حرارتی (TES) برای سیستم‌های حرارتی خورشیدی توجه فزاینده‌ای را به خود جلب کرده است، زیرا انرژی خورشیدی بطور متناوب در دسترس است. در این مطالعه، چندین ماده تغییرفازدهنده (PCM) جدید از جمله نوعی پارافین و برخی از ترکیبات معدنی مانند نیترات آمونیوم و هگزا‌هیدرات نیترات منیزیم بررسی و خواص ترموفیزیکی آنها مقایسه شدند. این مطالعه در فواصل دمایی مختلف در سیستم‌های گرمایش خورشیدی برای TES قابل استفاده است. یکی دیگر از رویکردهای جدید این مطالعه، کشف تأثیر نانولوله‌های کربنی چند جداره (MWCNTs) با دو قطر ۸ و ۱۰-۲۰ نانومتر بر خواص ترموفیزیکی پارافین برای بهبود این خواص است. نتایج نشان داد که بالاترین مقادیر بهبود نسبت به خواص پارافین مربوط به ۵ درصد افزودنی نانوذره برای هر دو قطر نانوذره در بین درصدهای مورد مطالعه بود. یک روش نوآورانه با اندازه‌گیری هدایت الکتریکی (EC) استفاده شده است، زیرا اندازه‌گیری آن آسان‌تر از هدایت حرارتی (K) برای مطالعه تأثیر نانوذرات بر رفتار PCM است. نتایج نشان می‌دهد که افزودن ۵ درصد نانوذرات با ۱۰-۲۰ نانومتر و ۸ نانومتر در دمای ۲۵ درجه سانتی‌گراد، هدایت حرارتی را به ترتیب ۱۴۲ و ۱۵۶ درصد افزایش می‌دهد. افزودن نانوذرات، EC را چندین بار بهبود بخشیده است، به طوری که قطر ۸ نانومتر در مقایسه با ۱۰-۲۰ نانومتر، ۳۰۰ درصد افزایش EC را نشان می‌دهد.

Residential Consumer's Willingness to Pay for Renewable Energy: Evidence from a Double-Bounded Dichotomous Choice Survey from India

Vasundhara Sen *

Department of Infrastructure, Symbiosis Centre for Management and Human Resource Development, Symbiosis International (Deemed University), Pune, India.

PAPER INFO

Paper History:

Received: 03 January 2022

Revised: 21 June 2022

Accepted: 06 July 2022

Keywords:

Green Energy Contracts,
Contingent Valuation,
Renewable Energy,
Willingness to Pay

ABSTRACT

Despite the falling costs of Renewable Energy (RE), RE adoption in Indian residential households is still at tepid growth rates. With the onset of retail electricity market deregulation in India, the introduction of "green tariffs" for residential households can be effective in resolving the issue of low RE adoption. This study investigates the willingness to pay for green tariffs/renewable energy-based electricity contracts using the contingent valuation method. Data collected from 476 Indian residential households are analyzed by the Double-Bounded Dichotomous Choice technique. The results of the conducted maximum Likelihood Estimation (MLE) method reveal the mean willingness to pay 308.52 Rs per household/month for consumption of green power in a premium-paying setting. Results indicate that although households hold positive perception of renewable energy, the willingness to pay is not commensurately high, indicating an attitude-action gap. The study recommends green energy defaults in residential energy contracts, direct marketing of non-use value of RE use (altruistic and bequest) by power supplying utilities, and promoting RE use through RE opinion champions/influencers as measures to enhance RE adoption amongst Indian residential energy consumers.

<https://doi.org/10.30501/jree.2022.314713.1302>

2423-7469/© 2023 The Author(s). Published by MERC. This is an open access article under the CC BY license (<https://creativecommons.org/licenses/by/4.0/>).



چکیده

علیرغم کاهش هزینه‌های انرژی‌های تجدیدپذیر (RE)، پذیرش این نوع انرژی در خانوارهای مسکونی هندی هنوز در نرخ رشد اندک است. با شروع مقررات زدایی از بازار خرده فروشی برق در هند، معرفی "تعرفه‌های سبز" برای خانوارهای مسکونی می‌تواند در حل مسئله نپذیرفتن انرژی تجدیدپذیر مؤثر باشد. این مطالعه به تعرفه‌های سبز/قراردادهای برق مبتنی بر انرژی‌های تجدیدپذیر با استفاده از روش ارزش‌گذاری مشروط می‌پردازد. داده‌های جمع‌آوری شده از 476 خانوار مسکونی هندی با تکنیک پیوند دوگانه بررسی می‌شوند. نتایج روش برآورد حداکثر احتمال بررسی تخصصی (MLE) نشان می‌دهد میانگین تمایل پرداخت به ازای هر خانوار/ماه برای مصرف برق سبز در یک محیط پرداخت حق بیمه مبلغ 308/52 روپیه است. نتایج نشان می‌دهد که اگرچه خانوارها درک مثبتی از انرژی‌های تجدیدپذیر دارند، اما تمایل به پرداخت بالا برای آن ندارند که این نشان‌دهنده خلایق بین نگرش و عمل است. این مطالعه، پیش‌فرض‌هایی از انرژی سبز را در بحث انرژی در قراردادهای مسکونی، بازاریابی مستقیم ارزش غیرکاربردی استفاده از انرژی تجدیدپذیر (نوع دوستانه و ارثی) توسط شرکت‌های تأمین برق، و ترویج استفاده از انرژی تجدیدپذیر از طریق مدافعان/تأثیرگذاران انرژی تجدیدپذیر، به عنوان اقداماتی برای افزایش پذیرش آن در میان مناطق مسکونی و مصرف‌کنندگان هند توصیه می‌کند.

Assessing the Environmental Impacts of Biomass Energy Production in Loka Abaya District, Sidama Region, Southern Ethiopia

Ararsa Derese Seboka^{a*}, Fiseha Bekele Teshome^b, Motuma Tolera Feyissa^a

^a Department of General Forestry, Wondo Genet College of Forestry and Natural Resources, Hawassa University, P. O. Box: 128, Shashemene, Ethiopia.

^b Department of Environmental Science, Wondo Genet College of Forestry and Natural Resources, Hawassa University, P. O. Box: 128, Shashemene, Ethiopia.

PAPER INFO

Paper History:

Received: 15 March 2022

Revised: 18 June 2022

Accepted: 23 June 2022

Keywords:

Biomass Energy,
Wood Fuel,
Charcoal,
Firewood,
Greenhouse Gases,
Environment Impacts

ABSTRACT

This study was conducted in the Loka Abaya District of Sidama Region, Southern Ethiopia to assess the environmental impacts of biomass energy production with particular emphasis on charcoal and firewood. The data collection was undertaken using the questionnaire survey administered to 186 randomly selected households. This task was followed by key informant interviews and an analysis of the literature. The sampled households produced 208 432.9 kg firewood yr⁻¹ for domestic consumption and 261 039.8 kg charcoal yr⁻¹ for sale in town. 2.3×10^{-6} km² of the forest is cleared to produce a single sack of charcoal. Charcoal and firewood production is totally responsible for the degradation of 39.4 ha of forest per year. The associated emissions of CO₂, CO, N₂O, CH₄, and TNMHC (total non-methane hydrocarbon) during the production and consumption of firewood and charcoal were calculated based on the emission factors indicated by previous studies. The results demonstrated that the trace gases produced during charcoal making were higher than that of charcoal burning. Further, the amounts of greenhouse gases generated during firewood burning were higher than the ones generated during charcoal burning. In order to minimize the challenges of deforestation and greenhouse gas emissions caused by charcoal and firewood consumption, a strategy of promoting the utilization of alternative clean energy sources such as solar and biogas should be implemented in parallel to the effort of adoption of improved biomass energy-saving cook stoves.

<https://doi.org/10.30501/jree.2022.334270.1346>

2423-7469/© 2023 The Author(s). Published by MERC. This is an open access article under the CC BY license (<https://creativecommons.org/licenses/by/4.0/>).



چکیده

این مطالعه در ناحیه لوکا آبا یا در منطقه سیداما، اتیوپی جنوبی برای ارزیابی اثرات زیست محیطی تولید انرژی زیست توده با تأکید ویژه بر زغال چوب و هیزم انجام شد. جمع آوری داده ها با استفاده از پرسشنامه پیمایشی بر روی ۱۸۶ خانوار که به صورت تصادفی انتخاب شدند، انجام شد. این کار با مصاحبه با خبرچینان کلیدی و تحلیل ادبیات دنبال شد. خانوارهای نمونه ۲۰۸۴۳۲/۹ کیلوگرم هیزم در سال برای مصرف داخلی و ۲۶۱۰۳۹/۸ کیلوگرم زغال چوب در سال برای فروش در شهر تولید کردند. $۲/۳ \times ۱۰^{-۶}$ کیلومتر مربع از جنگل برای تولید یک کیسه زغال چوب پاک سازی می شود. تولید زغال چوب و هیزم به طور کلی مسئول تخریب ۳۹/۴ هکتار از جنگل در سال است. انتشار مرتبط CO₂، CO، N₂O، CH₄ و TNMHC (کل هیدروکربن غیر متان) در طول تولید و مصرف هیزم و زغال چوب بر اساس متغیرهای انتشار نشان داده شده توسط مطالعات قبلی محاسبه شد. نتایج نشان داد که انتشار گازهای کمیاب تولید شده در حین تولید زغال چوب بیشتر از گازهای تولید شده از سوزاندن زغال آن است. علاوه بر این، مقدار گازهای گلخانه ای تولید شده در هنگام سوزاندن هیزم بیشتر از گازهای تولید شده در هنگام سوزاندن زغال چوب بود. به منظور به حداقل رساندن چالش های جنگل زدایی و انتشار گازهای گلخانه ای ناشی از مصرف زغال چوب و هیزم، یک استراتژی ترویج استفاده از منابع انرژی پاک جایگزین مانند انرژی خورشیدی و بیوگاز باید به موازات تلاش برای پذیرش بهبود انرژی زیست توده اجرا شود.

Impact of Organic Hydrocarbons on Fuel Properties and Engine Characteristics of Thermally Cracked Cashew Nut Shell Liquid

Gokul Raghavendra Srinivasan *, Aditya Mahajan, Rajiv Seth, Rakesh Mahajan

Research and Development Department, Steamax Envirocare India Private Limited, Janak Puri, Delhi-110058, India.

PAPER INFO

Paper History:

Received: 26 March 2022

Revised: 06 July 2022

Accepted: 07 July 2022

Keywords:

Cashew Nut Wastes,
Thermal Cracking,
Screw Press Extraction,
Anacardic Acid,
Cresol

ABSTRACT

The present study aims to explore the role of characterized hydrocarbons in thermally cracked shell liquid in determining its overall fuel properties and combustion characteristics in a CI engine. For this purpose, waste shell liquid was extracted from waste cashew nut shell by means of cold extraction technique using a simple electrically operated mechanical screw press, which reported maximum extractable oil content as 17.7 %. In addition, it was thermally cracked at 350-400 °C using conventional heating for both lab-scale and pilot-scale extraction. Based on its chemical composition, raw shell liquid contained anacardic acid and cardol, while thermally cracked shell liquid had cresol and methyl oleate as their dominant hydrocarbon compounds. Their composition was found to be 51.84 %, 33.68 %, 43.87 %, and 28.49 %, respectively. According to their contribution, both cyclic and aromatic as well as linear-chained hydrocarbons exhibited significant effect on the fuel properties of the cracked shell liquid, with carbon atoms contributing to its physical and thermal properties, whereas cyclic and aromatic hydrocarbons enhance its flow characteristics. Next, neat and blend samples of this cracked shell liquid with petro diesel reported higher peak in-cylinder pressure by 5.6 % (on average) due to the presence of fatty acid esters, which induced early ignition and provided sufficient time for combustion. Meanwhile, higher emission levels were attributed by both cyclic and aromatic and linear-chained hydrocarbons, citing aromaticity and unsaturation in their molecules, which also resulted in reduced thermal efficiencies by 12.5 % (on average), upon accounting for their inferior calorific content. In conclusion, it is evident that hydrocarbons in these treated shell liquids play a significant role in their fuel properties and engine characteristics.

<https://doi.org/10.30501/jree.2022.335041.1349>

2423-7469/© 2023 The Author(s). Published by MERC. This is an open access article under the CC BY license (<https://creativecommons.org/licenses/by/4.0/>).



چکیده

هدف از مطالعه حاضر، بررسی نقش هیدروکربن‌های مشخص شده از تجزیه حرارتی مایع بدست آمده از پوسته بادام هندی در تعیین خواص کلی سوخت و ویژگی‌های احتراق آن در یک موتور احتراق تراکمی (CI) است. برای این منظور، مایع ضایعات پوسته بادام هندی با استفاده از روش استخراج سرد و با استفاده از یک پرس مکانیکی ساده با کارکرد الکتریکی، از پوسته ضایعات بادام هندی استخراج شد که حداکثر میزان روغن قابل استخراج ۱۷/۷ درصد گزارش شد. علاوه بر این، مایع ضایعات با استفاده از گرمایش معمولی برای استخراج در مقیاس آزمایشگاهی و آزمایشی در دمای ۳۵۰-۴۰۰ درجه سانتیگراد تجزیه شد. بر اساس ترکیب شیمیایی، مایع پوسته خام حاوی اسید آناکاردیک و کاردول بود، در حالی که مایع پوسته تجزیه شده حرارتی دارای کرزول و متیل اولنات به عنوان ترکیبات هیدروکربنی غالب آنها بود. ترکیب آنها به ترتیب ۵۱/۸۴ درصد، ۳۳/۶۸ درصد، ۴۳/۸۷ درصد و ۲۸/۴۹ درصد بود. با توجه به سهم هریک، هیدروکربن‌های حلقوی و معطر و همچنین هیدروکربن‌های زنجیره‌ای خطی با تأکید بر نقش اتم‌های کربن در خواص فیزیکی و حرارتی، تأثیر قابل توجهی بر خواص سوخت مایع پوسته تجزیه شده نشان دادند. این در حالیست که هیدروکربن‌های حلقوی و معطر، ویژگی‌های جریان آن را افزایش می‌دهند. در مرحله بعد، نمونه‌های تمیز و ترکیبی از این مایع پوسته تجزیه شده حرارتی با پترو دیزل به دلیل وجود استرهای اسید چرب، که باعث اشتعال زود هنگام می‌شود و زمان کافی برای احتراق فراهم می‌کند، حداکثر فشار درون سیلندر را به میزان ۵/۶ درصد (به طور متوسط) بالاتر گزارش کردند. در همین حال، سطوح بالاتر انتشار توسط هیدروکربن‌های حلقوی و معطر و زنجیره خطی نسبت داده شد، که به معطر بودن و غیر اشباع بودن در مولکول‌های آنها اشاره دارد که همچنین منجر به کاهش بازده حرارتی تا ۱۲/۵٪ (به طور متوسط)، با توجه به محتوای کالری پایین آنها شد. در نتیجه، بدیهی است که هیدروکربن‌های موجود در این مایعات پوسته تصفیه شده نقش مهمی در خواص سوخت و ویژگی‌های موتور آنها دارند.

Energy Management of Multi-Microgrids in Joint Energy and Ancillary Service Market Considering Uncertainties of Renewables

Ritu Jain, Vasundhara Mahajan *

Department of Electrical Engineering, Sardar Vallabhbhai National Institute of Technology, P. O. Box: 395007, Surat, Gujarat, India.

PAPER INFO

Paper History:

Received: 14 February 2022

Revised: 05 August 2022

Accepted: 07 August 2022

Keywords:

Renewable Energy Sources,
Energy Management,
Multi-Microgrid,
Energy Market,
Ancillary Service Market

ABSTRACT

In this study, energy management of grid-connected Multi-Microgrid (MMG) is performed through joint optimization of the energy and ancillary service market. The test system comprises the IEEE 30 bus system as the main grid and the 16-bus system as an MMG. The MMG is comprised of dispatchable and non-dispatchable generation and loads. The non-dispatchable generators are based on renewable energy sources (RES) such as solar and wind. The uncertainty modeling for wind and solar is performed by Weibull and beta probability distribution function. The strategic integration of RES helps MMG deliver both energy and ancillary services to the utility grid. This research aims to reduce the total energy cost while reducing reserve cost by maximizing the use of RES under normal operation and during contingency conditions. It is observed that if MMG is incorporated into the system, then the total generation cost, reserve cost, and power losses are reduced to 0.11 %, 0.325 %, and 1.201 %, respectively, in normal operating conditions. Under contingency, when Generator 5 is out of service and the main grid is operating alone, the total generation cost increased significantly from 22118.92 \$ day⁻¹ to 22435.68 \$ day⁻¹ and the real power loss increased from 233.35 MW day⁻¹ to 245.11 MW day⁻¹. However, by interconnecting MMG with the main grid, generation cost and power loss get reduced to 22375.60 \$ day⁻¹ and 243.35 MW day⁻¹, respectively. It is analyzed that participation of MMG provides techno-economic benefits during normal operation and contingency conditions.

<https://doi.org/10.30501/jree.2022.329343.1334>

2423-7469/© 2023 The Author(s). Published by MERC. This is an open access article under the CC BY license (<https://creativecommons.org/licenses/by/4.0/>).



چکیده

در این مطالعه، مدیریت انرژی چند ریزشبکه متصل به شبکه (MMG) از طریق بهینه‌سازی مشترک بازار انرژی و خدمات جانبی انجام شده است. سیستم تست شامل سیستم گذرگاه سری IEEE شامل ۳۰ عدد باس (BUS) به عنوان شبکه اصلی و سیستم ۱۶ باس به عنوان یک MMG است. MMG از تولید و بارهای قابل ارسال و غیرقابل توزیع تشکیل شده است. ژنراتورهای غیرقابل توزیع مبتنی بر منابع انرژی تجدیدپذیر (RES) مانند خورشیدی و باد هستند. مدل‌سازی عدم قطعیت برای باد و خورشید توسط تابع توزیع احتمال Weibull و بتا انجام می‌شود. ادغام استراتژیک RES به MMG کمک می‌کند انرژی و خدمات جانبی را به شبکه برق ارائه دهد. هدف از این تحقیق، کاهش هزینه کل انرژی و در عین حال کاهش هزینه ذخیره با به حداکثر رساندن استفاده از RES در عملیات عادی و در شرایط اضطراری است. مشاهده می‌شود که اگر MMG در سیستم گنجانده شود، هزینه کل تولید، هزینه ذخیره و تلفات توان به ترتیب به ۰/۱۱٪، ۰/۳۲۵٪ و ۱/۲۰۱٪ در شرایط عملیاتی عادی کاهش می‌یابد. در شرایط اضطراری، زمانی که ژنراتور ۵ خارج از سرویس است و شبکه اصلی به تنهایی کار می‌کند، هزینه کل تولید به طور قابل توجهی از ۲۲۱۱۸/۹۲ دلار در روز به ۲۲۴۳۵/۶۸ دلار در روز افزایش یافته و تلفات برق واقعی از ۲۳۳/۳۵ مگاوات در روز به ۲۴۵/۱۱ مگاوات افزایش یافت. با اتصال MMG به شبکه اصلی، هزینه تولید و تلفات برق به ترتیب به ۲۲۳۷۵/۶۰ دلار در روز و ۲۴۳/۳۵ مگاوات در روز کاهش می‌یابد. چنین تجزیه و تحلیل می‌شود که مشارکت MMG مزایای فنی-اقتصادی را در طول عملیات عادی و شرایط اضطراری فراهم می‌کند.

Development of the Low-Economic-Risk Microgrids to Establish Environmental-Friendly Industries

Mohammad Hossein Jahangir*, Arash Kargarzadeh, Mohammad Montazeri

Department of Renewable Energies and Environment, Faculty of New Science and Technologies, University of Tehran, P. O. Box: 1439957131, Tehran, Iran.

PAPER INFO

Paper History:

Received: 26 February 2022

Revised: 18 June 2022

Accepted: 29 June 2022

Keywords:

Micro Grid,
Green Factory,
Carbon Emission,
Deferrable Load,
Economic Analysis

ABSTRACT

As one of the main consumers of electricity, industries account for in releasing a large amount of emission. Using renewable energies to feed factories is not an easy task and they should be economically viable to compete with fossil fuels. The goal of this study is to analyze the possibilities of using energy local area networks in off-grid and on-grid modes in an industrial project by considering and calculating all primary and deferrable loads in detail for the first time. The industrial project is sensitive and all possibilities should be considered closely to avoid economic losses. In this case, changes in electrical loads during the project, degradation of components, environmental risks, and economic risks of the investment (for each scenario) are considered and determined too. The results indicate that component degradation can cause 24,000 kWh drop in total electricity production at the end of the project and the total biogas consumption increases from 742 kg/yr to 9330 kg/yr. The results also show that the on-grid scenario (solar/battery) with the Net Present Cost of 200,000\$ will be an easy and low-risk choice for investment, but has high environmental risks. On the other hand, the stand-alone scenario (solar/wind/bio/battery) with Net Present Cost of 598,000\$ minimizes the environmental risks at the expense of high investment risk. A proper comparison between the multi-year and single-year modes at the end of the project ensures the high accuracy of techno-economic analysis in terms of optimum system types, emissions, and economics.

<https://doi.org/10.30501/jree.2022.330754.1338>

2423-7469/© 2023 The Author(s). Published by MERC. This is an open access article under the CC BY license (<https://creativecommons.org/licenses/by/4.0/>).



چکیده

صنایع به عنوان یکی از مصرف‌کنندگان اصلی برق از رتبه بالایی در انتشار مقادیر زیادی از آلاینده‌ها برخوردارند. استفاده از انرژی‌های تجدیدپذیر برای تغذیه کارخانه‌ها کار ساده‌ای نیست و برای رقابت با سوخت‌های فسیلی باید از نظر اقتصادی مقرون به صرفه باشند. هدف از این مطالعه، تجزیه و تحلیل احتمالات استفاده از شبکه‌های محلی انرژی در حالت‌های متصل به شبکه و منفصل از شبکه در یک پروژه صنعتی با در نظر گرفتن و محاسبه تمام بارهای اصلی و متغیر و با جزئیات کامل برای اولین بار است. پروژه صنعتی حساس است و برای جلوگیری از ضرر و زیان اقتصادی باید تمامی امکانات را مورد بررسی قرار داد. در این حالت تغییرات بارهای الکتریکی در طول پروژه، فرسودگی اجزاء، خطرات زیست‌محیطی و ریسک‌های اقتصادی سرمایه‌گذاری (برای هر سناریو) در نظر گرفته شده و تعیین می‌شود. نتایج تحقیق حاکی از آن است که فرسایش اجزاء می‌تواند باعث کاهش ۲۴,۰۰۰ کیلووات ساعتی در کل تولید برق در پایان پروژه شود و کل مصرف بیوگاز از ۷۴۲ کیلوگرم در سال به ۹۳۳۰ کیلوگرم در سال افزایش یابد. همچنین نتایج نشان می‌دهد که سناریوی متصل به شبکه (فوتوولتاییک/باتری) با هزینه خالص فعلی ۲۰۰,۰۰۰ دلار یک انتخاب آسان و کم‌ریسک برای سرمایه‌گذاری خواهد بود، اما دارای ریسک‌های زیست‌محیطی بالایی است. از سوی دیگر، سناریوی مستقل (خورشیدی/بادی/بیو/باتری) با هزینه خالص فعلی ۵۹۸,۰۰۰ دلار، خطرات زیست‌محیطی را به قیمت ریسک بالای سرمایه‌گذاری به حداقل می‌رساند. مقایسه حالت شبیه‌سازی "چند ساله" با حالت "یک ساله" در پایان پروژه، افزایش دقت تجزیه و تحلیل فنی-اقتصادی را -از نظر انتخاب سیستم بهینه، آلاینده‌گی و محاسبات اقتصادی- به وضوح نمایش می‌دهد.

Analysis of Biogas Recovery from Liquid Dairy Manure Waste by Anaerobic Digestion

Fatemeh Norouzi^a, Morteza Hosseinpour^{b*}, Saeed Talebi^a

^a Department of Energy Engineering and Physics, Amirkabir University of Technology (Tehran Polytechnic), P. O. Box: 15875-4413, Tehran, Iran.

^b Department of Renewable Energy Research, Niroo Research Institute (NRI), Tehran, Iran.

PAPER INFO

Paper History:

Received: 12 April 2022

Revised: 03 August 2022

Accepted: 12 August 2022

Keywords:

Anaerobic Digestion,

Biogas,

Process Simulation,

Liquid Dairy Manure

ABSTRACT

In this paper, an industrial dairy farm unit was taken as a case study to carry out the applicable technical assessment for the construction of a biogas plant using a combined heat and power (CHP) unit. A comprehensive sensitivity analysis was applied to examine the effectiveness of the operational parameters and feed composition in the purity and production rate of biogas. Aspen Plus was used to implement the anaerobic digestion process. The results showed that any increase in the digester's operational performance and mass rate of feedstock water led to the modification of biomethane content, but dropped in biogas mass flow rate. Moreover, an increase in the mass rate of carbohydrates, protein, and organic load rate (OLR) of feedstock reduces methane composition. Besides, increasing the rate of lipids has raised the rate of methane production and its composition.

<https://doi.org/10.30501/jree.2022.336371.1354>

2423-7469/© 2023 The Author(s). Published by MERC. This is an open access article under the CC BY license (<https://creativecommons.org/licenses/by/4.0/>).



چکیده

در این مطالعه، ارزیابی فنی کاربری یک دامداری صنعتی در ایران برای احداث نیروگاه بیوگاز با استفاده از واحد ترکیبی حرارت و برق (CHP) مورد مطالعه قرار گرفته است. همچنین، تجزیه و تحلیل حساسیت برای سنجش اثربخشی پارامترهای عملیاتی و ترکیب خوراک بر خلوص و میزان تولید بیوگاز اعمال گردید. از مدل شناخته شده ADM1 که شبیه‌سازی فرآیند هضم را در نرم افزار اسپن توسعه داده است، استفاده شده است. نتایج نهایی نشان می‌دهد که افزایش زمان ماند به‌عنوان یکی از مهم‌ترین پارامترهای عملیاتی هاضم و نرخ جرمی آب خوراک، منجر به افزایش خلوص بیومتان و کاهش نرخ تولید گاز متان می‌شود. افزایش نرخ جرمی کربوهیدرات‌ها، پروتئین و بار آلی (OLR) مواد اولیه نیز باعث کاهش خلوص بیومتان تولیدی و افزایش نرخ تولید گاز متان می‌شود. علاوه بر این، افزایش نرخ چربی نیز باعث افزایش تولید بیومتان و درجه خلوص آن می‌شود.

CONTENTS

<p>Krishnarao Rajaram Patil</p>	<p>Experimental Investigation into the Combustion, Performance, and Emission Characteristics of Oxygenated DEE and Ethanol Blending with KOMÉ Biodiesel Fuelled CI Engine</p>	<p>1-8</p>
<p>Ming Hung Lin Jiun Hung Lin Mamdouh El Haj Assad Reza Alayi Seyed Reza Seyednouri</p>	<p>Optimal Location and Sizing of Wind Turbines and Photovoltaic Cells in the Grid for Load Supply Using Improved Genetic Algorithm</p>	<p>9-18</p>
<p>Armin Motamed Sadr Mehran Ameri Ebrahim Jahanshahi Javaran</p>	<p>Evaluation of the Experimental Performance of an Asphalt Solar Air Collector</p>	<p>19-26</p>
<p>Zeinab Sabzian-Molaee Esmacel Rokrok Meysam Doostizadeh</p>	<p>An Optimal Master-Slave Model for Stochastic Planning of AC-DC Hybrid Distribution Systems</p>	<p>27-38</p>
<p>Uttam Bista Bhawana Rayamajhi Bipasyana Dhungana Sunil Prasad Lohani</p>	<p>Biogas Production by Co-Digestion of Food Waste with Sewage Sludge and Poultry Litter: A Way Towards Sustainable Waste-to-Energy Conversion</p>	<p>39-44</p>
<p>Seyed Amir Hassan Bathaei Masoud Iranmanesh Hossein Amiri Hajir Kourki</p>	<p>Investigation of the Enhancement of Thermophysical Properties of New Combinations of MWCNTs with Several PCMs Consisting of a Type of Paraffin in Comparison with Some Mineral Compounds (AN-MN-6H₂O)</p>	<p>45-55</p>
<p>Vasundhara Sen</p>	<p>Residential Consumer's Willingness to Pay for Renewable Energy: Evidence from a Double-Bounded Dichotomous Choice Survey from India</p>	<p>56-69</p>
<p>Ararsa Derese Seboka Fischa Bekele Teshome Motuma Tolera Feyissa</p>	<p>Assessing the Environmental Impacts of Biomass Energy Production in Loka Abaya Distriet, Sidama Region, Southern Ethiopia</p>	<p>70-80</p>
<p>Gokul Raghavendra Srinivasan Aditya Mahajan Rajiv Seth Rakesh Mahajan</p>	<p>Impact of Organic Hydrocarbons on Fuel Properties and Engine Characteristics of Thermally Cracked Cashew Nut Shell Liquid</p>	<p>81-94</p>
<p>Ritu Jain Vasundhara Mahajan</p>	<p>Energy Management of Multi-Microgrids in Joint Energy and Ancillary Service Market Considering Uncertainties of Renewables</p>	<p>95-107</p>
<p>Mohammad Hossein Jahangir Arash Kargarzadeh Mohammad Montazeri</p>	<p>Development of the Low-Economic-Risk Microgrids to Establish Environmental-Friendly Industries</p>	<p>108-124</p>
<p>Fatemeh Norouzi Morteza Hosseinpour Saeed Talebi</p>	<p>Analysis of Biogas Recovery from Liquid Dairy Manure Waste by Anaerobic Digestion</p>	<p>125-132</p>

